Heft 287   Kaan Koca

Advanced experimental methods for investigating flow-biofilm-sediment interactions

Advanced experimental methods for investigating flow-biofilm-sediment interactions

von der Fakultät Bau- und Umweltingenieurwissenschaften der Universität Stuttgart zur Erlangung der Würde eines Doktor-Ingenieurs (Dr.-Ing.) genehmigte Abhandlung

vorgelegt von

Kaan Koca

aus Istanbul, Türkei

Hauptberichterin: Prof. Dr.-Ing. Silke Wieprecht

Mitberichter: Prof. Dr. rer. nat. Andreas Lorke

Tag der mündlichen Prüfung: 29. September 2021

Institut für Wasser- und Umweltsystemmodellierung
der Universität Stuttgart
2022

Heft 287   **Advanced experimental methods for investigating flow-biofilm-sediment interactions**

von
Dr.-Ing.
Kaan Koca

D93   Advanced experimental methods for investigating flow-biofilm-sediment interactions

To Pinar, The Love of My Life…

Acknowledgement

First of all, I would like to take this opportunity to express my great gratitude and appreciation to my supervisor, Prof. Dr.-Ing. Silke Wieprecht, Chair of the Department of Hydraulic Engineering and Water Resources Management of the Institute for Modelling Hydraulic and Environmental Systems (IWS) at the University of Stuttgart, for her support, affirmation, and patience as well as for her continued encouragement and meticulous editing when preparing my dissertation. I am incredibly grateful that she has offered and motivated me to finalize my doctoral dissertation, continued to have faith in my research abilities over the years, whilst providing me with the opportunity to work in exciting projects.

I am also indebted to Prof. Dr. rer. nat. Andreas Lorke, Head of the Environmental Physics Group at the University of Koblenz-Landau, for kindly agreeing to act as the examiner of my dissertation. He generously took precious time out of his schedule to evaluate my work and provided continued support and patience. He also gave me the opportunity to conduct research in his team, which was a truly memorial experience. I have benefited greatly from his wealth of knowledge and scientific enthusiasm, which will inspire me all the time. I also thank to Prof. Dr. rer. nat. habil. Karl-Heinrich Engesser for accepting the chairmanship of my defense.

I would like to thank to all my co-authors, who contributed to the work that I present in this dissertation. I must say a special thank you to Dr.-Ing. Christian Noß and Dr. rer.nat Sabine U. Gerbersdorf. Dr. Noß graciously introduced me to the joys of macgyvering in experimental hydraulics and instrumentation. Dr. Gerbersdorf graciously introduced me to the fields of microbiology and biochemistry. They provided friendship, conversation, and advice, and their encouraging words were invaluable to me.

I would further like to express my thanks to Stefan Haun, Ph.D. and Prof. Dr.-Ing. Markus Noack, who have valued my work, supported my research through many fruitful discussions, and encouraged my ideas. I am also grateful to the entire team at the IWS, including researchers, students, and laboratory technicians, for providing a relaxing atmosphere and an enriching experience. I particularly appreciate the support of the workshop team. The flume tests would not have been possible without their help. I also had the full pleasure of working with my former officemate, Dr.-Ing. Felix Beckers. He always provided a relaxing atmosphere in the office and was always ready for assistance whenever I need. I wish him the best in his life with his lovely wife and daughters. I would also like to take this opportunity to thank to Ms. Maria Costa Jornet and Dr.-Ing. Kristina Terheiden, who have always been very kind and helpful, whenever I need any help, particularly regarding any bureaucratic formalities. Furthermore, I am grateful to my CHARM-colleagues from Freiburg and Konstanz, with whom I had the great pleasure of working in a transdisciplinary research project. I also cannot forget my colleagues at the Environmental Physics Group of University of Koblenz-Landau, who contributed to my research in multiple ways.

It is important to find a balance with the life outside the laboratory. In this respect, I cannot thank enough to a friend, who has always been there for me, not only at work, but also outside: Jan Görtz. I have had immense joys of our walks and captivating chats, which have made my life in Stuttgart more colourful. I wish him all the success in his defense and future career. Furthermore, my sincere thanks go to my longtime friends, Onur Bora and Serkan Zerman, who have always provided comfort with their sympathetic ears. I wish them all the best in their future career.

My wholehearted thanks to my parents, Nuray and Mehmet Ömer, for their unconditional love, emotional support, and trust. Thank you for supporting my choices of places to live since my undergraduate years, making a lot of things possible for me, and coming to visit us. And numerous thanks to my dearest brother, Emirhan. To have you as a brother and a friend is a priceless treasure. I am proud to see you studying with an excellent academic performance and wish all your dreams come true. I also deeply thank to my in-laws (Kemal, Gülay, and Arda Telal) for their always encouraging assistance and kindness as well as for coming to visit us wherever we go. We are looking forward to your next visit in the most positive way.

Finally, I would like to express my deepest gratitude to my wife, my friend, my rock, my world: Pinar. To thank you enough, the words fail me. None of this would have been possible without your endless support, encouragement, patience, and of course, your heartwarming smile. The journey we have travelled together was not always smooth, but we have managed to get over all the obstacles together and made our love stronger, for which I am eternally blessed. Over the past years, I have discovered how amazingly strong and resilient you are and learned a lot from you. You are my inspiration and driving force to keep on fighting and never give up. You have made countless sacrifices for me so that I can pursue what I love doing, and I owe you everything. Now it is my turn. I love you my powerful wife! This dissertation is dedicated to you.

Contents

List of Tables

List of Figures

Notations

The following symbols are used in this dissertation:

$\langle\ \rangle$	[–]	time average (mean)
BI	[–]	biostabilization index
D	[mm]	particle size diameter
D_{10}	[mm]	the 10th percentile of particle size diameter
D_{50}	[mm]	the 50th percentile of particle size diameter or median particle size diameter
D_{90}	[mm]	the 90th percentile of particle size diameter
F_D	[N]	hydrodynamic drag force
F_G	[N]	gravitational force
F_L	[N]	lift force
F_R	[N]	resistance force
k_s	[mm]	roughness height
K	[–]	von Karman constant
M_D	[N m]	overtopping moment due to F_D and F_L at the pivoting point
M_S	[N m]	resisting moment due to F_G at the pivoting point
$\langle N_u^2 \rangle$	[m^2 s^{-2}]	variance of the noise in u'
$\langle N_v^2 \rangle$	[m^2 s^{-2}]	variance of the noise in v'
$\langle N_{w1}^2 \rangle$	[m^2 s^{-2}]	variance of the noise in w_1'
$\langle N_{w2}^2 \rangle$	[m^2 s^{-2}]	variance of the noise in w_2'
PSD	[m^2 s^{-2} Hz^{-1}]	power spectral density
R	[–]	correlation coefficient
Re_*	[–]	particle Reynolds number
ρ	[kg m^{-3}]	density of the fluid
ρ_b	[kg m^{-3}]	bulk density of (wet) sediment
ρ_s	[kg m^{-3}]	density of the sediment
δ_v	[mm]	thickness of the laminar sublayer
SNR	[dB]	signal-to-noise ratio

τ_{cr}	[Pa]	critical shear stress for erosion
$\tau_{cr,1}$	[Pa]	critical shear stress for surface erosion
$\tau_{cr,2}$	[Pa]	critical shear stress for mass erosion
$\tau_{cr,S}$	[Pa]	critical shear stress associated with maximum change in slope of V_e
τ_t	[Pa]	instantaneous bed shear stress
$\tau_{t,g}$	[Pa]	instantaneous bed shear stress associated with incipient sediment motion
τ_* or θ	[–]	non-dimensional Shields parameter
TKE	[m^2 s^{-2}]	turbulent kinetic energy
u	[m s^{-1}]	longitudinal (x-direction) velocities
u'	[m s^{-1}]	fluctuating component of u
u_*	[m s^{-1}]	friction velocity
$\langle U_{mag} \rangle$	[m s^{-1}]	magnitude of the mean longitudinal and vertical velocity
v	[m s^{-1}]	transversal (y-direction) velocities
v'	[m s^{-1}]	fluctuating component of v
V_e	[mm^3]	cumulative erosion volume
υ	[m^2 s^{-1}]	fluid kinematic viscosity
w_1, w_2	[m s^{-1}]	first and second vertical velocity components obtained from Beams 1 and 3, and Beams 2 and 4 of the Vectrino Profiler
w_1', w_2'	[m s^{-1}]	fluctuating vertical velocity components of w_1 and w_2
$\langle w_{true1}'^2 \rangle$	[m^2 s^{-2}]	true variance of w_1
$\langle w_{true2}'^2 \rangle$	[m^2 s^{-2}]	true variance of w_2
$\langle w_1' w_2' \rangle$	[m^2 s^{-2}]	covariance of w_1 and w_2
z	[mm]	elevation, with the origin at the bed
z_{ir}	[mm]	position of the upper limit of the boundary interference region above the bed (mm)
z_{ss}	[mm]	position of the sweet-spot of the Vectrino Profiler above the bed

Abbreviations

The following abbreviations are used in this dissertation:

A, B	regions of sediment cores representing (0 – 10 cm) and >10 cm, respectively
ADV	acoustic Doppler velocimeter
ASSET	adjustable shear stress erosion and transport flume
BD	bulk density
C	cohesive bed
CEC	cation exchange capacity
Chl-a	chlorophyll-a
CMOS	complementary metal–oxide–semiconductor
Cs^{137}	cesium-137
CSM	cohesive strength meter
DNA	deoxyribonucleic acid
EFA	erosion function apparatus
EMD	erosion measurement device
EPS	extracellular polymeric substances
EPS-p	EPS protein
EPS-c	EPS carbohydrate
ETDC	erosion, transport, deposition, and consolidation
G, GF, S, M	bed type (gravel, geotextile, sand, and metal)
GBS, SBT	reservoirs of Großer Brombachsee and Schwarzenbach
GEMS	Gust erosion microcosm system
GRA	gamma ray attenuation
HERODE	hydraulics for erosion and deposit
HF, LF	high flow, low flow
HL-corrected	after Doppler noise correction of Hurther and Lemmin [1]
IA	interrogation area
IR	interference region

ISF	portable in situ flume
ISIS	instrument for measuring shear stress in situ
LDV	laser Doppler velocimeter
m.a.s.l.	meters above sea level
MRM	magnetic resonance microscopy
Na^+, Ca^{2+}, Mg^{2+}	sodium, calcium, magnesium
NaI (TI)	iodide doped with Thallium
Nc	non-cohesive bed
NIWA	National Institute of Water and Atmospheric Research
OCT	optical coherence tomography
PAR	photosynthetically active radiation
PCR	polymerase chain reaction
PD	percent difference (%)
PDF	probability density function
PHOTOSED	photogrammetric sediment erosion detection method
PIV	particle image velocimetry
PSD	particle size distribution
PTV	particle tracking velocimetry
PVC	polyvinyl chloride
RNA	ribonucleic acid
rRNA	ribosomal RNA
ROI	region of interest
SEDFLUME	sediment erosion at depth flume
SETEG	Strömungskanal zur Ermittlung der tiefenabhängigen Erosionsstabilität von Gewässersedimenten
SFM	structure-from-motion
SS	sweet-spot
SSC	suspended sediment concentration
TOC	total organic content
VP	Vectrino Profiler

Abstract

Understanding erosion and transport of sediment is of importance when dealing with many geomorphological and ecological concerns, such as the stability of riverbanks, the siltation of navigational channels, the distribution of sediments, nutrients, and pollutants as well as the loss of storage capacity of reservoirs. For example, by interrupting river connectivity, dams alter flow and sediment dynamics, leading to sediment accumulation in the reservoirs. Therefore, advancing the knowledge about erosion and sediment transport processes is also critical for effective management of water resources.

There is a relatively good understanding of the erosion processes of non-cohesive sediments on idealized geometries. The erosion processes in natural cohesive sediment mixtures, on the other hand, are greatly affected by a variety of physical, chemical, and biological sediment properties. These sediment properties and their complex site-specific interactions with flow and bed morphology considerably complicate modelling and management of sediment, resulting in high spatial and temporal variability of critical erosion thresholds in aquatic water bodies. Despite the importance of sediment dynamics, the relative roles of sediment properties on spatial and depth variable erosion resistance of cohesive sediments remain poorly understood. In addition, presence of microbial aggregates ("biofilm") has been increasingly recognized to mediate sediment properties and dynamics both in the laboratory and in the field through their self-secreted matrix of extracellular polymeric substances (EPS). In particular, adhesion and cohesion exerted by biofilms lead to increased erosion thresholds (biostabilization), both at the sediment surface and deeper layers. The biostabilization potential of biofilms is controlled by their biodiversity and community composition through the metabolic performance of involved microbial communities, which is also dictated by the complex interactions of flow, biofilm, and sediment. Therefore, to improve the understanding of sediment transport and biostabilization as well as to consider the multi-variate problem of natural cohesive sediment mixtures, interdisciplinary studies with integrated methodological approaches are needed. In this respect, controlled laboratory experiments are still ideal to investigate the three-way interaction between flow, biofilm, and sediment. The present dissertation explores the erosion of artificial and natural sediments through advanced experimental methods and approaches, with a focus on flow–biofilm–sediment interactions. The results of this study are presented in three scientific publications, which are core parts of this cumulative dissertation.

The first set of laboratory experiments deals with the performance of an acoustic Doppler velocity profiler (Vectrino Profiler) for measuring mean velocity and turbulence at the sediment–water interface. The flow measurements obtained by Vectrino Profiler were compared to those obtained by particle image velocimetry (PIV) on four types of bed material, involving geotextile bed as a scenario for loose sediment with high porosity, sand bed with a median particle size of 0.25 mm, coarse gravel bed having a nominal diameter between 18 and 36 mm as well as metal bed as a scenario for strongly acoustically reflective flat bed. During the experiments, the flow velocity, bed material,

and probe to bed distance of the Vectrino Profiler were varied whilst the flow depth remained constant at 0.23 m. The vertical profiles of mean velocity, turbulent kinetic energy, and power spectral density of velocity fluctuations were compared between the two instruments since they are most commonly used parameters for characterization of flow at the sediment–water interface. The results showed that the acoustic interference of the bed (boundary interference) adversely affects the velocity measurements as close as 1.7 – 5 mm above the bed, depending on the bed material. Accordingly, a practical criterion was provided to identify the vertical extent of the boundary interference region. It was shown that its vertical extent can be identified by a local minimum in the signal-to-noise ratio, recorded by the Vectrino Profiler itself. Outside the boundary interference region, the best agreement between the two instruments was found around the sweet-spot of the Vectrino Profiler, where the observed differences were <6% for mean velocities and <10% for turbulent kinetic energy. Overall, this study shows the limitations of acoustic-based velocity instruments for measuring flow and turbulence at the sediment–water interface. Therefore, optical methods, such as PIV, can be utilized to obtain non-destructive measurements of spatial velocity distribution near the bed.

The second set of laboratory experiments explores the interactions of flow, biofilm, and sediment using an integrated and interdisciplinary approach, which is rarely implemented in the fields of hydraulic engineering and ecohydraulics. The experiments were conducted in six identical laboratory flumes using the water and inoculation from the reservoir Großer Brombachsee. The biofilms were then cultivated on fine (median particle size = 0.16 mm) and medium sand (median particle size = 0.29 mm) under contrasting flow conditions: low flow (bed shear stress ~ 0.01 Pa) and high flow (bed shear stress ~ 0.04 Pa). The water depth, water temperature, and light intensity were kept constant during the experiments. Through a methodological workshop, a multitude of advanced optical instruments and approaches was utilized on the quasi-naturally grown biofilm samples to test the feasibility of an integrated experimental approach for investigation of flow–biofilm–sediment interactions, with a focus on biostabilization. It was observed that the flow speed influences the time of settlement, biofilm growth as well as surface topography. Mean surface roughness (0.46 to 1.97 mm) and biofilm thickness (1.92 to 3.74 mm) increased considerably with a decreasing flow regime (bed shear stress from 0.04 Pa to 0.01 Pa). Moreover, application of next-generation sequencing approach demonstrated that the abundance and species diversity were significantly higher for bacterial communities at high flow conditions, whereas they were higher for microalgal communities at low flow conditions. The advantages and challenges associated with the applied methods were also explored in view of sediment stability. It was suggested that the laboratory-scale observations should be linked to larger scales relevant for management of water resources.

To explore the interrelationships between site-specific sediment parameters and spatially and depth-varying erosion thresholds, the third set of experiments utilized 22 sediment cores that were collected from the deposits of two reservoirs: Großer Brombachsee (GBS) and Schwarzenbachtalsperre (SBT). The multi-variate relationships between critical

erosion thresholds of cohesive sediment mixtures and a collection of physical (bulk density, particle size distribution, sediment composition, and percentiles of particle size distribution), chemical (cation exchange capacity and total organic carbon), and biological (chlorophyll-a, EPS protein and carbohydrate) sediment characteristics were investigated. In contrast to the most previous studies that employed visual determination approaches only, the critical erosion thresholds were determined analytically (and visually) in a straight erosion flume using an advanced photogrammetric measurement method relying on a structured-light approach. The analyses revealed that the clay-dominated sediments of the GBS with comparatively low total organic carbon and sand content were, on average, 10 times more stable compared to the sandy sediments of the SBT. Consequently, for the clay-dominated sediments, critical erosion thresholds were strongly correlated with clay content, and to a lesser extent, with bulk density. In contrast, the comparatively sandy sediment layers of SBT exhibited strong positive correlations between critical erosion thresholds and sand content, whereas the relationship was inverse with clay content. The strength of these relations generally decreased for sediment layers deeper than 10 cm. EPS (protein and carbohydrate) and chlorophyll-a were not good indicators for the erosion thresholds, suggesting an ambiguous influence of biology and its varying interaction with other physico-chemical sediment properties. Therefore, identifying universal sediment parameters for estimating critical erosion thresholds is challenging for natural sediments, but the interrelationships can be simplified to site-dependent key parameters.

Overall, the findings of this research highlight the need to further study erosion processes in laboratory and various natural environments under variable regimes of flow, biofilm, and sediment. When studying flow–biofilm–sediment interactions and erosion processes, spatially heterogenous near–bed flow dynamics and its simultaneous interaction with sediment–biofilm matrix and (dynamic) bed roughness can be considered using non-destructive optical approaches, such as PIV and underwater laser scanner. Due to the complexity of natural sediments, the field studies should, ideally, be complemented with controlled laboratory studies by utilizing a combination of advanced optical and molecular approaches in an integrative way. A successful example of such integrated approach is demonstrated in this dissertation.

Kurzfassung

Das Verständnis der Erosion und des Transports von Sedimenten ist für viele geomorphologische und ökologische Probleme von Bedeutung, z. B. für die Stabilität von Flussufern, die Verschlammung von Schifffahrtskanälen, die Dynamik von Sedimenten, Nähr- und Schadstoffen sowie den Verlust der Stauraumkapazität von Wasserreservoirs. Durch die Unterbrechung der Flussdurchgängigkeit verändern Querbauwerke beispielsweise die Strömungs- und Sedimentdynamik, was zu Sedimentansammlungen in den Stauräumen führt. Daher ist ein besseres Verständnis der Erosions- und Sedimenttransportprozesse auch für eine wirksame Bewirtschaftung der Gewässer wichtig.

Die Erosionsprozesse von nicht kohäsiven Sedimenten auf idealisierten Geometrien sind relativ gut bekannt. Die Erosionsprozesse in natürlichen kohäsiven Sedimentmischungen werden dagegen stark von einer Vielzahl physikalischer, chemischer und biologischer Sedimenteigenschaften beeinflusst. Diese Sedimenteigenschaften und ihre komplexen standortabhängigen Wechselwirkungen mit der Strömung und der Sohlmorphologie erschweren die Modellierung und das Management von Sedimenten erheblich und führen zu einer hohen räumlichen und zeitlichen Variabilität der kritischen Erosionsschwellen. Trotz der Bedeutung der Sedimentdynamik sind die relativen Auswirkungen der Sedimenteigenschaften auf die räumlich und in der Tiefe variierende Erosionsstabilität kohäsiver Sedimente bisher nur wenig bekannt. Außerdem wird zunehmend erkannt, dass mikrobielle Aggregate ("Biofilm") durch ihre selbstproduzierte Matrix aus extrazellulären polymeren Substanzen (EPS) die Sedimenteigenschaften und -dynamik sowohl im Labor als auch in Felduntersuchungen beeinflussen. Insbesondere die Adhäsion und Kohäsion, die durch Biofilme erzeugt werden, führen zu erhöhten Erosionsschwellen (Biostabilisierung), sowohl an der Sedimentoberfläche als auch in tieferen Schichten. Das Biostabilisierungspotenzial von Biofilmen wird durch ihre Artenvielfalt und die Artenzusammensetzung durch die Stoffwechselleistung der beteiligten mikrobiellen Gemeinschaften kontrolliert, die auch durch die komplexen Wechselwirkungen von Strömung, Biofilm und Sediment beeinflusst wird. Um das Verständnis von Sedimenttransport und Biostabilisierung zu verbessern und das multivariate Problem natürlicher kohäsiver Sedimentmischungen zu berücksichtigen, sind daher interdisziplinäre Studien mit integrierten methodischen Ansätzen erforderlich. Daher sind kontrollierte Laborexperimente weiterhin ideal, um die Drei-Wege-Interaktion zwischen Strömung, Biofilm und Sediment zu untersuchen. In der vorliegenden Dissertation wird die Erosion von künstlichen und natürlichen Sedimenten mit Hilfe moderner experimenteller Methoden und Ansätze untersucht, mit einem Schwerpunkt auf den Wechselwirkungen zwischen Strömung, Biofilm und Sediment. Die Ergebnisse dieser Arbeit werden in drei wissenschaftlichen Publikationen vorgestellt, die am Ende dieser Dissertation zu finden sind.

Die ersten Laborexperimente beschäftigen sich mit der Leistung eines Ultraschall-Doppler-Profil-Geschwindigkeitsmessers (Vectrino Profiler) zur Messung der mittleren Geschwindigkeit und Turbulenz an der Sediment-Wasser-Grenzfläche. Die mit dem

Vectrino Profiler gewonnenen Strömungsmessungen wurden mit denen verglichen, die mit Hilfe der Particle Image Velocimetry (PIV) an vier Arten von Sohlmaterial gewonnen wurden. Dabei handelte es sich um einen Geotextilsohle als Szenario für lockeres Sediment mit hoher Porosität, eine Sandsohle mit einer mittleren Partikelgröße von 0,25 mm, eine grobe Kiessohle mit einem nominalen Durchmesser zwischen 18 und 36 mm sowie eine Metallsohle als Szenario für stark akustisch reflektierenden Sohlen. Während der Experimente wurden die Strömungsgeschwindigkeit, das Sohlmaterial und der Abstand zwischen dem Vectrino-Profiler-Sensor und der Sohle variiert, während die Wassertiefe konstant bei 0,23 m blieb. Die vertikalen Profile der mittleren Geschwindigkeit, der turbulenten kinetischen Energie und der spektralen Leistungsdichte der Geschwindigkeitsschwankungen wurden zwischen den beiden Instrumenten verglichen, da dies die am häufigsten verwendeten Parameter zur Charakterisierung der Strömung an der Sediment-Wasser-Grenzfläche sind. Die Ergebnisse zeigten, dass die akustische Interferenz der Sohle die Geschwindigkeitsmessungen in einem Bereich von 1,7 bis 5 mm über der Sohle beeinträchtigt, abhängig vom Sohlenmaterial. Folglich wurde ein praktisches Kriterium zur Bestimmung der vertikalen Ausdehnung der akustischen Interferenzzone entwickelt. Es wurde gezeigt, dass die vertikale Ausdehnung durch ein lokales Minimum im Signal-Rausch-Verhältnis, das vom Vectrino Profiler selbst aufgezeichnet wird, identifiziert werden kann. Außerhalb der akustischen Interferenzzone wurde die beste Übereinstimmung zwischen den beiden Instrumenten um den Sweetspot des Vectrino Profilers herum gefunden, in dem die beobachteten Unterschiede <6% für die mittleren Geschwindigkeiten und <10% für die turbulente kinetische Energie betrugen. Insgesamt zeigt diese Studie die Einschränkungen von akustischen Geschwindigkeitsmessgeräten für die Messung von Strömung und Turbulenz an der Sediment-Wasser-Grenzfläche. Daher können optische Methoden wie PIV eingesetzt werden, um zerstörungsfreie Messungen der räumlichen Geschwindigkeitsverteilung in der Sohlnähe zu ermitteln.

Die zweiten Laborexperimente untersuchen die Wechselwirkungen von Strömung, Biofilm und Sediment mit einem integrierten und interdisziplinären Ansatz, der in den Disziplinen Wasserbau und Ökohydraulik nur selten umgesetzt wird. Die Experimente wurden in sechs identischen Laborrinnen mit dem Wasser und der Inokulation aus dem Großen Brombachsee durchgeführt. Die Biofilme wurden auf Feinsand (mittlere Partikelgröße = 0,16 mm) und Mittelsand (mittlere Partikelgröße = 0,29 mm) unter unterschiedlichen Strömungsbedingungen aufgewachsen: geringe Strömung (Sohlschubspannung ~ 0,01 Pa) und hohe Strömung (Sohlschubspannung ~ 0,04 Pa). Die Wassertiefe, die Wassertemperatur und die Lichtintensität wurden während der Experimente konstant gehalten. Im Rahmen eines Methoden-Workshops wurden verschiedene fortschrittliche optische Instrumente und Ansätze an dem quasi-natürlich gewachsenen biofilmgebundenen Sediment verwendet, um die Durchführbarkeit eines integrierten experimentellen Ansatzes zur Untersuchung der Wechselwirkungen zwischen Strömung, Biofilm und Sediment zu testen, mit einem Schwerpunkt auf der Biostabilisierung. Es wurde festgestellt, dass die Strömungsgeschwindigkeit die Besiedlungszeit, das Biofilmwachstum und die Oberflächentopographie beeinflusst. Die

mittlere Oberflächenrauheit (0,46 bis 1,97 mm) und die Biofilmdicke (1,92 bis 3,74 mm) nahmen mit abnehmendem Strömungsregime (Sohlschubspannung von 0,04 Pa auf 0,01 Pa) deutlich zu. Darüber hinaus zeigte die Anwendung des Next-Generation-Sequencing-Ansatzes, dass die Abundanz und die Artenvielfalt für bakterielle Gemeinschaften bei hohen Strömungsbedingungen signifikant höher waren, während sie für Mikroalgengemeinschaften bei niedrigen Strömungsbedingungen höher waren. Die Vorteile und Herausforderungen, die mit den angewandten Methoden verbunden sind, wurden auch im Hinblick auf die Sedimentstabilität untersucht. Es wurde vorgeschlagen, die Messungen im Labormaßstab mit größeren Maßstäben zu verknüpfen, die für die Bewirtschaftung von Gewässern relevant sind.

Um die Wechselbeziehungen zwischen den standortabhängigen Sedimentparametern und den räumlich und tiefenabhängigen kritischen Erosionsschwellen zu erforschen, wurden in den dritten Experimenten 22 Sedimentkerne verwendet, die aus den Ablagerungen von zwei Stauräumen entnommen wurden: Großer Brombachsee (GBS) und Schwarzenbachtalsperre (SBT). Untersucht wurden die multivariaten Beziehungen zwischen kritischen Erosionsschwellen kohäsiver Sedimentmischungen und einer Reihe physikalischer (Lagerungsdichte, Sedimentzusammensetzung, Perzentilwerte der Partikelgrößenverteilung), chemischer (Kationenaustauschkapazität, gesamter organischer Kohlenstoff) und biologischer (Chlorophyll-a, EPS-Protein und Kohlenhydrate) Sedimenteigenschaften. Im Gegensatz zu den meisten früheren Studien, die nur visuelle Bestimmungsansätze verwendeten, wurden die kritischen Erosionsschwellen analytisch (und visuell) in einer geraden Erosionsrinne mit einer modernen photogrammetrischen Messmethode bestimmt, die auf einem strukturierten Lichtansatz basiert. Die Analysen ergaben, dass die tonhaltigen Sedimente der GBS mit vergleichsweise geringem Gesamtgehalt an organischem Kohlenstoff und Sand im Durchschnitt 10-fach stabiler waren als die sandigen Sedimente der SBT. Folglich waren die kritischen Erosionsschwellen für die tonhaltigen Sedimente stark mit dem Tongehalt und in geringerem Maße mit der Lagerungsdichte korreliert. Im Gegensatz dazu wiesen die vergleichsweise sandigen Sedimentschichten der SBT starke positive Korrelationen zwischen den kritischen Erosionsschwellen und dem Sandgehalt auf, während die Beziehung zum Tongehalt umgekehrt war. Die Stärke dieser Beziehungen nimmt für Sedimentschichten ab, die tiefer als 10 cm in den Sedimentkernen liegen. EPS (Protein und Kohlenhydrate) und Chlorophyll-a waren keine guten Indikatoren für die kritischen Erosionsschwellen, was auf einen unklaren Einfluss der Biologie und ihre unterschiedliche Wechselwirkung mit anderen physikalisch-chemischen Sedimenteigenschaften hinweist. Es zeigt sich also, dass die Identifizierung von universellen Sedimentparametern für die Abschätzung kritischer Erosionsschwellen natürlicher Sedimente sehr komplex ist, die Wechselbeziehungen jedoch vereinfacht auf einzelne standortabhängige Schlüsselparameter reduziert werden können.

Insgesamt unterstreichen die Ergebnisse dieser Forschung die Bedeutung der weiteren Untersuchung von Erosionsprozessen im Labor und in verschiedenen natürlichen Gewässern unter variablen Strömungs-, Biofilm- und Sedimentregimen. Bei der Untersuchung der Wechselwirkungen zwischen Strömung, Biofilm und Sediment sowie

der Erosionsprozesse können die räumlich heterogene sohlnahe Strömungsdynamik und ihre gleichzeitige Wechselwirkung mit der Sediment-Biofilm-Matrix und der (dynamischen) Oberflächenrauheit mit zerstörungsfreien optischen Ansätzen wie PIV und Unterwasser-Laserscanner berücksichtigt werden. Aufgrund der Komplexität natürlicher Sedimente sollten die Feldstudien idealerweise durch kontrollierte Laborstudien ergänzt werden, bei denen eine Kombination aus fortschrittlichen optischen und molekularen Ansätzen integrativ eingesetzt wird. Ein erfolgreiches Beispiel für einen solchen integrierten Ansatz wird in dieser Dissertation vorgestellt.

Declaration

The dissertation may contain similar and/or verbatim formulations, figures, and passages from my core articles:

1. Performance of the Vectrino Profiler at the sediment–water interface, Journal of Hydraulic Research, 55:4, 573-581
2. Exploring flow–biofilm–sediment interactions: Assessment of current status and future challenges, Water Research, 185, 116182
3. Functional relationships between critical erosion thresholds of fine reservoir sediments and their sedimentological characteristics, Journal of Hydraulic Engineering, accepted

I omit a clear identification for readability and use these parts from the articles in my dissertation, as well as reprint these articles in the appendices, with kind permissions from the publishers (Journal of Hydraulic Research – Taylor & Francis, Water Research – Elsevier, Journal of Hydraulic Engineering – ASCE). For the formal version of these articles, readers are referred to the respective journals through DOI links and original sources provided in the appendices.

1 Introduction

1.1 **Research Background and Motivation**

Erosion, transport, and deposition of sediment in rivers and reservoirs have been of great interest to engineers, sedimentologists, and geomorphologists for many years. This is mainly due to the complex interactions between flow and sediment that control morphology of the bed, and thus aquatic habitat, water quality, and beyond. The interaction of flow and sediment is so complex that, according to an anecdote, when Hans Albert Einstein told his father Albert Einstein that he would like to study sediment transport, Albert Einstein recommended him strongly not to delve into the mechanics of sediment transport due to difficulties in dealing with sediment transport processes [2].

Natural flows are typically characterized by three-dimensional (3D) flow velocities over a rough boundary consisting of a complex topography, hereafter called sediment–water interface. The sediment–water interface is dynamic and may change its shape due to the dynamic erosion, transport, deposition, and consolidation (ETDC) process, which is also governed by a complex interaction of physical, chemical, and biological factors. Consequently, flow in aquatic systems contains a range of temporal and spatial scales [3]. The complexity is further increased in the presence of "ecosystem engineers", such as biofilms, which act to change the geomorphology [4, 5] and the entire ecosystem [6]. Biofilms are genetically diverse surface-attached aggregates of microorganisms (Archaea, Bacteria, Eukarya) [7], which are wrapped in a self-secreted matrix of extracellular polymeric substances (EPS) and colonize beds in diverse environments, including rivers [8], and reservoirs [9].

Hughes [10] once stated: "Understanding sediment transport in coastal regions is a perplexing challenge that in all likelihood will continue to frustrate coastal researchers and engineers for generations to come". This opinion is still valid today and could also be applied to freshwater ecosystems such as rivers and reservoirs. Accordingly, understanding and modelling erosion processes are critical for many ecological and

geomorphological concerns, including the stability of riverbanks and bridge piers, the siltation of navigation channels and harbours, the distribution of particulate matter (sediments, organics, and pollutants) as well as the loss of storage capacity of reservoirs (figure 1). For example, erosion and deposition processes are usually in a state of dynamic equilibrium in most natural rivers. However, the global construction of >58,000 large dams [11] has significantly affected this balance by fragmenting the river network [12], leading to an estimated over 100 Gt sediment trapped in reservoirs [13]. Therefore, advancing our knowledge about erosion and sediment transport processes is also central to a range of management strategies, particularly in view of increased demands for hydropower [14, 15].

Figure 1: Sedimentation problem in Paonia Reservoir, Colorado, USA. a) before drawdown, b) after drawdown as part of the sediment management strategy. Left image shows that the mud interfered with the intake structure that controls releases to the stream below the dam

Sediment bed material can be non-cohesive and cohesive. The non-cohesive sediments range from sand (0.062 mm > diameter < 2.0 mm) to gravel (diameter > 2.0 mm), whereas the cohesive sediments consist of smaller particles, including silt (0.002 mm < diameter < 0.0062 mm) and clay (diameter < 0.002 mm) fractions [16, 17]. In river and reservoirs or any other aquatic ecosystems, cohesive sediments are usually encountered as a heterogenous mixture of inorganic particles (e.g., sand, silt, clay) enriched with diverse microbial communities forming biofilm [18] as well as pore water and gas (e.g., methane) [19]. A water-sediment mixture of silt, clay and organic matter is also called "mud" [20].

Erosion mechanisms and influencing factors differ considerably between cohesive and non-cohesive sediments. Whilst erosion resistance of non-cohesive sediment is mainly governed by particle size and weight, electrostatic charges on clay-sized particles determine the interparticle bonding between cohesive sediments [17]. These interparticle bonding forces can be several orders of magnitude larger than gravitational forces [21]. Cohesive sediment erosion takes place when the strength of the flow is sufficient to overcome interparticle forces [21, 22] and cohesive sediments erode as a bulk group (flocs or aggregates) with interparticle interactions. In contrast, non-cohesive sediments are detached from the bed and transported as individual particles without interparticle interaction [16].

The increased recognition of ecological effects on flow-sediment dynamics over the last two decades has resulted in the development of the field called "ecohydraulics". Among other biological influences, the role of biofilms in modifying sediment properties and

processes has been increasingly recognized. Indeed, when growing on sediment in the bed finer than approximately 2 mm (clay, silt, sand) [23], biofilms glue sediment particles to each other through their self-secreted EPS matrix [4, 5], leading to enhanced erosion resistance [24]. Such ability of biofilms to increase erosion thresholds (or sediment stability) by biological actions is called "biostabilization" [25–28] or "biogenic stabilization" [5]. Biostabilization has been reported to considerably mediate the sediment ETDC processes in aquatic ecosystems [5]. It must be noted that despite non-cohesive sediments act independently of each other, when they are coated with biofilms, they behave as cohesive particles, resulting from the adhesion exerted by biofilm [5]. Additionally, adhesion and cohesion exerted by biofilm are expected to enhance erosion resistance not only at the surface [18, 29], but also at deeper sediment layers [30].

A great deal of laboratory studies have been previously performed with non-cohesive sediments and sediments without any microbial involvement, yielding a relatively good understanding of the erosion processes occurring on idealized geometries [5, 18]. Since interparticle bonds between particles and presence of biofilm in natural sediments significantly complicate modelling and management of sediment in aquatic water bodies, there exists no generic relationships for the estimation of erosion thresholds in natural sediments. Additionally, the vast and complex interactions of physical, chemical, and biological factors can considerably affect erosion thresholds, resulting in high spatial and temporal variability [31, 32]. Therefore, when assessing erosive properties of cohesive sediments, site-specific sediment conditions should be considered [33], which makes cohesive erosion studies a multi-variate problem [22]. Therefore, future field studies are required to consider the multi-variate problem of natural cohesive sediment mixtures [34] with biofilm [5]. It is of critical importance since cohesive sediments can also bind contaminants and may lead to significant ecological and water quality problems. Due to growing concerns for ecological problems, the sediments are subject to several international guidelines, such as EU Water Framework Directive, which aims to achieve the "good" ecological status of water bodies in the EU by 2027 [35]. Despite the importance of sediment dynamics, the relative roles of sedimentological factors on spatial and depth variable erosion resistance of cohesive sediments remain poorly understood.

The biostabilization potential of biofilms is dictated by their biodiversity and community composition through the metabolic performance of involved microbial communities [5, 28, 36–38], which is governed by the interactions of flow, biofilm, and sediment. Indeed, many biofilms have complex morphologies and can develop long, oscillating filamentous structures called streamers [39, 40], which not only alter flow dynamism and bed topography, but also mass transport near the bed and thus biostabilization potential [24]. Whilst investigating the relationships between site-specific natural sediment characteristics and erosion thresholds is important to advance our understanding about cohesive erosion processes and to establish practical formulations for erosion thresholds, a fundamental understanding of flow–biofilm–sediment interactions which influence biostabilization is still elusive. Despite artificial and natural sediments and their erosion behaviour have received increasing attention over the last decades with or without

consideration of biofilm, their interrelationships to flow and bed topography co-evolving with biofilm growth have not been studied yet [5, 26, 41]. Challenges include i) creating realistic experimental settings and utilizing a combination of tools and approaches to describe the reciprocal relationships between flow–biofilm–sediment and associated mass transfer, which alters microbial processes and vice-versa and ii) understanding the role of key microbial players (and processes) for biogeochemical and morphological processes, and how microorganismal level functions can be linked to biostabilization [24]. Overcoming these challenges requires an integrated and interdisciplinary investigation of biostabilization by studying hydraulics, geomorphology, and microbial ecology as an integrated concept using advanced tools and approaches rather than viewing them as subordinately serving the other [42]. A decade after the "2020 vision" of Rice et al. [41] for integrated and interdisciplinary river science, a feasibility of an interdisciplinary approach bringing different tools and scientific communities together on the same research topic has yet to be tested.

1.2 **Research Objectives**

The main objective of this dissertation is to investigate the erosion of artificial and natural sediments through advanced experimental methods and approaches, with a focus on flow–biofilm–sediment interactions.

More specifically, the objectives of this research are:

- to demonstrate limitations of an acoustic-based velocity profiler for characterizing flow and turbulence at the sediment–water interface through controlled laboratory experiments,

- to provide the current state of the knowledge in the erosion process of non-cohesive and cohesive sediments (with and without biofilm) under the influence of various physical, chemical, and biological factors, including their interactions with flow, biofilm and sediment,

- to critically review current state of the flow–biofilm–sediment research across various spatial scales, currently employed measurement techniques and critically assess their advantages and limitations with particular reference to erosion processes,

- to investigate the interrelationships between physical, chemical, and biological sedimentological characteristics and erosion thresholds for natural sediments,

- to perform laboratory experiments on biostabilization and explore the feasibility of an interdisciplinary research by utilizing a variety of modern optical and laser-based tools, advanced molecular approaches as well as integrating knowledge from hydraulic engineering, geomorphology, and microbial ecology.

1.3 **Outline of Dissertation**

This doctoral dissertation is presented in a cumulative format. The dissertation contains an introduction and a literature review chapter, a material and methods chapter, and three appendices composed of three publications/manuscripts that are either published (Appendix I & II) or accepted for publication (Appendix III) in peer-reviewed journals (figure 2).

Chapter 2 discusses the erosion and sediment transport processes for non-cohesive and cohesive sediments as well as physical, chemical, and biological factors influencing the erosion resistance of these sediments. Methodological challenges for the measurements of erosion, flow dynamics, and bed topography are also discussed.

Chapter 3 presents an overview of materials and methods for conducting laboratory experiments and field sampling. Additional methods are also provided in the respective manuscripts.

Chapter 4 presents a synthesis of main findings and provides an outlook for potential future studies and further methodological challenges to be solved that can support predictions on erosion of natural sediments under variable regimes of flow–biofilm–sediment interactions.

Appendix I evaluates the measurement performance of an acoustic Doppler velocity profiler, namely Vectrino Profiler, and discusses how acoustic-based velocimeters pose challenges for mean velocity and turbulence measurements at the sediment–water interface despite their frequent use. Laboratory experiments were conducted on four types of bed material. Mean velocities and turbulence measured by Vectrino Profiler were compared to those measured by Particle Image Velocimetry. The influence and vertical extent of the boundary interference region (i.e., acoustic interference of the bed biasing velocities) as well as reliable measurement range were critically discussed [43].

Appendix II focuses on flow–biofilm–sediment interactions from an interdisciplinary perspective. It presents a combination of a controlled experimental study and application-oriented critical review on the state of the art and methodological approaches in the flow-biofilm-sediment research with an emphasis on biostabilization and fine sediment dynamics. A feasibility of an interdisciplinary approach for biostabilization research was explored through a methodological workshop. The chapter also addresses how advanced methods in the fields from hydraulics, sedimentation engineering, microbial ecology, and biochemistry can be applied to study flow–biofilm–sediment interactions, towards the same goal of biostabilization. The main experimental findings were incorporated into a critical review [24].

Appendix III focuses on the multivariate relationships between critical erosion thresholds of natural sediments and their physico–chemical and biological–sedimentological characteristics based on 22 sediment cores collected from two reservoirs in Germany. The interrelationships between erosion thresholds and a collection of sediment parameters, including bulk density, sediment composition, percentiles, cation exchange capacity, organic content, EPS (proteins and carbohydrates) as well as

chlorophyll-a (a proxy for photoautotrophic biomass/algae in sediments) were evaluated and discussed. Based on controlled laboratory experiments, this study also utilized an advanced photogrammetric method to quantify critical erosion thresholds for a succession of sediment layers within the collected sediment cores [44].
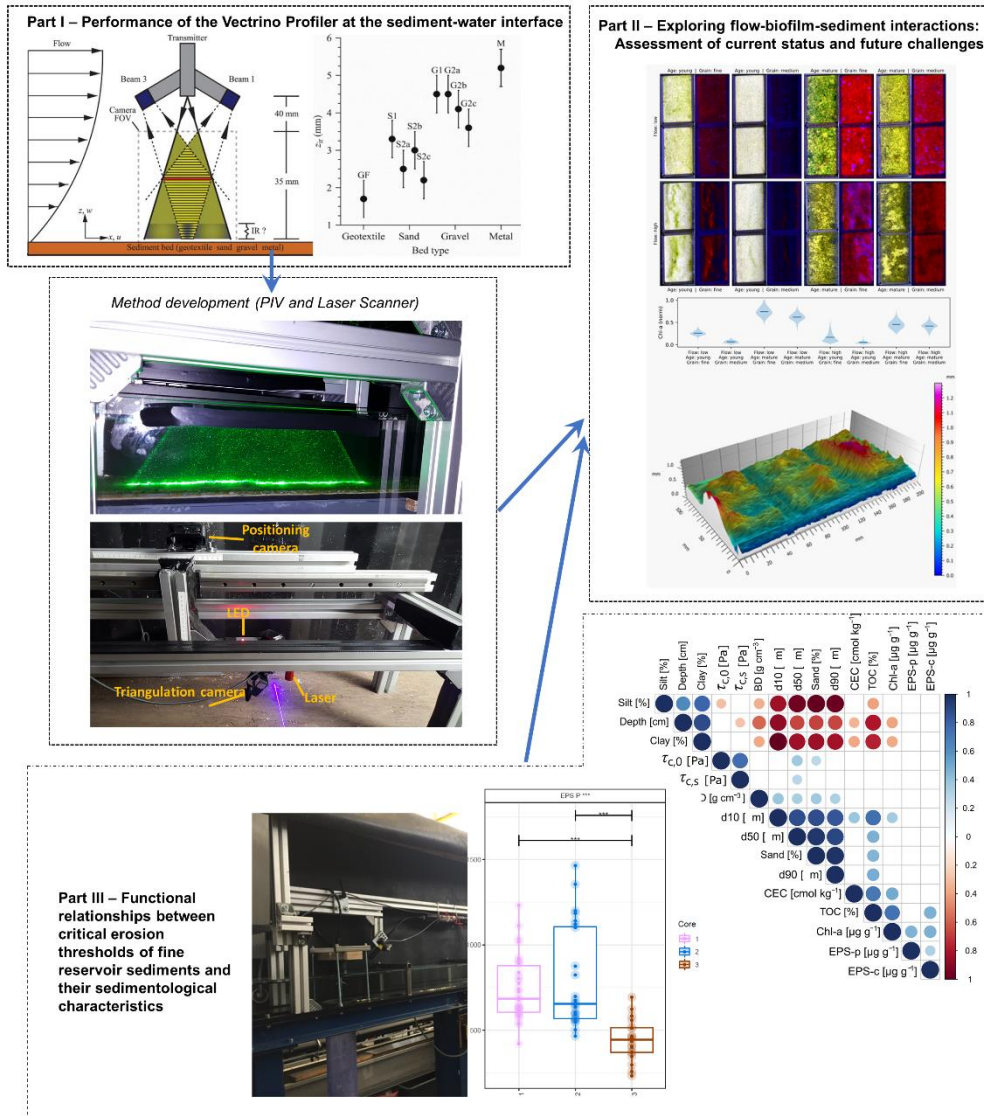

Figure 2: Overview of the achievements in exploring erosion process, with a particular focus on flow–biofilm–sediment interactions

2 Literature Review

This chapter focuses on sediment transport mechanisms for both non-cohesive and cohesive sediments. Incipient motion observation techniques and erosion devices for measuring incipient motion of sediments as well as associated methodological challenges are discussed in detail. Physical, chemical, and biological factors affecting erodibility of cohesive sediments are presented and discussed. Finally, the effect of biofilm on erosion thresholds is elaborated along with methodological challenges in exploring flow-biofilm-sediment interactions, which control growth and functions of biofilms.

2.1 Origin and Properties of Sediments

The characterization of sediment deposits is critical to understand their behaviour (mobility and stability) and fate in aquatic water bodies as well as to design engineering structures (e.g., reservoirs). In view of erosion and transport, sediments are generally characterized by their particle shape, composition and size, the latter being the most important parameter [45]. Based on the particle size distribution, sediments are usually classified into two categories using the Wentworth scale [46]: i) non-cohesive sediment and ii) cohesive sediment [21, 22]. The non-cohesive sediments range from sand (0.062 mm > diameter < 2.0 mm) to gravel (diameter > 2.0 mm), whereas the cohesive sediments consist of smaller particles, including silt (0.002 mm < diameter < 0.0062 mm) and clay (diameter < 0.002 mm) fractions. The sand and silt particles are produced as a consequence of physical weathering of primary materials (i.e., rocks), nearly spherical, and mostly contain quartz with feldspar and mica [20, 22]. Mainly containing tetrahedral sheets of silicon-oxygen and octahedral sheets of magnesium, or aluminium-oxygen, the clay particles are formed by chemical weathering of primary materials and are plate-shaped [22, 47]. The various combinations of these sheets with different anionic and cationic substitutions [17] lead to development of different clay minerals, holding together by electrostatic forces. The most common types of minerals comprise kaolinites, illites, vermiculites, and smectites (or montmorillonites) (see Grabowski et al. [22] for further details).

In natural environments, such as rivers, reservoirs, lakes, and estuaries, cohesive sediments are typically found as a heterogenous mixture of inorganic particles (e.g., fine

sand, silt, clay), organic matter, pore water, and gas (e.g., methane) [19]. A water–sediment mixture of silt, clay, and organic matter is also called "mud" [20] or fine sediments. The volumetric fractions, weight, and particle size distributions of natural sediments are highly variable [17, 19, 22].

The mechanisms for erosion and transport of sediments and affecting factors involved differ for non-cohesive and cohesive sediments. The behaviour of cohesive sediment particles is controlled by gravitational, interparticle electrochemical, and hydrodynamic forces. The relative contributions of these forces are mainly controlled by particle size. While the gravitational and hydrodynamic forces are critical for erosion resistance of non-cohesive sediments, the interparticle electrochemical forces, including Coulombian forces, London-van der Waals forces, and double-layer repulsion become increasingly dominant as the particle size reduces below 62 µm (see review by Santamarina [48]). Particularly, clay particles have large surface areas compared to their volumes (i.e., large specific area) and can attract and repel each other due to the presence of electrical charge. With the predominance of attractive forces, they become strongly cohesive. Since the cohesion is exerted by electrochemical forces present on the particle surface, the degree of cohesion also increases with decreasing size of particles, leading to maximum cohesion for the fine clay fractions ($< 2\,µm$) [17]. Sand and gravel particles, on the other hand, do not show any cohesive behaviour, do not stick together, and thus are practically non-cohesive (Table 1). Similarly, according to Mantz [49], coarse silt range exhibits little cohesion behaviour in terms of incipient motion similar to those of sand. While non-cohesive particles act independently of each other (without interacting), nevertheless when they are coated with microbial assemblages ("biofilms"), they act as cohesive particles due to the adhesion exerted by biofilm [5] (see section 2.8).

Under certain environmental conditions, cohesive particles can stick together and form larger particles with larger submerged weight – a process named "flocculation" [50]. The resulting particles or aggregates are called "flocs". Flocs are composite and flexible structures having various shapes (typically $100 - 200\,µm$) [51], sizes, and densities and can comprise both inorganic (e.g., clay and silt particles) and organic (e.g., biofilm) matter [19, 52]. Thereby, the sediment mechanics of fine cohesive particles is different than that of non-cohesive particles.

2.2 Concept of Erosion

In order to understand cohesive sediment transport and the effect of biofilm on erosion processes, it is necessary to describe the underlying physics. Erosion (or sediment entrainment) is defined as the detachment and movement of sediment particles at the sediment-water interface (e.g., in river or reservoir bed) [53]. For non-cohesive sediment, detachment of sediment particles from the bed and their transport take place when eroding forces are dominant over the resisting forces. The resisting forces are a function of size, weight, shape, and porosity of the particle, its position in the surrounding matrix of particles as well as packing density [16, 54–56].

Table 1: Sediment particle size and its relation to cohesion [17] (with permission from ASCE)[1]

Size range (µm)	Classification	Degree of cohesion
> 62	Coarse-grained	Non-cohesive
40 – 62	Fine grained: coarse silt	Practically non-cohesive
20 – 40	Fine grained: coarse silt	Cohesion increasingly important with decreasing size
2 – 20	Fine grained: medium and fine silt	Cohesion important
< 2	Fine-grained: coarse, medium, and fine clay	Cohesion very important

Cohesive sediments respond to hydraulic forces both physically (by absorbing water and swelling) and chemically through ion exchange in an attempt to preserve electroneutrality [57]. Hence, electrochemical properties of particles and their complex interactions (in the form of attraction and resistance) with water chemistry controls the erosion resistance (erodibility) of cohesive sediment [21, 58, 59]. The degree of interparticle attraction (sticking together) between sediment particles is influenced by, *inter alia*, clay minerology, grain size, cation-exchange-capacity (see section 2.7) while the water chemistry is a function of temperature, pH, and dissolved ions [22].

Cohesive sediments are usually transported as suspended load or wash load, whereas bed load consists of non-cohesive sediments. Cohesive sediment erosion occurs when the flow strength is large enough to dominate interparticle attraction forces [21, 22, 60]. Associated cohesive sediment behaviour is defined for bulk samples, implying that cohesive sediments are transported as a group with interparticle interactions [22, 61] in different erosion modes depending on the flow strength and bed composition [62]. Non-cohesive sediments are, on the other hand, typically detached from the sediment bed and transported as individual particles without interparticle interaction [16]. Withstanding the uncertainties in identifying sediment incipient motion described in section 2.4., erosion and transport of non-cohesive sediment is better understood compared to cohesive sediment erosion, yet the erosion process is even more complex when the biological factors, such as biofilm, are involved.

2.3 Theory of Sediment Incipient Motion

A non-cohesive sediment particle resting on the bed is subject to a combination of gravitational (F_G), hydrodynamic drag (F_D), and lift forces (F_L). Incipient motion represents the state of condition immediately before to movement of sediment particles at the bed surface. It is often related to increasing flow conditions. This includes increasing discharge or flow velocity due to e.g., storm events and snowmelt as well as reservoir management strategies, such as sediment flushing. When the flow rate is

---

[1] This material may be downloaded for personal use only. Any other use requires prior permission of the American Society of Civil Engineers. This material may be found at https://doi.org/10.1061/9780784408148.ch04.

increased, the bed shear stress also increases. The bed shear stress eventually reaches to a level at which sediment particles starts to move. This level is referred to as "critical shear stress for erosion" or "erosion threshold".

Considering a velocity profile in a river with a time-averaged velocity of U that corresponds to a level of u at the particle level, the forces acting on an individual particle are: i) the drag force (F_D), ii) the lift force (F_L), iii) the frictional resistance force (F_R), and iv) the gravitational force (F_G) (figure 3). Depending on the conditions, there exist three modes of particle motion, including rolling, sliding, and lifting [16, 63]. To reach the incipient motion, one of the following conditions must be satisfied:

$F_L \geq F_G$ (lifting mode)
$F_D \geq F_R = (F_G - F_L)tan\phi,$ with ϕ is the pivoting angle (sliding mode)
$M_D \geq M_S$ (rolling mode)

Where M_D is the overturning moment due to F_D and F_L at the pivoting point, and M_S is the resisting moment due to F_G about the pivoting point.
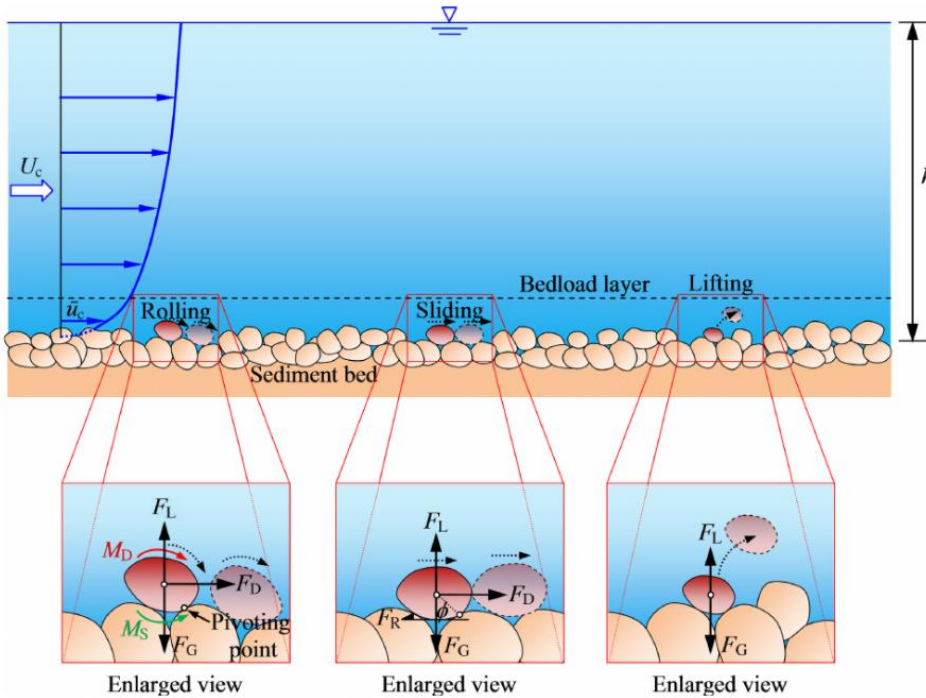
Figure 3: Conceptual sketch of sediment entrainment threshold for different sediment movement modes [16] (reproduced with permission from Wiley)

Whilst the underlying mechanics are clear, challenges include simultaneous measurements of these variables due to complex three-dimensional turbulence patterns and their interaction with the co-evolving bed [24, 64]. Since turbulence is considered as random fluctuations around a mean flow velocity [65], bulk properties based on flow velocity and particle properties have been found favourable, which have resulted in development of a variety of formulas and engineering curves for estimating incipient motion. Therefore, before describing cohesive erosion processes, incipient motion of non-cohesive sediment is described in the following sections.

2.4 **Identification of Sediment Incipient Motion**

Prior to describing the erodibility of cohesive sediment and biofilm-induced sediment stabilization, the approaches used for definitions of incipient motion of non-cohesive sediments shall be briefly summarized since a combination of visual and analytical approach will be utilized in this study to quantify the incipient motion.

Whilst knowledge of incipient motion of sediment particles is needed for estimating sediment transport, different definitions of incipient motion exist, which include: i) the visual observation approach [66], ii) the reference transport approach [67, 68], iii) the largest grain approach [69], and the probabilistic approach [53]. The first three approaches assume that incipient motion is a deterministic process and time-averaged bed shear stress moves the sediment particles [66, 68, 70–72], whereas the probabilistic approach considers incipient motion as a stochastic process by recognizing the probabilistic features of turbulent fluctuations caused by particle-flow interactions [53, 73–82]. The contributors to the stochastic processes also include, *inter alia*, surface roughness of the bed [83], heterogeneities in size, shape and density of particles [84–87], sheltering effect [88, 89], and packing [56, 90], which are also mutually influenced by the presence of biofilm [5, 26]. Therefore, estimating or quantifying the initiation of motion is challenging and mostly subjective. The "visual observation approach", as the name suggests, is based on the direct observation of movement of sediment particles at the bed. Incipient motion is considered to occur when the first particles start moving. Accordingly, Kramer [66] qualitatively defines four types of flow conditions for the incipient motion:

i. **No transport:** No particles move on the bed

ii. **Weak transport:** A countable number of the smallest particles are in motion in isolated zones.

iii. **Medium transport:** An uncountable number of particles of mean size are in motion.

iv. **General transport:** Particles of all sizes are in continuous motion at all parts of the bed, leading to morphological changes.

Other qualitative visual definitions of incipient motion involve, *inter alia*, motion of a single particle [56, 91, 92], motion of 1-2 particles [93], motion of the most exposed particle(s) [94], general motion on the bed [95, 96], and first motion of a plane sediment bed [97].

The "reference transport approach" is an indirect but quantitative approach and defines a critical shear stress associated with zero bedload (i.e., rolling, sliding, lifting) transport rate (i.e., the average particle momentum per unit bed area), which is performed by extrapolating the backward measured transport rate to shear stress at zero or at a low reference level [67, 98, 99]. However, in cases of sediment mixtures with a wide range of particle sizes, a unique reference transport rate cannot be observed [67, 100], making the approach sensitive to the properties of the sediment particles and their particle size distribution as well as extrapolation techniques employed. While it is accurately unknown

which approach Shields [68] used for measuring and comparing his data to those by Casey [101], Gilbert [71], Kramer [102] and USWES [103], the analysis of large datasets on erosion thresholds suggests that a combination of visual observation and reference transport approaches was employed [104, 105]. According to the experiments by Taylor and Vanoni [106], the Shields curve represents the conditions of a small observable transport rate, rather than zero transport rate.

The "largest grain method" is a quantitative approach based on the critical shear stress (flow competence functions) required to mobilize the largest particle [69, 107]. In this approach, flow functions are developed based on the collection of sediment particles in a sediment trap. While the approach can be easily applied in small streams where the near-bed measurements of flow is difficult, the size and efficiency of the sediment trap as well as the measurement duration play a critical role [108]. Differences in these factors may lead to underestimation of the maximum size of transported sediment [107] or to equivocal results for sediment that exhibits equal mobility since the flow functions approach is based on selective transport [109].

The "probabilistic approach" considers the effect of turbulence and variability in particle properties on the incipient motion. Compared to the other approaches, it acknowledges that the bed shear stress varies over time, and thus the incipient motion is associated with complex interactions of particles (and their properties) with turbulent fluctuations of flow. In this case, while the conceptual sketch (figure 3) employs the average flow velocity, the probabilistic approaches consider instantaneous flow velocities, including turbulent bursting events (i.e., outward interactions, inward interactions, ejection, and sweep events) and their frequencies and durations [110]. Figure 4 presents probability density functions (PDFs) of instantaneous bed shear stress (τ_t) and instantaneous bed shear stress $(\tau_{t,g})$ associated with sediment incipient motion. When the flow velocity increases, a slight overlapping of both PDFs can take place, leading to the state of incipient motion. The degree of particle motion is controlled by the degree of PDF overlapping. When there is no overlapping, no particle motion takes place. In cases of a significant overlapping of both PDF distributions, a significant amount of particles are set in motion [16]. As discussed later in this section, the probabilistic approach is arguably the most accurate approach for describing sediment entrainment process since the dynamic interaction between near-bed flow velocities and associated sediment particle motions can be simultaneously quantified.
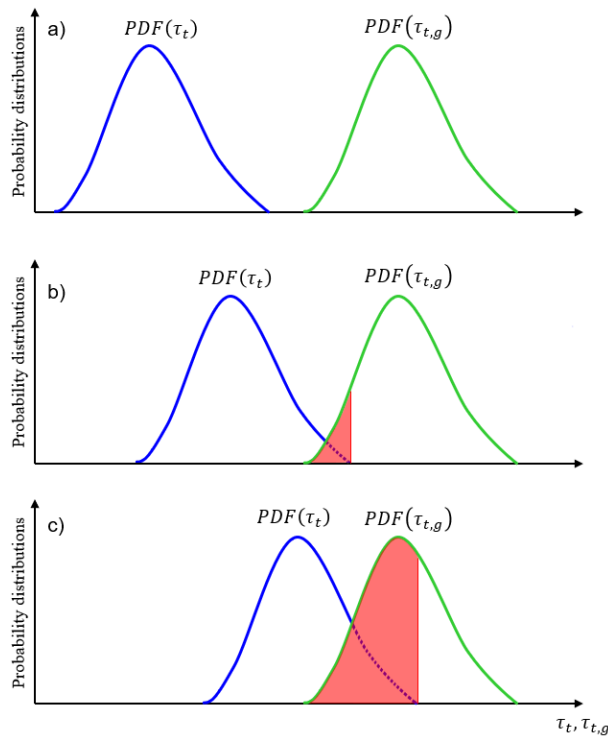
Figure 4: Conceptual diagram of sediment entrainment probabilities: a) Probability density functions (PDFs) of instantaneous bed shear stress (τ_t) and instantaneous bed shear stress governing vulnerability of individual particle entrainment $(\tau_{t,g})$, b) a slight overlapping of both PDFs leading to particle entrainment, and c) a substantial overlapping of both PDFs, leading to entrainment of considerable amount of sediments (modified from Dey and Ali [16], with permission from Wiley)

The visual observations of incipient motion have shown that incipient motion is related to flow strength, which can be described using discharge [111], flow velocity [112, 113], bed shear stress [68], and stream power [114]. Among these quantities, the concepts of mean flow velocity [113] and critical shear stress [68] have long been used. Hjulström [113] established a diagram between particle diameter and depth-averaged velocity to determine whether the flow will erode, transport or deposit sediment based on a water depth of 1.0 m, which was extended by Sundborg [115] and Miedema [116] considering different water depths and also cohesive sediments. Even though the Hjulström – Sundborg diagram is extensively used by geologists due to its simplicity [117], there exist several drawbacks. One of them is the absence of data for particle sizes smaller than 0.1 mm [22] and for sediment mixtures. Another drawback is that it disregards the effect of flow heterogeneity near the sediment bed. It is well known that there exists a complex interaction of flow and sediment (with or without biofilm) at the sediment-water interface, which cannot be estimated reliably from mean velocity measurements only [5, 26, 40, 118–120]. Accordingly, near-bed shear stress is of greater importance for describing the incipient motion in natural waters, where biota even makes the flow more complicated. However, its measurements in natural flow conditions are difficult due to limitations of the methods.

Therefore, the concept of critical shear stress and the widely used Shields curve [68] have been central issues in erosion and sediment transport and most of the experimental and theoretical studies have been built on the work by Shields [68] (see reviews, books, and guidelines by Dey [63], Dey and Ali [16], Dey and Papanicolaou [54], Garcia [121], Vanoni [122], van Rijn [59], Yalin [123], and Yang et al. [61], among others). Based on a series of laboratory experiments on a flatbed using four different non-cohesive sediment types with sizes ranging from 0.36 mm to 3.44 mm and densities ranging from 1.06 to 4.25 g cm^{-3} and applying the principles of similarity theory for the first time, Shields [68] described a non-dimensional relation between particle size and critical shear stress. The nondimensional Shields parameter (τ_* or θ), which is used to calculate the state of the incipient motion, is given by:

$$\tau_* = \theta = \frac{\tau_{cr}}{(\rho_s - \rho)gD}$$

where ρ_s is the density of the sediment, ρ is the density of the fluid, g the value of gravitational acceleration, D the characteristic particle diameter of the sediment, which usually corresponds to median grain size of sediment mixtures ($D = D_{50}$), and τ_{cr} is the critical shear stress. The Shields parameter is defined as a function of the particle Reynolds number $\left(Re_* = \frac{u_* k_s}{v}\right)$, where $u_* = (\tau_{cr}/\rho)^{1/2}$ is the friction velocity, $k_s (= 2.5D_{50})$ is the roughness height, and v is fluid kinematic viscosity. Accordingly, the Shields diagram [68] presents the variation of Re_* with respect to θ. In this diagram, the curve represents the boundary between stability (below the curve) and erosion (above the curve). Re_* represents the characteristics of the flow around roughness elements, by defining i) hydraulicly smooth ($Re_* \leq 5$), ii) hydraulicly transitional ($5 \leq Re_* \leq 70$), and hydraulicly rough ($Re_* \geq 70$) regimes [16]. Therefore, Re_* can be considered as the interrelationship between near-bed flow and surface roughness. In hydraulicly smooth flow, the sediment particles are smaller than the thickness of the laminar sublayer (δ_v), and thus the local roughness elements are often sheltered. δ_v can be estimated by $\delta_v = 5v/u_*$ [124] and has a typical height of $O(1\ cm)$ [3]. In hydraulicly rough flows, on the other hand, sediment size or local roughness becomes larger than the laminar sublayer and interacts with the overlying flow. Due to the development of filamentous structures, biofilms often generate additional flow resistance and thus the effective roughness is larger than the geometric roughness k_s [125–128].

Despite a century of studies on sediment incipient motion, there is no generally accepted approach for estimating sediment incipient motion. For instance, while the reference transport approach is better suited for bedload transport studies, it can lead to the overestimation of actual bed shear stress in the presence of developing bedforms during the experiment. The Shields diagram and its modifications (see review by Yang et al. [61]) is still widely used today, but large scatters exist (up to tenfold) around the mean Shields diagram of the experimental data obtained in similar flow conditions, morphologies, and median grain sizes [105, 129]. This can be mainly attributed to the different descriptions of sediment incipient motion since utilizing different or subjective

incipient motion criteria can result in different estimations of critical flow conditions. For detailed elaboration of the limitations of the Shields diagram, the reader is referred to the papers by Buffington [104], Buffington and Montgomery [105], Pähtz et al. [55], Sherman et al. [45], and Yang et al. [61]. The accurate determination of the associated erosion thresholds for the incipient sediment motion can be further complicated by varying degrees of sediment bed heterogeneity involving mixed grain sizes (cohesive contributions), macro-roughness, bed roughness [16, 54, 105], including biofilm-associated surface roughness [5, 26]. The Shields diagram is limited to the abiotic sediments (without biological involvement) on a flat bed, and some field studies reported its restricted application for incipient sediment motion estimation for biotic sediments [18, 130] and cohesive sediments [18], where erosion resistance and thus critical shear stress required for incipient motion may drastically increase due to cohesive forces between the particles and adhesive forces binding to the bed.

I argue that, to identify incipient motion objectively and accurately regardless of biotic involvement, the best practice would be to adopt a "probabilistic approach" by obtaining simultaneous measurements of instantaneous flow velocities and the sediment entrainment processes across the bed. Thereby, the interaction of the highly turbulent flow field and sediment particles can be considered. Some authors indeed argue that sediment transport rate appears to never reach precisely to zero due to strong turbulent bursting events [55, 56, 121]. While performing simultaneous measurements of velocity and bed is easier for non-cohesive sediment transport, it is deemed to be challenging for cohesive sediments and biofilm-coated sediments due to i) a high density of suspended particles in the water column preventing optical access to spatially-resolved flow measurements with advanced velocity measurement techniques, such as Particle Image Velocimetry (PIV), and ii) carpet-like erosion mode of biofilm-coated sediment, where instead of bedload particle motions, a catastrophic failure of the bed is often observed [131, 132]. Additionally, for biofilm-coated beds, heterogeneous surface topography imposes additional measurement challenges and uncertainties and make the flow even more complex. Therefore, in this dissertation, a combination of visual and analytical approach will be utilized to identify erosion thresholds based on spatially resolved measurements of erosion. As discussed above, since near-bed shear stress is more relevant for representing particle-flow interaction, near-bed shear stress determined a priori by a laser Doppler velocimeter (LDV) as a function of discharge will be used (see chapter 3).

Since the incipient motion and thus the mobility or stability of sediment are influenced by cohesion and adhesion due to the presence of clay fractions and biological matters (e.g., biofilm), the erosion potential of cohesive sediments and influencing physical, chemical, and biological factors (with the main focus on biofilm) is presented in the following sections.

2.5 **Erodibility of Fine Cohesive Sediments**

In non-cohesive sediments, critical shear stress for erosion is reached when the gravity force of the individual particle is exceeded by the bed shear stress. When the sediment bed consists of clay fractions with a certain amount, erosion resistance of sediment considerably increases and sediment transport concepts for non-cohesive sediment become invalid [59]. There is no consensus about the amount of clay fraction (e.g., 5 – 15%) [59, 133, 134] required for transition from non-cohesive to cohesive erosion regime since it depends on clay mineralogy, organic matter content, and sand size in the mixture [135].

Erosion of fine cohesive sediment takes place when the flow forces are larger than the synergistic interparticle forces in an individual particle or in particle groups. Whether non-cohesive or cohesive sediment, the onset of erosion is defined by the critical shear stress (τ_{cr}). Owing to the complex and widely varying bonds between cohesive sediment particles and their interactions with flow and biota, much less is known about erosion of cohesive sediments. Unlike non-cohesive sediments, erosion of cohesive sediments cannot be characterized solely based on their physical characteristics, such as particle size distribution and particle shape. Cohesive sediments mainly consist of clay-sized sediments, which have strong interparticle forces due to electrostatic charges on the surface. The interparticle forces can be several orders of magnitude larger than gravitational forces [21]. The degree of interparticle bonds increase with the decrease in particle size (see Table 1). These complex interparticle bonds substantially complicate the modelling of sediment transport for streams and reservoirs with cohesive bed and/or bank, and thus the management of these water resources. Even disregarding the effect of biological components, there exist more than 20 parameters [see 136]. Biological factors, in some cases, may be more important than the electrochemical forces [137]. The most important factors are discussed in the following sections. For a more comprehensive overview, the reader is referred to Black et al. [18], Grabowski [22], Mehta [138], Mehta and McAnally [17], and Raudkivi [21]. These vast and complex physical, chemical, and biological factors can considerably influence fine cohesive erosion, leading to high spatial and temporal erosion variability [31, 32]. Therefore, when assessing erosive properties of cohesive sediments, site-specific sediment conditions should be considered [33], which make cohesive erosion studies a multi-variate problem [22]. The erosion of cohesive sediment is governed by the frictional forces of site-specific hydrodynamic regimes (e.g., currents, wind-induced surface waves) and their complex and dynamic interactions with multi-variate properties of the sediments [21, 22, 138].

It must also be recognized that cohesive sediments can exist in multiple states, including i) eroded sediment, ii) transported sediment (sediment in suspension – fluid mud), iii) deposited sediment, and iv) partially consolidated or consolidated sediment, known as ETDC (Erosion-Transport-Deposition-Consolidation) processes. This means that sand, silt, and clay particles are continuously eroded, transported, and deposited (though not necessarily in this order) in rivers, lakes, and reservoirs due to flow and turbulence. The dynamics of these processes are controlled by the interactions between flow

characteristics, sediment properties (with or without biota) and water chemistry [26]. The erosion and transport of cohesive sediment have been extensively studied in estuarine environments using a variety of laboratory and field-deployable methods (see section 2.6). However, our knowledge about riverine environments, particularly reservoir sediments, remains limited despite the importance of the topic for ecological and engineering investigations.

By ignoring the effect of organic matter and biological forces, most studies have identified two main types of erosion modes [139–141], centering around alternative definitions [142, 143]:

Surface Erosion $(\tau_{cr,1})$: Surface erosion takes place when a critical shear stress for individual particles and aggregates (or flocs) is locally exceeded, leading to entrainment of individual surficial sediment (particle, aggregates or flocs), also known as Type-1 erosion [139, 141]

Mass Erosion $(\tau_{cr,2})$: Mass erosion take place when a critical threshold for the bulk strength of the sediment is exceeded, resulting in instantaneous entrainment of clusters or lumps of aggregates or flocs, also known as Type-2 erosion [139, 141]

Figure 5 shows the idealized relationship between erosion rate and shear stress assuming that erosion rates are estimated through SSC over time [139, 141]. Surface erosion occurs at the point where first sediment or floc is detached from the bed $(\tau_{cr,1})$. As the shear stress increases, surface erosion also increases gradually until large aggregates of the bed are removed $(\tau_{cr,2})$. The erosion rate and suspended sediment concentration (SSC) is estimated to be linear [139, 140, 144]. It must be mentioned that some measurements are challenging to fit this idealized relationship (figure 5) due to the large variability in data stemming from the natural variability of cohesive sediments (Tables 2 and 3). The discrepancies are due to subjective SSC threshold levels and regression approaches (e.g., linear or logarithmic). Whilst some researchers assumed the erosion threshold being equal to the background SSC level, others considered the critical erosion threshold level for surface erosion subjectively (e.g., 10 mg/L by Widdows et al. [145] and 100 mg/L by Lucas [146]). Therefore, the erosion thresholds for surface erosion vary widely in the literature. Similarly, time-series of the SSC can be considered for a certain time period or the entire time period, the latter biasing towards the surface erosion [147].

Additional erosion mode observations include multistep entrainment phenomenon by Righetti and Lucarelli [130]. Righetti and Lucarelli [130] reported a sporadic, intermittent motion of relatively small aggregates (at low shear stress) called primary aggregates, followed by an increase of primary aggregate flux (at higher shear stress), defined as aggregates of higher clustering order. Finally, with further increase in shear stress, a sudden erosion occurs, leading to an increasing number (size) of aggregates (or flocs).
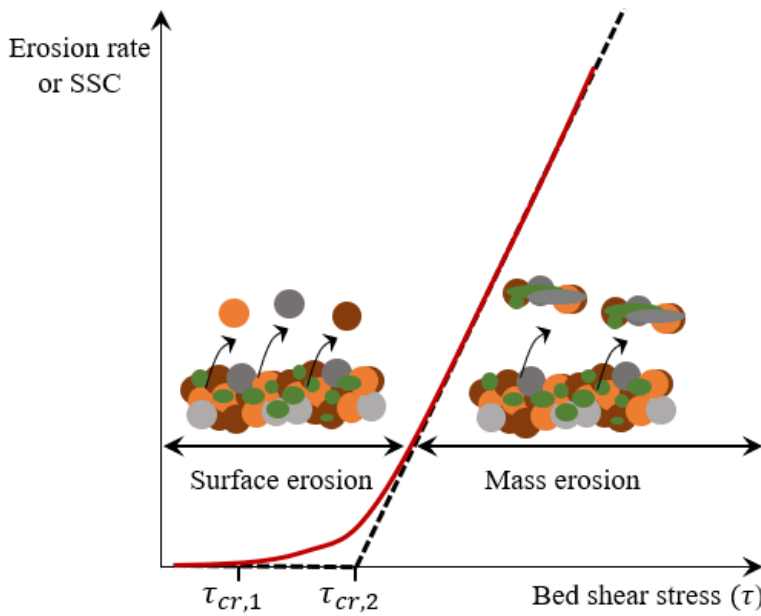
Figure 5: Idealized relationship between shear stress and erosion rates. Units are intentionally omitted (inspired by Tolhurst et al. [149])

In the context of biofilm-mediated sediments, which is usually the case for natural cohesive sediments [5], several different thresholds exist [148–150], making a comparison between these studies highly difficult, particularly for erosion thresholds obtained using field-deployable erosion devices (see section 2.6). Furthermore, when biofilm covers the surface of the superficial sediment, a sudden catastrophic failure of the bed is directly observed, followed by mass erosion at considerably higher bed shear stresses [5, 131, 132].

Since the idealized approach (figure 5) operates based on measurements of SSC using either optical or acoustic sensors, erosion measurements on biologically mediated sediment surfaces can be challenging, particularly when the flocs are transported near the bed far away from these sensors (see section 2.6 for discussion). In the context of this thesis, a combination of visual and quantitative approach was used to quantitatively obtain erosion thresholds using a camera in combination with a structured light (PHOTOSED) [151], which enables measurements of sediment volume over time [152]. The method is further discussed in chapter 3.

Over the last few decades, in order to estimate erosion thresholds for cohesive sediments, various mathematical formulas have been developed (see Zhu et al. [153]), yet they result in significantly different erosion thresholds due to site-specific, cohesive nature of the sediment (see van Rijn [135]).

Prior to proceeding with erosion devices and factors influencing cohesive sediment erosion, it is worth summarizing key terms used to describe erosion in various disciplines. Some of these terms have been used interchangeably by different researchers.

Erosion: Entrainment of sediment by action of wind and water [59].

Erodibility: *"Erodibility is the propensity for the sediment to be eroded and is represented typically as an erosion threshold or erosion rate. It is an attribute of the sediment itself, and is dependent on the sediment properties that dictate the resistive forces in the sediment, such as gravity, friction, cohesion, and adhesion"* [22].

Erosion threshold: The threshold level at which structural failure of the sediment occurs due to velocity of an eroding fluid or an applied shear stress [154].

Cohesive strength: The strength of sediment due to attractive electrochemical forces or electrical charges on particles, which are related to surface area to volume of particles [22].

Adhesive strength: The strength of sediment due to surface tension resulting from electrochemical attraction between particle and other materials (i.e., organic matter, EPS) [22].

2.6 **Measurement Devices for Erosion**

In order to estimate erosion rates and critical shear stress for erosion, a variety of devices/techniques have been developed and tested, both in laboratories and in the field. Laboratory flumes include conventional straight recirculating flumes (or ducts) [140] and rotating cylinders (annular flumes) [155]. Laboratory flumes are often used to test field-collected sediment samples (cores) or artificially reconstructed sediments with different size and mineralogy (table 2).

While field studies are comparatively less than laboratory studies, a diversity of benthic in situ flumes have been developed to quantify erosion rates and erosion thresholds of sediments in natural rivers, lakes, reservoirs, estuaries, and oceans. These erosion devices include submerged impinging jets, known as Cohesive Strength Meter (CSM) [29], Gust Erosion Microcosm System [156], benthic annular flumes [157], benthic in situ flumes [158–161]. They can be mainly categorized under straight recirculating flumes and recirculating systems. In these devices, suspended sediment concentration (SSC) is measured using the backscatter signal intensity from particles with an optical or acoustic instrument and related to certain hydrodynamic conditions. Thanks to their portability, CSM and Gust Microcosm chamber have been used to quantify temporally and spatially varying erosion thresholds. CSM works by delivering a jet of pressurized water (vertical jet) onto the sediment surface and is also commercially available. After an incremental increase of the jet pressure and eroding the sediment, the light transmission in the water column (thus SSC) is then measured with infrared transmissometer and related to hydrodynamic conditions. The Gust Erosion Microcosm System (GEMS) is a circular erosion device consisting of a rotating shear plate on the top. The rotation rate of the top shear plate is used to exert various shear stresses on the bed [156]. Both CSM and GEMS have been extensively used in the field over the last three decades, particularly in the estuarine environment, but only recently in field environments (see table 3). Indeed, the review of existing devices indicates that most of the erosion devices (both laboratory and

field-deployable) have been utilized either in the marine and coastal environments or for field-collected samples from these environments, with comparatively much less studies from rivers and reservoirs (table 3).

Each field-deployable device (or category) has certain advantages and disadvantages depending on their complexity, portability, cost, and operating principle [149, 162]. For example, even though CSM has been extensively used in the field, it does not generate shear stress parallel to the bed, and therefore lacks reality. It also defines the erosion threshold e.g., a 10% decrease in light transmission within the test chamber, which is dependent not only the configuration (type, diameter of the nozzle, and its height from the bed), but also sediment properties. Additionally, it is only capable of quantifying erosion thresholds for the surficial sediment [162]. A major disadvantage of recirculating erosion devices (e.g., GEMS, ISEF, Sea Carousel, benthic annular flumes) is the development of curvature secondary flows, leading to complex three-dimensional flow patterns and thus heterogenous shear stress on the sediment surface [163]. In these flumes, the bed shear stress is radially increased from inner to the outer flume wall [163].

Benthic in situ flumes can vary in size and shape. In these flumes, abrupt changes in SSC are monitored and linked to prevailing hydrodynamic conditions. The main advantage of the flumes is that they can deliver flow parallel to the sediment surface to exert consistent shear stress [162], but they are costly and complex setups [32].

In natural conditions, the bed can be coated by biofilm [29]. The initial increase in SSC can be related to the breakdown of this surficial surface instead of sediment resuspension [160]. Furthermore, even without a biofilm cover, rolling/sliding sediment particles (bed load) cannot be observed with such erosion devices in the field since the background signal intensity cannot distinguish whether the suspended particles are in the vicinity of the bed or further above in the water column (transported from other sites) [160]. An additional problem is the insensitivity of sensors to detect SSC at high sediment concentrations [164].

Whilst the physical, chemical, and biological properties of the natural sediment can be altered (disturbed) by the process of extracting, transporting and testing sediment cores [32, 158], conventional laboratory flumes are still the most reliable way of generating controlled and reproducible flow conditions that can be used to observe and measure erosion thresholds visually and quantitatively. Depth-dependent erosion behaviour of sediments and its relation to sediment properties is also required to advance management of water resources (e.g., reservoirs) and assess their ecological conditions. Whilst most field-deployable erosion devices focus on the erosion of surficial layers [162], depth-dependent erosion behaviour can be obtained with laboratory flumes (see table 2), such as the SEDFLUME (Sediment Erosion at Depth Flume, [143]), EFA flume (Erosion Function Apparatus, [165, 166]), and ASSET flume (Adjustable Shear Stress Erosion and Transport Flume [167], by fitting sediment cores to a hole at the bottom of the flume, and lifting and aligning the core flush with the flume bottom layer-by-layer. In this study, the SETEG erosion flume [168], a straight recirculating duct similar to SEDFLUME, was

used to examine depth-dependent erosion behaviour of natural cohesive sediments and surface erosion of biofilm-coated sediments.

Additionally, observations of a wide range of erosion thresholds in the literature for similar flow and bed conditions [105] can be attributed to approaches used to identify erosion thresholds (see section 2.4) as well as a variety of erosion devices employed, each having different operating principles [149, 162]. In most erosion devices, bed shear stress measurements are pre-calibrated as a function of discharge based on indirect measurements of the flow velocity approx. 8 – 10 cm above the bed [135]. However, the bed shear stress obtained with different methods, including the law of the wall (i.e., obtaining logarithmic velocity-depth profile), Prandtl's seventh power, turbulent kinetic energy, Reynolds stress, and the quadratic stress law [169] can substantially vary due to the complex nature of the turbulent flow near the bed [170]. Therefore, velocity measurements should be performed in the immediate vicinity of the bed.

Among bed shear stress estimation methods, the most common methods are law of the wall and Reynolds stress method. In the law of the wall method, velocity measurements are performed in discrete measurement points, so that the velocity gradient can be obtained. Based on the assumption of linear depth varying eddy viscosity, steady flow conditions, and constant shear stress, bed shear stress can be calculated using the law of the wall [see 21]. Apart from these assumptions, another limitation of the method is the involvement of the universal von Kármán coefficient (κ). Recent studies have shown the non-universality of the von Kármán coefficient in fluvial streams [171], particularly on biofilm-covered surfaces [172]. Furthermore, accurate measurements of velocity and elevations above the "unclear" bed level is very challenging [169], resulting in errors in bed shear stress estimation [169, 173].

In the Reynolds stress method, vertical momentum flux is required to estimate Reynolds stress at a particular elevation. There exists a diffusional process for the transport of fluid momentum towards the bed. The exchange of fluid eddies across the planes of mean shear parallel to the bottom tends to even out the velocity distribution by diffusing momentum towards the bed. This rate of momentum transport due to turbulent velocity fluctuations is known as Reynolds stress [174] and is calculated as:

$$\tau_{x,y} = -\rho \langle u'v' \rangle$$

where overbar denotes the temporal average, u' and v' denote fluctuations of longitudinal and vertical velocity, respectively and are defined as

$$u' = u - \langle u \rangle \text{ and } v' = v - \langle v \rangle$$

where u and v denote instantaneous velocities and prime denotes turbulent fluctuations.

In curvature flows (e.g., annular flume, GEMS), the method has a limitation since it assumes isotropic turbulence conditions, which is not the case due to strong flow curvature [163]. In this study, the Reynolds stress method was adopted to quantify the spatial distribution of near-bed shear stress in the erosion flume, but a comparison to law of the wall method showed similar results.

Table 2: Overview of erosion devices used in the laboratory (modified and updated after Wang [175])

Flume type	Sediment type – source / Equipment name (if available)	Author(s)
Straight recirculating flume	San Francisco Bay mud in marine water	Partheniades [140]
	Kaolinite; freshwater (river); SEDFLUME	Dennett et al. [176, 177]
	Undisturbed samples from riverbeds: SEDFLUME	McNeil et al. [143]
	Reconstructed samples for riverbeds; SEDFLUME	Jepsen et al. [178]
	Undisturbed muddy sediment from a reservoir	Haag et al. [179]
	Quartz particles; SEDFLUME and ASSET	Roberts et al. [167, 180]
	Undisturbed and reconstructed samples from field; pure clay (Kaolinite, Bentonite); Quartz particles; SEDFLUME	Lick and McNeil [181]
	Sediment mixtures (D_{50} = 152.5 µm and 215 µm) and cohesive estuarine mud	Panagiotopoulos et al. [182]
	Mud-sand mixtures and natural mud from the Mississippi River	Perkey et al. [183]
	Georgia kaolinite in fresh water	Ravisangar et al. [184, 185]
	Undisturbed loess-derived soils in cropland tested in freshwater (Belgium)	Nachtergaele and Poesen [186]
	Reconstructed sediment mixtures of mud and sand and natural mixed sediments (intertidal); ERODIMETRE	Le Hir et al. [187]
	Sand and clay mixture	Barry et al. [188]
	Undisturbed samples from riverbed and coastal area	Ganaoui et al. [189]
	Undisturbed samples from lakes; SEDFLUME	Righetti and Lucarelli [130]
	Undisturbed samples from riverbeds	Ternat et al. [190]
Straight recirculating duct	Silt and clay mixture; Kaolinite	Briaud et al. [165, 191, 192]
	Sediment cores from three reservoirs, River Neckar, Germany; SETEG	Gerbersdorf et al. [193, 194]
	Natural sediment cores from Durance and Rhône rivers; HERODE	Ternat et al. [190]
	Undisturbed natural soil samples from riverbanks in Manitoba, Canada Erosion Measurement Device (EMD)	Kimiaghalam et al. [195]
	Cohesive/non-cohesive sediment mixture; SETEG-PHOTOSED	Noack et al. [151]
	Reservoir mud; SETEG-PHOTOSED	Beckers et al. [196]

Flume type	Sediment type – source / Equipment name (if available)	Author(s)
	Cohesive and non-cohesive soil mixtures with mud contents varying from 0% to 100%; Erosion Function Apparatus (EFA)	Gao et al. [166, 197]
Rotating cylinder or annular flume	Boston Blue Clay	Zreik et al. [198]
	Yolo loam soil	Arulanandan et al. [199]
	30% Illite	Ariathurai and Arulanandan [200]
	Hong Kong mud and King's Lynn Sand (230 pm); SEA CAROUSEL	Ockenden and Delo [201]
	Mudflat at Hythe, Southampton Water, Southern England; Lab Carousel	Neumeier et al. [202]
	Reconstructed cohesive sediment mixtures with varying clay contents	Grabowski et al. [154]
	Sediment sizes (0.17–4 mm)	Baar et al. [203]
	Cohesive sediment collected from the upper River Taw in South-West England	Krishnappan et al. [204]
Submerged impinging jet – cohesive strength meter	Mixture of clay (40%), silt (53%), and fine sand (7%)	Mazurek et al. [205]
	Clay-sand mixtures	Ansari et al. [206]
	Reconstructed cohesive sediment mixtures with varying clay contents	Grabowski et al. [154]
	Reconstructed sediments with varying ratios of kaolinite and smectite clay (estuarine)	Kilkie [207]
	Biologically mediated fluvial streambank erosion	Smith et al. [208]
Vertical tube with rotating propeller	Mixed mudflat at intertidal sites in the German and Danish Wadden Sea	Andersen et al. [209, 210]
	Mud-sand mixtures EROMES	van Rijn [135]
Circular inverted bell-shaped funnel	Muddy bed Instrument for measuring shear stress in situ (ISIS)	Lintern et al. [211]

Table 3: Overview of field-deployable erosion devices (modified and updated after Wang [175])

Flume type	Sediment type – source / Equipment name (if available)	Author(s)
Circular inverted bell-shaped funnel	Mudflats in Severn estuary (Portishead and Blue Anchor Bay), UK Instrument for measuring Shear stress in situ (ISIS)	Williamson and Ockenden [212]
Submerged impinging jet – cohesive strength meter or jet erosion device	Allen et al. [213, 214]	Paterson [29]
	Intertidal mudflat, Westerschelde estuary, the Netherlands,	Tolhurst et al. [215]
	Sylt mudflat, Germany (biostabilization index of 6.2)	Tolhurst et al. [215]
	Cohesive clay soils to non-cohesive sandy soils (in streams – thirty sample sites)	Allen et al. [213, 214]
	Muddy sediment Humber estuary Skeffling mudflats	Tolhurst et al. [150]
	Agricultural soils	Potter et al. [216]
	Saltmarshmud in Essex (UK)	Watts et al. [217]
	Streambank erodibility, southwestern Virginia, USA	Wynn et al. [218]
	Cohesive channels in the Powder River Basin (PRB) of Wyoming, USA	Thoman and Niezgoda [219]
	Urbanizing basin near Toronto, Canada	Shugar et al. [220]
	Lowland streams, UK	Grabowski et al. [221]
	Streambank erodibility, Illinois River watershed in Oklahoma, USA	Daly et al. [222]
	Riverbanks sediments at each site of Selangor River, Bernam River and Lui River, Malaysia	Ibrahim et al. [223]
	Estuarine mud at14 sites	Kilkie [207]
	Streambank erodibility, Tennessee, USA	Mahalder et al. [224, 225]
	Intertidal area near Rimouski (Quebec, Canada)	Waqas et al. [226]
	Mudflat-salt marsh transition area on the Jiangsu Coast, China	Watts et al. [217], Chen et al. [227]
	4 types of cohesive soils	Wahl [228]
	Bay of Fundy, Canada Lake Ontario, Canada	Amos et al. [229, 230]
	Fine-grained sediment in Fraser River delta	Amos et al. [231]

Flume type	Sediment type – source / Equipment name (if available)	Author(s)
Benthic annular flume	Biofilm-mediated sediment, Upper South Cove, Nova Scotia; Sea Carousel	Sutherland et al. [232]
	Chesapeake Bay and Middle Atlantic Bight	Maa et al. [233]
	Baltimore Harbour	Sanford and Maa [144]
	Muddy sediment from tidal flat in the Westerschelde estuary, Netherlands	Lucas et al. [234]
	Humber estuary, UK	Widdows et al. [145, 235]
	Reconstructed mud from Wadden sea	Johansen et al. [236]
	Sediment at in Baynes Sound, British Columbia, Canada; SEA CAROUSEL	Sutherland and Amos [157]
Gust erosion (U-GEMS)	Estuarine sediment	Gust [156], Gust and Müller [237]
	Ship-born sediment samples (seabed, western European continental margin)	Thomsen and Gust [238]
	Accumulation of sediment on continental margins, Gulf of Lions, Mediterranean Sea	Law et al. [239]
	23 sediment cores from Arc and Isère alpine rivers	Legout et al. [240]
	Sand-mud mixed sediment on the Yeochari tidal flat, Gyeonggi Bay, Korea	Ha et al. [241]
	Surface soils in the Yolo Bypass, California, USA	Work and Schoellhamer [242]
	106 sediment cores (flood deposit on the middle Louisiana shelf)	Xu et al. [243]
	Mud, Pearl River Estuary, China	Huang et al. [244]
Benthic race-track shaped flume	South Wales, UK	Black and Cramp [159]
Benthic vertical recirculating flume	Intertidal mudflat along the Dutch Wadden Sea coast; ISEF	Houwing [245], Houwing and van Rijn [161]
Benthic flow-through flume	Buzzards Bay, Mass	Young [246]
	Undisturbed bottom sediment, Puget Sound Basin, Washington, US (SEAFLUME)	Gust and Morris [247]
	Boston harbour mud, 12% clay, 51% silt	Ravens and Gschwend [248]
	Several rivers, wetlands, and lakes in New Zealand NIWA in situ Flume I and 2	Aberle et al. [31, 249, 250] Debnath et al. [32, 251]
	River sediment Portable in-situ flume (ISF)	He and Nguyen [252]

2.7 **Factors Affecting Erodibility of Cohesive Sediments**

In the natural environment, a variety of factors affect erodibility or erosion thresholds of cohesive sediments [22] (figure 6). According to Winterwerp et al. [136], there are more than 20 parameters, even when the biological factors are ignored. In the following sections, most important physical, chemical, and biological factors are discussed in detail.

Physical
‣ Mean particle size
‣ Particle size distribution
‣ Bulk density
‣ Water content
‣ Temperature

Erosion

Biological
‣ Biogenic structures (Burrows, Networks, Biofilm, EPS, etc.)
‣ Sediment disturbance
‣ Feeding and egestion

Geochemical
‣ Clay mineralogy
‣ CEC
‣ pH
‣ Metal ions and SAR
‣ Organic content
‣ Salinity
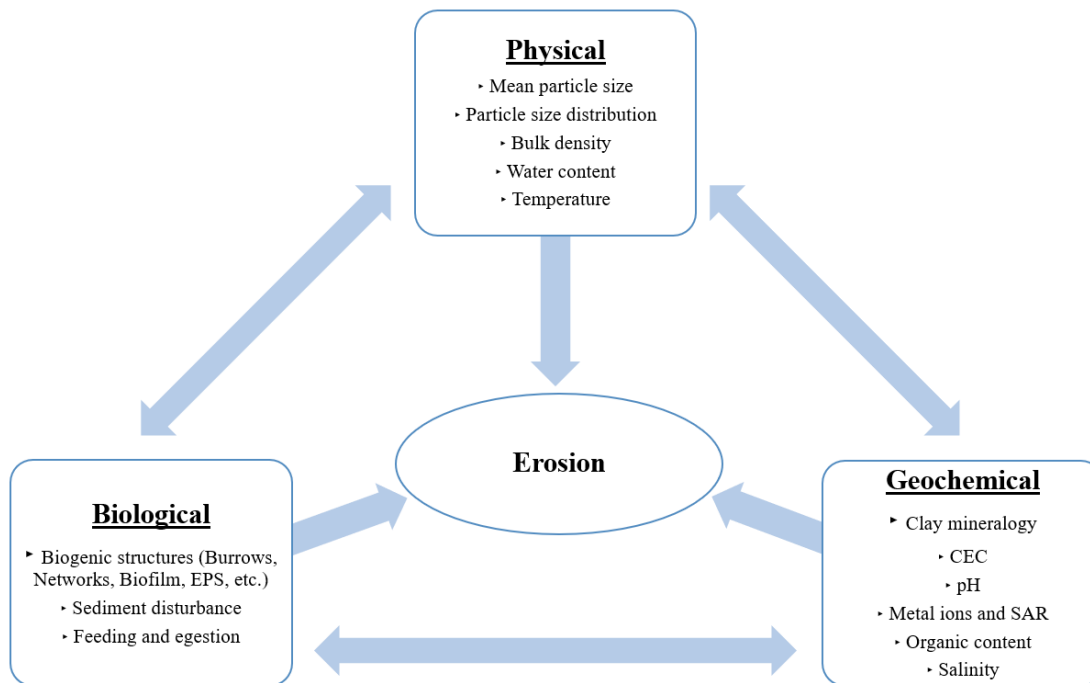
Figure 6:   Physical, chemical, and biological factors affecting cohesive sediment erodibility. The direction of the arrows show dynamic interaction between sediment properties (modified from Grabowski et al. [22], Copyright (2011), with permission from Elsevier)

2.7.1 Physical factors affecting erodibility of cohesive sediments

The physical factors influencing cohesive sediment erosion include flow and sediment properties (site-specific) and their interactions [22]. The key sediment properties that have been recognized to influence fine sediment erodibility are bulk density, water and gas content, mean (or median) particle or aggregate size, particle size distribution (clay, silt, and sand content), sediment structure, and water temperature [135, 142, 155, 183, 187, 200, 213, 216, 218, 219, 222, 224, 225, 253–263]. All these properties can vary substantially from one site to another [22]. Particularly, the effect of clay or mud (defined as a mixture of clay and silt therein) content on the critical shear stress has been extensively studied in the laboratory [34, 133, 135, 142, 166, 183, 187, 191, 258, 264, 265]. Despite a large body of laboratory experiments, comparatively less field studies exist [31, 32, 187, 213, 245, 265–267]. In general, erosion thresholds increase with increasing clay content [34, 135, 182, 183, 258, 261, 265, 268] and increasing bulk density (or decreasing water content) [133, 213, 218, 254, 265].

Based on the laboratory and field experiments of non-cohesive and cohesive sediment mixtures, Mitchener and Torfs [265] found an increase in critical shear stress by a factor of 10 by 30% mud addition to a sand bed and an increase by a factor of 2 by adding 50% sand to a mud bed. Furthermore, in case of mud addition of 50% to a sand bed, the critical shear stress was as high as to those observed in homogeneous mud beds, which was also supported by the findings by Panagiotopoulos et al. [182]. Houwing [245] observed a factor of 100 decrease in erosion rates of intertidal sediment with the increase in mud content (from 4% to 35%). For riverine sediments, Debnath et al. [32] reported a negative relationship between mud content and erosion coefficient, with a small erosion coefficient representing a low erosion rate. Interestingly, Gerbersdorf et al. [194] and Gerbersdorf et al. [193] reported negative relationships between sand content and critical shear stress for erosion for the field collected samples from a riverine environment.

Panagiotopoulos et al. [182] and van Ledden [269] showed that the clay content is a more generic indicator compared to the mud content to define the transition from non-cohesive to cohesive erosion behaviour. The clay (or mud) content is of importance since it determines the packing mode of the bed and thus its erosion behaviour [34]. When the clay content is large, the coarse particles are dispersed by fine sediments, resulting in fine packing [134, 270]. On the other hand, fine sediments are filled into the pore space (voids) of non-cohesive sediments when the clay content is small, resulting in coarse packing [134, 270]. According to Raudkivi [21], a presence of 10% clay is sufficient to control cohesive properties of the sediment. More recently, based on extensive experiments with artificially mixed sediments (kaolinite and bentonite) and natural mud collected from the lower Mississippi River, Perkey et al. [183] reported an increase in critical shear stress by a factor of 2-3 when mud content addition to the sand reached to 8%. Similar to the findings by Mitchener and Torfs [265] and Panagiotopoulos et al. [182], Grabowski [154], Kothyari and Jain [142], and Perkey et al. [183] reported maximum critical shear stress for erosion when the mud content was 30% – 40%. While increasing clay content is critical for increasing erosion thresholds [31], clay mineral composition also plays an important role [265]. For example, the transition from non-cohesive to cohesive erosion behaviour was shown to be between 7% and 13% for smectite. Similarly, a bentonite addition of 2% to quartz particles was observed to cause considerable increase in critical shear stress for erosion [264]. By using freshwater and marine water on sediment mixtures with various ratios of kaolinite and smectite clay, Kilkie [207] recently found a decrease in critical shear stress for the smectite rich sediments in freshwater, underlining the importance of clay mineral composition and its reaction to water chemistry. Recently, Perkey et al. [183] reported an increase in critical shear stress by a factor of 2 for erosion of the natural sediment samples from the lower Mississippi River and kaolinite–bentonite mixtures as compared to kaolinite only mixtures. Despite the observed effect of clay mineral composition on erosion thresholds [264, 271], most experimental studies have been hitherto conducted with kaolinite and in many studies the type of clay mineral is not mentioned. The variations in clay content often leads to changes in bulk density of sediments [182]. Therefore, both clay (or mud) content and bulk density should be considered as integrative parameters.

Bulk density (the ratio of the mass and apparent volume of a sediment sample) and water content indicate consolidation or packing of sediments [22]. Previous investigations have generally found positive correlations between critical shear stress and bulk density of fine cohesive sediments in laboratories, marine and freshwater environments [22 and the references therein] [31, 180, 183, 272], with exceptions being Gerbersdorf et al. [194] and Gerbersdorf et al. [193] in which the authors observed negative relationship in between based on sediment samples collected from riverine environments. According to Roberts et al. [180], bulk density is an important property of fine sediments with a size smaller than 0.125 mm, beyond which the particle size is of importance. Best generalizations for critical shear stress have been hitherto obtained using bulk density based on samples from both riverine and coastal environments [22]. For example, *inter alia*, using sediment and water samples from a lake, Hwang and Mehta [273] obtained relationships between bulk density and critical shear stress (and erosion rates) using an annual flume. These expressions obtained from riverine and coastal environments were later generalized and parametrized by [59]. Yet, bulk density cannot be used alone to estimate critical shear stress for erosion [180].

In general, bulk density increases or water content decreases with sediment depth in both artificially mixed and field-sampled fine cohesive sediments [143, 181, 184, 274–277]. Therefore, deeper sediment layers are expected to be more resistant to erosion compared to surface layers. It must be mentioned that the natural sediments also contain biota (e.g., biofilm, among others), which is generally dominant at the sediment surface and vertically distributed through sediment depth [30, 215]. Therefore, the adhesion and cohesion exerted by biofilm is expected to increase critical shear stress for erosion at the sediment surface [18, 29] and at deeper layers [30].

Despite the role of bulk density on erosion resistance of cohesive sediment has been noted by many researchers (in some cases of intertidal sediments, increasing critical shear stress up to 20 times [217, 278]) Grabowski [22] argues that water content is a more generic indicator since it affects the mechanical properties of clay [22]. Most experimental and field studies have relied on the assumption that the sediment is saturated (pores are filled with water and no gas is present). Therefore, bulk density and water content have been used interchangeably [180, 279]. Yet, gases (e.g., methane or carbon dioxide) are usually stored in natural sediments [280, 281] and thus expected to decrease the mechanical stability of sediment.

Natural rivers and reservoirs are characterized by complex geometries, including deltas, bends, and a diversity of bed and channel roughness. The latter also includes biological players, such as vegetation and biofilm, both of which are known to considerably affect flow characteristics [5, 40, 282, 283]. Accordingly, hydrodynamic characteristics affecting erodibility (and its spatial variability) of sediment comprise a magnitude of the shear stress and turbulence [138], including secondary flows [140, 259, 284–288] as well as flow variability, including flow duration and peaks [268].

As described in the preceding sections, mean (or median) particle size is often positively correlated with erosion thresholds for non-cohesive sediments. On the other hand, studies

on cohesive sediments generally report a negative correlation between particle (or aggregate) size and critical shear stress for fine (clay – silt size) sediments [142, 165, 180, 191, 238, 264]. By performing laboratory experiments, Roberts et al. [180] studied the influence of bulk density and mean particle size (5 μm to 1350 μm) on the erosion of quartz particles. The authors observed a positive correlation with critical shear stress for the mean size range of 100μm to 1350 μm, and a negative correlation for sediment particles below 100 μm. While the latter was attributed by Roberts et al. [180] to the increased cohesivity, Lick et al. [264] and Grabowski et al. [22] argue that the interparticle attraction was partly due to organic matter resulting from long consolidation time rather than the cohesion between the quartz sediments. Grabowski et al. [22] further argue that the relationship between particle size and erosion thresholds can be positive or negative for fine cohesive sediments depending on the flow and turbulence characteristics in the water column during deposition of sediments, which can lead to varying aggregate sizes and thus varying erosion response. Utilizing a field-deployable cohesive strength meter (CSM), Thomsen and Gust [238] performed field experiments on natural marine mud and observed a negative correlation with D_{50}. The authors observed clay-liked behaviour of silty sediments (for $D_{50} < 30$μm) comparing with the erosion thresholds reported in the literature. This was attributed by the authors to biological stabilization of sediment. Using a special erosion function apparatus (EFA), Briaud et al. [165] found a negative correlation between critical shear stress and D_{50} for consolidated cohesive sediment mixtures from the field. For a wide range of sediment mixtures with clay proportion varying in the range of 10% to 50% (with fine gravel, or with fine sand and gravel), Kothyari and Jain [142] conducted extensive experiments and similarly observed a negative correlation of critical shear stress with particle size for the clay range. More recently, Briaud et al. [191] reported a negative correlation with critical shear stress for cohesive sediment mixtures, suggesting the use of D_{50} for defining upper- and lower limits of the critical shear stress. Based on the digitized data from the published literature, the variation of critical shear stress with mean particle (aggregate) size (or D_{50}) is depicted in Appendix III (accepted manuscript). It is clear from the figure that there is a general agreement on the negative correlation between particle size and critical shear stress for mean (and median) particle (aggregate) sizes smaller than approx. 0.150 mm and a positive correlation for particle sizes larger than 0.150 mm.

2.7.2 Chemical factors affecting erodibility of cohesive sediments

Despite numerous studies on physical sediment properties affecting erodibility of fine cohesive sediment, chemical properties have received considerably less attention. The erodibility of cohesive sediment is affected by various chemical factors, involving contributions from the chemistry of sediment, eroding fluid (water in this case), and pore fluid.

The factors related to water chemistry that can affect cohesive sediment erodibility include pH, dissolved ions, metals, and salinity [22]. Water chemistry does this by altering physicochemical forces between cohesive particles [22]. While studies on the

effect of pH on cohesive sediment erodibility is mostly limited to laboratory setups [22], a decrease in erosion thresholds up to a factor of 14 was observed with increasing pH [185]. Since pH can be regulated by biological activities (e.g., biofilm) [289, 290], more studies on the effect of pH on erosion thresholds are needed. Temperature also influences the erodibility of fine cohesive sediments. Ariathurai and Arulanandan [200] found a decrease in erosion thresholds with increasing temperature, likely due to decreased electrochemical attraction between clay particles.

The chemistry of pore fluid and its interaction with overlying fluid also affect physicochemical forces between cohesive particles [22, 291]. The chemical composition of dissolved ions in these pore fluids, specifically the ratio of exchangeable sodium ions (Na^+) to calcium (Ca^{2+}) and magnesium (Mg^{2+}) ions, was reported to influence erosion thresholds of fine cohesive sediments [200, 291, 292]. Grabowski et al. [22] also argue that the existence of metal ions can affect erodibility of cohesive sediments by enhancing the electrochemical attraction between clay particles and enhancing the elasticity of biofilms. Furthermore, pore fluid pH affects the orientation of particles during interparticle bonding by interfering with the surface or edge charges of the particles, leading to orientations of Edge-Edge (E-E), Edge-Face (E-F), Face-Face (F-F), which changes the structure of the sediment. For example, low pH conditions ($5 \leq pH \leq 7$) result mostly in E-F particle orientations. This leads to stratification of the bed structure with high void ratio and high-water content, resulting in high erosion rates near the surface [176]. On the other hand, high pH conditions ($pH > 7$) result mostly in F-F particle orientations, for which the interparticle attraction is highly enhanced due to increased surface contact. This leads to denser aggregate and sediment structures, with a low water content and a strong erosion resistance [176].

One of the most important parameters influencing erodibility of cohesive sediment is the clay mineralogy. Clay minerals are mainly responsible for the cohesive nature of the sediment (crosslinking of particles with each other in water, for types of the crosslinking see review by Dai and Zhao [293]) and form approximately one third of sedimentary rocks [294]. Mainly containing tetrahedral "sheets" of silicon-oxygen and octahedral "sheets" of magnesium or aluminium-oxygen [21] in a "crystal-like" structure (also called crystal layer), the clay particles are formed by chemical weathering of silicate minerals within rocks and are plate-shaped [22, 47]. The ionic composition of these sheets can vary considerably due to isomorphic substitution of exchangeable ions between clay minerals [21, 294, 295]. Due to ionic exchange and associated broken bonds between clay minerals, the crystal-like structure of clay minerals becomes negatively charged. This negative charge is then balanced by adsorption of exchangeable cations in the vicinity of the crystal structure to keep neutrality [21].The total negative charge in clay is known as Cation Exchange Capacity (CEC) [17]. The CEC, expressed as milliequivalents of exchangeable cations per 100 grams of dry sediment, is a specific property of clay minerals that determine the degree of mineral cohesion and the adsorption capability. The higher CEC results in greater cohesion. This leads to coagulation or flocculation of micro-meter-sized individual clay particles to form larger aggregates or flocs [17].

The various combinations or bonding of the tetrahedral and octahedral sheets with different anionic- and cationic substitutions [17] lead to the development of different clay minerals, holding together by electrostatic (attractive and repulsive) forces. Cohesion results from net attraction interparticle forces. The most common types of minerals include kaolinites, illites, vermiculites, and smectites (or montmorillonites) (see Grabowski et al. [22] for further details), which are mainly characterized by their sheet configuration (1:1 or 2:1, see table 4) [294]. These clay mineral groups have different layer structures, particle sizes, CEC values, textures, plasticities, water adsorption capacities (table 4), and reactions to biological effects [22]. Therefore, different erosion thresholds are observed. In general, increasing levels of CEC were reported to increase erosion thresholds (or decrease erosion rates) based on laboratory and field-sampled sediments from riverine and coastal environments [193–195, 200]. Yet, Torfs [296] observed a lower critical shear stress for a mixture of smectite (Montmorillonite) and sand in comparison to kaolinite or natural marine mud. This further shows the complexity of cohesive sediment erosion processes since kaolinites are the least electrochemically active minerals owing to their larger sizes and lowest CEC. Despite CEC is a distinct property of clay particles (defining clay mineralogy) and thus fine cohesive sediments in natural waters, the influence of CEC on erosion of natural cohesive sediments has not been sufficiently addressed.

Clay minerals have also space between their layers [293]. Since the interlayer bonding is strong in kaolinites, there is no or little interlayer swelling, which leads to little isomorphic substitution and thus lower CEC levels. On the other side, the interlayer bonding in smectites is weak, enabling water and exchangeable ions to access. Another aspect of clay minerals is that when they swell due to their electronegative surface and CEC, the interlayer spacing will increase and thus their adsorption capacity for heavy metals [297] and other organic contaminants [298].

Consisting of waste and secretion of dead organisms (flora and fauna), organic matter in natural waters can widely range in size [22]. Clay particles in natural waters are negatively charged due to adsorption of natural organic matter (NOM) [176]. NOM is typically expressed as a percent of organic carbon adsorbed to the clay particles [176]. Interparticle bonding between clay particles and thus stability of fine cohesive sediments can be positively or negatively influenced by NOM and its interaction with sediment [299]. Based on laboratory experiments, Dennett et al. [176] found decreased critical shear stress with an increase in NOM (0.0% to 0.12%). On the other hand, Gerbersdorf et al. [194] and Gerbersdorf et al. [193] found positive relationships between total organic carbon (TOC) and critical shear stress for erosion from field collected samples from riverine environments. Similarly, Aberle et al. [31] observed that the erosion resistance increases due to presence of fibrous organic matter (e.g., decomposing leaves and roots).

Mehta [300] showed that higher TOC results in lower particle density based on the measurements from Rodman Reservoir (Florida) [301]. Gowland and Mehta [302] and Gowland et al. [303] collected data on erodibility of organic-rich sediments from various sites in Florida (USA) and showed that 5% by weight of TOC, the bulk density reduced

to 1700 kg/m^3, which is supported by the findings of Parchure and Davis [301]. For example, among many other riverine sites, Parchure and Davis [301] observed a decrease of particle density from 2700 kg/m^3 (sand) to 1400 kg/m^3 when organic content increased to 75%. The authors also reported an increase by a factor of 7.5 in erosion rates when organic content increased from 10% to 60% for Newnan's Lake (Florida). Due to adsorption of clay particles, Parchure and Davis [301] also reported an increase in TOC with increasing mud ratio. Righetti and Lucarelli [130] observed an increase by a factor of 5 in erosion resistance with varying TOC content (8 – 25%), the maximum resistance being at a TOC of 12 –14%. Since TOC or NOC can vary highly from one site to another, it should be considered in cohesive erosion studies. Note that the amount of organic content in these studies are denoted as TOC in this thesis.

2.7.3 Biological factors affecting erodibility of cohesive sediments
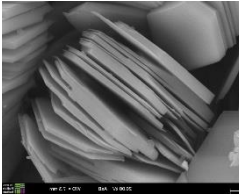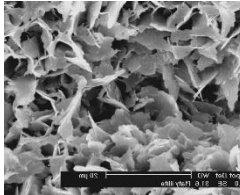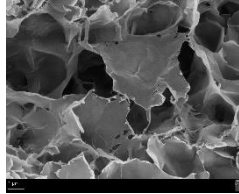
Organisms (e.g., macrofauna, meiofauna, microalgae and bacteria) living in sediments of rivers, reservoirs and estuaries can increase or decrease erodibility of sediment [18, 22]. They also interact differently with electrochemical properties of cohesive sediments depending on site-specific sediment and water properties [17]. In general, the increase in erosion thresholds or sediment stability is called "biostabilization" [27] or "biogenic stabilization" [5]. Alternatively, it is defined as *"a decrease in sediment erodibility caused directly or indirectly by biological action"* [304]. In contrast, increase in sediment erodibility by biological actions is known as "bioturbation" [27]. Bioturbation is caused by reworking of sediment by inhabiting organisms [22]. According to Black et al. [18], stabilizing effects by biological actions include, *inter alia*, mucus called extracellular polymer substances (EPS) secreted by microorganisms, networking effects, sediment compaction, sediment armouring, biofiltration, and biodeposition, whereas the destabilizing effects include, *inter alia*, grazing blistering, burrow cleaning, and boundary layer effects.

The organisms inhabiting in natural sediments include bacteria, diatoms, microalgae, and burrowing organisms. These benthic communities are abundant in sediment [6, 305]. By studying the effect of bacteria and diatoms on erosion thresholds, Paterson [27] showed that non-cohesive particles become cohesive when bacteria and diatoms grow on them, resulting in substantial increase in erosion thresholds This is due to EPS that form cohesive networks between particles and microorganisms. Paterson [27] and USBR [292] argue that microorganisms have a stronger influence on erosion thresholds than the interparticle electrochemical forces within cohesive sediments. The stabilizing effect of microbial organisms, "biostabilization", is discussed in detail in the following sections.

Burrowing organisms can positively or negatively affect sediment erodibility of surficial sediment. For example, Brekhovskikh et al. [306] showed a decrease by a factor of 10 in erosion thresholds in the presence of Oligochaeta, which are frequently observed worms in freshwater environment. Brekhovskikh et al. [306] also found an initial decrease in erosion thresholds for Chironomids (midges with burrowing larva observed in freshwater environment). However, the authors observed that the erosion thresholds increased over

time due to mucus secreted by Chironomids. A similar stabilizing effect of burrowing organisms was later demonstrated by Meadows and Meadows [307]. The reader is further referred to the reviews by Black et al. [18] and Grabowski et al. [22].

Table 4: Properties of mostly studied clay minerals for erodibility [17, 22, 207, 293, 297, 308–311]. Images reproduced from the 'Images of Clay Archive' of the Mineralogical Society of Great Britain & Ireland and The Clay Minerals Society (https://www.minersoc.org/images-of-clay.html)

Properties	Kaolinite	Illite	Smectite
Sheet type	1:1 (two layer)	2:1 (three layer)	2:1 (three-layer)
Particle size (μm)*	0.36 (large)	0.062 (medium)	0.011 (small)
CEC (Meq/100 g)	3 – 15	10 – 40	80 – 150
Water adsorption capacity	No swelling Low expansive coefficient	No swelling Medium expansive coefficient	High expansive coefficient
Critical salinity (ppm)**	0.6	1.1	2.4
Plasticity	Low	Medium	High
Erodibility in soils	Low	Medium	High
Erodibility in sediment with low SAR	Medium	Low	Low
Erodibility in sediment with high SAR	Medium	High	High
Specific	Low	Medium	Very High
Surface area	8 – 26 m^2 g^{-1}		
SEM Image			

* Defined here as the diameter of a circle with the same surface area as platelike clay particles.

** Critical salinity for floc formation.

2.8 **Biostabilization of Sediment by Biofilm**

This section is partially reproduced from Appendix II [24]. Biofilms are genetically diverse surface-attached aggregates of microorganisms (Archaea, Bacteria, Eukarya) [7], which are wrapped in a self-produced matrix of EPS. Aquatic biofilms are capable of colonizing various soft (e.g., sediment or soil surface) and hard (e.g., stone, plant, pipe, or vessel surfaces) surfaces that exist across diverse environments, including streams and rivers [6], lakes [312], estuarine [313], and marine [137] waters, as well as drinking water distribution systems [314, 315]. Whether growing on mud (epipelic), sand (epipsammic), stone (epilithic) or plant (epiphythic), whether addressed as microphytobenthos (in shallow coastal waters, intertidal flats), microbial mat (among others, in habitats of hot springs, hypersaline ponds, groundwater) or periphyton (on any submerged surface in the aquatic habitat), all communities possess emergent features, such as production of EPS, tolerance towards external stresses, cell-cell communication and collective behavior as well as synergetic use of nutrients that distinguish them as biofilm [26, 316–318].

When growing on sediment in the bed finer than about 2 mm (clay, silt, sand) [23], biofilms also glue the sediment particles to each other through their EPS matrix [4, 5]. This, in turn, alters the sediment-bed properties, e.g., density, morphology, size gradation [319–322], and dynamics, e.g., erosion and transport [30, 64, 323–329] and, finally, the accumulation and transport of contaminants [330, 331].

As defined in the previous section, the ability of biofilms to increase erosion thresholds by biological actions is called "biostabilization" [25–28] or "biogenic stabilization" [5]. Hereafter it is referred to as "biostabilization" throughout the dissertation. Biostabilization has been reported to mediate the sediment ETDC processes in aquatic ecosystems [5]. It must be noted that biostabilization can also occur through smoothing of the bed surface and therefore reduction of the hydraulic roughness, as observed over gravel-like hemispheres [119]. These interactions of sediment and biofilm are critical to the biogeochemical processes at the entire ecosystem level [332].

The biostabilization index (BI) is often used as an indicator for the stabilizing effect of biofilm and is defined as [27, 333]:

$$\frac{\tau_{cr,bio}}{\tau_{cr}}$$

where $\tau_{cr,bio}$ is the critical shear stress for biostabilized sediment and τ_{cr} is its abiotic reference. An overview of some studies reporting BI from diverse environments is given in Table 5. Many of these laboratory and field studies employed different erosion devices and different definitions of erosion thresholds, which results in a wide range of erosion thresholds and BI. This raises questions about comparability of the results. It must also be mentioned that most of these studies represent sediment characteristics at intertidal areas, with only three studies representing freshwater environment [9, 334, 335].

Biostabilization potential of biofilms and biofilm-induced biogeochemical processes are dictated by their biodiversity and community composition through the metabolic

performance of involved microbial communities [5, 28, 36–38]. The physical structure, composition and diversity of the biofilms in aquatic ecosystems vary widely depending on the physical (e.g., grain size, porosity), chemical (e.g., sediment nutrient content), biological (e.g., growth rate, cell-cell communication), and environmental (e.g., light, temperature and flow regime) factors [36, 336] and processes [337]. This also includes their complex interactions with nutrient and organic matter cycling [6, 338], growth habitat [339, 340] as well as flow and bed topography [8, 341–343]. Many biofilms have complex morphologies and can develop long, oscillating filamentous structures called streamers [39, 40], which not only alter flow dynamics and bed topography, but also mass transport near the bed.

Table 5: A list of observed biostabilization index (*BI*) values in the literature (modified and updated after Vignaga [344]). "nc" denotes non-cohesive bed, whereas "c" denotes cohesive bed

BI [−]	Bed	Sediment environment / Erosion device (if available)	Author(s)
2 – 6	nc	Subtidal biological mats binding sandy carbonate sediments / Laboratory flume and in situ underwater flume	Neumann et al. [345]
10 – 15	nc	Marine sand bar (0.189 mm) covered with purple sulphur bacteria / Straight laboratory flume	Grant and Gust [346]
3	nc	0.125 – 0.177 mm quartz grains in seawater / Laboratory flume	Dade et al. [347]
4	nc	Subtidal sediment / Straight laboratory flume	Madsen et al. [348]
> 10.6	nc	Marine sediment colonized by autotrophic assemblages / Cohesive strength meter	Yallop et al. [137]
2.5	nc	Sediment (gravel and d = 1 mm sand) / Recirculating laboratory flume	Vignaga et al. [349]
> 3	nc	River water, 0.150 mm glass beads / Straight recirculating flume	Thom [335]
3	c	Estuarine sediment / Annular flume	Parchure and Mehta [277]
4	c	Intertidal sandy beach / Cohesive strength meter	Yallop et al. [137]
6.2	c	Intertidal mudflat / Cohesive strength meter	Tolhurst et al. [215]
5 – 10	c	Intertidal mudflat / Annular flume	Neumeier et al. [202]
1.5	c	Lake sediments / Straight recirculating flume	Righetti and Lucarelli [130]
3.4	c/nc	Tidal mudflats / Two different annular flumes	Amos et al. [350]
1.5 – 1.7	c/nc	Reservoir, 0 – 0.02 mm, 0.02 – 0.05 mm, 0.05 – 0.10 mm / Straight recirculating flume	Fang et al. [334]
2.65 – 5.01	c/nc	River water, 0 – 0.02 mm, 0.02 – 0.05 mm, 0.05 – 0.10 mm / Straight recirculating flume, river water	Fang et al. [9]

Therefore, of particular importance for biostabilization is, the complex and dynamic interaction between flow, biofilm, and sediment, which substantially influences both cohesive and adhesive properties of the bed [27, 130, 329], leading to increased erosion thresholds at the sediment surface [5, 18] and at deeper layers [30]. The erosion behaviour of both, non-cohesive and cohesive sediment with biofilm cover, is similar to that of natural cohesive sediments [132, 329]. Specifically, electrochemical and biological properties of natural sediment interact with each other, which is further complicated by reciprocal flow-biofilm-sediment interactions. Accordingly, distinguishing between adhesion and cohesion and understanding their relative contributions to erosion process is very difficult.

In order to better predict the behavior of fine sediment or develop sediment management scenarios (e.g., flushing) [351, 352], experiments have been largely performed in laboratory flumes with sediments that were retrieved and transferred from the field [9, 193, 334]. However, there also exist in-situ measurements to avoid sediment disturbance associated with transportation of sediment from the field to the laboratory flume and sediment aging [250, 353]. However, as discussed in section 2.6, this imposes additional challenges, such as inaccurate determination of erosion thresholds due to a subjective selection of threshold definitions and methodological limitations (e.g., application of horizontal flow or vertical flow, generation of heterogenous flow conditions due to flume curvatures), yielding a diverse range of critical shear stress values even for similar flow and bed conditions.

Accordingly, whilst investigating the relationships between site-specific natural sediment characteristics and erosion thresholds is important to advance our understanding about cohesive erosion process and to establish practical formulations for erosion thresholds, a fundamental understanding is still elusive and is derived from controlled laboratory experiments. In this respect, in order to better understand biostabilization and sediment dynamics as well as to effectively manage our water bodies for the benefits of human society and ecosystem functioning, a better understanding of flow-biofilm-sediment interactions is needed. Challenges include i) creating realistic experimental settings and utilizing a combination of tools and approaches to describe the reciprocal relationships between flow-biofilm-sediment and associated mass transfer, which alters microbial processes and vice-versa, and ii) understanding the role of key microbial players (and processes) for biogeochemical and morphological processes at the entire ecosystem level, and how organismal level functions can be linked to ecosystem functions. These challenges require acquisition of large bodies of information across various spatial scales by studying hydraulics, geomorphology, and ecology as an integrated concept using advanced tools and approaches rather than studying them in isolation. To foster interdisciplinary research with little or no destruction to flow and sediment, a combination of optical methods and approaches would be ideal. A comprehensive elaboration of research on flow-biofilm-sediment interactions as well as associated methodological challenges and research gaps in relation to biostabilization and fine sediment dynamics are provided in the publication in Appendix II. Herein, a brief overview of

methodological discussion is provided, with some passages quoted verbatim from the publication (Appendix II).

Hydraulics: As discussed above, the understanding of flow-biofilm-sediment interactions is currently hampered by the lack of velocity measurements at the sediment-water interface. Most studies represent flow with a single (bulk) value for the entire channel either as a depth-averaged or cross-sectional average velocity (and discharge) [354 and references therein] or temporally-averaged flow and turbulence parameters far above the bed [341, 342, 355]. For example, Risse-Buhl et al. [342] and [341] conducted velocity measurements around biofilm-covered sediment using acoustic Doppler velocity profiler (i.e., Vectrino Profiler), but could not obtain accurate near-bed flow velocities due to acoustic interference of the bed [43]. Since most studies employ conventional ADV sensors [282, 325, 356–358], they mostly ignore heterogenous nature of turbulence parameters over a natural living surface, such as biofilms. Yet, to understand how biofilms affect the turbulent boundary layer and vice versa, as well as its erosion response, near-bed flow measurements are critical. Additionally, many measurement techniques are capable of recording velocity measurements at single probe locations or along a vertical profile and disturb the flow field (intrusive). Whilst an optical technique, called, laser Doppler velocimetry [125, 126], is non-intrusive, it does not give access the simultaneous dynamics of the flow since it is also capable of measuring at a single probe location. In this regard, optical and non-intrusive approaches, such as PIV and PTV (particle tracking velocimetry), are the most favourable techniques to obtain high resolution, simultaneous two-dimensional measurements of flow and turbulence over a large region (few dm^2). For example, by using PIV, Graba [118], Murphy [359], and Shang et al. [322] showed i) the highly complex and heterogenous distribution of turbulent flow structures around biofilm, and ii) the increased drag due to high levels of momentum transport, resulting in an effective hydrodynamic roughness significantly larger (a factor of 2 reported by Murphy [357]) than the biofilm geometrical roughness. Due to is non-intrusive nature, PIV technique can easily be combined with other optical measurement techniques, e.g., underwater laser scanner for bed roughness and hyperspectral imaging for biochemistry (Chlorophyll-a) measurements, which often co-evolve with flow over time. Since commercial PIV systems are very expensive (>100k€), a low-cost PIV system was developed and applied in this study.

Bed topography: Many measurement techniques exist for bed topography or roughness measurements, including, *inter alia*, airborne laser scanning [360], terrestrial laser scanning [361, 362], multibeam echo sounding [363] over large domains as well as structure-from-motion [364, 365] and laser-triangulation [342, 366, 367] for roughness calculations in smaller domains. While structure-from-motion (SFM) outweigh the literature [364, 368, 369], the technique also has some limitations [368]. The main limitations include refraction at the water surface and image degradation when the SFM is applied from the air [370], requiring modelling the distortion of the light [371]. However, during the experiments, the water surface also has a variable surface roughness due to interactions of flow and biofilm filaments, making SFM measurements from

outside impossible. This means that the flume must be drained in order to perform SFM measurements over dynamic surfaces. However, draining the flume also disturbs biofilm, both structurally and microbially. Additionally, SFM technique is computationally expensive [369]. Even though the laser-triangulation sensors have not been intensively used in fluvial hydraulics, they can address the limitations of the commonly used SFM techniques. For example, using a boat-mounted laser triangulation sensor, Noss and Lorke [367] investigated high-resolution depth and width measurements of shallow streams. Thom [335] quantified surface topography of biofilms using a commercial laser triangulation, but the measurements had to be performed outside of the flume, and the measurement process was quite timely. Since commercial laser-triangulation sensors are not designed to operate underwater and are expensive, a self-made underwater laser scanner was developed and applied to assess feasibility of an interdisciplinary research.

Molecular approaches: Insights into the microbial community composition have been traditionally gained by microscopic evaluation of morphological, taxonomically unique features [372]. This classical approach is for example common for the determination of diatom species that – by their appearance and certain requirements – are excellent indicators of different water qualities or various hydrodynamics scenarios [118]. Whilst these insights are very valuable on the microalgae level, addressing the occurrence of certain bacterial species requires metagenomics approaches. Nowadays, thanks to the advances in molecular ecology and computational power, it has become possible to decipher the previously unprecedented diversity of biofilms and taxonomic differences using high-throughput technologies [372, 373]. Furthermore, metagenomic approaches prevents problems associated with conventional polymerase chain reaction (PCR) amplification [372]. Specifically, Ribonucleic acid (RNA)-based approaches, instead of Deoxyribonucleic acid (DNA)-based approaches, have the capability to provide a clearer picture of taxonomic and functional diversity of the metabolically active microbial communities in biofilms [374]. In this regard, the molecular analysis of 16S Ribosomal RNA (rRNA) and 18S rRNA is now central to many studies addressing diversity of biofilm communities [375–379].

3 Materials and Methods

As reviewed in chapter 2, the erosion processes in natural environment are highly influenced by physical, chemical, and biological properties of sediments and their site-specific interactions. Therefore, controlled laboratory experiments are ideal to understand the interactions of flow, biofilm, and sediment as well as the resulting ecosystem process, i.e., "biostabilization". Since there exists mutual and dynamic feedback between flow, sediment, and biofilm-induced sediment reworking process, interdisciplinary approaches are required to better comprehend biostabilization mechanisms. In this respect, a combination of non-destructive optical methods and approaches would be ideal. In addition to laboratory studies, the process of natural erosion should be explored in the field in order to understand the relative roles of site-specific sedimentological parameters on spatially- and depth-variable erosion thresholds, with the possibility to transfer findings to different environments.

3.1 **Laboratory Study**

The *first set of experiments* were motivated by the increasing use of acoustic Doppler velocity profilers for characterizing velocities and turbulence at the sediment – water interface under both laboratory [380, 381] and field conditions [382, 383]. Specifically, the Vectrino Profiler has become increasingly popular due to its high spatial resolution (1 mm) and velocity profiling range (35 mm) (http://cs.nortek.no/). Since it can also provide simultaneous measurements of distance, thus the instrument is well suited for studies involving flow–biofilm–sediment interactions. However, boundaries located in the measurement range of conventional acoustic Doppler velocimeters (ADV) are known to have adverse influence on velocity measurements due to the acoustic interference of the bed, biasing velocities as far as 10 mm above the bed [384–386], the region named as "boundary interference region". Particularly, as discussed in chapter 2, the interactions between flow and biofilm take place predominantly at scales ranging from $100 \, \mu m$ to 10 cm in vertical length [387]. Therefore, near-bed measurements (< 10 mm) is of great importance.

To evaluate the measuring performance of the Vectrino Profiler as well as to investigate the influence and vertical extent of the boundary interference region on mean velocity

and turbulence measured by the Vectrino Profiler, laboratory experiments were conducted in a flume (0.36 m wide, 3 m long) on four types of bed material, including (i) geotextile bed (Polypropylen, GreenLife GmbH, Schwerin, Germany) as a scenario for fluffy sediment with high porosity, (ii) sand bed with a median grain size (D_{50}) of 0.25 mm, (iii) gravel bed having a nominal diameter between 18 and 36 mm (coarse gravel), and (iv) metal bed as a scenario for strongly reflective flat bottom. During the measurements the flow depth was kept constant at 0.23 m, while flow velocity, bed material, and distance of the Vectrino Profiler probe to the bed were altered. The measurements were performed both with Vectrino Profiler and Particle Image Velocimetry (PIV, Dantec Dynamics, Skovlunde, Denmark). The comparison included vertical profiles of mean flow velocity, turbulent kinetic energy (TKE) as well as power spectral density of velocity fluctuations since they are essential parameters, which are commonly used to characterize flow fields at the sediment–water interface. More information about the experimental set-up, methods, and data processing is given in Appendix I [43]. This study showed and highlighted the limitations of the Vectrino Profiler (or other ADV techniques) for measuring velocities in the close vicinity of the bed. Therefore, in order to obtain high spatial and temporal measurements of velocities without disturbing the bed, optical methods, such as PIV should be used.

The *second set of experiments* focused on flow–biofilm–sediment interactions from an "interdisciplinary" perspective. Although fine sediments and their erosional behavior have received increasing attention over the last decades with or without the consideration of biofilm, their link to spatio-temporally varying bed topography, hydrodynamics, and microbial community, and metabolic activity co-evolving with biofilm growth have not been studied yet [41, 326, 388]. Such studies require integrated investigations of hydrodynamics, biogeomorphology and microbiology [41, 42]. However, even a decade after the "2020 vision" of Rice et al. [41] for integrated and interdisciplinary river science, a feasibility of an interdisciplinary approach bringing different tools and scientific communities together on the same topic, "biostabilization" in the context of this study, has yet to be tested.

Therefore, in this experiment, we have tested the feasibility of such an integrated and interdisciplinary approach by co-applying advanced instruments and methods from the disciplines of hydrodynamics, microbial ecology, and sedimentation engineering on freshwater biofilm samples that were quasi-naturally grown on non-cohesive sediment. Since, flow velocity is the main driver for biofilm growth and EPS production [5, 8, 375], biofilms developed at contrasting flow conditions are expected to have different morphology (e.g., thickness, roughness) and different levels of EPS secretion, which may influence sediment stability. Hence, biofilms were cultivated in six identical laboratory flumes (each 0.15 m wide and 3 m long) at contrasting flow conditions: i) low flow (LF) scenario with a bed shear stress of ~ 0.01 Pa and ii) high flow (HF) scenario with a bed shear stress of ~ 0.04 Pa. Three LF flumes and HF flumes were located in separate containers to avoid cross-contamination of ambient light. The flumes were modified versions of the ones used by Thom et al. [132] and each possess an individual water tank,

pipes, and cooling circuits to cultivate biofilm under controlled conditions of hydrodynamics, temperature, and light. The entire bottom of each flume was reconstructed as "one block" to avoid any water leakage to the bottom as well as any height inconsistencies across the flume (e.g., cartridges are not perfectly parallel), which, otherwise, could significantly affect flow conditions by generating step-change in the roughness. The biofilms were cultivated on 16 removable cartridges with dimensions of 88 x 58 x 50 mm³ (*l* x *w* x *h*). The advantage of such design is that it enables the transfer of cartridges outside the flume when *in situ* measurements cannot be performed. Before inserting these cartridges into the flumes, they were filled with fine ($D_{50} = 0.16$ mm) and medium sand ($D_{50} = 0.29$ mm), saturated in water, compacted and flattened to achieve a planar surface parallel with the cartridges edges. In order to reproduce nutrient conditions, water chemistry, and site-specific microbial organisms, 1.2 m^3 of natural freshwater was withdrawn from the reservoir Großer Brombachsee (meso-eutrophic) [281], which was then transported to the laboratory, well-mixed through aeration, filtered to avoid large particles that can disturb sediment surface or stuck in the flume, and distributed to the water tanks equally. Additionally, a homogeneous solution was prepared using site-specific sand and scratched stones (for diatom and algae) and equally distributed into the flumes. During the experiments, water depth in the flumes were maintained (in the beginning) at 75 mm through gates at the flumes' outlets. The water temperature was also fixed at 15°C with the help of heat exchangers, which supplied colder water at 8 °C. A full PAR (photosynthetically active radiation) spectrum was utilized [132] and the light intensity was kept constant at 50 µE $m^{-2}s^{-1}$. After a growth period, the biofilm growth and related parameters were regularly monitored and linked to prevailing conditions.

Through a joint methodological workshop, we utilized advanced methods with capabilities of measuring at various spatial scales and high spatial resolutions to address the interdisciplinary question of how advanced methods in the fields of hydraulics, sedimentation engineering, microbial ecology, and biochemistry can be applied to study flow–biofilm–sediment interactions, towards the same goal: Biostabilization. The measurements included flow dynamics (Particle Image Velocimetry), bed topography (laser-triangulation scanner and light microscopy), biofilm structure (optical coherence tomography), mass transfer (microsensors), microbial community (16s and 18s rRNA gene sequencing), mechanical properties (rheometer), and biostabilization potential through erosion thresholds (see section 3.2 for SETEG flume). We also explored advantages and limitations of the methods applied. The main findings of this experimental study were combined with an application-oriented review on the current state of the knowledge and methodological approaches in the flow-biofilm-sediment research with a focus on biostabilization and fine sediment dynamics mainly in the benthic zone of lotic and lentic environments. More information about the application of these methodological approaches can be found in Appendix II [24].

3.2 **Field Study**

To investigate multi-variate relationships between sedimentological properties and erosion thresholds, 9 and 13 sediment cores (22 in total) were collected from the deposits of reservoirs Großer Brombachsee (GBS) and Schwarzenbach (SBT), respectively. Both reservoirs are shallow with mean depths of ~16.5 m (maximum depth = 33 m at maximum capacity) and ~21.8 m (maximum depth = 65 m at maximum capacity) for GBS and SBT. With typical total phosphorus concentrations of < 30 mg m^{-3}, they can be considered as meso-eutrophic [281].

The GBS (inauguration date = 2000) is located in Bavaria in Germany (the Franconian Lake District) at an elevation of approximately 410 meters above sea level (m.a.s.l.). It has a surface area of ~8 km^2 [389]. The main purpose of the reservoir is to store water and regulate water levels in the Regnitz-Main catchment area. The GBS is also used for leisure, recreation, and fishing.

Located in the Black Forest in the south-west of Germany (Baden-Württemberg) at an elevation of approximately 669 meters above sea level (m.a.s.l.), the Schwarzenbach reservoir (inauguration date = 1926) is a shallow, mesotrophic reservoir, with a surface area of ~0.54 km^2 [389]. The reservoir is mainly used to balance the load in energy supply and drains into the first large-scale hydroelectric pumped-storage system. Similar to the GBS, the SBT is also used for leisure, recreation, and fishing. The reservoir is fed by two inflows, one transition tunnel and pumped water.

Of particular importance is the difference of sediment composition between the two reservoirs. The SBT is sand-dominated, whereas the GBS is clay-dominated. In addition, total organic content varied between both reservoirs, all of which are expected to influence the erosion thresholds (see chapter 2).

Sediment cores from these deposits were extracted using the "Frahm Sediment Sampler" (MBT GmbH – MacArtney Germany), which was originally developed by "Leibniz Institute for Baltic Sea Research". The main advantage of this corer, compared to conventional gravity and piston cores, is the generation of the vacuum by the lid, when extracting sediment from the bottom. Thanks to the movable clamps, it also facilitates quick sealing immediately after sediment core collection [390], resulting in a collection of relatively undisturbed sediment core samples. To enable a smoother entry into the sediment, we used PVC (Polyvinyl chloride) cores of 0.10 m in diameter (wall thickness = 0.005 m) and 1 m in length, with a lower end bevelled to an angle of 5°. The Frahm Sediment Sampler was operated from a floating platform powered by an electric motor. The floating platform was also equipped with a tripod and an electric winch (12 V), whose speed can change between 20 and 10 m min^{-1} without and with load, respectively.

After withdrawal of the sediment cores, they were immediately transferred to the laboratory with core lids closed to mitigate disturbances due to water fluctuations [150, 194]. The vertical profiles of wet bulk density was non-destructively measured for all cores based on Gamma Ray Attenuation (GRA) measurements by emitting a collimated gamma beam (Cesium Cs^{137} with a decay energy of 661 KeV) through the sediment cores

and detecting the gamma quants with a scintillator detector unit made of Sodium Iodide doped with Thallium (NaI (TI)) at the other side of the cores at a room temperature of 27 °C (see Mayar et al. [391, 392] for details of the technique). The attenuation of gamma rays passing through the cores rely strongly on the bulk density. This results in vertical profiles of bulk-density distribution with a vertical resolution of 2 cm. After the bulk density measurements, the sediment cores were stored in a climate-controlled chamber, with temperatures being close to the *in situ* temperatures. Based on the similarity of the vertical bulk density profiles, the group of sediment cores collected from GBS and SBT were separately categorized into two sub-groups for the analyses of i) physico-chemical and biological analyses (table 6), and ii) critical shear stress for erosion. The cores in sub-groups were then sectioned into different layers at vertical intervals of 1 – 5 cm. To ensure the comparability between the sediment cores and to assess uncertainties associated with assigning different sediment cores (and layers) to each other for characterization of sediment properties and critical erosion thresholds, a maximum bulk density deviation of 7.5 % (percentage error) was allowed between two layers. This resulted in a correlation matrix consisting of 92 elements to explore multivariate relationships between selected sedimentological properties and erosion thresholds.

For the physico-chemical sediment properties, particle size distribution was measured by laser diffraction with a Malvern Mastersizer 2000 (Malvern Instruments Ltd, Malvern, UK). On the basis of the particles size measurements, the sediments were then categorized into clay, silt (fine, medium, coarse) and sand (find, medium, coarse) according to the ISO 14688-1 (2017) and finally the 10th, 50th, and 90th percentiles (D_{10}, D_{50}, D_{90}) were calculated. Total Organic Carbon (TOC) was indirectly measured by loss on ignition (in percentage) of dried sediment according to the European standard DIN EN 13137 (2001). Therefore, TOC considers both living and dead organisms. The Cation Exchange Capacity (CEC) was determined using hexamminecobalt (III)chloride as an extracting solution and quantifying the exchangeable cations photometrically according to ISO 23470:2018 (2018). The individual exchange ions (e.g., Na^+, Ca^{2+}, Mg^{2+}) were not quantified.

Table 6: Overview of analysed sedimentological parameters

Physical	Bulk density
	Sediment composition
Chemical	Total organic carbon
	Cation exchange capacity
Biological	Chlorophyll-a
	EPS (protein, carbohydrate)

For biological sediment properties, chlorophyll-a, a proxy for photoautotrophic biomass/algae in sediments, was determined within $0.5 \, cm^3$ wet sediment samples of each sediment layer (in triplicates) by ethanol extraction (96%) and acidification by

Hydrochloric acid (HCl). The spectrophotometric determination of supernatant was performed before and after acidification according to DIN 38412-16:1985-12 (1985) and Gerbersdorf et al. [326]. The EPS contents were characterized by extracting the colloidal (water-extractable) fractions of the biofilm and centrifuging (Sigma 202MK Centrifuge, Sigma GmbH, Osterode, Germany) according to Gerbersdorf et al. [326]. Subsequently, the supernatants were analysed spectrophotometrically for EPS-protein (EPS-p) and EPS-carbohydrate (EPS-c) contents (in triplicates) using the modified Lowry method [393] and phenol-sulfuric acid method [394], respectively.

For the critical shear stress measurements, the sediment cores were eroded at various vertical intervals (representing the interval for sedimentological characterization) in the SETEG ("Strömungskanal zur Ermittlung der tiefenabhängigen Erosionsstabilität von Gewässersedimenten") flume [168, 276]. The SETEG flume is a pressurized recirculating flume, which has a clear glass window of 2 m in length (total length = 8 m), 0.142 m in width, and 0.10 m in depth. The flume enables the control of the velocity by varying discharge (0.001 to 0.065 m^3 s^{-1}). The water is pumped through pipes from a large annually drained water tank (1200 m^3) in the basement of the laboratory. The SETEG flume has a circular hole at the measurement section (7.64 m from the flume entrance) as well as an electric motor driven lifting shaft, on which sediment cores can be locked, moved (in vertical), and positioned to the flume zero-bed level. Two-dimensional (2D) laser Doppler velocimeter (LDV) (TSI Inc., Shoreview, MN, USA) measurements were used to characterize the spatial distribution of the shear stress across the measurement section. The bed shear stress was calculated as a function of discharge using the Reynolds stress method at 2 mm above the bed (see section 2.6), but a comparison to the law of the wall method showed similar results (with percent difference of < 4 %). The flow was fully developed at the measurement section and Kolmogorov's inertial subrange (-*5/3* law) [395] was present in the spectrum of velocity fluctuations, confirming that the measurements represent typical characteristics of turbulence. For further details about the SETEG flume as well as bed-shear stress–discharge relationships, the reader is referred to Beckers et al. [152].

After inserting a sediment core into the flume bed, any protruding or loose sediment was cut off with a wire, so that the sediment surface was flush with the flume bed. Further, the sediment cores fitted snugly into the circular hole in the flume bed, creating minimum disturbance. The sediment surfaces (layers) were then exposed to a stepwise increment of discharge. Each discharge was maintained for a period of 600s until a surface failure of the bed was observed, after which another sediment layer was elevated to the flume level by means of the lifting shaft. During the erosion process, the sediment surface was continuously monitored by a photogrammetric system, namely PHOTOSED (Photogrammetric Sediment Erosion Detection Method). The details about the method can be found in Noack et al. [151]. Briefly, the method operates based on the structured-light technique, in which a semi-conductor laser coupled with a diffraction optic projects a structured (known) dot pattern (approximately 24,000 points) onto the sediment surface and a CMOS camera (Complementary metal–oxide–semiconductor, Imaging

Development Systems GmbH, Obersulm, Germany) continuously records deflection and appearance of these light patterns at 10 frames per second (2 MP images) [151]. The volumetric change of the sediment layer between consecutive frames (here: $\Delta t = 60$ s) and thus time-series of the recorded erosion volumes within a specified region of interest of the sediment surface can be calculated using Farnebaeck's Dense Optical Flow algorithm [396], which enables estimation of different types of critical shear stress for erosion [152].

Further details about the erosion set-up, identification of erosion thresholds as well as statistical analysis between sedimentological parameters and erosion thresholds can be found in Appendix III [44].

4 Synthesis and Conclusions

The research presented herein was based on laboratory flume studies focused on flow–sediment interactions (with and without biofilm) and erosion resistance of artificial and natural sediments. To this end, multiple experimental methods for investigating the interactions between flow and sediment (with or without biofilm) were utilized. The study also illustrated a successful application of an interdisciplinary approach bringing together methods from the fields of hydraulics, sedimentation engineering, microbial ecology, and biochemistry. In general, the findings underline the need to further study erosion processes in various natural environments under variable regimes of flow, biofilm, and sediment. Due to complex interactions between physico-chemical and biological bed properties, the field studies should, ideally, be complemented with controlled laboratory studies by utilizing a combination of advanced optical and molecular approaches in an integrative way. In the following the main findings of this dissertation are presented (see Appendices I, II, and III for the articles).

Assessing performance of a commonly used acoustic Doppler velocity profiler for measuring flow and turbulence in the near-bed region

The laboratory study on the comparison between Vectrino Profiler and PIV measurements of velocities and turbulence at the sediment–water interface demonstrated that the sediment bed adversely influenced velocity measurements as close as $1.7 - 5$ mm above the bed, depending on the bed material. The vertical extent of the boundary interference region – the acoustic interference region of the bed leading to underestimation of velocities – and velocity differences between two instruments decreased with decreasing proximity of the Vectrino Profiler. It was also shown that the vertical extent of this boundary interference region can be practically identified by a local minimum in signal-to-noise ratio recorded by the Vectrino Profiler itself. It must be mentioned that even though the Vectrino Profiler is capable of providing accurate measurements of bed distance in addition to velocities over solid surfaces (e.g., gravel), alternative distance measurements are required on softer sediment beds (e.g., sand, fluffy sediments) due to the penetration of the acoustic signal. In the measurements, a reasonable agreement (<10%) of mean velocities and turbulence was observed between both instruments around the sweet-spot (the region of largest overlapping between the

receivers) of the Vectrino Profiler only. Whilst the mean velocities were reliable over a larger region (± 8 bins centered at the sweet-spot), the spectral analysis of turbulent fluctuations showed that turbulence measurements are only reliable within 3 mm around the sweet-spot, which is approximately one-third of the previously suggested region by MacVicar et al. [397]. A remarkable observation was to persistent appearance of a local minimum of TKE and velocity variances at the sweet-spot of the Vectrino Profiler, where the Doppler noise is minimum. The application of the Doppler noise correction method by Hurther and Lemmin [1] could not correct the TKE profiles, suggesting that the noise is not solely due to geometrical configuration of the VP. Therefore, measurements from Vectrino Profiler should be interpreted with caution, particularly for measurements above fine sediment beds. This study further confirms the limitations of acoustic-based velocity instruments for measuring flow and turbulence at the sediment–water interface. Future studies should explore placing the sweet-spot of the Vectrino Profiler within the boundary interference region of the bed in addition to considering the probe's potential flow disturbance. For non-destructive, high-resolution velocity and turbulence measurements over larger areas, optical methods, such as PIV and PTV, can be used, which also give access to visual observations of sediment surface or moving boundaries (e.g., biofilm filaments).

Identifying the gaps and challenges in flow-biofilm-sediment research and addressing them with an integrative approach

Motivated by the needs for integrative and interdisciplinary approaches to investigate the interactions of flow, biofilm, and sediment in order to better understand biostabilization, this study presents results of a laboratory study and methodological workshop focused on flow–biofilm–sediment interactions on biofilm-covered non-cohesive sediment bed developed at contrasting flow conditions. We also presented a successful application of an interdisciplinary approach, bringing a variety of advanced methods from different scientific disciplines together. The results were incorporated into an applicated-oriented review focusing on flow-biofilm-sediment research across various spatial scales.

On the basis of their co-application for the same goal towards understanding biostabilization, we made several observations about reciprocal relationships between flow, biofilm, and sediment as well as advantages and challenges associated with applied methods. We found that the flow speed influences the time of settlement, biofilm growth as well as surface topography. Mean surface roughness (0.46 to 1.97 mm) and biofilm thickness (1.92 to 3.74 mm) increased considerably with a decreasing flow regime (bed shear stress from 0.04 Pa to 0.01 Pa). The changes in surface topography affected the magnitude and distribution of Reynolds shear stress and enhanced effective roughness. Whilst measuring bed topography with scanning microscopy was time-consuming with a potential to disturb sediment due to transportation of cartridges outside the flume, underwater laser-triangulation scanner demonstrated similar results quickly, both in terms of time and measurements. Therefore, even though the underwater laser-triangulation method is not frequently used in geomorphological investigations (section 2.8), it can be considered as a suitable choice at scales ranging from cm^2 to dm^2 since it provides non-

destructive measurements of the bed. In addition, the method can easily be combined with the PIV method, giving insights into dynamic interactions between bed and flow. Further, the application of microsensors to measure metabolic activity within the sediment bed led to observation of bursts of H_2O_2 when touching a diatom colony with sensors. This could be a self-defense mechanism of these microalgae against predators, which have not been previously observed in a similar environment. Optical Coherence Tomography (OCT) provided *in situ* and non-destructive internal structure of biofilm-bed in the surficial sediment layer, giving access to observations of filament networks connecting sediment particles together. However, the method was limited to surficial sediment layers (~2 mm) due to the limited probe depth. Overall, microsensor measurements could be used together with PIV, laser scanner, and OCT measurements in analyzing the external and internal mass and momentum transfer by combining substrate distribution, flow dynamics, and biofilm structure. Furthermore, in an attempt to observe changes in the microbial community that drive important ecosystem functions (i.e., biostabilization), advanced molecular methods were applied and significant shifts in species composition and diversity at both prokaryotic and eukaryotic level were observed. The abundance and species diversity were significantly higher for bacterial communities at high flow conditions, whereas they were higher for microalgal communities at low flow conditions. Measurements by hyperspectral imaging illustrated that imaging density, composition, and distribution of phototrophic biofilms may create a strong predictor for sediment stability and metabolic activity. Rheological measurements showed that viscoelasticity of biofilm varies with biofilm age, presenting more elastic behaviour for mature biofilm. Whilst commonly used magnetic particle induction technique [398] enabled measurements of surface adhesion (a proxy for sediment stabilization) at high-resolution (< 5mm), the measurements were limited to the surface of low-profile biofilms, with no protruding filaments due to limited optical access. To facilitate the comparison between different experimental studies and to obtain realistic (i.e., horizontally applied stress) results representative for natural conditions, straight laboratory flumes are still the most reliable way to obtain critical erosion thresholds of sediments.

Investigating the role of site-specific sedimentological parameters on erodibility of natural sediments

Whilst controlled laboratory experiments are ideal to understand complex erosion processes and flow–biofilm–sediment interactions, there exists no generic relationship between erosion thresholds and sedimentological properties. In order to explore the relative roles of site-specific sedimentological parameters on depth-variable erosion thresholds, 22 natural sediment cores were collected from two reservoirs (GBS, SBT) in Germany. By characterizing physico-chemical and biological sediment properties as well as measuring erosion thresholds in a straight laboratory flume utilizing an advanced photogrammetric measurement method relying on a structured-light approach, multivariate relationships between sedimentological properties and two types of erosion thresholds at various sediment layers were observed. The sedimentological properties of sediment cores collected from GBS and SBT were different. The clay-dominated

sediments of the GBS with comparatively low total organic carbon and sand content were, on average, 10 times more stable compared to the sandy sediments of the SBT. Consequently, for the clay-dominated sediments, strong positive correlations were found between the erosion thresholds, clay content, and bulk density, supporting previous studies discussed in section 2.7.1. In contrast, the comparatively sandy sediment layers of SBT exhibited strong positive correlations between erosion thresholds and sand content, whereas the relationship was inverse with clay content. This is, in contrast, to the study by Gerbersdorf et al. [193] and Gerbersdorf et al. [194], who reported negative relationships between sand content and critical shear stress in a similar riverine environment. Interestingly, a negative correlation between organic carbon content and erosion thresholds was also observed, which is opposed to the other studies in riverine environments [31, 193, 194]. Furthermore, EPS and chlorophyll-a were not good indicators for the erosion thresholds, suggesting an ambiguous influence of biology and its varying interaction with other physico-chemical parameters. Overall, the results stress the need to further investigate the site-specific influence of sedimentological properties and their relative roles on sediment erodibility at various natural environments in order to predict the behavior of fine cohesive sediments and develop sediment management scenarios (e.g., reservoir flushing) [351, 352] .

5 References

[1]   Hurther, D., and Lemmin, U. "A Correction Method for Turbulence Measurements with a 3D Acoustic Doppler Velocity Profiler." *Journal of Atmospheric and Oceanic Technology*, Vol. 18, No. 3, 2001, pp. 446–458. https://doi.org/10.1175/1520-0426(2001)018<0446:ACMFTM>2.0.CO;2.

[2]   Nelson, J. "Erosion and Sedimentation." *EOS Transactions*, Vol. 80, 1999, pp. 176–177. https://doi.org/10.1029/99EO00128.

[3]   Lorke, A., and Macintyre, S. The Benthic Boundary Layer (in Rivers, Lakes, and Reservoirs). 2009.

[4]   Jones, S. "Goo, Glue, and Grain Binding: Importance of Biofilms for Diagenesis in Sandstones." *Geology*, Vol. 45, No. 10, 2017, pp. 959–960. https://doi.org/10.1130/focus102017.1.

[5]   Paterson, D. M., Hope, J. A., Kenworthy, J., Biles, C. L., and Gerbersdorf, S. U. "Form, Function and Physics: The Ecology of Biogenic Stabilisation." *Journal of Soils and Sediments*, Vol. 18, No. 10, 2018, pp. 3044–3054. https://doi.org/10.1007/s11368-018-2005-4.

[6]   Battin, T. J., Besemer, K., Bengtsson, M. M., Romani, A. M., and Packmann, A. I. "The Ecology and Biogeochemistry of Stream Biofilms." *Nature Reviews Microbiology*, Vol. 14, No. 4, 2016, pp. 251–263. https://doi.org/10.1038/nrmicro.2016.15.

[7]   Flemming, H.-C., and Wuertz, S. "Bacteria and Archaea on Earth and Their Abundance in Biofilms." *Nature Reviews Microbiology*, Vol. 17, No. 4, 2019, pp. 247–260. https://doi.org/10.1038/s41579-019-0158-9.

[8]   Battin, T. J. "Hydrodynamics Is a Major Determinant of Streambed Biofilm Activity: From the Sediment to the Reach Scale." *Limnology and Oceanography*, Vol. 45, No. 6, 2000, pp. 1308–1319. https://doi.org/10.4319/lo.2000.45.6.1308.

[9]   Fang, H., Fazeli, M., Cheng, W., Huang, L., and Hu, H. "Biostabilization and Transport of Cohesive Sediment Deposits in the Three Gorges Reservoir." *PLoS ONE*, Vol. 10, No. 11, 2015. https://doi.org/10.1371/journal.pone.0142673.

[10]   Hughes, S. A. *Physical Models and Laboratory Techniques in Coastal Engineering*. World Scientific, 1993.

[11] Mulligan, M., van Soesbergen, A., and Sáenz, L. "GOODD, a Global Dataset of More than 38,000 Georeferenced Dams." *Scientific Data*, Vol. 7, No. 1, 2020, p. 31. https://doi.org/10.1038/s41597-020-0362-5.

[12] Nilsson, C., Reidy, C. A., Dynesius, M., and Revenga, C. "Fragmentation and Flow Regulation of the World's Large River Systems." *Science*, Vol. 308, No. 5720, 2005, pp. 405–408. https://doi.org/10.1126/science.1107887.

[13] Syvitski, J. P. M., Vörösmarty, C. J., Kettner, A. J., and Green, P. "Impact of Humans on the Flux of Terrestrial Sediment to the Global Coastal Ocean." *Science*, Vol. 308, No. 5720, 2005, pp. 376–380. https://doi.org/10.1126/science.1109454.

[14] Gernaat, D. E. H. J., Bogaart, P. W., Vuuren, D. P. van, Biemans, H., and Niessink, R. "High-Resolution Assessment of Global Technical and Economic Hydropower Potential." *Nature Energy*, Vol. 2, No. 10, 2017, pp. 821–828. https://doi.org/10.1038/s41560-017-0006-y.

[15] Zarfl, C., Lumsdon, A. E., Berlekamp, J., Tydecks, L., and Tockner, K. "A Global Boom in Hydropower Dam Construction." *Aquatic Sciences*, Vol. 77, No. 1, 2015, pp. 161–170. https://doi.org/10.1007/s00027-014-0377-0.

[16] Dey, S., and Ali, S. Z. "Bed Sediment Entrainment by Streamflow: State of the Science." *Sedimentology*, Vol. 66, No. 5, 2019, pp. 1449–1485. https://doi.org/10.1111/sed.12566.

[17] Mehta, A. J., and McAnally, W. H. "Fine Grained Sediment Transport." 2013, pp. 253–306. https://doi.org/10.1061/9780784408148.ch04.

[18] Black, K. S., Tolhurst, T. J., Paterson, D. M., and Hagerthey, S. E. "Working with Natural Cohesive Sediments." *Journal of Hydraulic Engineering*, Vol. 128, No. 1, 2002, pp. 2–8. https://doi.org/10.1061/(ASCE)0733-9429(2002)128:1(2).

[19] Winterwerp, J. C., and van Kesteren, W. G. M. The Nature of Cohesive Sediment. In *Developments in Sedimentology*, Elsevier, 2004, pp. 29–85.

[20] Bosboom, J., and Stive, M. J. F. *Coastal Dynamics*. 2021.

[21] Raudkivi, A. J. *Loose Boundary Hydraulics*. CRC Press, 1998.

[22] Grabowski, R. C., Droppo, I. G., and Wharton, G. "Erodibility of Cohesive Sediment: The Importance of Sediment Properties." *Earth-Science Reviews*, Vol. 105, No. 3, 2011, pp. 101–120. https://doi.org/10.1016/j.earscirev.2011.01.008.

[23] Statzner, B., Arens, M.-F., Champagne, J.-Y., Morel, R., and Herouin, E. "Silk-Producing Stream Insects and Gravel Erosion: Significant Biological Effects on Critical Shear Stress." *Water Resources Research*, Vol. 35, No. 11, 1999, pp. 3495–3506. https://doi.org/10.1029/1999WR900196.

[24] Gerbersdorf, S. U., Koca, K., de Beer, D., Chennu, A., Noss, C., Risse-Buhl, U., Weitere, M., Eiff, O., Wagner, M., Aberle, J., Schweikert, M., and Terheiden, K. "Exploring Flow-Biofilm-Sediment Interactions: Assessment of Current Status and Future Challenges." *Water Research*, Vol. 185, 2020, p. 116182. https://doi.org/10.1016/j.watres.2020.116182.

[25] de Brouwer, J. F. C., Wolfstein, K., Ruddy, G. K., Jones, T. E. R., and Stal, L. J. "Biogenic Stabilization of Intertidal Sediments: The Importance of Extracellular

Polymeric Substances Produced by Benthic Diatoms." *Microbial Ecology*, Vol. 49, No. 4, 2005, pp. 501–512. https://doi.org/10.1007/s00248-004-0020-z.

[26] Gerbersdorf, S. U., and Wieprecht, S. "Biostabilization of Cohesive Sediments: Revisiting the Role of Abiotic Conditions, Physiology and Diversity of Microbes, Polymeric Secretion, and Biofilm Architecture." *Geobiology*, Vol. 13, No. 1, 2015, pp. 68–97. https://doi.org/10.1111/gbi.12115.

[27] Paterson, D. M. Biological Mediation of Sediment Erodibility: Ecology and Physical Dynamics. In *Cohesive Sediments*, John Wiley and Sons, 1997, pp. 215–229.

[28] Roncoroni, M., Brandani, J., Battin, T. I., and Lane, S. N. "Ecosystem Engineers: Biofilms and the Ontogeny of Glacier Floodplain Ecosystems." *Wiley Interdisciplinary Reviews: Water*, Vol. 6, No. 6, 2019, p. e1390. https://doi.org/10.1002/wat2.1390.

[29] Paterson, D. M. "Short-Term Changes in the Erodibility of Intertidal Cohesive Sediments Related to the Migratory Behavior of Epipelic Diatoms." *Limnology and Oceanography*, Vol. 34, No. 1, 1989, pp. 223–234. https://doi.org/10.4319/lo.1989.34.1.0223.

[30] Chen, X. D., Zhang, C. K., Zhou, Z., Gong, Z., Zhou, J. J., Tao, J. F., Paterson, D. M., and Feng, Q. "Stabilizing Effects of Bacterial Biofilms: EPS Penetration and Redistribution of Bed Stability Down the Sediment Profile." *Journal of Geophysical Research: Biogeosciences*, Vol. 122, No. 12, 2017, pp. 3113–3125. https://doi.org/10.1002/2017JG004050.

[31] Aberle, J., Nikora, V., and Walters, R. "Effects of Bed Material Properties on Cohesive Sediment Erosion." *Marine Geology*, Vol. 207, No. 1, 2004, pp. 83–93. https://doi.org/10.1016/j.margeo.2004.03.012.

[32] Debnath, K., Nikora, V., Aberle, J., Westrich, B., and Muste, M. "Erosion of Cohesive Sediments: Resuspension, Bed Load, and Erosion Patterns from Field Experiments." *Journal of Hydraulic Engineering*, Vol. 133, No. 5, 2007, pp. 508–520. https://doi.org/10.1061/(ASCE)0733-9429(2007)133:5(508).

[33] Wynn, T. M., and Mostaghimi, S. "Effects of Riparian Vegetation on Stream Bank Subaerial Processes in Southwestern Virginia, USA." *Earth Surface Processes and Landforms*, Vol. 31, No. 4, 2006, pp. 399–413. https://doi.org/10.1002/esp.1252.

[34] Perera, C., Smith, J., Wu, W., Perkey, D., and Priestas, A. "Erosion Rate of Sand and Mud Mixtures." *International Journal of Sediment Research*, Vol. 35, No. 6, 2020, pp. 563–575. https://doi.org/10.1016/j.ijsrc.2020.06.004.

[35] Carvalho, L., Mackay, E. B., Cardoso, A. C., Baattrup-Pedersen, A., Birk, S., Blackstock, K. L., Borics, G., Borja, A., Feld, C. K., Ferreira, M. T., Globevnik, L., Grizzetti, B., Hendry, S., Hering, D., Kelly, M., Langaas, S., Meissner, K., Panagopoulos, Y., Penning, E., Rouillard, J., Sabater, S., Schmedtje, U., Spears, B. M., Venohr, M., van de Bund, W., and Solheim, A. L. "Protecting and Restoring Europe's Waters: An Analysis of the Future Development Needs of the Water Framework Directive." *Science of The Total Environment*, Vol. 658, 2019, pp. 1228–1238. https://doi.org/10.1016/j.scitotenv.2018.12.255.

[36]   Allan, D. J., and Castillo, M. M. *Stream Ecology - Structure and Function of Running Waters*. Springer, Dordrecht, The Netherlands, 2007.

[37]   Besemer, K. "Biodiversity, Community Structure and Function of Biofilms in Stream Ecosystems." *Research in microbiology*, Vol. 166, No. 10, 2015, pp. 774–781. https://doi.org/10.1016/j.resmic.2015.05.006.

[38]   Loreau, M., Naeem, S., Inchausti, P., Bengtsson, J., Grime, J. P., Hector, A., Hooper, D. U., Huston, M. A., Raffaelli, D., Schmid, B., Tilman, D., and Wardle, D. A. "Biodiversity and Ecosystem Functioning: Current Knowledge and Future Challenges." *Science*, Vol. 294, No. 5543, 2001, p. 804. https://doi.org/10.1126/science.1064088.

[39]   Larned, S. T., Packman, A. I., Plew, D. R., and Vopel, K. "Interactions between the Mat-Forming Alga Didymosphenia Geminata and Its Hydrodynamic Environment." *Limnology and Oceanography: Fluids and Environments*, Vol. 1, No. 1, 2011, pp. 4–22. https://doi.org/10.1215/21573698-1152081.

[40]   Nikora, V. "Hydrodynamics of Aquatic Ecosystems: An Interface between Ecology, Biomechanics and Environmental Fluid Mechanics." *River Research and Applications*, Vol. 26, No. 4, 2010, pp. 367–384. https://doi.org/10.1002/rra.1291.

[41]   Rice, S. P., Lancaster, J., and Kemp, P. "Experimentation at the Interface of Fluvial Geomorphology, Stream Ecology and Hydraulic Engineering and the Development of an Effective, Interdisciplinary River Science." *Earth Surface Processes and Landforms*, Vol. 35, No. 1, 2010, pp. 64–77. https://doi.org/10.1002/esp.1838.

[42]   Viles, H. "Biogeomorphology: Past, Present and Future." *Geomorphology*, Vol. 366, 2020, p. 106809. https://doi.org/10.1016/j.geomorph.2019.06.022.

[43]   Koca, K., Noss, C., Anlanger, C., Brand, A., and Lorke, A. "Performance of the Vectrino Profiler at the Sediment–Water Interface." *Journal of Hydraulic Research*, 2017, pp. 1–9. https://doi.org/10.1080/00221686.2016.1275049.

[44]   Beckers, F., Koca, K., Haun, S., Noack, M., Gerbersdorf, S. U., and Wieprecht, S. "Functional Relationships between Critical Erosion Thresholds of Fine Reservoir Sediments and Their Sedimentological Characteristics." *Journal of Hydraulic Engineering*, Forthcoming. https://doi.org/10.1061/(ASCE)HY.1943-7900.00019864.

[45]   Sherman, D., Davis, L., and Namikas, S. L. 1.13 Sediments and Sediment Transport. In *Treatise on Geomorphology*, 2013, pp. 233–256.

[46]   Wentworth, C. K. "A Scale of Grade and Class Terms for Clastic Sediments." *The Journal of Geology*, Vol. 30, No. 5, 1922, pp. 377–392.

[47]   Velde, B., Ed. *Origin and Mineralogy of Clays: Clays and the Environment*. Springer-Verlag, Berlin Heidelberg, 1995.

[48]   Santamarina, J. C., Klein, K. A., and Fam, M. A. *Soils and Waves: Particulate Materials Behavior, Characterization and Process Monitoring*. Wiley, Chichester ; New York, 2001.

[49]   Mantz, P. A. "Incipient Transport of Fine Grains and Flakes by Fluids — Extended Shields Diagram." *Journal of the Hydraulics Division*, Vol. 103, No. 6, 1977, pp. 601–615.

[50]   Droppo, I. G., and Stone, M. "In-Channel Surficial Fine-Grained Sediment Laminae. Part I: Physical Characteristics and Formational Processes." *Hydrological Processes*, Vol. 8, No. 2, 1994, pp. 101–111. https://doi.org/10.1002/hyp.3360080202.

[51]   Wang, X. H., and Andutta, F. P. "Sediment Transport Dynamics in Ports, Estuaries and Other Coastal Environments." *Sediment Transport Processes and Their Modelling Applications*, 2013. https://doi.org/10.5772/51022.

[52]   Winterwerp, J. C., and van Kesteren, W. G. M. Flocculation Processes. In *Developments in Sedimentology*, Elsevier, 2004, pp. 87–119.

[53]   Einstein, H. A. "Formulas for the Transportation of Bed Load." *Transactions of the American Society of Civil Engineers*, Vol. 107, No. 1, 1942, pp. 561–577.

[54]   Dey, S., and Papanicolaou, A. "Sediment Threshold under Stream Flow: A State-of-the-Art Review." *KSCE Journal of Civil Engineering*, Vol. 12, No. 1, 2008, pp. 45–60. https://doi.org/10.1007/s12205-008-8045-3.

[55]   Pähtz, T., Clark, A. H., Valyrakis, M., and Durán, O. "The Physics of Sediment Transport Initiation, Cessation, and Entrainment Across Aeolian and Fluvial Environments." *Reviews of Geophysics*, Vol. 58, No. 1, 2020, p. e2019RG000679. https://doi.org/10.1029/2019RG000679.

[56]   Papanicolaou, A. N., Diplas, P., Evaggelopoulos, N., and Fotopoulos, S. "Stochastic Incipient Motion Criterion for Spheres under Various Bed Packing Conditions." *Journal of Hydraulic Engineering*, Vol. 128, No. 4, 2002, pp. 369–380. https://doi.org/10.1061/(ASCE)0733-9429(2002)128:4(369).

[57]   Mitchell, J. K., and Soga, K. *Fundamentals of Soil Behavior*. Wiley, Hoboken, N.J, 2005.

[58]   Le Hir, P., Monbet, Y., and Orvain, F. "Sediment Erodability in Sediment Transport Modelling: Can We Account for Biota Effects?" *Continental Shelf Research*, Vol. 27, No. 8, 2007, pp. 1116–1142. https://doi.org/10.1016/j.csr.2005.11.016.

[59]   Van Rijn, L. C. *Principles of Sediment Transport in Rivers, Estuaries and Coastal Seas*. Delft Hydraulics, Universiteit Utrecht, Aqua Publications, 1993.

[60]   Winterwerp, J. C., and van Kesteren, W. G. M. Sediment-Fluid Interaction. In *Developments in Sedimentology*, Elsevier, 2004, pp. 161–210.

[61]   Yang, Y., Gao, S., Wang, Y. P., Jia, J., Xiong, J., and Zhou, L. "Revisiting the Problem of Sediment Motion Threshold." *Continental Shelf Research*, Vol. 187, 2019, p. 103960. https://doi.org/10.1016/j.csr.2019.103960.

[62]   Mehta, A. J. Laboratory Studies on Cohesive Sediment Deposition and Erosion. Berlin, Heidelberg, 1988.

[63]   Dey, S. *Fluvial Hydrodynamics - Hydrodynamic and Sediment Transport Phenomena*. Springer, 2014.

[64] Vignaga, E., Sloan, D. M., Luo, X., Haynes, H., Phoenix, V. R., and Sloan, W. T. "Erosion of Biofilm-Bound Fluvial Sediments." *Nature Geoscience*, Vol. 6, No. 9, 2013, pp. 770–774. https://doi.org/10.1038/ngeo1891.

[65] Reynolds, O. "III. An Experimental Investigation of the Circumstances Which Determine Whether the Motion of Water Shall Be Direct or Sinuous, and of the Law of Resistance in Parallel Channels." *Proceedings of the Royal Society of London*, Vol. 35, Nos. 224–226, 1883, pp. 84–99. https://doi.org/10.1098/rspl.1883.0018.

[66] Kramer, H. "Sand Mixtures and Sand Movement in Fluvial Model." *Transactions of the American Society of Civil Engineers*, Vol. 100, No. 1, 1935, pp. 798–838.

[67] Paintal, A. S. "Concept Of Critical Shear Stress In Loose Boundary Open Channels." *Journal of Hydraulic Research*, Vol. 9, No. 1, 1971, pp. 91–113. https://doi.org/10.1080/00221687109500339.

[68] Shields, A. Application of Similarity Principles and Turbulence Research to Bed-Load Movement. https://resolver.caltech.edu/CaltechKHR:HydroLabpub167. Accessed Jun. 10, 2020.

[69] Andrews, E. D. "Entrainment of Gravel from Naturally Sorted Riverbed Material." *GSA Bulletin*, Vol. 94, No. 10, 1983, pp. 1225–1231. https://doi.org/10.1130/0016-7606(1983)94<1225:EOGFNS>2.0.CO;2.

[70] Carling, P. A. "Threshold of Coarse Sediment Transport in Broad and Narrow Natural Streams." *Earth Surface Processes and Landforms*, Vol. 8, No. 1, 1983, pp. 1–18. https://doi.org/10.1002/esp.3290080102.

[71] Gilbert, G. K., and Murphy, E. C. *The Transportation of Debris by Running Water*. Publication 86. U.S. Geological Survey, 1914.

[72] Yalin, M. S., and Karahan, E. "Inception of Sediment Transport." *Journal of the Hydraulics Division*, Vol. 105, No. 11, 1979, pp. 1433–1443.

[73] Dancey, C. L., Diplas, P., Papanicolaou, A., and Bala, M. "Probability of Individual Grain Movement and Threshold Condition." *Journal of Hydraulic Engineering*, Vol. 128, No. 12, 2002, pp. 1069–1075. https://doi.org/10.1061/(ASCE)0733-9429(2002)128:12(1069).

[74] Dey, S., and Raikar, R. V. "Characteristics of Loose Rough Boundary Streams at Near-Threshold." *Journal of Hydraulic Engineering*, Vol. 133, No. 3, 2007, pp. 288–304. https://doi.org/10.1061/(ASCE)0733-9429(2007)133:3(288).

[75] Dixit, S., and Patel, P. L. "Stochastic Nature of Turbulence over Mobile Bed Channels." *ISH Journal of Hydraulic Engineering*, Vol. 26, No. 1, 2020, pp. 104–111. https://doi.org/10.1080/09715010.2018.1460628.

[76] Grass, A. J. *The Influence of Boundary Layer Turbulence on the Mechanics of Sediment Transport**. CRC Press, 1983.

[77] Kalinske, A. A. "Movement of Sediment as Bed Load in Rivers." *Eos, Transactions American Geophysical Union*, Vol. 28, No. 4, 1947, pp. 615–620. https://doi.org/10.1029/TR028i004p00615.

[78] Spiliotis, M., Kitsikoudis, V., Ozgur Kirca, V. S., and Hrissanthou, V. "Fuzzy Threshold for the Initiation of Sediment Motion." *Applied Soft Computing*, Vol. 72, 2018, pp. 312–320. https://doi.org/10.1016/j.asoc.2018.08.006.

[79] Sumer, B. M., and Deigaard, R. "Particle Motions near the Bottom in Turbulent Flow in an Open Channel. Part 2." *Journal of Fluid Mechanics*, Vol. 109, 1981, pp. 311–337. https://doi.org/10.1017/S0022112081001092.

[80] Sumer, B. M., and Oguz, B. "Particle Motions near the Bottom in Turbulent Flow in an Open Channel." *Journal of Fluid Mechanics*, Vol. 86, No. 1, 1978, pp. 109–127. https://doi.org/10.1017/S0022112078001020.

[81] Wu, F.-C., and Chou, Y.-J. "Rolling and Lifting Probabilities for Sediment Entrainment." *Journal of Hydraulic Engineering*, Vol. 129, No. 2, 2003, pp. 110–119. https://doi.org/10.1061/(ASCE)0733-9429(2003)129:2(110).

[82] Zanke, U. "On the Influence of Turbulence on the Initiation of Sediment Motion." *International Journal of Sediment Research*, Vol. 18, 2003.

[83] Papanicolaou, A. N., Diplas, P., Dancey, C. L., and Balakrishnan, M. "Surface Roughness Effects in Near-Bed Turbulence: Implications to Sediment Entrainment." *Journal of Engineering Mechanics*, Vol. 127, No. 3, 2001, pp. 211–218. https://doi.org/10.1061/(ASCE)0733-9399(2001)127:3(211).

[84] Bridge, J. S., and Bennett, S. J. "A Model for the Entrainment and Transport of Sediment Grains of Mixed Sizes, Shapes, and Densities." *Water Resources Research*, Vol. 28, No. 2, 1992, pp. 337–363. https://doi.org/10.1029/91WR02570.

[85] Cassel, M., Lavé, J., Recking, A., Malavoi, J.-R., and Piégay, H. "Bedload Transport in Rivers, Size Matters but so Does Shape." *Scientific Reports*, Vol. 11, No. 1, 2021, p. 508. https://doi.org/10.1038/s41598-020-79930-7.

[86] Komar, P. D., and Li, Z. "Pivoting Analyses of the Selective Entrainment of Sediments by Shape and Size with Application to Gravel Threshold." *Sedimentology*, Vol. 33, No. 3, 1986, pp. 425–436. https://doi.org/10.1111/j.1365-3091.1986.tb00546.x.

[87] Lane, E. W., and Carlson, E. J. "Some Observations on the Effect of Particle Shape on the Movement of Coarse Sediments." *Eos, Transactions American Geophysical Union*, Vol. 35, No. 3, 1954, pp. 453–462. https://doi.org/10.1029/TR035i003p00453.

[88] Kirchner, J. W., Dietrich, W. E., Iseya, F., and Ikeda, H. "The Variability of Critical Shear Stress, Friction Angle, and Grain Protrusion in Water-Worked Sediments." *Sedimentology*, Vol. 37, No. 4, 1990, pp. 647–672. https://doi.org/10.1111/j.1365-3091.1990.tb00627.x.

[89] McEwan, I., and Heald, J. "Discrete Particle Modeling of Entrainment from Flat Uniformly Sized Sediment Beds." *Journal of Hydraulic Engineering*, Vol. 127, No. 7, 2001, pp. 588–597. https://doi.org/10.1061/(ASCE)0733-9429(2001)127:7(588).

[90] Dey, S., and Ali, S. Z. "Stochastic Mechanics of Loose Boundary Particle Transport in Turbulent Flow." *Physics of Fluids*, Vol. 29, No. 5, 2017, p. 055103. https://doi.org/10.1063/1.4984042.

[91] Frank, D., Foster, D., Sou, I. M., Calantoni, J., and Chou, P. "Lagrangian Measurements of Incipient Motion in Oscillatory Flows." *Journal of Geophysical Research: Oceans*, Vol. 120, No. 1, 2015, pp. 244–256. https://doi.org/10.1002/2014JC010183.

[92] Neill, C. R. Mean Velocity Criterion for Scour of Coarse Uniform Bed Material. No. 3, Fort Collins, CO, USA, 1967, pp. 46–54.

[93] Rakoczi, L. Influence of Grain-Size Composition on the Incipient Motion and Self-Pavement of Bed Materials. No. 2, Delft, Netherlands, 1975, pp. 150–157.

[94] Laursen, E. M. "Discussion of 'The Legend of A. F. Shields' by Emmett M. Laursen." *Journal of Hydraulic Engineering*, Vol. 126, No. 9, 2000, pp. 720–721. https://doi.org/10.1061/(ASCE)0733-9429(2000)126:9(720).

[95] Misri, R. L., Garde, R. J., and Ranga-Raju, K. G. Experiments on Bed Load Transport of Nonuniform Sands and Gravels. Beijing, China, 1983.

[96] Petit, F. "Dimensionless Critical Shear Stress Evaluation from Flume Experiments Using Different Gravel Beds." *Earth Surface Processes and Landforms*, Vol. 19, No. 6, 1994, pp. 565–576. https://doi.org/10.1002/esp.3290190608.

[97] White, S. J. "Plane Bed Thresholds of Fine Grained Sediments." *Nature*, Vol. 228, No. 5267, 1970, pp. 152–153. https://doi.org/10.1038/228152a0.

[98] Beheshti, A. A., and Ataie-Ashtiani, B. "Analysis of Threshold and Incipient Conditions for Sediment Movement." *Coastal Engineering*, Vol. 55, No. 5, 2008, pp. 423–430. https://doi.org/10.1016/j.coastaleng.2008.01.003.

[99] Parker, G., Klingeman, P. C., and McLean, D. G. "Bedload and Size Distribution in Paved Gravel-Bed Streams." *Journal of the Hydraulics Division*, Vol. 108, No. 4, 1982, pp. 544–571.

[100] Komar, P. D. "Selective Grain Entrainment by a Current from a Bed of Mixed Sizes; a Reanalysis." *Journal of Sedimentary Research*, Vol. 57, No. 2, 1987, pp. 203–211. https://doi.org/10.1306/212F8AE4-2B24-11D7-8648000102C1865D.

[101] Casey, H. J. *Über Geschiebebewegung*. Preuß. Versuchsanst. f. Wasserbau u. Schiffbau, 1935.

[102] Kramer, H. *Modellgeschiebe Und Schleppkraft [Modelling Bed Load and Drag Force]*. Preuß ische Versuchsanstalt für Wasserbau und Schiffbau, 1932.

[103] USWES. *Study of River-Bed Material and Their Use with Special Reference to the Lower Mississippi River*. Publication Paper 17. US Waterways Experimental Station, Vicksburg, Mississippi, USA, 1935.

[104] Buffington, J. M. "The Legend of A. F. Shields." *Journal of Hydraulic Engineering*, Vol. 125, No. 4, 1999, pp. 376–387. https://doi.org/10.1061/(ASCE)0733-9429(1999)125:4(376).

[105] Buffington, J. M., and Montgomery, D. R. "A Systematic Analysis of Eight Decades of Incipient Motion Studies, with Special Reference to Gravel-Bedded Rivers." *Water Resources Research*, Vol. 33, No. 8, 1997, pp. 1993–2029. https://doi.org/10.1029/96WR03190.

[106] Taylor, B. D., and Vanoni, V. A. "Temperature Effects in Low-Transport, Flat-Bed Flows." *Journal of the Hydraulics Division*, Vol. 98, No. 8, 1972, pp. 1427–1445.

[107] Wilcock, P. R. "Methods for Estimating the Critical Shear Stress of Individual Fractions in Mixed-Size Sediment." *Water Resources Research*, Vol. 24, No. 7, 1988, pp. 1127–1135. https://doi.org/10.1029/WR024i007p01127.

[108] Wathen, S. J., Ferguson, R. I., Hoey, T. B., and Werritty, A. "Unequal Mobility of Gravel and Sand in Weakly Bimodal River Sediments." *Water Resources Research*, Vol. 31, No. 8, 1995, pp. 2087–2096. https://doi.org/10.1029/95WR01229.

[109] Shvidchenko, A. B., Pender, G., and Hoey, T. B. "Critical Shear Stress for Incipient Motion of Sand/Gravel Streambeds." *Water Resources Research*, Vol. 37, No. 8, 2001, pp. 2273–2283. https://doi.org/10.1029/2000WR000036.

[110] Diplas, P., Dancey, C. L., Celik, A. O., Valyrakis, M., Greer, K., and Akar, T. "The Role of Impulse on the Initiation of Particle Movement Under Turbulent Flow Conditions." *Science*, Vol. 322, No. 5902, 2008, pp. 717–720. https://doi.org/10.1126/science.1158954.

[111] Schoklitsch, A. *Handbuch des Wasserbaues I*. Springer-Verlag, Wien, 1950.

[112] Forchheimer, P. *Hydraulik*. Leipzig, Teubner, 1914.

[113] Hjulström, F. *Studies of the Morphological Activity of Rivers as Illustrated by the River Fyris*. Almqvist & Wiksells, 1935.

[114] Bagnold, R. A. "An Empirical Correlation of Bedload Transport Rates in Flumes and Natural Rivers." *Proceedings of the Royal Society of London. A. Mathematical and Physical Sciences*, Vol. 372, No. 1751, 1980, pp. 453–473. https://doi.org/10.1098/rspa.1980.0122.

[115] Sundborg, Å. "The River Klarälven a Study of Fluvial Processes." *Geografiska Annaler*, Vol. 38, Nos. 2–3, 1956, pp. 125–316. https://doi.org/10.1080/20014422.1956.11880887.

[116] Miedema, S. A. Constructing the Shields Curve: Part C — Cohesion by Silt, Hjulstrom, Sundborg. Presented at the ASME 2013 32nd International Conference on Ocean, Offshore and Arctic Engineering, 2013.

[117] Southard, J. Introduction to Fluid Motions, Sediment Transport, and Current-Generated Sedimentary Structures. *MIT OpenCourseWare*. https://ocw.mit.edu/courses/earth-atmospheric-and-planetary-sciences/12-090-introduction-to-fluid-motions-sediment-transport-and-current-generated-sedimentary-structures-fall-2006/. Accessed Feb. 20, 2021.

[118] Graba, M., Sauvage, S., Moulin, F. Y., Urrea, G., Sabater, S., and Sanchez-Pérez, J. M. "Interaction between Local Hydrodynamics and Algal Community in Epilithic Biofilm." *Water Research*, Vol. 47, No. 7, 2013, pp. 2153–2163. https://doi.org/10.1016/j.watres.2013.01.011.

[119] Graba, M., Moulin, F. Y., Boulêtreau, S., Garabétian, F., Kettab, A., Eiff, O., Sánchez-Pérez, J. M., and Sauvage, S. "Effect of Near-Bed Turbulence on Chronic Detachment of Epilithic Biofilm: Experimental and Modeling

Approaches." *Water Resources Research*, Vol. 46, No. 11, 2010. https://doi.org/10.1029/2009WR008679.

[120] Nikora, V. I., Goring, D. G., and Biggs, B. J. F. "Some Observations of the Effects of Micro-Organisms Growing on the Bed of an Open Channel on the Turbulence Properties." *Journal of Fluid Mechanics*, Vol. 450, 2002, pp. 317–341. https://doi.org/10.1017/S0022112001006486.

[121] Garcia, M., Ed. *Sedimentation Engineering: Processes, Measurements, Modeling, and Practice*. American Society of Civil Engineers, Reston, VA, 2008.

[122] Vanoni, V. A. *Sedimentation Engineering*. American Society of Civil Engineers, Reston, Va, 2006.

[123] Yalin, M. S. *Mechanics of Sediment Transport*. Pergamon Press, Oxford ; New York, 1977.

[124] Nikuradse, J. "Strömungsgesetze in Rauhen Rohren [Laws of Flow in Rough Pipes]." *VDI Forschungsheft, Beilage zu "Forschung auf dem Gebiete des Ingenieurwesens,"* Vol. Ausgabe B, Band 4, No. 361, 1933, p. 26.

[125] Andrewartha, J., Perkins, K., Sargison, J., Osborn, J., Walker, G., Henderson, A., and Hallegraeff, G. "Drag Force and Surface Roughness Measurements on Freshwater Biofouled Surfaces." *Biofouling*, Vol. 26, No. 4, 2010, pp. 487–496. https://doi.org/10.1080/08927014.2010.482208.

[126] Schultz, M. P. "Effects of Coating Roughness and Biofouling on Ship Resistance and Powering." *Biofouling*, Vol. 23, No. 5, 2007, pp. 331–341. https://doi.org/10.1080/08927010701461974.

[127] Schultz, M. P., Walker, J. M., Steppe, C. N., and Flack, K. A. "Impact of Diatomaceous Biofilms on the Frictional Drag of Fouling-Release Coatings." *Biofouling*, Vol. 31, Nos. 9–10, 2015, pp. 759–773. https://doi.org/10.1080/08927014.2015.1108407.

[128] Walker, J. M., Sargison, J. E., and Henderson, A. D. "Turbulent Boundary-Layer Structure of Flows over Freshwater Biofilms." *Experiments in Fluids*, Vol. 54, No. 12, 2013, p. 1628. https://doi.org/10.1007/s00348-013-1628-x.

[129] Frey, P., and Church, M. "How River Beds Move." *Science*, Vol. 325, No. 5947, 2009, pp. 1509–1510. https://doi.org/10.1126/science.1178516.

[130] Righetti, M., and Lucarelli, C. "May the Shields Theory Be Extended to Cohesive and Adhesive Benthic Sediments?" *Journal of Geophysical Research: Oceans*, Vol. 112, No. C5, 2007. https://doi.org/10.1029/2006JC003669.

[131] Koca, K., Wieprecht, S., and Gerbersdorf, S. U. Biostabilization of Fine Sediment in River and Reservoirs: Exploring the Interplay between Flow, Substrate and Community. Presented at the International Conferrence onCohesive Sediment Transport Processes 2019 (INTERCOH), Istanbul, Turkey, 13 -17.10.2019, 2019.

[132] Thom, M., Schmidt, H., Gerbersdorf, S. U., and Wieprecht, S. "Seasonal Biostabilization and Erosion Behavior of Fluvial Biofilms under Different Hydrodynamic and Light Conditions." *International Journal of Sediment Research*, Vol. 30, No. 4, 2015, pp. 273–284. https://doi.org/10.1016/j.ijsrc.2015.03.015.

[133] Panagiotopoulos, I., Voulgaris, G., and Collins, M. B. "The: Influence of Clay on the Threshold of Movement of Fine Sandy Beds." *COAST ENG*, 1997. https://doi.org/10.1016/S0378-3839(97)00013-6.

[134] Wu, W., Perera, C., Smith, J., and Sanchez, A. "Critical Shear Stress for Erosion of Sand and Mud Mixtures." *Journal of Hydraulic Research*, Vol. 56, No. 1, 2018, pp. 96–110. https://doi.org/10.1080/00221686.2017.1300195.

[135] van Rijn, L. C. "Erodibility of Mud–Sand Bed Mixtures." *Journal of Hydraulic Engineering*, Vol. 146, No. 1, 2020, p. 04019050. https://doi.org/10.1061/(ASCE)HY.1943-7900.0001677.

[136] Winterwerp, J. C., Cornelisse, J. M., and Kuijper, C. Parameters to Characterize Natural Muds. Presented at the International Workshop on Cohesive Sediments, Brussels, Belgium, 1990.

[137] Yallop, M. L., de Winder, B., Paterson, D. M., and Stal, L. J. "Comparative Structure, Primary Production and Biogenic Stabilization of Cohesive and Non-Cohesive Marine Sediments Inhabited by Microphytobenthos." *Estuarine, Coastal and Shelf Science*, Vol. 39, No. 6, 1994, pp. 565–582. https://doi.org/10.1016/S0272-7714(06)80010-7.

[138] Mehta, A. J., Hayter, E. J., Parker, W. R., Krone, R. B., and Teeter, A. M. "Cohesive Sediment Transport. I: Process Description." *Journal of Hydraulic Engineering*, Vol. 115, No. 8, 1989, pp. 1076–1093. https://doi.org/10.1061/(ASCE)0733-9429(1989)115:8(1076).

[139] Mehta, A. J., and Partheniades, E. Resuspension of Deposited Cohesive Sediment Beds. Presented at the 18th Conference on Coastal Engineering, Cape Town, South Africa, 1982.

[140] Partheniades, E. "Erosion and Deposition of Cohesive Soils." *Journal of the Hydraulics Division*, Vol. Issue 1, 1965, pp. 105–139.

[141] Vermeyen, T. *Erosional and Depositional Characteristics of Cohesive Sediments Found in Elephant Butte Reservoir, New Mexico*. Publication Technical Report R-95-15. Water Resources Services, Technical Service Center, Bureau of Reclamation, Denver, CO, USA, 1995.

[142] Kothyari, U. C., and Jain, R. K. "Influence of Cohesion on the Incipient Motion Condition of Sediment Mixtures." *Water Resources Research*, Vol. 44, No. 4, 2008. https://doi.org/10.1029/2007WR006326.

[143] McNeil, J., Taylor, C., and Lick, W. "Measurements of Erosion of Undisturbed Bottom Sediments with Depth." *Journal of Hydraulic Engineering*, Vol. 122, No. 6, 1996, pp. 316–324. https://doi.org/10.1061/(ASCE)0733-9429(1996)122:6(316).

[144] Sanford, L. P., and Maa, J. P.-Y. "A Unified Erosion Formulation for Fine Sediments." *Marine Geology*, Vol. 179, No. 1, 2001, pp. 9–23. https://doi.org/10.1016/S0025-3227(01)00201-8.

[145] Widdows, J., Brinsley, M. D., Bowley, N., and Barrett, C. "A Benthic Annular Flume ForIn SituMeasurement of Suspension Feeding/Biodeposition Rates and Erosion Potential of Intertidal Cohesive Sediments." *Estuarine, Coastal and Shelf Science*, Vol. 46, No. 1, 1998, pp. 27–38. https://doi.org/10.1006/ecss.1997.0259.

[146] Lucas, C. H., Widdows, J., and Wall, L. "Relating Spatial and Temporal Variability in Sediment Chlorophyll a and Carbohydrate Distribution with Erodibility of a Tidal Flat." *Estuaries*, Vol. 26, 2003, pp. 885–893.

[147] WorleyParsons. *Roberts Ban Terminal 2*. Publication 307071-00790-01-EN-REP-4001. Worley Parsons Canada, 2015.

[148] Andersen, T. J., Lund-Hansen, L. C., Pejrup, M., Jensen, K. T., and Mouritsen, K. N. "Biologically Induced Differences in Erodibility and Aggregation of Subtidal and Intertidal Sediments: A Possible Cause for Seasonal Changes in Sediment Deposition." *Journal of Marine Systems*, Vol. 55, Nos. 3–4, 2005, pp. 123–138. https://doi.org/10.1016/j.jmarsys.2004.09.004.

[149] Tolhurst, T. J., Black, K. S., Paterson, D. M., Mitchener, H. J., Termaat, G. R., and Shayler, S. A. "A Comparison and Measurement Standardisation of Four in Situ Devices for Determining the Erosion Shear Stress of Intertidal Sediments." *Continental Shelf Research*, Vol. 20, No. 10, 2000, pp. 1397–1418. https://doi.org/10.1016/S0278-4343(00)00029-7.

[150] Tolhurst, T. J., Riethmüller, R., and Paterson, D. M. "In Situ versus Laboratory Analysis of Sediment Stability from Intertidal Mudflats." *Continental Shelf Research*, Vol. 20, No. 10, 2000, pp. 1317–1334. https://doi.org/10.1016/S0278-4343(00)00025-X.

[151] Noack, M., Schmid, G., Beckers, F., Haun, S., and Wieprecht, S. "PHOTOSED—PHOTOgrammetric Sediment Erosion Detection." *Geosciences*, Vol. 8, No. 7, 2018, p. 243. https://doi.org/10.3390/geosciences8070243.

[152] Beckers, F., Inskeep, C., Haun, S., Schmid, G., Wieprecht, S., and Noack, M. "High Spatio-Temporal Resolution Measurements of Cohesive Sediment Erosion." *Earth Surface Processes and Landforms*, 2020, p. esp.4889. https://doi.org/10.1002/esp.4889.

[153] Zhu, Y., Lu, J., Liao, H., Wang, J., Fan, B., and Yao, S. "Research on Cohesive Sediment Erosion by Flow: An Overview." *Science in China Series E: Technological Sciences*, Vol. 51, No. 11, 2008, p. 2001. https://doi.org/10.1007/s11431-008-0232-4.

[154] Grabowski, R. C., Droppo, I. G., and Wharton, G. "Estimation of Critical Shear Stress from Cohesive Strength Meter-Derived Erosion Thresholds." *Limnology and Oceanography: Methods*, Vol. 8, No. 12, 2010, pp. 678–685. https://doi.org/10.4319/lom.2010.8.0678.

[155] Arulanandan, K., Krone, R. B., and Loganathan, P. "Pore and Eroding Fluid Influences on Surface Erosion on Soil." *Journal of the Geotechnical Engineering Division*, Vol. 101, No. 1, 1975, pp. 51–66. https://doi.org/10.1061/AJGEB6.0000141.

[156] Gust, G. Fluid Velocity Measuring Instrument, , 1990.

[157] Sutherland, T. F., and Amos, C. L. "An In Situ Assessment of Seabed Stability in Baynes Sound, British Columbia, Canada." *Journal of Coastal Research*, Vol. 36, No. 3, 2020, pp. 472–486. https://doi.org/10.2112/JCOASTRES-D-19-00133.1.

[158] Aberle, J., Nikora, V., and Walters, R. "In Situ Measurement of Cohesive Sediment Dynamics with a Straight Benthic Flume." 2012, pp. 1–10. https://doi.org/10.1061/40655(2002)110.

[159] Black, K., and Cramp, A. "A Device to Examine the in Situ Response of Intertidal Cohesive Sediment Deposits to Fluid Shear." *Continental Shelf Research*, Vol. 15, No. 15, 1995, pp. 1945–1954. https://doi.org/10.1016/0278-4343(95)00003-J.

[160] He, C., Taylor, J. N., Rochfort, Q., and Nguyen, D. "A New Portable in Situ Flume for Measuring Critical Shear Stress on River Beds." *International Journal of Sediment Research*, Vol. 36, No. 2, 2021, pp. 235–242. https://doi.org/10.1016/j.ijsrc.2020.08.004.

[161] Houwing, E.-J., and van Rijn, L. C. "In Situ Erosion Flume (ISEF): Determination of Bed-Shear Stress and Erosion of a Kaolinite Bed." *Journal of Sea Research*, Vol. 39, No. 3, 1998, pp. 243–253. https://doi.org/10.1016/S1385-1101(98)00007-0.

[162] Grabowski, R. C. "Measuring the Shear Strength of Cohesive Sediment in the Field." *Geomorphological Techniques*, 2014, p. 7.

[163] Booij, R. "Measurements of the Flow Field in a Rotating Annular Flume." *Communications on hydraulic and geotechnical engineering, No. 1994-02*, 1994.

[164] Lemon, H. R. *Calibration of an Annular Flume for Measurements of Sediment Stability*. Master's Thesis. University of Stuttgart, Stuttgart, Germany, 2018.

[165] Briaud, J. L., Ting, F. C. K., Chen, H. C., Cao, Y., Han, S. W., and Kwak, K. W. "Erosion Function Apparatus for Scour Rate Predictions." *Journal of Geotechnical and Geoenvironmental Engineering*, Vol. 127, No. 2, 2001, pp. 105–113. https://doi.org/10.1061/(ASCE)1090-0241(2001)127:2(105).

[166] Gao, X., Wang, Q., Xu, C., and Su, R. "Experimental Study on Critical Shear Stress of Cohesive Soils and Soil Mixtures." *Transactions of the ASABE*, 2020. https://doi.org/doi: 10.13031/trans.14065.

[167] Roberts, J. D., Jepsen, R. A., and James, S. C. "Measurements of Sediment Erosion and Transport with the Adjustable Shear Stress Erosion and Transport Flume." *Journal of Hydraulic Engineering*, Vol. 129, No. 11, 2003, pp. 862–871.

[168] Kern, U., Haag, I., Schürlein, V., Holzwarth, M., and Westrich, B. "Ein Strömungskanal Zur Ermittlung Der Tiefenabhängigen Erosionsstabilität von Gewässersedimenten: Das SETEG-System." *Wasserwirtschaft*, Vol. 89, 1999, pp. 72–77.

[169] Thompson, C. E. L., Amos, C. L., Jones, T. E. R., and Chaplin, J. "The Manifestation of Fluid-Transmitted Bed Shear Stress in a Smooth Annular Flume-a Comparison of Methods." *Journal of Coastal Research*, Vol. 19, No. 4, 2003, pp. 1094–1103.

[170] Dey, S., Sarkar, S., and Solari, L. "Near-Bed Turbulence Characteristics at the Entrainment Threshold of Sediment Beds." *Journal of Hydraulic Engineering*, Vol. 137, No. 9, 2011, pp. 945–958. https://doi.org/10.1061/(ASCE)HY.1943-7900.0000396.

[171] Gaudio, R., Miglio, A., and Dey, S. "Non-Universality of von Kármán's κ in Fluvial Streams." *Journal of Hydraulic Research*, Vol. 48, No. 5, 2010, pp. 658–663. https://doi.org/10.1080/00221686.2010.507338.

[172] Cowle, M. W., Babatunde, A. O., and Bockelmann-Evans, B. N. "The Frictional Resistance Induced by Bacterial Based Biofouling in Drainage Pipelines." *Journal of Hydraulic Research*, Vol. 55, No. 2, 2017, pp. 269–283. https://doi.org/10.1080/00221686.2016.1212411.

[173] Whiting, P. J., and Dietrich, W. E. "Boundary Shear Stress and Roughness Over Mobile Alluvial Beds." *Journal of Hydraulic Engineering*, Vol. 116, No. 12, 1990, pp. 1495–1511. https://doi.org/10.1061/(ASCE)0733-9429(1990)116:12(1495).

[174] Lumley, J. L., and Tennekes, H. *A First Course in Turbulence*. MIT Press, Cambridge, Mass, 1972.

[175] Wang, Y.-C. (Becky). "Effects of Physical Properties and Rheological Characteristics on Critical Shear Stress of Fine Sediments." 2013.

[176] Dennett, K. E., Sturm, T. W., Amirtharajah, A., and Mahmood, T. "Effects of Adsorbed Natural Organic Matter on the Erosion of Kaolinite Sediments." *Water Environment Research*, Vol. 70, No. 3, 1998, pp. 268–275.

[177] Dennett, K. E., Sturm, T. W., Amirtharajah, A., and Mahmood, T. Flume Studies on the Erosion of Cohesive Sediments. In *International Water Resources Engineering Conference*, No. 1:199-203, 1995.

[178] Jepsen, R., Roberts, J., and Lick, W. "Effects of Bulk Density on Sediment Erosion Rates." *Water, Air, and Soil Pollution*, Vol. 99, No. 1, 1997, pp. 21–31. https://doi.org/10.1007/BF02406841.

[179] Haag, I., Kern, U., and Westrich, B. "Erosion Investigation and Sediment Quality Measurements for a Comprehensive Risk Assessment of Contaminated Aquatic Sediments." *Science of The Total Environment*, Vol. 266, No. 1, 2001, pp. 249–257. https://doi.org/10.1016/S0048-9697(00)00753-1.

[180] Roberts, J., Jepsen, R., Gotthard, D., and Lick, W. "Effects of Particle Size and Bulk Density on Erosion of Quartz Particles." *Journal of Hydraulic Engineering*, Vol. 124, No. 12, 1998, pp. 1261–1267. https://doi.org/10.1061/(ASCE)0733-9429(1998)124:12(1261).

[181] Lick, W., and McNeil, J. "Effects of Sediment Bulk Properties on Erosion Rates." *Science of The Total Environment*, Vol. 266, No. 1, 2001, pp. 41–48. https://doi.org/10.1016/S0048-9697(00)00747-6.

[182] Panagiotopoulos, I., Voulgaris, G., and Collins, M. B. "The Influence of Clay on the Threshold of Movement of Fine Sandy Beds." *Coastal Engineering 32 (1997) 19-43*, 1997. https://doi.org/10.1016/S0378-3839(97)00013-6.

[183] Perkey, D. W., Smith, S. J., and Priestas, A. M. *Erosion Thresholds and Rates for Sand Mud Mixtures*. Engineer Research and Development Center (U.S.) Vicksburg United States, 2020.

[184] Ravisangar, V., Sturm, T. W., and Amirtharajah, A. "Influence of Sediment Structure on Erosional Strength and Density of Kaolinite Sediment Beds."

Journal of Hydraulic Engineering, Vol. 131, No. 5, 2005, pp. 356–365. https://doi.org/10.1061/(ASCE)0733-9429(2005)131:5(356).

[185] Ravisangar, V., Dennett, K. E., Sturm, T. W., and Amirtharajah, A. "Effect of Sediment PH on Resuspension of Kaolinite Sediments." *Journal of Environmental Engineering*, Vol. 127, No. 6, 2001, pp. 531–538. https://doi.org/10.1061/(ASCE)0733-9372(2001)127:6(531).

[186] Nachtergaele, J., and Poesen, J. "Spatial and Temporal Variations in Resistance of Loess-Derived Soils to Ephemeral Gully Erosion." *European Journal of Soil Science*, Vol. 53, No. 3, 2002, pp. 449–463. https://doi.org/10.1046/j.1365-2389.2002.00443.x.

[187] Hir, P. L., Cann, P., Waeles, B., Jestin, H., and Bassoullet, P. Chapter 11 Erodibility of Natural Sediments: Experiments on Sand/Mud Mixtures from Laboratory and Field Erosion Tests. In *Proceedings in Marine Science* (T. Kusuda, H. Yamanishi, J. Spearman, and J. Z. Gailani, eds.), Elsevier, 2008, pp. 137–153.

[188] Barry, K. M., Thieke, R. J., and Mehta, A. J. "Quasi-Hydrodynamic Lubrication Effect of Clay Particles on Sand Grain Erosion." *Estuarine, Coastal and Shelf Science*, Vol. 67, No. 1, 2006, pp. 161–169. https://doi.org/10.1016/j.ecss.2005.11.009.

[189] Ganaoui, O. E., Schaaff, E., Boyer, P., Amielh, M., Anselmet, F., and Grenz, C. "Erosion of the Upper Layer of Cohesive Sediments: Characterization of Some Properties." *Journal of Hydraulic Engineering*, Vol. 133, No. 9, 2007, pp. 1087–1091. https://doi.org/10.1061/(ASCE)0733-9429(2007)133:9(1087).

[190] Ternat, F., Boyer, P., Anselmet, F., and Amielh, M. "Erosion Threshold of Saturated Natural Cohesive Sediments: Modeling and Experiments." *Water Resources Research*, Vol. 44, No. 11, 2008. https://doi.org/10.1029/2007WR006537.

[191] Briaud, J.-L., Govindasamy, A. V., and Shafii, I. "Erosion Charts for Selected Geomaterials." *Journal of Geotechnical and Geoenvironmental Engineering*, Vol. 143, No. 10, 2017, p. 04017072. https://doi.org/10.1061/(ASCE)GT.1943-5606.0001771.

[192] Briaud, J.-L., Ting, F. C. K., Chen, H. C., Gudavalli, R., Perugu, S., and Wei, G. "SRICOS: Prediction of Scour Rate in Cohesive Soils at Bridge Piers." *Journal of Geotechnical and Geoenvironmental Engineering*, Vol. 125, No. 4, 1999, pp. 237–246. https://doi.org/10.1061/(ASCE)1090-0241(1999)125:4(237).

[193] Gerbersdorf, S. U., Jancke, T., and Westrich, B. "Sediment Properties for Assessing the Erosion Risk of Contaminated Riverine Sites. An Approach to Evaluate Sediment Properties and Their Covariance Patterns over Depth in Relation to Erosion Resistance. First Investigations in Natural Sediments (11 Pp)." *Journal of Soils and Sediments*, Vol. 7, No. 1, 2007, pp. 25–35. https://doi.org/10.1065/jss2006.11.190.

[194] Gerbersdorf, S. U., Jancke, T., and Westrich, B. "Physico-Chemical and Biological Sediment Properties Determining Erosion Resistance of Contaminated Riverine Sediments – Temporal and Vertical Pattern at the Lauffen

Reservoir/River Neckar, Germany." *Limnologica*, Vol. 35, No. 3, 2005, pp. 132–144. https://doi.org/10.1016/j.limno.2005.05.001.

[195] Kimiaghalam, N., Clark, S. P., and Ahmari, H. "An Experimental Study on the Effects of Physical, Mechanical, and Electrochemical Properties of Natural Cohesive Soils on Critical Shear Stress and Erosion Rate." *International Journal of Sediment Research*, Vol. 31, No. 1, 2016, pp. 1–15. https://doi.org/10.1016/j.ijsrc.2015.01.001.

[196] Beckers, F., Haun, S., and Noack, M. "Experimental Investigation of Reservoir Sediments." *E3S Web of Conferences*, Vol. 40, 2018, p. 03030. https://doi.org/10.1051/e3sconf/20184003030.

[197] Gao, X., Wang, Q., and Ma, G. Experimental Investigation on the Erosion Threshold and Rate of Gravel and Silty Clay Mixtures. 2019.

[198] Zreik, D. A., Krishnappan, B. G., Germaine, J. T., Madsen, O. S., and Ladd, C. C. "Erosional and Mechanical Strengths of Deposited Cohesive Sediments." *Journal of Hydraulic Engineering*, Vol. 124, No. 11, 1998, pp. 1076–1085. https://doi.org/10.1061/(ASCE)0733-9429(1998)124:11(1076).

[199] Arulanandan, K., Krone, R. B., and Loganathan, P. "Pore and Eroding Fluid Influences on Surface Erosion on Soil." *Journal of the Geotechnical Engineering Division*, Vol. 101, No. 1, 1975, pp. 51–66. https://doi.org/10.1061/AJGEB6.0000141.

[200] Ariathurai, R., and Arulanandan, K. "Erosion Rates of Cohesive Soils." *Journal of the Hydraulics Division*, Vol. 104, No. 2, 1978, pp. 279–283. https://doi.org/10.1061/JYCEAJ.0004937.

[201] Ockenden, M. C., and Delo, E. *Consolidation and Erosion of Estuarine Mud and Sand Mixtures - an Experimental Study*. Hydraulics Research Wallingford, 1988.

[202] Neumeier, U., Lucas, C. H., and Collins, M. "Erodibility and Erosion Patterns of Mudflat Sediments Investigated Using an Annular Flume." *Aquatic Ecology*, Vol. 40, No. 4, 2006, pp. 543–554. https://doi.org/10.1007/s10452-004-0189-8.

[203] Baar, A. W., Smit, J. de, Uijttewaal, W. S. J., and Kleinhans, M. G. "Sediment Transport of Fine Sand to Fine Gravel on Transverse Bed Slopes in Rotating Annular Flume Experiments." *Water Resources Research*, Vol. 54, No. 1, 2018, pp. 19–45. https://doi.org/10.1002/2017WR020604.

[204] Krishnappan, B., Stone, M., Granger, S. J., Upadhayay, H. R., Tang, Q., Zhang, Y., and Collins, A. L. "Experimental Investigation of Erosion Characteristics of Fine-Grained Cohesive Sediments." *Water*, Vol. 12, No. 5, 2020, p. 1511. https://doi.org/10.3390/w12051511.

[205] Mazurek, K. A., Rajaratnam, N., and Sego, D. C. "Scour of Cohesive Soil by Submerged Circular Turbulent Impinging Jets." *Journal of Hydraulic Engineering*, Vol. 127, No. 7, 2001, pp. 598–606. https://doi.org/10.1061/(ASCE)0733-9429(2001)127:7(598).

[206] Ansari, S. A., Kothyari, U. C., and Raju, K. G. R. "Influence of Cohesion on Scour under Submerged Circular Vertical Jets." *Journal of Hydraulic Engineering*, Vol. 129, No. 12, 2003, pp. 1014–1019. https://doi.org/10.1061/(ASCE)0733-9429(2003)129:12(1014).

[207] Kilkie, P. "The Temporal and Spatial Variations in the Erosion Thresholds of Intertidal Cohesive Sediment, with a Focus on Clay Mineralogy." 2017, p. 271.

[208] Smith, D. J., Wynn-Thompson, T. M., Williams, M. A., and Seiler, J. R. "Do Roots Bind Soil? Comparing the Physical and Biological Role of Plant Roots in Fluvial Streambank Erosion: A Mini-JET Study." *Geomorphology*, Vol. 375, 2021, p. 107523. https://doi.org/10.1016/j.geomorph.2020.107523.

[209] Andersen, T. J. "Seasonal Variation in Erodibility of Two Temperate, Microtidal Mudflats." *Estuarine, Coastal and Shelf Science*, Vol. 53, No. 1, 2001, pp. 1–12. https://doi.org/10.1006/ecss.2001.0790.

[210] Andersen, T. J., Lanuru, M., van Bernem, C., Pejrup, M., and Riethmueller, R. "Erodibility of a Mixed Mudflat Dominated by Microphytobenthos and Cerastoderma Edule, East Frisian Wadden Sea, Germany." *Estuarine, Coastal and Shelf Science*, Vol. 87, No. 2, 2010, pp. 197–206. https://doi.org/10.1016/j.ecss.2009.10.014.

[211] Lintern, D. G., Sills, G. C., Feates, N., and Roberts, W. Erosion Properties of Mud Beds Deposited in Laboratory Settling Columns. In *Proceedings in Marine Science* (J. C. Winterwerp and C. Kranenburg, eds.), Elsevier, 2002, pp. 343–357.

[212] Williamson, H., and Ockenden, M. "ISIS: An Instrument for Measuring Erosion Shear Stress In Situ." *Estuarine Coastal and Shelf Science*, Vol. 42, 1996, pp. 1–18. https://doi.org/10.1006/ecss.1996.0001.

[213] Allen, P. M., Arnold, J., and Jakubowski, E. "Prediction of Stream Channel Erosion Potential." *Environmental and Engineering Geoscience*, Vol. V, No. 3, 1999, pp. 339–351. https://doi.org/10.2113/gseegeosci.V.3.339.

[214] Allen, P. M., Arnold, J., and Jakubowski, E. "Design and Testing of a Simple Submerged-Jet Device for Field Determination of Soil Erodibility." *Environmental and Engineering Geoscience*, Vol. III, No. 4, 1997, pp. 579–584. https://doi.org/10.2113/gseegeosci.III.4.579.

[215] Tolhurst, T. J., Black, K. S., Shayler, S. A., Mather, S., Black, I., Baker, K., and Paterson, D. M. "Measuring the in Situ Erosion Shear Stress of Intertidal Sediments with the Cohesive Strength Meter (CSM)." *Estuarine, Coastal and Shelf Science*, Vol. 49, No. 2, 1999, pp. 281–294. https://doi.org/10.1006/ecss.1999.0512.

[216] Potter, K. N., Velázquez-Garcia, J. de J., and Torbert, H. A. "Use of a Submerged Jet Device to Determine Channel Erodibility Coefficients of Selected Soils of Mexico." *Journal of Soil and Water Conservation*, Vol. 57, No. 5, 2002, pp. 272–277.

[217] Watts, C. W., Tolhurst, T. J., Black, K. S., and Whitmore, A. P. "In Situ Measurements of Erosion Shear Stress and Geotechnical Shear Strength of the Intertidal Sediments of the Experimental Managed Realignment Scheme at Tollesbury, Essex, UK." *Estuarine, Coastal and Shelf Science*, Vol. 58, No. 3, 2003, pp. 611–620. https://doi.org/10.1016/S0272-7714(03)00139-2.

[218] Wynn, T. M., Henderson, M. B., and Vaughan, D. H. "Changes in Streambank Erodibility and Critical Shear Stress Due to Subaerial Processes along a Headwater Stream, Southwestern Virginia, USA." *Geomorphology*, Vol. 97, No. 3, 2008, pp. 260–273. https://doi.org/10.1016/j.geomorph.2007.08.010.

[219] Thoman, R. W., and Niezgoda, S. L. "Determining Erodibility, Critical Shear Stress, and Allowable Discharge Estimates for Cohesive Channels: Case Study in the Powder River Basin of Wyoming." *Journal of Hydraulic Engineering*, Vol. 134, No. 12, 2008, pp. 1677–1687. https://doi.org/10.1061/(ASCE)0733-9429(2008)134:12(1677).

[220] Shugar, D., Kostaschuk, R., Ashmore, P., Desloges, J., and Burge, L. "In Situ Jet-Testing of the Erosional Resistance of Cohesive Streambeds." *Canadian Journal of Civil Engineering*, 2011. https://doi.org/10.1139/l07-024.

[221] Grabowski, R. C., Wharton, G., Davies, G. R., and Droppo, I. G. "Spatial and Temporal Variations in the Erosion Threshold of Fine Riverbed Sediments." *Journal of Soils and Sediments*, Vol. 12, No. 7, 2012, pp. 1174–1188. https://doi.org/10.1007/s11368-012-0534-9.

[222] Daly, E. R., Fox, G. A., Al-Madhhachi, A.-S. T., and Storm, D. E. "Variability of Fluvial Erodibility Parameters for Streambanks on a Watershed Scale." *Geomorphology*, Vol. 231, 2015, pp. 281–291. https://doi.org/10.1016/j.geomorph.2014.12.016.

[223] Ibrahim, S. L., Ariffin, J., Abdullah, J., and Muhamad, N. S. "JET EROSION DEVICE (JED) Â€" MEASUREMENT OF SOIL ERODIBILITY COEFFICIENTS." *Jurnal Teknologi*, Vol. 78, Nos. 5–5, 2016. https://doi.org/10.11113/jt.v78.8577.

[224] Mahalder, B., Schwartz, J. S., Palomino, A. M., and Zirkle, J. "Relationships between Physical-Geochemical Soil Properties and Erodibility of Streambanks among Different Physiographic Provinces of Tennessee, USA." *Earth Surface Processes and Landforms*, Vol. 43, No. 2, 2018, pp. 401–416. https://doi.org/10.1002/esp.4252.

[225] Mahalder, B., Schwartz, J. S., Palomino, A. M., and Zirkle, J. "Estimating Erodibility Parameters for Streambanks with Cohesive Soils Using the Mini Jet Test Device: A Comparison of Field and Computational Methods." *Water*, Vol. 10, No. 3, 2018, p. 304. https://doi.org/10.3390/w10030304.

[226] Waqas, A., Neumeier, U., and Rochon, A. "Seasonal Changes in Sediment Erodibility Associated with Biostabilization in a Subarctic Intertidal Environment, St. Lawrence Estuary, Canada." *Estuarine, Coastal and Shelf Science*, Vol. 245, 2020, p. 106935. https://doi.org/10.1016/j.ecss.2020.106935.

[227] Chen, D., Li, M., Zhang, Y., Zhang, L., Tang, J., Wu, H., and Wang, Y. P. "Effects of Diatoms on Erosion and Accretion Processes in Saltmarsh Inferred from Field Observations of Hydrodynamic and Sedimentary Processes." *Ecohydrology*, Vol. 13, No. 8, 2020, p. e2246. https://doi.org/10.1002/eco.2246.

[228] Wahl, T. Methods for Analyzing Submerged Jet Erosion Test Data to Model Scour of Cohesive Soils. 2021.

[229] Amos, C. L., Droppo, I. G., Gomez, E. A., and Murphy, T. P. "The Stability of a Remediated Bed in Hamilton Harbour, Lake Ontario, Canada." *Sedimentology*, Vol. 50, No. 1, 2003, pp. 149–168. https://doi.org/10.1046/j.1365-3091.2003.00542.x.

[230] Amos, C. L., Grant, J., Daborn, G. R., and Black, K. "Sea Carousel—A Benthic, Annular Flume." *Estuarine, Coastal and Shelf Science*, Vol. 34, No. 6, 1992, pp. 557–577. https://doi.org/10.1016/S0272-7714(05)80062-9.

[231] Amos, C. L., Feeney, T., Sutherland, T. F., and Luternauer, J. L. "The Stability of Fine-Grained Sediments from the Fraser River Delta." *Estuarine, Coastal and Shelf Science*, Vol. 45, No. 4, 1997, pp. 507–524. https://doi.org/10.1006/ecss.1996.0193.

[232] Sutherland, T. F., Amos, C. L., and Grant, J. "The Effect of Buoyant Biofilms on the Erodibility of Sublittoral Sediments of a Temperate Microtidal Estuary." *Limnology and Oceanography*, Vol. 43, No. 2, 1998, pp. 225–235. https://doi.org/10.4319/lo.1998.43.2.0225.

[233] Maa, J. P.-Y., Wright, L. D., Lee, C.-H., and Shannon, T. W. "Vims Sea Carousel: A Field Instrument for Studying Sediment Transport." *Marine Geology*, Vol. 115, No. 3, 1993, pp. 271–287. https://doi.org/10.1016/0025-3227(93)90056-2.

[234] Lucas, C. H., Widdows, J., and Wall, L. "Relating Spatial and Temporal Variability in Sediment Chlorophylla and Carbohydrate Distribution with Erodibility of a Tidal Flat." *Estuaries*, Vol. 26, No. 4, 2003, pp. 885–893. https://doi.org/10.1007/BF02803347.

[235] Widdows, J., Friend, P. L., Bale, A. J., Brinsley, M. D., Pope, N. D., and Thompson, C. E. L. "Inter-Comparison between Five Devices for Determining Erodability of Intertidal Sediments." *Continental Shelf Research*, Vol. 27, No. 8, 2007, pp. 1174–1189. https://doi.org/10.1016/j.csr.2005.10.006.

[236] Johansen, C., Larsen, T., and Petersen, O. Experiments on Erosion of Mud from the Danish Wadden Sea. Presented at the Experiments on Erosion of Mud from the Danish Wadden Sea, 1994.

[237] Gust, G., and Müller, V. Interfacial Hydrodynamics and Entrainment Functions of Currently Used Erosion Devices. In *Cohesive Sediments : 4th Nearshore and Estuarine Cohesive Sediment Transport Conference, INTERCOH '94, 11-15 July 1994: Wallingford, England, UK* (N. Burt, ed.), Wiley, New York, USA, 1997, pp. 149–174.

[238] Thomsen, L., and Gust, G. "Sediment Erosion Thresholds and Characteristics of Resuspended Aggregates on the Western European Continental Margin." *Deep Sea Research Part I: Oceanographic Research Papers*, Vol. 47, No. 10, 2000, pp. 1881–1897. https://doi.org/10.1016/S0967-0637(00)00003-0.

[239] Law, B. A., Hill, P. S., Milligan, T. G., Curran, K. J., Wiberg, P. L., and Wheatcroft, R. A. "Size Sorting of Fine-Grained Sediments during Erosion: Results from the Western Gulf of Lions." *Continental Shelf Research*, Vol. 28, No. 15, 2008, pp. 1935–1946. https://doi.org/10.1016/j.csr.2007.11.006.

[240] Legout, C., Droppo, I. G., Coutaz, J., Bel, C., and Jodeau, M. "Assessment of Erosion and Settling Properties of Fine Sediments Stored in Cobble Bed Rivers: The Arc and Isère Alpine Rivers before and after Reservoir Flushing." *Earth Surface Processes and Landforms*, Vol. 43, No. 6, 2018, pp. 1295–1309. https://doi.org/10.1002/esp.4314.

[241] Ha, H. J., Choi, S. M., Seo, J. Y., and Ha, H. K. "Erodibility of Sand-Mud Mixed Sediment on the Yeochari Tidal Flat, Gyeonggi Bay, Korea." *Journal of Coastal*

Research, No. 85 (10085), 2018, pp. 416–420. https://doi.org/10.2112/SI85-084.1.

[242] Work, P. A., and Schoellhamer, D. H. *Measurements of Erosion Potential Using Gust Chamber in Yolo Bypass near Sacramento, California*. Publication 2018–1062. U.S. Geological Survey, Reston, VA, 2018.

[243] Xu, K., Corbett, D. R., Walsh, J. P., Young, D., Briggs, K. B., Cartwright, G. M., Friedrichs, C. T., Harris, C. K., Mickey, R. C., and Mitra, S. "Seabed Erodibility Variations on the Louisiana Continental Shelf before and after the 2011 Mississippi River Flood." *Estuarine, Coastal and Shelf Science*, Vol. 149, 2014, pp. 283–293. https://doi.org/10.1016/j.ecss.2014.09.002.

[244] Huang, W., Zhang, H., Zhu, L., Chen, L., Zhang, G., Gong, W., and Liu, J. "In-Situ Study of the Spatiotemporal Variability of Sediment Erodibility in a Microtidal Estuary." *Estuarine, Coastal and Shelf Science*, Vol. 232, 2020, p. 106530. https://doi.org/10.1016/j.ecss.2019.106530.

[245] Houwing, E.-J. "Determination of the Critical Erosion Threshold of Cohesive Sediments on Intertidal Mudflats Along the Dutch Wadden Sea Coast." *Estuarine, Coastal and Shelf Science*, Vol. 49, No. 4, 1999, pp. 545–555. https://doi.org/10.1006/ecss.1999.0518.

[246] Young, R. A. "Seaflume: A Device for in-Situ Studies of Threshold Erosion Velocity and Erosional Behavior of Undisturbed Marine Muds." *Marine Geology*, Vol. 23, No. 1, 1977, pp. M11–M18. https://doi.org/10.1016/0025-3227(77)90091-3.

[247] Gust, G., and Morris, M. J. "Erosion Thresholds and Entrainment Rates of Undisturbed in Situ Sediments." *Journal of Coastal Research*, 1989, pp. 87–99.

[248] Ravens, T. M., and Gschwend, P. M. "Flume Measurements of Sediment Erodibility in Boston Harbor." *Journal of Hydraulic Engineering*, Vol. 125, No. 10, 1999, pp. 998–1005. https://doi.org/10.1061/(ASCE)0733-9429(1999)125:10(998).

[249] Aberle, J., Nikora, V., and Walters, R. "Data Interpretation for In Situ Measurements of Cohesive Sediment Erosion." *Journal of Hydraulic Engineering*, Vol. 132, No. 6, 2006, pp. 581–588. https://doi.org/10.1061/(ASCE)0733-9429(2006)132:6(581).

[250] Aberle, J., Nikora, V., McLean, S., Doscher, C., McEwan, I., Green, M., Goring, D., and Walsh, J. "Straight Benthic Flow-Through Flume for In Situ Measurement of Cohesive Sediment Dynamics." *Journal of Hydraulic Engineering*, Vol. 129, No. 1, 2003, pp. 63–67. https://doi.org/10.1061/(ASCE)0733-9429(2003)129:1(63).

[251] Debnath, K., Nikora, V., and Elliott, A. "Stream Bank Erosion: In Situ Flume Tests." *Journal of Irrigation and Drainage Engineering*, Vol. 133, No. 3, 2007, pp. 256–264. https://doi.org/10.1061/(ASCE)0733-9437(2007)133:3(256).

[252] He, C., and Nguyen, D. "Erodibility Study of Sediment in a Fast-Flowing River." *International Journal of Sediment Research*, Vol. 34, No. 2, 2019, pp. 144–154. https://doi.org/10.1016/j.ijsrc.2018.09.002.

[253] Grissinger, E. H., Little, W. C., and Murphey, J. B. "Erodibility of Streambank Materials of Low Cohesion." *Transactions of the ASAE*, Vol. 24, No. 3, 1981, pp. 0624–0630.

[254] Hanson, G. J., and Robinson, K. M. "The Influence of Soil Moisture and Compaction on Spillway Erosion." *Transactions of the ASAE (USA)*, 1993.

[255] Harder, L., and Arulanandan, K. "Laboratory Techniques in the Prediction of Soil Erodibility." *PB - U.S. National Technical Information Service*, 1976.

[256] Hollick, M. "Towards a Routine Test for the Assessment of the Critical Tractive Forces of Cohesive Soils." *Transactions of the ASAE*, Vol. 19, No. 6, 1976, pp. 1076–1081.

[257] Jain, R. K., and Kothyari, U. C. "Cohesion Influences on Erosion and Bed Load Transport." *Water Resources Research*, Vol. 45, No. 6, 2009. https://doi.org/10.1029/2008WR007044.

[258] Kamphuis, J., and Hall, K. "Cohesive Material Erosion by Unidirectional Current." *J. Hydraul. Eng.*, Vol. 109, No. 1, 1983, pp. 49–61.

[259] Knighton, D. *Fluvial Forms and Processes: A New Perspective*. Hodder Arnold, Sheffield, UK, 1998.

[260] Lyle, W. M., and Smerdon, E. T. "Relation of Compaction and Other Soil Properties to Erosion Resistance of Soils." *Transactions of the ASAE*, Vol. 8, No. 3, 1965. https://doi.org/10.13031/2013.40536.

[261] Smerdon, E. T., and Beasley, R. P. "Critical Tractive Forces in Cohesive Sediments." *Agricultural Engineering*, Vol. 42, No. 1, 1961, pp. 26–29.

[262] Wan, C. F., and Fell, R. "Investigation of Rate of Erosion of Soils in Embankment Dams." *Journal of Geotechnical and Geoenvironmental Engineering*, Vol. 130, No. 4, 2004, pp. 373–380. https://doi.org/10.1061/(ASCE)1090-0241(2004)130:4(373).

[263] Winterwerp, J. C., and Van Kesteren, W. G. M. Erosion and Entrainment. In *Developments in Sedimentology*, Elsevier, 2004, pp. 343–381.

[264] Lick, W., Jin, L., and Gailani, J. "Initiation of Movement of Quartz Particles." *Journal of Hydraulic Engineering*, Vol. 130, No. 8, 2004, pp. 755–761. https://doi.org/10.1061/(ASCE)0733-9429(2004)130:8(755).

[265] Mitchener, H., and Torfs, H. "Erosion of Mud/Sand Mixtures." *Coastal Engineering*, Vol. 29, No. 1, 1996, pp. 1–25. https://doi.org/10.1016/S0378-3839(96)00002-6.

[266] Dickhudt, P. J., Friedrichs, C. T., and Sanford, L. P. "Mud Matrix Solids Fraction and Bed Erodibility in the York River Estuary, USA, and Other Muddy Environments." *Continental Shelf Research*, Vol. 31, Nos. 10, Supplement, 2011, pp. S3–S13. https://doi.org/10.1016/j.csr.2010.02.008.

[267] Dickhudt, P. J., Friedrichs, C. T., Schaffner, L. C., and Sanford, L. P. "Spatial and Temporal Variation in Cohesive Sediment Erodibility in the York River Estuary, Eastern USA: A Biologically Influenced Equilibrium Modified by Seasonal Deposition." *Marine Geology*, Vol. 267, No. 3, 2009, pp. 128–140. https://doi.org/10.1016/j.margeo.2009.09.009.

[268] Julian, J. P., and Torres, R. "Hydraulic Erosion of Cohesive Riverbanks." *Geomorphology*, Vol. 76, No. 1, 2006, pp. 193–206. https://doi.org/10.1016/j.geomorph.2005.11.003.

[269] van Ledden, M., van Kesteren, W. G. M., and Winterwerp, J. C. "A Conceptual Framework for the Erosion Behaviour of Sand–Mud Mixtures." *Continental Shelf Research*, Vol. 24, No. 1, 2004, pp. 1–11. https://doi.org/10.1016/j.csr.2003.09.002.

[270] Marion, D., Nur, A., Yin, H., and Han, D. "Compressional Velocity and Porosity in Sand-clay Mixtures." *GEOPHYSICS*, Vol. 57, No. 4, 1992, pp. 554–563. https://doi.org/10.1190/1.1443269.

[271] Kasanin-Grubin, M. "Clay Mineralogy as a Crucial Factor in Badland Hillslope Processes." *CATENA*, Vol. 106, 2013, pp. 54–67. https://doi.org/10.1016/j.catena.2012.08.008.

[272] Fukuda, M. K., and Lick, W. "The Entrainment of Cohesive Sediments in Freshwater." *Journal of Geophysical Research: Oceans*, Vol. 85, No. C5, 1980, pp. 2813–2824. https://doi.org/10.1029/JC085iC05p02813.

[273] Mehta, A. J., and Hwang, K.-N. Fine Sediment Erodibility in Lake Okeechobee, Florida. 89/019. http://aquaticcommons.org/127/. Accessed Feb. 26, 2021.

[274] Bale, A. J., Stephens, J. A., and Harris, C. B. "Critical Erosion Profiles in Macro-Tidal Estuary Sediments: Implications for the Stability of Intertidal Mud and the Slope of Mud Banks." *Continental Shelf Research*, Vol. 27, No. 18, 2007, pp. 2303–2312. https://doi.org/10.1016/j.csr.2007.05.015.

[275] Beckers, F., Haun, S., and Noack, M. "Experimental Investigation of Reservoir Sediments." *E3S Web of Conferences*, Vol. 40, 2018, p. 03030. https://doi.org/10.1051/e3sconf/20184003030.

[276] Noack, M., Gerbersdorf, S. U., Hillebrand, G., and Wieprecht, S. "Combining Field and Laboratory Measurements to Determine the Erosion Risk of Cohesive Sediments Best." *Water*, Vol. 7, No. 9, 2015, pp. 5061–5077. https://doi.org/10.3390/w7095061.

[277] Parchure, T. M., and Mehta, A. J. "Erosion of Soft Cohesive Sediment Deposits." *Journal of Hydraulic Engineering-Asce*, Vol. 111, 1985, pp. 1308–1326.

[278] Amos, C. L., Van Wagoner, N. A., and Daborn, G. R. "The Influence of Subaerial Exposure on the Bulk Properties of Fine-Grained Intertidal Sediment from Minas Basin, Bay of Fundy." *Estuarine, Coastal and Shelf Science*, Vol. 27, No. 1, 1988, pp. 1–13. https://doi.org/10.1016/0272-7714(88)90028-5.

[279] Wang, Y.-C., and Sturm, T. W. "Effects of Physical Properties on Erosional and Yield Strengths of Fine-Grained Sediments." *Journal of Hydraulic Engineering*, Vol. 142, No. 11, 2016, p. 04016049. https://doi.org/10.1061/(ASCE)HY.1943-7900.0001193.

[280] Liu, L., Wilkinson, J., Koca, K., Buchmann, C., and Lorke, A. "The Role of Sediment Structure in Gas Bubble Storage and Release." *Journal of Geophysical Research: Biogeosciences*, Vol. 121, No. 7, 2016, pp. 1992–2005. https://doi.org/10.1002/2016JG003456.

[281] Peeters, F., Encinas Fernandez, J., and Hofmann, H. "Sediment Fluxes Rather than Oxic Methanogenesis Explain Diffusive CH 4 Emissions from Lakes and Reservoirs." *Scientific Reports*, Vol. 9, No. 1, 2019, p. 243. https://doi.org/10.1038/s41598-018-36530-w.

[282] Cheng, W., Fang, H., Lai, H., Huang, L., and Dey, S. "Effects of Biofilm on Turbulence Characteristics and the Transport of Fine Sediment." *Journal of Soils and Sediments*, Vol. 18, No. 10, 2018, pp. 3055–3069. https://doi.org/10.1007/s11368-017-1859-1.

[283] Tinoco, R. O., Juan, J. E. S., and Mullarney, J. C. "Simplification Bias: Lessons from Laboratory and Field Experiments on Flow through Aquatic Vegetation." *Earth Surface Processes and Landforms*, Vol. 45, No. 1, 2020, pp. 121–143. https://doi.org/10.1002/esp.4743.

[284] Duarte, C. F., Nadim, N., and Chandratilleke, T. T. "Experimental Study of Granular Bed Erosion and Sedimentation Subjugated to the Secondary Flow Structures in Curved Ducts." *Advances in Mechanical Engineering*, Vol. 11, No. 11, 2019, p. 1687814019885255. https://doi.org/10.1177/1687814019885255.

[285] Papanicolaou, A. N., Elhakeem, M., and Hilldale, R. "Secondary Current Effects on Cohesive River Bank Erosion." *Water Resources Research*, Vol. 43, No. 12, 2007. https://doi.org/10.1029/2006WR005763.

[286] Partheniades, E. *Engineering Properties and Hydraulic Behavior of Cohesive Sediments*. CRC, Boca Raton, Fla. ; London, 2007.

[287] Qin, C., Shao, X., and Xiao, Y. "Secondary Flow Effects on Deposition of Cohesive Sediment in a Meandering Reach of Yangtze River." *Water*, Vol. 11, No. 7, 2019, p. 1444. https://doi.org/10.3390/w11071444.

[288] Sheng, Y. P. "Consideration of Flow in Rotating Annuil for Sediment Erosion and Deposition Studies." *Journal of Coastal Research*, 1989, pp. 207–216.

[289] Heinzelmann, C., and Wallisch, S. "Benthic Settlement and Bed Erosion. A Review." *Journal of Hydraulic Research*, Vol. 29, No. 3, 1991, pp. 355–371. https://doi.org/10.1080/00221689109498439.

[290] Montague, C. L. Influence of Biota on Erodibility of Sediments. New York, NY, 1986.

[291] Mehta, A. J. Characterization of Cohesive Sediment Properties and Transport Processes in Estuaries. New York, NY, 1986.

[292] USBR. *Erosion and Sedimentation Manual*. United States Bureau of Reclamation (USBR), 2006.

[293] Dai, C., and Zhao, F. Clay Minerals. In *Oilfield Chemistry* (C. Dai and F. Zhao, eds.), Springer, Singapore, 2018, pp. 3–19.

[294] Moore, D. M., and Reynolds, R. C. *X-Ray Diffraction and the Identification and Analysis of Clay Minerals*. Oxford University Press, Oxford ; New York, 1997.

[295] Terzaghi, K. *Soil Mechanics in Engineering Practice*. Warren Press, Alcester, 2010.

[296] Torfs, H. *Erosion of Mud/Sand Mixtures*. PhD Thesis. Katholieke Universiteit Leuven, Leuven, Belgium, 1995.

[297]   Uddin, M. K. "A Review on the Adsorption of Heavy Metals by Clay Minerals, with Special Focus on the Past Decade." *Chemical Engineering Journal*, Vol. 308, 2017, pp. 438–462. https://doi.org/10.1016/j.cej.2016.09.029.

[298]   Sarkar, B., Rusmin, R., Ugochukwu, U. C., Mukhopadhyay, R., and Manjaiah, K. M. Chapter 5 - Modified Clay Minerals for Environmental Applications. In *Modified Clay and Zeolite Nanocomposite Materials* (M. Mercurio, B. Sarkar, and A. Langella, eds.), Elsevier, 2019, pp. 113–127.

[299]   Bennett, R. H., O'Brien, N. R., and Hulbert, M. H. Determinants of Clay and Shale Microfabric Signatures: Processes and Mechanisms. In *Microstructure of Fine-Grained Sediments: From Mud to Shale* (R. H. Bennett, W. R. Bryant, M. H. Hulbert, W. A. Chiou, R. W. Faas, J. Kasprowicz, H. Li, T. Lomenick, N. R. O'Brien, S. Pamukcu, P. Smart, C. E. Weaver, and T. Yamamoto, eds.), Springer, New York, NY, 1991, pp. 5–32.

[300]   Mehta, A. J. *Studies on Erosion and Settling of Organic-Rich Sediment from Newnans Lake and Other Water Bodies in Florida*. U.S. Army Engineer Research and Development Center, Vicksburg, MS, USA, 2002.

[301]   Parchure, T. M., and Davis, J. E. *Effect of Organic Materials on Bulk Density and Erodibility of Fine Sediment Beds*. 2005.

[302]   Gowland, J. E., and Mehta, A. J. *Properties of Sediment from Newnans Lake, Florida*. Publication Report No. 2002/012. Coastal and Oceanographic Engineering Program, University of Florida, Gainesville, FL, USA, 2002, p. 172.

[303]   Gowland, J. E., Mehta, A. J., Stuck, J. D., John, C. V., and Parchure, T. M. Organic-Rich Fine Sediments in Florida, Part II: Resuspension in a Lake. In *Proceedings in Marine Science* (J. P.-Y. Maa, L. P. Sanford, and D. H. Schoellhamer, eds.), Elsevier, 2007, pp. 167–188.

[304]   Paterson, D. M., and Daborn, G. R. *Sediment Stabilisation by Biological Action: Significance for Coastal Engineering*. University of Bristol Press, 1991.

[305]   Whitehouse, R., Soulsby, R., Roberts, W., and Mitchener, H. *Dynamics of Estuarine Muds: A Manual for Practical Applications*. Institution of Civil Engineers, London, 2000.

[306]   Brekhovskikh, V. F., Debolsky, V. K., Vishnevskaya, G. N., and Zolotareva, N. S. "Erosion of Cohesive Bottom Sediments: The Influence of Benthos." *Journal of Hydraulic Research*, Vol. 29, No. 2, 1991, pp. 149–160. https://doi.org/10.1080/00221689109499000.

[307]   Meadows, P. S., and Meadows, A. The Environmentul Impact of Burrows and Burrowing Animals. 1991.

[308]   McAnally, W. H. *Aggregation and Deposition of Estuarial Fine Sediment*. PhD Thesis. University of Florida, 1999.

[309]   Miranda-Trevino, J. C., and Coles, C. A. "Kaolinite Properties, Structure and Influence of Metal Retention on PH." *Applied Clay Science*, Vol. 23, No. 1, 2003, pp. 133–139. https://doi.org/10.1016/S0169-1317(03)00095-4.

[310]   Murray, H. H. "Applied Clay Mineralogy Today and Tomorrow." *Clay Minerals*, Vol. 34, No. 1, 1999, pp. 39–49.

[311] Zhang, D., Zhou, C.-H., Lin, C.-X., Tong, D.-S., and Yu, W.-H. "Synthesis of Clay Minerals." *Applied Clay Science*, Vol. 50, No. 1, 2010, pp. 1–11. https://doi.org/10.1016/j.clay.2010.06.019.

[312] Zhang, L., Shen, T., Cheng, Y., Zhao, T., Li, L., and Qi, P. "Temporal and Spatial Variations in the Bacterial Community Composition in Lake Bosten, a Large, Brackish Lake in China." *Scientific Reports*, Vol. 10, No. 1, 2020, p. 304. https://doi.org/10.1038/s41598-019-57238-5.

[313] Vijsel, R. C. van de, Belzen, J. van, Bouma, T. J., Wal, D. van der, Cusseddu, V., Purkis, S. J., Rietkerk, M., and Koppel, J. van de. "Estuarine Biofilm Patterns: Modern Analogues for Precambrian Self-Organization." *Earth Surface Processes and Landforms*, Vol. 45, No. 5, 2020, pp. 1141–1154. https://doi.org/10.1002/esp.4783.

[314] Chan, S., Pullerits, K., Keucken, A., Persson, K. M., Paul, C. J., and Rådström, P. "Bacterial Release from Pipe Biofilm in a Full-Scale Drinking Water Distribution System." *npj Biofilms and Microbiomes*, Vol. 5, No. 1, 2019, pp. 1–8. https://doi.org/10.1038/s41522-019-0082-9.

[315] Douterelo, I., Sharpe, R. L., Husband, S., Fish, K. E., and Boxall, J. B. "Understanding Microbial Ecology to Improve Management of Drinking Water Distribution Systems." *Wiley Interdisciplinary Reviews: Water*, Vol. 6, No. 1, 2019, p. e01325. https://doi.org/10.1002/wat2.1325.

[316] Flemming, H.-C., Neu, D. T. R., and Wingender, D. J. *The Perfect Slime: Microbial Extracellular Polymeric Substances (EPS)*. IWA Publishing, 2016.

[317] Flemming, H.-C., and Wingender, J. "The Biofilm Matrix." *Nature Reviews Microbiology*, Vol. 8, No. 9, 2010, pp. 623–633. https://doi.org/10.1038/nrmicro2415.

[318] West, S. A., Diggle, S. P., Buckling, A., Gardner, A., and Griffin, A. S. "The Social Lives of Microbes." *Annual Review of Ecology, Evolution, and Systematics*, Vol. 38, No. 1, 2007, pp. 53–77. https://doi.org/10.1146/annurev.ecolsys.38.091206.095740.

[319] Fang, H., Zhao, H., Shang, Q., and Chen, M. "Effect of Biofilm on the Rheological Properties of Cohesive Sediment." *Hydrobiologia*, Vol. 694, No. 1, 2012, pp. 171–181. https://doi.org/10.1007/s10750-012-1140-y.

[320] Gibbs, R. J. "Effect of Natural Organic Coatings on the Coagulation of Particles." *Environmental Science & Technology*, Vol. 17, No. 4, 1983, pp. 237–240. https://doi.org/10.1021/es00110a011.

[321] Huiming, Z., Hongwei, F., and Minghong, C. "Floc Architecture of Bioflocculation Sediment by ESEM and CLSM." *Scanning*, Vol. 33, No. 6, 2011, pp. 437–445. https://doi.org/10.1002/sca.20247.

[322] Shang, Q., Fang, H., Zhao, H., He, G., and Cui, Z. "Biofilm Effects on Size Gradation, Drag Coefficient and Settling Velocity of Sediment Particles." *International Journal of Sediment Research*, Vol. 29, No. 4, 2014, pp. 471–480. https://doi.org/10.1016/S1001-6279(14)60060-3.

[323] Banasiak, R., Verhoeven, R., De Sutter, R., and Tait, S. "The Erosion Behaviour of Biologically Active Sewer Sediment Deposits: Observations from a

Laboratory Study." *Water Research*, Vol. 39, No. 20, 2005, pp. 5221–5231. https://doi.org/10.1016/j.watres.2005.10.011.

[324] Droppo, I. G., D'Andrea, L., Krishnappan, B. G., Jaskot, C., Trapp, B., Basuvaraj, M., and Liss, S. N. "Fine-Sediment Dynamics: Towards an Improved Understanding of Sediment Erosion and Transport." *Journal of Soils and Sediments*, Vol. 15, No. 2, 2015, pp. 467–479. https://doi.org/10.1007/s11368-014-1004-3.

[325] Fang, H. W., Lai, H. J., Cheng, W., Huang, L., and He, G. J. "Modeling Sediment Transport with an Integrated View of the Biofilm Effects." *Water Resources Research*, Vol. 53, No. 9, 2017, pp. 7536–7557. https://doi.org/10.1002/2017WR020628.

[326] Gerbersdorf, S. U., Jancke, T., Westrich, B., and Paterson, D. M. "Microbial Stabilization of Riverine Sediments by Extracellular Polymeric Substances." *Geobiology*, Vol. 6, No. 1, 2008, pp. 57–69. https://doi.org/10.1111/j.1472-4669.2007.00120.x.

[327] Malarkey, J., Baas, J. H., Hope, J. A., Aspden, R. J., Parsons, D. R., Peakall, J., Paterson, D. M., Schindler, R. J., Ye, L., Lichtman, I. D., Bass, S. J., Davies, A. G., Manning, A. J., and Thorne, P. D. "The Pervasive Role of Biological Cohesion in Bedform Development." *Nature Communications*, Vol. 6, 2015. https://doi.org/10.1038/ncomms7257.

[328] Parsons, D. R., Schindler, R. J., Hope, J. A., Malarkey, J., Baas, J. H., Peakall, J., Manning, A. J., Ye, L., Simmons, S., Paterson, D. M., Aspden, R. J., Bass, S. J., Davies, A. G., Lichtman, I. D., and Thorne, P. D. "The Role of Biophysical Cohesion on Subaqueous Bed Form Size." *Geophysical Research Letters*, Vol. 43, No. 4, 2016, pp. 1566–1573. https://doi.org/10.1002/2016GL067667.

[329] Righetti, M., and Lucarelli, C. "Resuspension Phenomena of Benthic Sediments: The Role of Cohesion and Biological Adhesion." *River Research and Applications*, Vol. 26, No. 4, 2010, pp. 404–413. https://doi.org/10.1002/rra.1296.

[330] Burns, A., and Ryder, D. S. "Potential for Biofilms as Biological Indicators in Australian Riverine Systems." *Ecological Management & Restoration*, Vol. 2, No. 1, 2001, pp. 53–64. https://doi.org/10.1046/j.1442-8903.2001.00069.x.

[331] Förstner, U., Heise, S., Schwartz, R., Westrich, B., and Ahlf, W. "Historical Contaminated Sediments and Soils at the River Basin Scale." *Journal of Soils and Sediments*, Vol. 4, No. 4, 2004, p. 247. https://doi.org/10.1007/BF02991121.

[332] Packman, A. "Building Bacterial Bridges." *Nature Geoscience*, Vol. 6, No. 9, 2013, pp. 682–683. https://doi.org/10.1038/ngeo1938.

[333] Manzenrieder, H. "Retardation of Initial Erosion under Biological Effects in Sandy Tidal Flats." *1985 Australasian Conference on Coastal and Ocean Engineering*, 1985, p. 455.

[334] Fang, H., Shang, Q., Chen, M., and He, G. "Changes in the Critical Erosion Velocity for Sediment Colonized by Biofilm." *Sedimentology*, Vol. 61, No. 3, 2014, pp. 648–659. https://doi.org/10.1111/sed.12065.

[335] Thom, M. *Towards a Better Understanding of the Biostabilization Mechanisms of Sediment Beds*. Stuttgart : Eigenverlag des Instituts für Wasser- und Umweltsystemmodellierung, 2019.

[336] Stevenson, R. J., Bothwell, M. L., and Lowe, R. L. *Algal Ecology: Freshwater Benthic Ecosystems*. Academic Press, San Diego, 1996.

[337] Leibold, M. A., Holyoak, M., Mouquet, N., Amarasekare, P., Chase, J. M., Hoopes, M. F., Holt, R. D., Shurin, J. B., Law, R., Tilman, D., Loreau, M., and Gonzalez, A. "The Metacommunity Concept: A Framework for Multi-Scale Community Ecology." *Ecology Letters*, Vol. 7, No. 7, 2004, pp. 601–613. https://doi.org/10.1111/j.1461-0248.2004.00608.x.

[338] Schiller, D. V., Martí, E., Riera, J. L., and Sabater, F. "Effects of Nutrients and Light on Periphyton Biomass and Nitrogen Uptake in Mediterranean Streams with Contrasting Land Uses." *Freshwater Biology*, Vol. 52, No. 5, 2007, pp. 891–906. https://doi.org/10.1111/j.1365-2427.2007.01742.x.

[339] Salta, M., Wharton, J. A., Blache, Y., Stokes, K. R., and Briand, J.-F. "Marine Biofilms on Artificial Surfaces: Structure and Dynamics." *Environmental Microbiology*, Vol. 15, No. 11, 2013, pp. 2879–2893. https://doi.org/10.1111/1462-2920.12186.

[340] Wilhelm, L., Besemer, K., Fasching, C., Urich, T., Singer, G. A., Quince, C., and Battin, T. J. "Rare but Active Taxa Contribute to Community Dynamics of Benthic Biofilms in Glacier-Fed Streams." *Environmental Microbiology*, Vol. 16, No. 8, 2014, pp. 2514–2524. https://doi.org/10.1111/1462-2920.12392.

[341] Risse-Buhl, U., Anlanger, C., Chatzinotas, A., Noss, C., Lorke, A., and Weitere, M. "Near Streambed Flow Shapes Microbial Guilds within and across Trophic Levels in Fluvial Biofilms." *Limnology and Oceanography*, Vol. n/a, No. n/a, 2020. https://doi.org/10.1002/lno.11451.

[342] Risse-Buhl, U., Anlanger, C., Kalla, K., Neu, T. R., Noss, C., Lorke, A., and Weitere, M. "The Role of Hydrodynamics in Shaping the Composition and Architecture of Epilithic Biofilms in Fluvial Ecosystems." *Water Research*, Vol. 127, 2017, pp. 211–222. https://doi.org/10.1016/j.watres.2017.09.054.

[343] Woodcock, S., Besemer, K., Battin, T. J., Curtis, T. P., and Sloan, W. T. "Modelling the Effects of Dispersal Mechanisms and Hydrodynamic Regimes upon the Structure of Microbial Communities within Fluvial Biofilms." *Environmental Microbiology*, Vol. 15, No. 4, 2013, pp. 1216–1225. https://doi.org/10.1111/1462-2920.12055.

[344] Vignaga, E. *The Effect of Biofilm Colonization on the Stability of Non-Cohesive Sediments*. PhD. University of Glasgow, 2012.

[345] Neumann, A. C., Gebelein, C. D., and Scoffin, T. P. "The Composition, Structure and Erodability of Subtidal Mats, Abaco, Bahamas." *Journal of Sedimentary Research*, Vol. 40, No. 1, 1970, pp. 274–297. https://doi.org/10.1306/74D71F2D-2B21-11D7-8648000102C1865D.

[346] Grant, J., and Gust, G. "Prediction of Coastal Sediment Stability from Photopigment Content of Mats of Purple Sulphur Bacteria." *Nature*, Vol. 330, No. 6145, 1987, pp. 244–246. https://doi.org/10.1038/330244a0.

[347] Dade, W. B., Davis, J. D., Nichols, P. D., Nowell, A. R. M., Thistle, D., Trexler, M. B., and White, D. C. "Effects of Bacterial Exopolymer Adhesion on the Entrainment of Sand." *Geomicrobiology Journal*, Vol. 8, No. 1, 1990, pp. 1–16. https://doi.org/10.1080/01490459009377874.

[348] Madsen, K. N., Nilsson, P., and Sundbäck, K. "The Influence of Benthic Microalgae on the Stability of a Subtidal Sediment." *Journal of Experimental Marine Biology and Ecology*, Vol. 170, No. 2, 1993, pp. 159–177. https://doi.org/10.1016/0022-0981(93)90150-M.

[349] Vignaga, E., Haynes, H., and Sloan, W. T. "Quantifying the Tensile Strength of Microbial Mats Grown over Noncohesive Sediments." *Biotechnology and Bioengineering*, Vol. 109, No. 5, 2012, pp. 1155–1164. https://doi.org/10.1002/bit.24401.

[350] Amos, C. L., Bergamasco, A., Umgiesser, G., Cappucci, S., Cloutier, D., DeNat, L., Flindt, M., Bonardi, M., and Cristante, S. "The Stability of Tidal Flats in Venice Lagoon—the Results of in-Situ Measurements Using Two Benthic, Annular Flumes." *Journal of Marine Systems*, Vol. 51, No. 1, 2004, pp. 211–241. https://doi.org/10.1016/j.jmarsys.2004.05.013.

[351] Haun, S., Kjærås, H., Løvfall, S., and Olsen, N. R. B. "Three-Dimensional Measurements and Numerical Modelling of Suspended Sediments in a Hydropower Reservoir." *Journal of Hydrology*, Vol. 479, 2013, pp. 180–188. https://doi.org/10.1016/j.jhydrol.2012.11.060.

[352] Haun, S., and Olsen, N. R. B. "Three-Dimensional Numerical Modelling of Reservoir Flushing in a Prototype Scale." *International Journal of River Basin Management*, Vol. 10, No. 4, 2012, pp. 341–349. https://doi.org/10.1080/15715124.2012.736388.

[353] Witt, O., and Westrich, B. "Quantification of Erosion Rates for Undisturbed Contaminated Cohesive Sediment Cores by Image Analysis." *Hydrobiologia*, Vol. 494, No. 1, 2003, pp. 271–276. https://doi.org/10.1023/A:1025495122246.

[354] Moulin, F. Y., and Eiff, O. Biofilms, Hydraulics and Sediment Dynamics. In *Critical Review of Ecohydraulic Experiments: Biofilm*, Hydralab, 2011.

[355] Singer, G., Besemer, K., Schmitt-Kopplin, P., Hödl, I., and Battin, T. J. "Physical Heterogeneity Increases Biofilm Resource Use and Its Molecular Diversity in Stream Mesocosms." *PLOS ONE*, Vol. 5, No. 4, 2010, p. e9988. https://doi.org/10.1371/journal.pone.0009988.

[356] Andersen, T. J., Fredsoe, J., and Pejrup, M. "In Situ Estimation of Erosion and Deposition Thresholds by Acoustic Doppler Velocimeter (ADV)." *Estuarine, Coastal and Shelf Science*, Vol. 75, No. 3, 2007, pp. 327–336.

[357] Besemer, K., Singer, G., Hödl, I., and Battin, T. J. "Bacterial Community Composition of Stream Biofilms in Spatially Variable-Flow Environments." *Applied and Environmental Microbiology*, Vol. 75, No. 22, 2009, pp. 7189–7195. https://doi.org/10.1128/AEM.01284-09.

[358] Fang, H., Huang, L., Zhao, H., Cheng, W., Chen, Y., Fazeli, M., and Shang, Q. Biofilm Growth and the Impacts on Hydrodynamics. In *Mechanics of Bio-Sediment Transport* (H. Fang, L. Huang, H. Zhao, W. Cheng, Y. Chen, M. Fazeli, and Q. Shang, eds.), Springer, Berlin, Heidelberg, 2020, pp. 153–208.

[359] Murphy, E. A. K., Barros, J. M., Schultz, M. P., Flack, K. A., Steppe, C. N., and Reidenbach, M. A. "Roughness Effects of Diatomaceous Slime Fouling on Turbulent Boundary Layer Hydrodynamics." *Biofouling*, Vol. 34, No. 9, 2018, pp. 976–988. https://doi.org/10.1080/08927014.2018.1517867.

[360] Bowen, Z. H., and Waltermire, R. G. Evaluation of Light Detection and Ranging (LIDAR) for Measuring River Corridor Topography. Journal of the American Water Resources Association, 38, 1, , 2002, p. 3341.

[361] Milan, D., and Heritage, G. Gravel-Bed Rivers: Processes, Tools, Environments. In (R. A. Church M. Biron P., ed.), John Wiley & Sons Ltd, Chichester, UK, 2012, pp. 286–302.

[362] Smith, M., Vericat, D., and Gibbins, C. "Through-Water Terrestrial Laser Scanning of Gravel Beds at the Patch Scale." *Earth Surface Processes and Landforms*, Vol. 37, No. 4, 2012, pp. 411–421. https://doi.org/10.1002/esp.2254.

[363] Parsons, D. R., Best, J. L., Orfeo, O., Hardy, R. J., Kostaschuk, R., and Lane, S. N. "Morphology and Flow Fields of Three-Dimensional Dunes, Rio Paraná, Argentina: Results from Simultaneous Multibeam Echo Sounding and Acoustic Doppler Current Profiling." *Journal of Geophysical Research: Earth Surface*, Vol. 110, No. F4, 2005. https://doi.org/10.1029/2004JF000231.

[364] Morgan, J. A., Brogan, D. J., and Nelson, P. A. "Application of Structure-from-Motion Photogrammetry in Laboratory Flumes." *Geomorphology*, Vol. 276, 2017, pp. 125–143. https://doi.org/10.1016/j.geomorph.2016.10.021.

[365] Seitz, L., Haas, C., Noack, M., and Wieprecht, S. "From Picture to Porosity of River Bed Material Using Structure-from-Motion with Multi-View-Stereo." *Geomorphology*, Vol. 306, 2018, pp. 80–89. https://doi.org/10.1016/j.geomorph.2018.01.014.

[366] Noss, C., Wilkinson, J., and Lorke, A. "Triangulation Hand-Held Laser-Scanning (TriHaLaS) for Micro- and Meso-Habitat Surveys in Streams." *Earth Surface Processes and Landforms*, Vol. 43, No. 6, 2018, pp. 1241–1251. https://doi.org/10.1002/esp.4310.

[367] Noss, C., and Lorke, A. "Roughness, Resistance, and Dispersion: Relationships in Small Streams." *Water Resources Research*, Vol. 52, No. 4, 2016, pp. 2802–2821. https://doi.org/10.1002/2015WR017449.

[368] Carrivick, J. L., and Smith, M. W. "Fluvial and Aquatic Applications of Structure from Motion Photogrammetry and Unmanned Aerial Vehicle/Drone Technology." *WIREs Water*, Vol. 6, No. 1, 2019, p. e1328. https://doi.org/10.1002/wat2.1328.

[369] Tomsett, C., and Leyland, J. "Remote Sensing of River Corridors: A Review of Current Trends and Future Directions." *River Research and Applications*, Vol. 35, No. 7, 2019, pp. 779–803. https://doi.org/10.1002/rra.3479.

[370] Qiao, X., Ji, Y., Yamashita, A., and Asama, H. "Structure from Motion of Underwater Scenes Considering Image Degradation and Refraction." *IFAC-PapersOnLine*, Vol. 52, No. 22, 2019, pp. 78–82. https://doi.org/10.1016/j.ifacol.2019.11.051.

[371] Chadebecq, F., Vasconcelos, F., Lacher, R., Maneas, E., Desjardins, A., Ourselin, S., Vercauteren, T., and Stoyanov, D. "Refractive Two-View Reconstruction for Underwater 3D Vision." *International Journal of Computer Vision*, Vol. 128, No. 5, 2020, pp. 1101–1117. https://doi.org/10.1007/s11263-019-01218-9.

[372] Clark, D. R., Ferguson, R. M. W., Harris, D. N., Nicholass, K. J. M., Prentice, H. J., Randall, K. C., Randell, L., Warren, S. L., and Dumbrell, A. J. "Streams of Data from Drops of Water: 21st Century Molecular Microbial Ecology." *WIREs Water*, Vol. 5, No. 4, 2018, p. e1280. https://doi.org/10.1002/wat2.1280.

[373] Rice, S. A., Wuertz, S., and Kjelleberg, S. "Next-Generation Studies of Microbial Biofilm Communities." *Microbial Biotechnology*, Vol. 9, No. 5, 2016, pp. 677–680. https://doi.org/10.1111/1751-7915.12390.

[374] Griffiths, R. I., Whiteley, A. S., O'Donnell, A. G., and Bailey, M. J. "Rapid Method for Coextraction of DNA and RNA from Natural Environments for Analysis of Ribosomal DNA- and RRNA-Based Microbial Community Composition." *Applied and Environmental Microbiology*, Vol. 66, No. 12, 2000, pp. 5488–5491.

[375] Besemer, K., Peter, H., Logue, J. B., Langenheder, S., Lindström, E. S., Tranvik, L. J., and Battin, T. J. "Unraveling Assembly of Stream Biofilm Communities." *The ISME Journal*, Vol. 6, No. 8, 2012, pp. 1459–1468. https://doi.org/10.1038/ismej.2011.205.

[376] Compte-Port, S., Fillol, M., Gich, F., and Borrego, C. M. "Metabolic Versatility of Freshwater Sedimentary Archaea Feeding on Different Organic Carbon Sources." *PLOS ONE*, Vol. 15, No. 4, 2020, p. e0231238. https://doi.org/10.1371/journal.pone.0231238.

[377] Wagner, K., Bengtsson, M. M., Besemer, K., Sieczko, A., Burns, N. R., Herberg, E. R., and Battin, T. J. "Functional and Structural Responses of Hyporheic Biofilms to Varying Sources of Dissolved Organic Matter." *Applied and Environmental Microbiology*, Vol. 80, No. 19, 2014, pp. 6004–6012. https://doi.org/10.1128/AEM.01128-14.

[378] Weisbrod, B., Wood, S. A., Steiner, K., Whyte-Wilding, R., Puddick, J., Laroche, O., and Dietrich, D. R. "Is a Central Sediment Sample Sufficient? Exploring Spatial and Temporal Microbial Diversity in a Small Lake." *Toxins*, Vol. 12, No. 9, 2020, p. 580. https://doi.org/10.3390/toxins12090580.

[379] Wilhelm, L., Singer, G. A., Fasching, C., Battin, T. J., and Besemer, K. "Microbial Biodiversity in Glacier-Fed Streams." *The ISME Journal*, Vol. 7, No. 8, 2013, pp. 1651–1660. https://doi.org/10.1038/ismej.2013.44.

[380] Leng, X., and Chanson, H. "Transverse Velocity Profiling under Positive Surges in Channels." *Flow Measurement and Instrumentation*, Vol. 64, 2018, pp. 14–27. https://doi.org/10.1016/j.flowmeasinst.2018.10.006.

[381] Hooshmand, A., Horner-Devine, A. R., and Lamb, M. P. "Structure of Turbulence and Sediment Stratification in Wave-Supported Mud Layers." *Journal of Geophysical Research: Oceans*, Vol. 120, No. 4, 2015, pp. 2430–2448. https://doi.org/10.1002/2014JC010231.

[382] Przyborowski, Ł., Łoboda, A. M., Karpiński, M., and Bialik, R. J. Characteristics of Flow Around Aquatic Plants in Natural Conditions: Experimental Setup, Challenges and Difficulties. Cham, 2018.

[383] Wengrove, M. E., and Foster, D. L. "Field Evidence of the Viscous Sublayer in a Tidally Forced Developing Boundary Layer." *Geophysical Research Letters*, Vol. 41, No. 14, 2014, pp. 5084–5090. https://doi.org/10.1002/2014GL060709.

[384] Dombroski, D. E., and Crimaldi, J. P. "The Accuracy of Acoustic Doppler Velocimetry Measurements in Turbulent Boundary Layer Flows over a Smooth Bed." *Limnology and Oceanography: Methods*, Vol. 5, No. 1, 2007, pp. 23–33. https://doi.org/10.4319/lom.2007.5.23.

[385] Finelli, C. M., Hart, D. D., and Fonseca, D. M. "Evaluating the Spatial Resolution of an Acoustic Doppler Velocimeter and the Consequences for Measuring Near-Bed Flows." *Limnology and Oceanography*, Vol. 44, No. 7, 1999, pp. 1793–1801. https://doi.org/10.4319/lo.1999.44.7.1793.

[386] Voulgaris, G., and Trowbridge, J. H. "Evaluation of the Acoustic Doppler Velocimeter (ADV) for Turbulence Measurements*." *Journal of Atmospheric and Oceanic Technology*, Vol. 15, No. 1, 1998, pp. 272–289. https://doi.org/10.1175/1520-0426(1998)015<0272:EOTADV>2.0.CO;2.

[387] Cameron, S. M., Nikora, V. I., Albayrak, I., Miler, O., Stewart, M., and Siniscalchi, F. "Interactions between Aquatic Plants and Turbulent Flow: A Field Study Using Stereoscopic PIV." *Journal of Fluid Mechanics*, Vol. 732, 2013, pp. 345–372. https://doi.org/10.1017/jfm.2013.406.

[388] Hannah, D. M., Wood, P. J., and Sadler, J. P. "Ecohydrology and Hydroecology: A New Paradigm'?" *Hydrological processes*, Vol. 18, 2004, pp. 3439–3445. https://doi.org/10.1002/hyp.5761.

[389] Deutsches TalsperrenKomitee e. V., ed. *Talsperren in Deutschland [Dams and Reservoirs in Germany]*. Springer Fachmedien Wiesbaden, Wiesbaden, Germany, 2013.

[390] Beckers, F., Biserov, R., and Wieprecht, S. *Experimental Investigation of Sediment Stability at Reservoirs on the Rhône River*. Publication 09/2019. Institute for Modelling Hydraulic and Environmental Systems (IWS), Stuttgart, Germany. http://doi.org/10.5281/zenodo.3739802, 2019, p. 54.

[391] Mayar, M. A., Schmid, G., Wieprecht, S., and Noack, M. "Proof-of-Concept for Nonintrusive and Undisturbed Measurement of Sediment Infiltration Masses Using Gamma-Ray Attenuation." *Journal of Hydraulic Engineering*, Vol. 146, No. 5, 2020, p. 04020032. https://doi.org/10.1061/(ASCE)HY.1943-7900.0001734.

[392] Mayar, M. A., Schmid, G., Wieprecht, S., and Noack, M. "Optimizing Vertical Profile Measurements Setup of Gamma Ray Attenuation." *Radiation Physics and Chemistry*, Vol. 164, 2019, p. 108376. https://doi.org/10.1016/j.radphyschem.2019.108376.

[393] Raunkjær, K., Hvitved-Jacobsen, T., and Nielsen, P. H. "Measurement of Pools of Protein, Carbohydrate and Lipid in Domestic Wastewater." *Water Research*, Vol. 28, No. 2, 1994, pp. 251–262. https://doi.org/10.1016/0043-1354(94)90261-5.

[394] Dubois, G. *Modeling and Simulation - Challenges and Best Practices for Industry*. CRC Press (Taylor & Francis Group), Boca Raton, FL, USA, 2018.

[395] Kolmogorov, A. N. The Local Structure of Turbulence in Incompressible Viscous Fluid for Very Large Reynolds' Numbers. No. 30, 1941, pp. 301–305.

[396] Farnebäck, G. Two-Frame Motion Estimation Based on Polynomial Expansion. In *Image Analysis* (J. Bigun and T. Gustavsson, eds.), Springer Berlin Heidelberg, Berlin, Heidelberg, 2003, pp. 363–370.

[397] MacVicar, B., Dilling, S., Lacey, J., and Hipel, K. A Quality Analysis of the Vectrino II Instrument Using a New Open-Source MATLAB Toolbox and 2D ARMA Models to Detect and Replace Spikes. Presented at the River Flow 2014, Lausanne, Switzerland, Sept 03.

[398] Larson, F., Lubarsky, H., Gerbersdorf, S. U., and Paterson, D. M. "Surface Adhesion Measurements in Aquatic Biofilms Using Magnetic Particle Induction: MagPI." *Limnology and Oceanography: Methods*, Vol. 7, No. 7, 2009, pp. 490–497. https://doi.org/10.4319/lom.2009.7.490.

6 Appendices

Appendix I: Performance of the Vectrino Profiler at the sediment–water interface

Appendix II: Exploring flow–biofilm–sediment interactions: Assessment of current status and future challenges

Appendix III: Functional relationships between critical erosion thresholds of fine reservoir sediments and their sedimentological characteristics

Appendix I

Performance of the Vectrino Profiler at the sediment–water interface[i]

Performance of the Vectrino Profiler at the sediment–water interface

Kaan Koca, Christian Noss, Christine Anlanger, Andreas Brand & Andreas Lorke

Technical note

Performance of the Vectrino Profiler at the sediment–water interface

KAAN KOCA, PhD Student, *Institute for Environmental Sciences, University of Koblenz-Landau, Landau, Germany.*
Email: koca@uni-landau.de (author for correspondence)

CHRISTIAN NOSS, Postdoctoral Researcher, *Institute for Environmental Sciences, University of Koblenz-Landau, Landau, Germany.*
Email: noss@uni-landau.de

CHRISTINE ANLANGER, PhD Student, *Institute for Environmental Sciences, University of Koblenz-Landau, Landau, Germany.*
Email: anlanger@uni-landau.de

ANDREAS BRAND, Postdoctoral Researcher, *Institute for Biogeochemistry and Pollutant Dynamics, ETH Zurich, Zurich, Switzerland*; *Surface Waters – Research and Management, Eawag, Swiss Federal Institute of Aquatic Science and Technology, Kastanienbaum, Switzerland.*
Email: andreas.brand@eawag.ch

ANDREAS LORKE, Professor, *Institute for Environmental Sciences, University of Koblenz-Landau, Landau, Germany.*
Email: lorke@uni-landau.de

ABSTRACT
The Vectrino Profiler is increasingly recognized as a promising instrument for characterizing near-bed velocities and turbulence due to its high spatio-temporal resolution and velocity profiling range. However, its measurement performance in the vicinity of the bed (< 10 mm) is not well documented. This study reports on the comparisons of mean velocity, turbulent kinetic energy, and power spectral density above various bed materials between the Vectrino Profiler and particle image velocimetry in a laboratory flume. Our analyses demonstrate that the bed interference adversely influences the measurements as close as 1.7–5 mm above the bed, depending on the bed material. We provide a criterion to identify the vertical extent of the interference region. Outside of the interference region, best agreement between the Vectrino Profiler and particle image velocimetry was found around the sweet-spot of the profiler where the observed differences were < 6% for mean velocities and < 10% for turbulent kinetic energy.

Keywords: Acoustic Doppler profiler; boundary layer; particle image velocimetry (PIV); sediment–water interface; turbulence; velocity measurements

1 Introduction

Measurements of velocities and turbulence with high spatio-temporal resolution are of critical importance for a variety of hydraulic applications. In 2012, the Vectrino Profiler (Vectrino II, Nortek AS, Rud, Norway) was introduced to meet the needs for increased spatial resolution. The Vectrino Profiler (VP) is a multi-static acoustic Doppler velocity profiler and its probe comprises four receivers around a central transmitter. It is capable of measuring three-dimensional flow velocities over a profiling range of 35 mm with an adjustable vertical resolution (bin size) of 1 to 4 mm, and at a sampling rate of up to

100 Hz. The instrument also allows for simultaneous measurements of the distance to a solid boundary at a sampling rate of up to 10 Hz, and a spatial resolution between 1 and 4 mm (Craig, Loadman, Clement, Rusello, & Siegel, 2011).

This work is motivated by the increasing use of the VP for measuring velocities and turbulence at the sediment–water interface (SWI) under both laboratory (Hooshmand, Horner-Devine, & Lamb, 2015) and field (Puleo et al., 2014; Wengrove & Foster, 2015) conditions. Its enhanced spatial resolution and velocity profiling range, together with simultaneous distance measurements, will most likely make the VP increasingly popular, particularly for the investigation of sediment–water

interactions. However, in spite of its high potential for boundary layer studies, there have been only few investigations on the effect of a boundary located in the measurement range on the performance of the VP (Brand, Noss, Dinkel, & Holzner, 2016; MacVicar, Dilling, Lacey, & Hipel, 2014), although boundaries are known to have adverse effects on other Doppler-based velocity measurements (Dombroski & Crimaldi, 2007; Finelli, Hart, & Fonseca, 1999; Precht, Janssen, & Huettel, 2006; Voulgaris & Trowbridge, 1998). Based on measurements away from solid boundaries, Brand et al. (2016) observed in comparison to standard acoustic Doppler velocimeter (ADV) measurements that (i) mean velocities measured by the VP are only reliable in the upper 25 mm of its profiling range, and (ii) turbulence quantities are most reliable at the sweet-spot (SS) of the VP, which will be discussed below.

The boundary interference region (IR) is defined as the near-bed region of the velocity profile, where the measurements are biased by the presence of the interface. Estimation of the vertical extent of the IR above the bed is of critical importance and requires independent reference flow measurements, which were lacking in the studies of MacVicar et al. (2014) and Brand et al. (2016). The focus of this contribution is therefore on the investigation of the influence and vertical extent of the IR on mean velocities and turbulence measured by the VP over different types of bed material. We also provide a comparison between the VP and particle image velocimetry (PIV) measurements away from the bed.

2 Methods

2.1 *Methodology and data*

Laboratory experiments were carried out in a flume (36 cm wide, 3 m long), which was instrumented with a PIV system (Dantec Dynamics, Skovlunde, Denmark) and a VP. A Cartesian coordinate system was used: the VP and therefore three-dimensional flow velocities (u, v, w) were accurately aligned with longitudinal (x), transversal (y), and vertical (z) directions of the flume (Fig. 1). The overlapping sampling volumes of both instruments were located at a fixed position at the centreline of the flume, 120 cm downstream of the flume inlet. PIV measurements were performed subsequently to the VP measurements.

The flume water was seeded with particles (20 µm polyamide) until the signal-to-noise ratio (SNR) of the VP measurements was at least 30 dB at the SS and 20 dB at the upper and lower end of the VP profiling range, which are the thresholds recommended by the manufacturer (http://www.nortekusa.com/usa/knowledge-center/). The SS corresponds to the location within the VP sampling volume, where the overlap of the four acoustic beams is largest. This corresponds to bin 12 in our case (52 mm below the transmitter, Fig. 1). During the measurements the flow depth was kept constant at 23 cm, while flow velocity, bed material, and distance of the probe to the bed were altered. Four types of beds were used: (i) geotextile bed (GF, Polypropylen, GreenLife GmbH, Schwerin, Germany) as
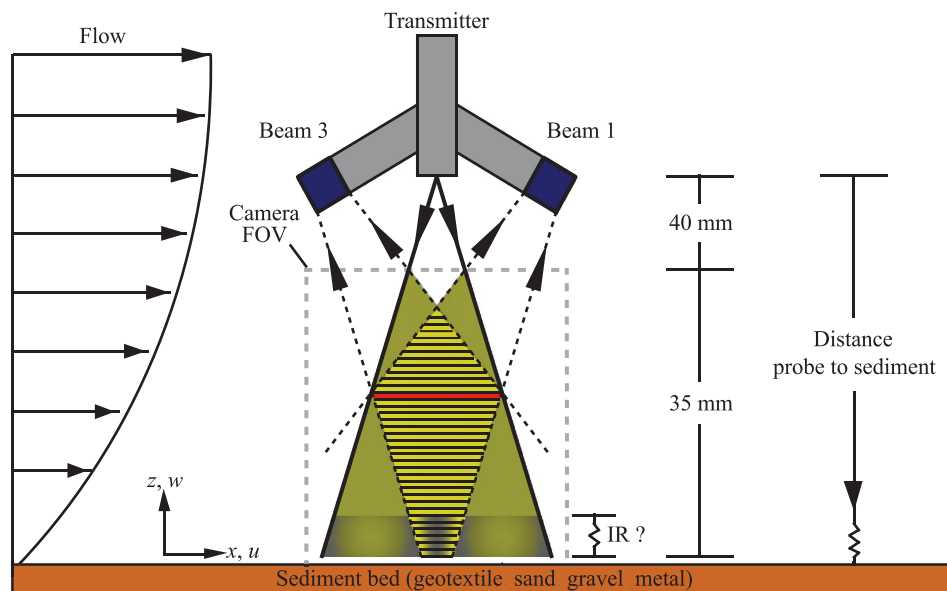
Figure 1   Side view of a schematic diagram showing the experimental set-up (not to scale). Only one pair of receivers are shown, with beam 1 (*x*- direction) aligned with the mean flow. Transmitter and receivers (beams) have a divergence angle for transmitting (solid lines with arrows) the acoustic signal and receiving backscattered signal (dashed black lines with arrows) within a sampling volume (shaded yellow area). The light yellow area in the sampling volume represents the region in which all beams overlap and observe the same particles. The darker yellow area represents the region where the beams receive backscattered signals from different regions of the sampling volume. The red bar in the sampling volume shows the position of the sweet-spot (SS, bin 12), where the overlapping region of the beams is the largest. The rectangular area enclosed by the grey dashed lines shows the field-of-view (FOV) of the PIV camera. The interference region (IR), where the velocity measurements are affected by the presence of the bed, is shown by a colour-gradient near the bed and a zigzag pattern for its variable vertical extent

Table 1   Per cent difference (PD) in mean velocity $\langle U_{\text{mag}} \rangle$ and turbulent kinetic energy $\langle \text{TKE} \rangle$ measured by PIV and VP for the different bed materials and flow velocities

Test			Probe distance by		PD			
ID	Bed type	$\langle U_{\text{mag}} \rangle$ (m s^{-1})	VP (mm)	PIV camera (mm)	z_{ir} z_{ss} (mm)	$\langle U_{\text{mag}} \rangle$ (%)	$\langle \text{TKE} \rangle$ (%)	$\langle \text{TKE} \rangle$ (HL) (%)
GF	Geotextile	0.026	74.0	66.3	1.7	− 19.3	− 32.6	− 60.1
					15.0	− 5.8	− 19.7	− 25.7
S1	Sand	0.039	74.1	73.0	3.3	− 14.7	− 48.1	− 89.9
					21.7	0.6	− 5.1	− 9.7
S2a	Sand	0.026	61.0	59.9	2.5	− 33.2	− 50.6	− 63.2
					8.6	− 17.0	− 20.5	− 26.7
S2b	Sand	0.026	73.8	72.7	3.0	− 26.4	− 21.6	− 52.0
					21.4	− 12.7	13.7	9.3
S2c[a]	Sand	0.026	50.5	49.4	3.3	− 7.0	− 35.0	− 46.1
G1	Gravel	0.031	74.2	74.2	4.5	− 20.9	10.5	− 41.8
					23.0	− 4.5	7.5	3.0
G2a	Gravel	0.056	74.2	74.2	4.5	− 11.8	8.3	− 43.8
					23.0	− 1.6	10.9	6.1
G2b	Gravel	0.056	60.4	60.5	4.1	5.2	3.5	− 14.9
					9.2	5.2	− 15.8	− 23.5
G2c[a]	Gravel	0.056	50.8	50.8	3.6	3.0	− 0.5	− 14.0
M	Metal	0.110	74.1	74.1	5.2	8.2	2.3	− 36.5
					22.8	4.6	− 4.4	− 12.1

Note: The height of the interference region (z_{ir}) and the position of the sweet-spot (z_{ss}, bin 12) were superimposed for PD comparison in terms of their elevations above the bed (mm).
[a]No comparison at z_{ss} (bin 12) exists for these tests since z_{ss} is located within the bed. PIV measurements were performed subsequently to these tests for S2 and G2 datasets.

a scenario for fluffy sediment with high porosity; (ii) sand bed (S) with a median grain size (D_{50}) of 0.25 mm; (iii) gravel bed (G) having a nominal diameter between 18 and 36 mm (coarse gravel); and (iv) metal bed (M) as a scenario for strongly reflective flat bottom. Furthermore, the distance between the probe and the bed was varied for tests S2 and G2 (Table 1). Vertical profiles of mean velocity, turbulent kinetic energy (TKE), as well as power spectral density (PSD) of velocity fluctuations were compared because they are essential parameters, which are frequently used to characterize the near-bed flow fields.

2.2   *Vectrino Profiler and data processing*

Three-dimensional velocity measurements were sampled for 6 min at 74 Hz with a vertical bin resolution of 1 mm over a range of 35 mm, starting 40 mm away from the transmitter (Fig. 1). The manufacturer recommends either to use the maximum interval ping algorithm and to adjust the velocity range to limit the influence of the acoustic interference on the velocity data, or to use the adaptive ping algorithm (http://cs.nortek.no/). The effect of different ping algorithms on SNR and correlation values was tested before the measurements. The maximum interval ping algorithm, which produces the longest ping interval to match the ambiguity velocity, was indeed found to be best suited for investigating the effect of acoustic interference close to the bed. Acoustic interference is related to the ping timing, and to obtain

good-quality data close to the bed, the ping interval needs to be long enough to reduce the signal contamination due to the pulse-to-pulse interference caused by reflections at the bed (see fig. 7 of Craig et al., 2011). We selected the maximum interval ping algorithm and adjusted the velocity range between 0.2 and 0.6 m s^{-1} depending on the flow conditions.

The instrument provides four velocity values, of which the longitudinal (u) and one vertical component (w_1) are obtained from receivers 1 and 3, and the transversal (v) and the second vertical component (w_2) are obtained from receivers 2 and 4. Such a set-up facilitates the estimation of the measurement noise in each velocity component (Hurther & Lemmin, 2001). It is based on the covariance of the two redundantly measured vertical velocity estimates $\langle w'_1 w'_2 \rangle$, for which the noise is assumed to be uncorrelated such that $\langle w'_1 w'_2 \rangle = \langle w'^2_{\text{true1}} \rangle = \langle w'^2_{\text{true2}} \rangle$. w'_1 and w'_2 are the fluctuating components (e.g. $w'_1 = w_1 - \langle w_1 \rangle$) of the two independently measured vertical velocities, $\langle w'^2_{\text{true1}} \rangle$ and $\langle w'^2_{\text{true2}} \rangle$ are their true variances, and angle brackets denote the time average. Following Hurther and Lemmin (2001), the variance of the noise for each vertical velocity component was estimated by subtracting the covariance from the measured variance (e.g. $\langle N^2_{w1} \rangle = \langle w'^2_1 \rangle - \langle w'_1 w'_2 \rangle$). Finally, the average noise variance $\langle N^2_w \rangle$ was calculated (i.e. $\langle N^2_w \rangle = 0.5(\langle N^2_{w1} \rangle + \langle N^2_{w2} \rangle)$). The corresponding Doppler noise in the longitudinal and transversal velocity components ($\langle N^2_{u,v} \rangle$) was estimated from the calibration matrix provided by

the VP, and subtracted from the measured variances $\langle u'^2 \rangle$ and $\langle v'^2 \rangle$ to calculate noise-corrected variances.

By careful examination of velocities and turbulence after trying various SNR and correlation thresholds, raw data were first filtered in beam coordinates with thresholds of SNR > 15 dB and correlation > 70%, and then despiked following the method of Goring and Nikora (2002), modified by Wahl (2003). Both procedures resulted in rejection of unreliable data below 1% and 3%, respectively, and affected neither normality of velocity distributions nor variance of the velocities. The outliers were replaced by the nearest valid data points. The filtered data were transformed back into the Cartesian coordinates, and the Doppler noise correction method (hereafter referred as "HL-corrected") of Hurther and Lemmin (2001) was applied.

2.3   *Particle image velocimetry and data processing*

Two-dimensional velocities (u, w) around the sampling volume of the VP were measured by PIV. The system consisted of a Dantec Dynamics FlowSense 4M charge-coupled (CCD) digital camera (2048 × 2048 pixels, 8 bit, greyscale), a 200-mJ Nd:YAG double-pulse laser (Litron Lasers, wave length: 532 nm), fitted with a cylindrical lens to generate a planar light sheet. The camera recorded double frame images within a field of view (FOV) of 46 × 46 mm (0.022 mm px^{-1}), at a rate of 7.4 Hz for 6 min. The time interval between two successive laser pulses was adjusted depending on the flow speed. The image pairs were processed using an adaptive correlation algorithm (DynamicStudio V4.0, Dantec Dynamics) with interrogation areas (IAs) of 32 × 32 pixels without overlapping, and with a 3 × 3 moving average validation for outlier detection. The final resolution of the two-dimensional velocity vectors was 0.7 mm in the longitudinal and vertical direction.

2.4   *Instrument comparison*

To locate the sampling volume of the VP within the FOV of the PIV camera and to align the velocity vectors measured by both instruments, the VP's probe position was measured by its internal boundary distance detection and by a combination of optical and physical surveys using the PIV camera and a micrometer screw. The distance between the central transmitter of the VP (Fig. 1) and the solid boundary is measured by the VP's transmitter via detecting the position of the maximum return signal intensity (Craig et al., 2011). This measurement process is influenced by the properties of the bed materials. Porous materials are expected to absorb and attenuate more of the acoustic signal due to their lower acoustic impedance (Kuczmarski & Johnston, 2011). The precise longitudinal and vertical position of the probe was first surveyed in images (resolution: 0.022 mm px^{-1}, accuracy: ± 2 pixels) close to the bed (approximately 30 mm above the bed), before the VP was moved upward to the position of the velocity measurements by the micrometer screw. A relative difference between the vertical increments adjusted by the

micrometer screw (30, 40, 50, 60, 70 and 74 mm from the bed, accuracy: ± 50 μm), and bed distances measured by the VP did not show any difference, irrespective of the bed material. This indicates that acoustic penetration and reflection of the VP's signal are independent of bed distance and vertical probe position. Therefore, bed distance measured by the VP's internal boundary detection was corrected to correspond to the topmost position of the bed elevation for different bed materials as observed by the PIV camera. We estimate an accuracy of ± 0.5 mm for the position of the solid bed, which corresponds to the nominal accuracy of the VP's distance measurements (Nortek, 2016). The locations of the measurement bins were taken from the "velocity header range matrix", which was calculated internally by the VP.

The PIV provided only two components of the velocity vectors (u, w), whereas the VP provided all three components (u, v, w). To compare the velocities measured by the PIV and by the VP, the velocity measurements at the intersections of both sampling volumes were considered for further analyses: (i) the width of the sampling volume of the VP was approximated by a cylinder with a diameter of 6 mm similar to the study of Poindexter, Rusello, and Variano (2011), and velocity vectors within the *xz*-plane obtained by the PIV were horizontally averaged in the *x*-direction (eight IAs) across the width of the VP's sampling volume; and (ii) velocity vectors within single IAs along the centreline of the VP's sampling volume were considered. The former method was selected because bulk flow statistics (i.e. mean velocity and TKE) were not affected by the degree of spatial averaging at these scales. The magnitudes of the mean velocities and the TKE were calculated using the following relations: $\langle U_{\mathrm{mag}} \rangle = (\langle u \rangle^2 + \langle w_1 \rangle^2)^{0.5}$, and $\langle \mathrm{TKE} \rangle = 0.5(\langle u'^2 \rangle + \langle w_1'^2 \rangle)$. w_1 was selected since it was obtained from the same pair of beams as u. PSDs of velocity fluctuations were estimated using Welch's method (Welch, 1967) for time-series segments of 512 points with 50% overlap, and a Hanning window function.

The effect of potential misalignment of both instruments was tested by rotating the measured velocity vectors by ± 1° around the three axes, which resulted in a maximum variation of 0.5% for $\langle \mathrm{TKE} \rangle$ and approximately 4% for the covariance of longitudinal and vertical velocity fluctuations $\langle u'w_1' \rangle$. Covariance is known to be most sensitive to misalignment errors (Peltier et al., 2013). We restricted the comparison between the VP and PIV to scalar quantities ($\langle U_{\mathrm{mag}} \rangle$, $\langle \mathrm{TKE} \rangle$) and PSD of velocity components to minimize the effect of small misalignment errors. The per cent differences between mean velocities and TKE measured by the PIV and VP were calculated as PD = $[(\langle \mathrm{VP} \rangle - \langle \mathrm{PIV} \rangle)/((\langle \mathrm{VP} \rangle + \langle \mathrm{PIV} \rangle)/2)] \times 100\%$.

3   Results

In this section, we illustrate the vertical extent of the IR and its effect on the near-bed velocities and turbulence by
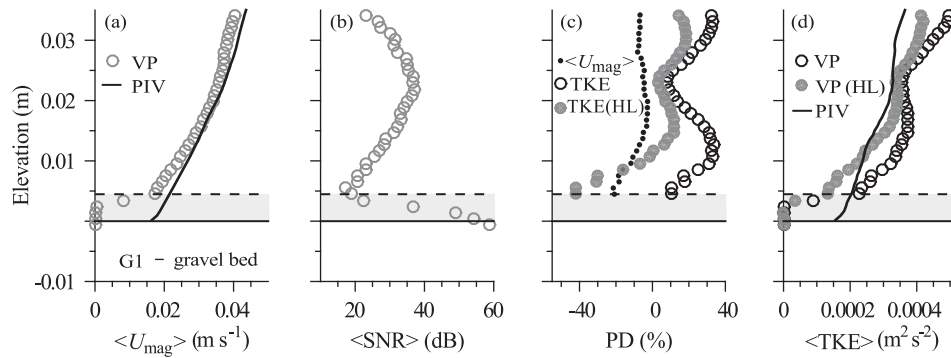
Figure 2   Mean velocity $\langle U_{mag} \rangle$ and turbulent kinetic energy $\langle TKE \rangle$ profiles measured by the VP and PIV over gravel bed (G1). (a) Mean velocities measured by the two instruments; (b) mean SNR values of all beams measured by the VP; (c) PD between the VP and PIV measurements; (d) comparison of uncorrected and HL-corrected $\langle TKE \rangle$ profiles. The shaded grey area represents the interference region (IR), with the horizontal dashed lines denoting the upper end of the IR ($z_{ir} = 4.5$ mm). The solid black lines at an elevation (z) of 0 mm show the locations of the bed surfaces
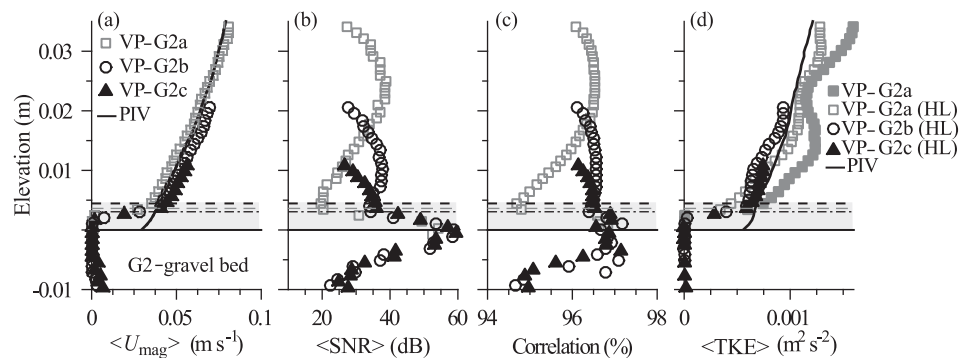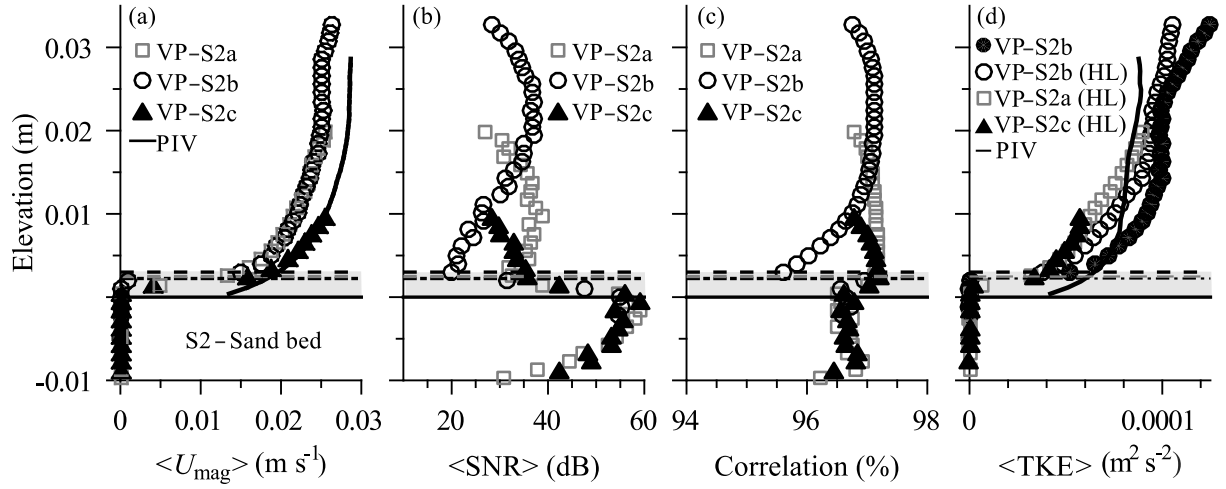

Figure 3   Mean velocity $\langle U_{mag} \rangle$ and turbulent kinetic energy $\langle TKE \rangle$ profiles measured by the PIV and VP with varying proximity to the gravel bed (G2a–G2c). (a) Mean velocities measured by the two instruments; (b) mean SNR values of all beams measured by the VP; (c) mean correlation values of all beams measured by the VP; (d) comparison of uncorrected and HL-corrected $\langle TKE \rangle$ profiles. The shaded grey area represents the interference region (IR), with the horizontal dashed lines denoting the upper end of the IR. The solid black lines at an elevation (z) of 0 mm show the locations of the bed surfaces

representative plots from gravel bed experiments (Figs 2 and 3), because measurements above all the bed materials showed a similar pattern. The velocity and turbulence profiles above geotextile (GF), sand (S1–S2), and metal (M) beds can be found in the supplementary material.

3.1 *Mean velocities*

Good agreement between the VP and PIV measurements was observed in the upper region of the profile, where PD $< 10\%$ for mean velocities estimated over ± 8 bins centred at the SS (bin 12) of the VP, and PD $< 6\%$ at bin 12 (Table 1, e.g. Fig. 2), except for sand tests (S2a and S2b, Fig. S2). On the other hand, large differences were observed close to the bed (Fig. 2a). This is most likely caused by bed interference of the acoustic measurements (Rusello & Allard, 2012). Within this zone, the quality parameters measured by the VP remained above critical thresholds (correlation $> 70\%$, SNR > 20 dB), which makes it difficult to identify the potentially contaminated range of the velocity profile. The SNR profile of the VP measurements always had a parabolic shape with the highest values ($c.38$ dB) around the SS of the profiling range (Fig. 2b). A local minimum of SNR was observed at the lower end of this parabola, whose

height varied with bed material. Below this minimum, the SNR increased sharply, reaching a maximum of 55–60 dB. The height at which the SNR reached a local minimum (horizontal dashed lines in Figs 2 and 3) corresponded to the upper end of the IR, below which the velocities began to deviate most strongly from the PIV measurements. This suggests that the vertical extent of the IR can be identified by the location of a minimum in the mean SNR profile.

The thickness of the IR (z_{ir}) varied between 1.7 ± 0.5 mm and 5.2 ± 0.5 mm (Fig. 4) for different bed materials. This suggests that velocity measurements with VP can be reliable as close as 1.7 ± 0.5 (mm) to the SWI, which is at least one-fifth of the distance suggested by Voulgaris and Trowbridge (1998) for a standard ADV. Above the IR the differences between the PIV and VP velocities were as small as 3% for Test G2c (Table 1), yet as high as -19.3% for Test GF (Table 1), and -26.4% for Test S2b (Table 1). Within the IR, the differences between the VP and PIV velocities increased steadily (reaching 200%) whilst approaching the bed.

The vertical extent of the IR decreased with decreasing probe's proximity to the bed, i.e. from 4.5 mm to 3.6 mm for the gravel bed, and varied between 3.3 and 2.5 mm for the sand bed, which is close to the accuracy (± 0.5 mm) of the distance
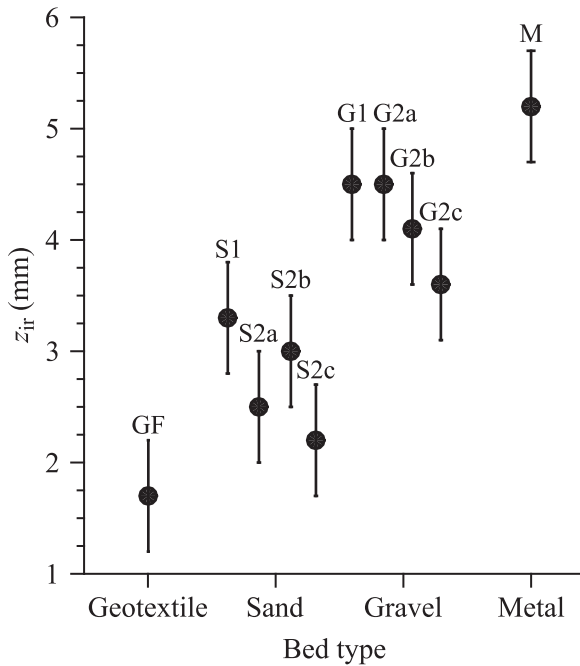
Figure 4   Observed height of the interference region (z_{ir}) for the measurements performed over geotextile, sand, gravel and metal beds. Error bars represent the accuracy of the distance measurements related to identification of the solid bed surface

measurements (Table 1 and Fig. 4). Also the PD between the measured mean velocities varied with varying the probe's proximity to the bed, between -33.2% and -7% for the sand bed, and between -11.8% and 3% for the gravel bed (Table 1). Best agreement between the VP and the PIV was found when the probe was closest to the bed (PD $= -7\%$ and PD $= 3\%$ in mean velocities for the sand and gravel bed, respectively). A potential explanation for the effect of the probe's proximity to the bed on the measured velocities could be the flow disturbance caused by the presence of the VP. While mean velocities were increasing with decreasing probe's proximity to the gravel bed (G2, Fig. 3a), no systematic increase in mean velocities was observed on sand bed (S2, Fig. S2a). Brand et al. (2016) estimated the effect of flow disturbance to be $< 0.9\%$ in the horizontal and $< 0.6\%$ in the vertical velocity component along VP's profiling range. The reason for the clear differences in measured mean velocities with different probe's proximity in the present measurements remains unclear.

The local maximum of SNR (55–60 dB) at the end of the VP profiling range was identical with the rigid bed level for gravel and metal beds (Figs 3b and S1j). This is likely due to the fact that no (or very little) acoustic signal was absorbed by the bed, and the acoustic signals were reflected mainly at the surface of the gravel and metal beds. Indeed, the PIV camera and the VP distance measurements were in a very good agreement for these types of beds (Table 1). However, 7.7 mm and 1.7 mm differences in distance readings (Table 1) between the surveys of the PIV camera and the VP were observed for the geotextile and sand bed, respectively, which confirms that the acoustic signal

penetrated into the bed for softer materials. Hence, the identification of the bed surface on soft materials is difficult, because none of the quality parameters (i.e. SNR and correlation) can be used to precisely identify the position of the bed in the measured velocity profiles. While we were unable to obtain a quantitative measure of softness and absorbance of the different bed materials used in our study, the effect of these measures on the extent of the IR should be considered in future studies.

3.2   *Turbulent kinetic energy and power spectral density*

The best agreement between $\langle TKE \rangle$ estimated from the VP and PIV measurements was observed at ± 4 bins around the SS of the VP (Fig. 2c). Differences between $\langle TKE \rangle$ from the VP and $\langle TKE \rangle$ from the PIV were below 10% (Fig. 2c) at this region for tests S1, G1, G2a and M. In these tests the VP was located approximately 74 mm above the bed (see Table 1) and therefore the entire profiling range of the VP could be analysed. Contrary to measurements around the SS, PD exceeded 20% in the lowest 15 mm of the profile (Fig. 2c). The uncorrected and HL-corrected $\langle TKE \rangle$ profiles showed a persistent local minimum around the SS (Fig. 2d), which suggests that the data quality varied along the VP's sampling volume. This local minimum was observed in $\langle u'^2 \rangle$ and $\langle v'^2 \rangle$ (not shown), but was not observed for ($\langle w_1'^2 \rangle$ and $\langle w_2'^2 \rangle$). MacVicar et al. (2014) and Brand et al. (2016) also observed similar profiles of velocity variances with a local minimum at the SS (e.g. see Fig. 3c of MacVicar et al., 2014). According to Brand et al. (2016), the profile shape is most likely caused by the Doppler noise contamination and decorrelation of the signals (decreasing overlap of the acoustic beams towards the edges of the velocity profile, Fig. 1), both of which are the result of geometric arrangement of the beams. Brand et al. (2016) observed that Doppler noise mainly contaminated the variance of the horizontal velocities, while the variance of the vertical velocities was mainly affected by the decorrelation of the beam signals. After applying the HL-correction, we observed a local minimum of $\langle N_u^2 \rangle$ at the SS, which increased on either side of the SS (Fig. S3), and dropped rapidly to zero at the upper end of the IR. $\langle N_u^2 \rangle$ was at least a factor of 10 higher in comparison to $\langle N_w^2 \rangle$ (1×10^{-4} vs. 7×10^{-6} for $\langle N_u^2 \rangle$ and $\langle N_w^2 \rangle$ at the SS, respectively for test G2a). Hence, the observed local minimum of $\langle TKE \rangle$ at the SS (Figs 2d and 3d) is not surprising since $\langle TKE \rangle$, by definition, involves contributions from both longitudinal and vertical velocity fluctuations.

Similar to the mean velocities, large differences in uncorrected and HL-corrected $\langle TKE \rangle$ were observed between the VP measurements with different probe proximities to the bed. Differences in uncorrected $\langle TKE \rangle$ at 9 mm above the bed varied between -2.7% and -20.5% for sand bed tests (S2), and between -13.6% and 23.4% for gravel bed tests (G2) (Figs 3d and S2d). Differences in HL-corrected $\langle TKE \rangle$ varied between -8.4% and -31.1% for sand bed tests (S2), and between -8.5% and -21.1% for gravel bed tests (G2). Surprisingly, the HL-correction did not result in a consistent improvement

throughout the profiles, although it improved the agreement at the SS for Tests S2b, G1 and G2a (Table 1). When the probe was located closest to the bed, the uncorrected $\langle$TKE$\rangle$ estimates matched favourably with a PD of -0.5% at 3.6 mm above the gravel bed (G2c, Table 1). Still, there was no improvement for sand bed (PD $= -35\%$ at 3.3 mm above the bed in Test S2c, Table 1). It should be noted that the SS (z_{ss}, bin 12) was located within the bed in tests S2c and G2c, and z_{ir} was located at bin 9 and 8 of the VP, respectively. While no consistent improvement in PD between the VP and PIV was observed for $\langle$TKE$\rangle$ in both cases, the performance of the VP under conditions when the SS is located in the IR deserves further investigation.

PSD of longitudinal velocity fluctuations (u') measured at elevations of $z = 13.7$, 23, and 30 mm above the bed (corresponding to bins 5, 12 and 21, respectively) are shown in Fig. 5 for test G2a, in which the full profiling range of the VP was located above the bed. The PSD of u' at bin 12 (the SS) showed an inertial subrange $-5/3$ slope for frequencies between 0.5 and 12 Hz with a noise floor of 1.6×10^{-6} m^2 s^{-2} Hz^{-1}, whereas the PSD at bins 5 and 21 strongly deviated at 0.9 Hz (Fig. 5) even though the noise floor was comparable (1.8 and 2×10^{-6} m^2 s^{-2} Hz^{-1}, respectively). The PSD estimated from the PIV measurements, in contrast, showed an inertial subrange between frequencies 0.5 and 2.4 Hz at all compared distances from the bed (Fig. 5). Considering the curvature of the velocity PSD for bins 5 and 21, it became clear that the PSDs cannot be only compensated by Doppler noise removal. Based on spectral analysis, MacVicar et al. (2014) concluded that the VP can be used for turbulence characterization only within a 10 mm subregion centred at the SS. When comparing the PSD within the inertial subrange between VP and PIV, only bins 10–12 were

found to be most reliable. This is approximately one-third of the previously suggested region by MacVicar et al. (2014) and confirms the recent findings of Brand et al. (2016).

4 Conclusions

A comparison between PIV and VP measurements of velocities and turbulence in the near bed region of a laboratory flume was carried out using different bed materials. Particular attention was paid to the vertical extent of the IR, in which acoustic interference of the bed leads to underestimation of the flow velocity and turbulent kinetic energy. From this comparison we identified the following important aspects for the use of the VP for near boundary measurements:

1. The bed strongly affected the measurements as close as 1.7– 5 mm above the bed. We also observed that the vertical extent of the IR and the velocity differences decreased with decreasing probe proximity to the bed. The vertical extent of this IR depended on bed material and could be identified by a local minimum in the SNR profile.
2. The location of the bed surface can be precisely identified with the VP's distance measurements over solid materials; however, alternative distance measurements are needed for measurements over soft materials.
3. Reasonable agreement of mean velocities and turbulence between VP and PIV measurements was observed only around the SS of the profiler. The difference between both instruments was below 10% for a range of $\pm$ 8 bins centred at the SS for mean velocities (excluding sand tests, S2a and S2b), and below 10% within $\pm$ 4 bins centred at the SS for $\langle$TKE$\rangle$. Spectral analysis showed that velocity spectra obtained at bins 10–12 followed a $-5/3$ slope in agreement with PIV measurements, which suggests that turbulence characterization will be most reliable within 3 mm around the SS. Positioning of the SS at the IR should be considered in future studies, along with experimental investigations of potential effects of the transmitter head on the flow field within the sampling volume.
4. In contrast to the PIV measurements, the $\langle$TKE$\rangle$ profiles measured by the VP showed a persistent local minimum at the SS, and the Doppler noise correction method of Hurther and Lemmin (2001) did not result in a consistent improvement in $\langle$TKE$\rangle$ profiles, which suggests that an increase in $\langle$TKE$\rangle$ below and above the SS cannot be compensated by this Doppler noise correction method.

Figure 5   Power spectral density (PSD) for longitudinal velocity fluctuations (u') of the PIV and VP at $z = 13.7$, 23, and 30 mm for test G2a and corresponding measurement bins of the VP. The sampling rate of the VP was 74 Hz compared to 7.4 Hz of PIV

Considering these aspects we conclude that VP data should be interpreted with caution, particularly for measurements above soft bed materials, where the location of the SWI is uncertain. This problem is especially critical in field applications with limited visual access to the bottom.

Supplemental data

Supplemental data for this article can be accessed 10.1080/0022 1686.2016.1275049.

Notation

$\langle\rangle$	=	time-average (mean) (–)
D_{50}	=	median grain size (mm)
$\langle N_u^2 \rangle, \langle N_{w1}^2 \rangle, \langle N_{w2}^2 \rangle$	=	variance of the noise in u', w_1', and w_2' ($m^2\,s^{-2}$)
$\langle N_{u,v}^2 \rangle$	=	variance of noise in u' and v' ($m^2\,s^{-2}$)
$\langle N_w^2 \rangle$	=	average noise variance obtained from w_1' and w_2' ($m^2\,s^{-2}$)
u, v	=	longitudinal (x-direction) and transversal (y-direction) velocities ($m\,s^{-1}$)
u', v', w_1', w_2'	=	fluctuating components of u, v, w_1, and w_2 ($m\,s^{-1}$)
$\langle u'^2 \rangle, \langle v'^2 \rangle$	=	variances of u and v ($m^2\,s^{-2}$)
$\langle U_{mag} \rangle$	=	magnitude of the mean longitudinal and vertical velocity ($m\,s^{-1}$)
w_1, w_2	=	first and second vertical velocity components obtained from Beams 1 and 3, and Beams 2 and 4 of the VP ($m\,s^{-1}$)
$\langle w_1 \rangle$	=	time-average w_1 ($m\,s^{-1}$)
$\langle w_{true1}'^2 \rangle, \langle w_{true2}'^2 \rangle$	=	true variances of w_1 and w_2 ($m^2\,s^{-2}$)
$\langle w_1' w_2' \rangle$	=	covariance of w_1 and w_2 ($m^2\,s^{-2}$)
z	=	elevation, with the origin at the bed (mm)
z_{ir}	=	position of the upper limit of the interference region above the bed (mm)
z_{ss}	=	position of the sweet-spot of the VP above the bed (mm)

Abbreviations

ADV	=	acoustic Doppler velocimeter
G, GF, S, M	=	bed type (gravel, geotextile, sand, and metal)
HL-corrected	=	after Doppler noise correction of Hurther and Lemmin (2001)
IA	=	interrogation area
IR	=	interference region
PD	=	per cent difference (%)
PIV	=	particle image velocimetry
PSD	=	power spectral density ($m^2\,s^{-2}\,Hz^{-1}$)
SNR	=	signal-to-noise ratio (dB)
SS	=	sweet-spot
TKE	=	turbulent kinetic energy ($m^2\,s^{-2}$)
VP	=	Vectrino Profiler

References

Brand, A., Noss, C., Dinkel, C., & Holzner, M. (2016). High-resolution measurements of turbulent flow close to the sediment–water interface using a bistatic acoustic profiler. *Journal of Atmospheric and Oceanic Technology*, *33*(4), 769–788. doi:10.1175/JTECH-D-15-0152.1

Craig, R. G. A., Loadman, C., Clement, B., Rusello, P. J., & Siegel, E. (2011). *Characterization and testing of a new bistatic profiling acoustic Doppler velocimeter: The Vectrino-II*. Proceedings of the IEEE/OES/CWTM Tenth Working Conference on Current Measurement Technology, Monterey, USA, 246–252. doi:10.1109/CWTM.2011. 5759559

Dombroski, D. E., & Crimaldi, J. P. (2007). The accuracy of acoustic Doppler velocimetry measurements in turbulent boundary layer flows over a smooth bed. *Limnology and Oceanography: Methods*, *5*(1), 23–33. doi:10.4319/ lom.2007.5.23

Finelli, C. M., Hart, D. D., & Fonseca, D. M. (1999). Evaluating the spatial resolution of an acoustic Doppler velocimeter and the consequences for measuring near-bed flows. *Limnology and Oceanography*, *44*(7), 1793–1801. doi:10.4319/lo.1999.44.7.1793

Goring, D. G., & Nikora, V. I. (2002). Despiking acoustic Doppler velocimeter data. *Journal of Hydraulic Engineering*, *128*(1), 117–126. doi:10.1061/(ASCE)0733-9429(2002)128: 1(117)

Hooshmand, A., Horner-Devine, A. R., & Lamb, M. P. (2015). Structure of turbulence and sediment stratification in wave-supported mud layers. *Journal of Geophysical Research: Oceans*, *120*(4), 2430–2448. doi:10.1002/2014JC010231

Hurther, D., & Lemmin, U. (2001). A correction method for turbulence measurements with a 3D acoustic Doppler velocity profiler. *Journal of Atmospheric and Oceanic Technology*, *18*(3), 446–458. doi:10.1175/1520-0426(2001)018 < 0446: ACMFTM > 2.0.CO;2

Kuczmarski, M. A., & Johnston, J. C. (2011). *Acoustic absorption in porous materials* (Report No: NASA/TM—2011-216995). Retrieved from NASA STI website http://ntrs.nasa. gov/archive/nasa/casi.ntrs.nasa.gov/20110011143.pdf

MacVicar, B.J., Dilling, S., Lacey, R.W.J., & Hipel, K. (2014). A quality analysis of the Vectrino II instrument using a new open-source MATLAB toolbox and 2D ARMA models to detect and replace spikes. In: A. J. Schleiss, G. De Cesare, M. J. Franca, M. Pfister, M. (Eds.), *River flow 2014* (1951–1959). London: Taylor & Francis.

Nortek. (2016). Vectrino Profiler − 3D profiling velocimeter [Data sheet]. Retrieved June 22, 2016, from http://www.nortek-as.com/lib/brochures/vectrino-ii

Peltier, Y., Riviere, N., Proust, S., Mignot, E., Paquier, A., & Shiono, K. (2013). Estimation of the error on the mean velocity and on the Reynolds stress due to a misoriented ADV probe in the horizontal plane: Case of experiments in a compound open-channel. *Flow Measurement and Instrumentation*, *34*, 34–41. doi:10.1016/j.flowmeasinst.2013.08.002

Poindexter, C. M., Rusello, P. J., & Variano, E. A. (2011). Acoustic Doppler velocimeter-induced acoustic streaming and its implications for measurement. *Experiments in Fluids*, *50*(*5*), 1429–1442. doi:10.1007/s00348-010-1001-2

Precht, E., Janssen, F., & Huettel, M. (2006). Near-bottom performance of the Acoustic Doppler Velocimeter (ADV) − a comparative study. *Aquatic Ecology*, *40*(*4*), 481–492. doi:10.1007/s10452-004-8059-y

Puleo, J., Blenkinsopp, C., Conley, D., Masselink, G., Turner, I., Russell, P., . . . Poate, T. (2014). Comprehensive field study of swash-zone processes. I: Experimental design with examples of hydrodynamic and sediment transport measurements. *Journal of Waterway, Port, Coastal, and Ocean Engineering*, *140*(*1*), 14–28. doi:10.1061/(ASCE)WW.1943-5460.0000210

Rusello, P. J., & Allard, M. P. (2012). Near boundary measurements with a profiling acoustic Doppler velocimeter. *Proceedings of 2012 Hydraulic Measurements & Experimental Methods Conference (HMEM 2012)*, Snowbird, UT, USA.

Voulgaris, G., & Trowbridge, J. H. (1998). Evaluation of the acoustic Doppler velocimeter (ADV) for turbulence measurements. *Journal of Atmospheric and Oceanic Technology*, *15*(*1*), 272–289. doi:10.1175/1520-0426(1998)015,0272: EOTADV.2.0.CO;2

Wahl, T. L. (2003). Discussion of "despiking acoustic Doppler velocimeter data" by Derek G. Goring and Vladimir I. Nikora. *Journal of Hydraulic Engineering*, *129*(6), 484–487. doi:10.1061/(ASCE)0733-9429(2003)129:6(484)

Welch, P. D. (1967). The use of fast fourier transform for the estimation of power spectra: A method based on time averaging over short, modified periodograms. *IEEE Transactions on Audio and Electroacoustics*, *15*(*2*), 70–73. doi:10.1109/TAU.1967.1161901

Wengrove, M., & Foster, D. (2015). Field evidence of the viscous sublayer in a tidally forced developing boundary layer. *Geophysical Research Letters*, *41*(*14*), 5084–5090. doi:10.1002/2014GL060709
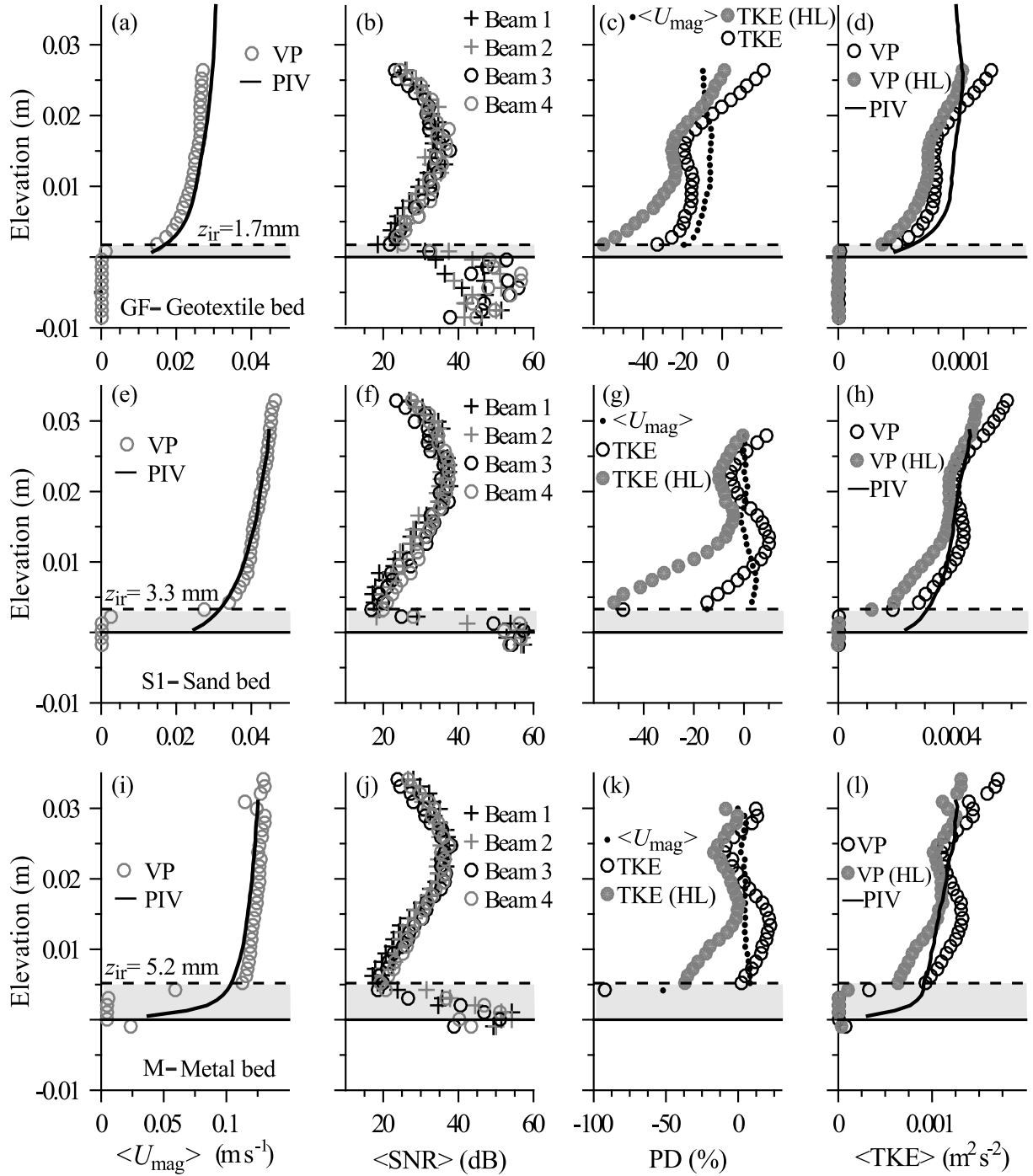
Figure S1 Mean velocity $\langle U_{mag} \rangle$ and turbulent kinetic energy $\langle TKE \rangle$ measured by the VP and PIV over geotextile (GF – top panel), sand (S1 – middle panel), and metal (M – bottom panel) beds. (a) Mean velocities measured by the two instruments; (b) mean signal-to-noise ratio (SNR) values of all beams measured by the VP; (c) percent difference (PD) between the VP and PIV measurements; (d) comparison of uncorrected and HL-corrected $\langle TKE \rangle$ profiles. The shaded grey area represents the interference region (IR), with the horizontal dashed lines denoting the upper end of the IR (z_{ir}). The solid black lines at an elevation (z) of 0 mm show the locations of the bed surfaces

Figure S2 Mean velocity $\langle U_{mag} \rangle$ and turbulent kinetic energy $\langle TKE \rangle$ profiles measured by the PIV and VP with varying proximity to the sand bed (S2a–S2c). (a) Mean velocities measured by the two instruments; (b) mean signal-to-noise ratio (SNR) values of all beams measured by the VP; (c) mean correlation values of all beams measured by the VP; (d) comparison of uncorrected and HL-corrected $\langle TKE \rangle$ profiles. The shaded grey area represents the interference region (IR), with the horizontal dashed lines denoting the upper end of the IR. The solid black lines at an elevation (z) of 0 mm show the locations of the bed surfaces
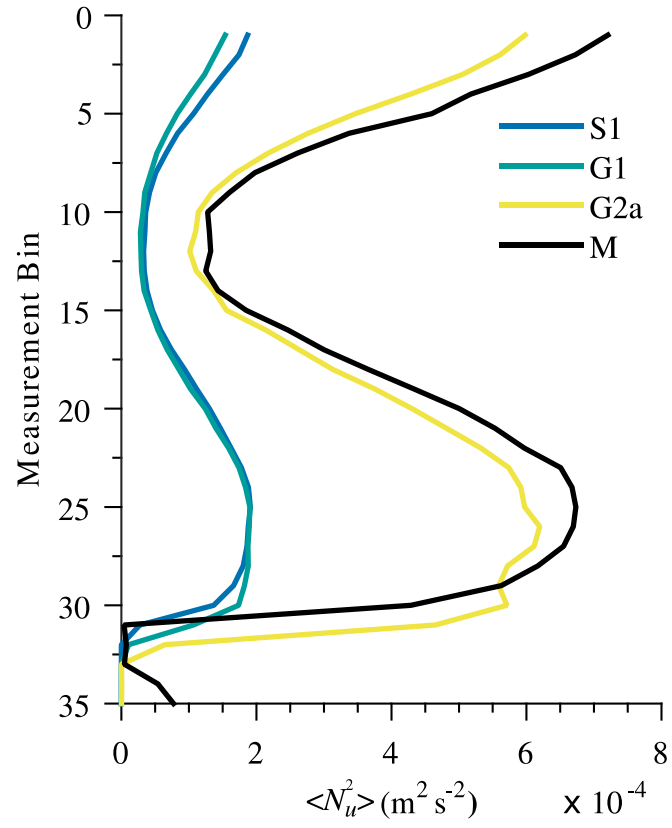
Figure S3 Estimates of the noise variance profiles in the fluctuating component of the longitudinal velocity (u') over sand (S1), gravel (G1, G2a), and metal (M) beds using the Doppler noise correction method of Hurther and Lemmin (2001)

Appendix II

Exploring flow–biofilm–sediment interactions: Assessment of current status and future challenges[ii]
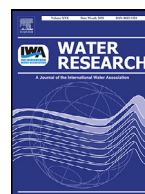
Review

Exploring flow-biofilm-sediment interactions: Assessment of current status and future challenges

Sabine Ulrike Gerbersdorf [a,1,*], Kaan Koca [a,1], Dirk de Beer [b], Arjun Chennu [b,c], Christian Noss [d,e], Ute Risse-Buhl [f], Markus Weitere [f], Olivier Eiff [g], Michael Wagner [h], Jochen Aberle [i], Michael Schweikert [j], Kristina Terheiden [a]

[a] *University of Stuttgart, Institute for Modelling Hydraulic and Environmental Systems, Pfaffenwaldring 61, 70569 Stuttgart, Germany*
[b] *Max Planck Institute for Marine Microbiology, Celsiusstraße 1, 28359 Bremen, Germany*
[c] *Leibniz Center for Tropical Marine Research, Fahrenheitstraße 6, 28359 Bremen, Germany*
[d] *University of Koblenz-Landau, Institute for Environmental Sciences, Fortstraße 7, 76829 Landau, Germany*
[e] *Federal Waterways Engineering and Research Institute, Hydraulic Engineering in Inland Areas, Kußmaulstraße 17, 76187 Karlsruhe, Germany*
[f] *Helmholtz Centre for Environmental Research – UFZ, Department of River Ecology, Brückstraße 3a, 39114 Magdeburg, Germany*
[g] *KIT Karlsruhe Institute of Technology, Institute for Hydromechanics, Otto-Ammann Platz 1, 76131 Karlsruhe, Germany*
[h] *KIT Karlsruhe Institute of Technology, Engler-Bunte-Institute, Water Chemistry and Water Technology, Engler-Bunte-Ring 9a, 76131 Karlsruhe, Germany*
[i] *Technische Universität Braunschweig, Leichtweiß-Institute for Hydraulic Engineering and Water Resources, Beethovenstraße 51a, 38106 Braunschweig, Germany*
[j] *University of Stuttgart, Institute of Biomaterials and Biomolecular Systems, Pfaffenwaldring 57, 70569 Stuttgart, Germany*

A R T I C L E   I N F O

A B S T R A C T

Biofilm activities and their interactions with physical, chemical and biological processes are of great importance for a variety of ecosystem functions, impacting hydrogeomorphology, water quality and aquatic ecosystem health. Effective management of water bodies requires advancing our understanding of how flow influences biofilm-bound sediment and ecosystem processes and vice-versa. However, research on this triangle of flow-biofilm-sediment is still at its infancy. In this Review, we summarize the current state of the art and methodological approaches in the flow-biofilm-sediment research with an emphasis on biostabilization and fine sediment dynamics mainly in the benthic zone of lotic and lentic environments. Example studies of this three-way interaction across a range of spatial scales from cell (nm – μm) to patch scale (mm – dm) are highlighted in view of the urgent need for interdisciplinary approaches. As a contribution to the review, we combine a literature survey with results of a pilot experiment that was conducted in the framework of a joint workshop to explore the feasibility of asking interdisciplinary questions. Further, within this workshop various observation and measuring approaches were tested and the quality of the achieved results was evaluated individually and in combination. Accordingly, the paper concludes by highlighting the following research challenges to be considered within the forthcoming years in the triangle of flow-biofilm-sediment:

i) Establish a collaborative work among hydraulic and sedimentation engineers as well as ecologists to study mutual goals with appropriate methods. Perform realistic experimental studies to test hypotheses on flow-biofilm-sediment interactions as well as structural and mechanical characteristics of the bed.

ii) Consider spatially varying characteristics of flow at the sediment-water interface. Utilize combinations of microsensors and non-intrusive optical methods, such as particle image velocimetry and laser scanner to elucidate the mechanism behind biofilm growth as well as mass and momentum flux exchanges between biofilm and water. Use molecular approaches (DNA, pigments, staining, microscopy) for sophisticated community analyses. Link varying flow regimes to microbial communities (and processes) and fine sediment properties to explore the role of key microbial players and functions in enhancing sediment stability (biostabilization).

iii) Link laboratory-scale observations to larger scales relevant for management of water bodies. Conduct field experiments to better understand the complex effects of variable flow and sediment regimes on biostabilization. Employ scalable and informative observation techniques (e.g., hyperspectral imaging, particle tracking) that can support predictions on the functional aspects, such as metabolic activity, bed stability, nutrient fluxes under variable regimes of flow-biofilm-sediment.

© 2020 Elsevier Ltd. All rights reserved.

1. Introduction

Microbial life in most water bodies grows in "biofilm", which are genetically diverse surface-attached aggregates of microorganisms (Archaea, Bacteria, Eukarya) (Flemming and Wuertz, 2019) that are wrapped in a self-produced matrix of extracellular polymeric substances (EPS). Aquatic biofilms are capable of colonizing various soft (e.g., sediment or soil surface) and hard (e.g., stone, plant, pipe or vessel surfaces) surfaces that exist across diverse environments, including streams and rivers (Battin et al., 2016), lakes (Zhang et al., 2020), estuarine (Vijsel et al., 2020) and marine (Yallop et al., 1994) waters, as well as drinking water distribution systems (Chan et al., 2019; Douterelo et al., 2019). Whether growing on mud (epipelic), sand (epipsammic), stone (epilithic) or plant (epiphytic), whether addressed as microphytobenthos (in shallow coastal waters, intertidal flats), microbial mat (among others, in habitats of hot springs, hypersaline ponds, groundwater) or periphyton (on any submerged surface in the aquatic habitat), all communities possess emergent features, such as production of EPS, tolerance towards external stresses, cell-cell communication and collective behavior as well as synergetic use of nutrients that distinguish them as biofilm (Flemming et al., 2016; Flemming and Wingender, 2010; Flemming and Wuertz, 2019; Gerbersdorf and Wieprecht, 2015; West et al., 2007).

Biofilm lifestyle is distinctly different and more common than planktonic lifestyle, with an estimated 40–80% of cells contributing to the global biomass residing in biofilms (Flemming and Wuertz, 2019). The transition of one microbe from the planktonic to the biofilm lifestyle, and vice-versa, depends on a range of environmental conditions among which the local hydrodynamics are of paramount importance (Berke et al., 2008; McDougald et al., 2012; Wheeler et al., 2019). Hydrodynamics largely dictate initial "touch-down" and the residence time of the microbes on surfaces (Rusconi et al., 2014). When exceeding a certain hydrodynamic force or experiencing a hydraulic retention time shorter than the doubling-time of the cells, the microbes will disperse again and leave the habitat. Those cells that still stick are selected towards stronger adherence, and the further biofilm development strongly shapes their adjacent physical and chemical surrounding in a reciprocal way (Gerbersdorf and Wieprecht, 2015). Thereby, biofilm growth and its influence on the surrounding strongly depend on the microbial metabolic activity which leads to redox-relevant small-scale stratification and impacts large-scale biogeochemical budgets (Packman, 2013). However, these metabolic processes are determined by mass transfer in the water column and towards the biofilm, which is again controlled by hydrodynamics regulating nutrient supply to the microbes (Gerbersdorf and Wieprecht, 2015). For a comprehensive review on the processes related to surface attachment and subsequent colonization, we refer readers to reviews by Berne et al. (2018), Gerbersdorf and Wieprecht (2015) and Tolker-Nielsen (2015).

When growing on sediment in the bed finer than about 2 mm (clay, silt, sand) (Statzner et al., 1999), biofilms also glue the sediment grains to each other through their EPS matrix (Jones, 2017; Paterson et al., 2018). This, in turn, alters the sediment-bed properties, e.g., density, morphology, size gradation

* Corresponding author.

E-mail addresses: sabine.gerbersdorf@mwk.bwl.de (S.U. Gerbersdorf), kaan.koca@iws.uni-stuttgart.de (K. Koca), dbeer@mpi-bremen.de (D. de Beer), achennu@mpi-bremen.de, arjun.chennu@leibniz-zmt.de (A. Chennu), christian.noss@baw.de (C. Noss), ute.risse-buhl@ufz.de (U. Risse-Buhl), markus.weitere@ufz.de (M. Weitere), olivier.eiff@kit.edu (O. Eiff), michael.wagner@kit.edu (M. Wagner), jochen.aberle@tu-braunschweig.de (J. Aberle), michael.schweikert@bio.uni-stuttgart.de (M. Schweikert), kristina.terheiden@iws.uni-stuttgart.de (K. Terheiden).

¹ Both authors share the first authorship.

(Fang et al., 2012; Gibbs, 1983; Huiming et al., 2011; Shang et al., 2014), and dynamics, e.g., erosion and transport (Banasiak et al., 2005; C. Chen et al., 2017; Droppo et al., 2015; Fang et al., 2017; Gerbersdorf et al., 2008; Malarkey et al., 2015; Righetti and Lucarelli, 2010; Vignaga et al., 2013) and, finally, the accumulation and transport of contaminants (Burns and Ryder, 2001; Förstner et al., 2004). The ability of biofilms to increase erosion thresholds by biological actions is an ecologically essential ecosystem function named "biostabilization" (de Brouwer et al., 2005; Gerbersdorf and Wieprecht, 2015; Passarelli et al., 2014; Roncoroni et al., 2019) and has been reported to mediate sediment erosion, transport, deposition and consolidation (ETDC) cycle in aquatic ecosystems (Paterson et al., 2018). It should be noted that biostabilization can also occur through smoothing of the bed surface and therefore reduction of the hydraulic roughness, as observed over gravel-like hemispheres (Graba et al., 2010). These interactions of sediment and biofilm are critical to the biogeochemical processes at the entire ecosystem level (Packman, 2013). Along with their impact on nutrient fluxes (Battin et al., 2016; Falkowski et al., 2008; Madsen, 2011), biofilms possess further fundamental ecosystem services such as water self-purification (Gerbersdorf and Wieprecht, 2015; Shannon et al., 2008) and they also regulate and mediate primary production and food web processes (Battin et al., 2008; Demars, 2019; Graba et al., 2013).
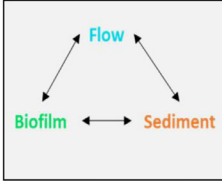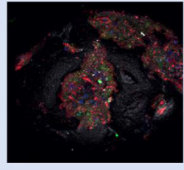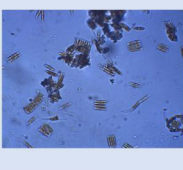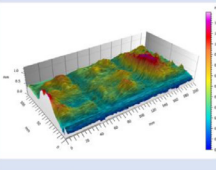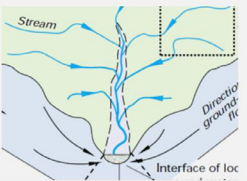
Such fundamental ecosystem processes and functions of the biofilms are determined by their biodiversity and community composition through the metabolic performance of involved microbial communities (Allan and Castillo, 2007; Besemer, 2015; Loreau et al., 2001). The physical structure, composition and diversity of the biofilms in aquatic ecosystems vary widely depending on the physical (e.g., grain size, porosity), chemical (e.g., sediment nutrient content), biological (e.g., growth rate, cell-cell communication) and environmental (e.g., light, temperature and flow regime) factors (Allan and Castillo, 2007; Stevenson et al., 1996) and processes (Leibold et al., 2004), including interactions with nutrient and organic matter cycling (Battin et al., 2016; Schiller et al., 2007), growth habitat (Salta et al., 2013; Wilhelm et al., 2014) as well as flow and bed topography (Battin, 2000; Risse-Buhl et al., 2017; Woodcock et al., 2013). Indeed, many biofilms have complex morphologies and can develop long, oscillating filamentous structures called streamers (Larned et al., 2011; Nikora, 2010), which not only alter flow dynamism and bed topography, but also mass transport near the bed.

The preceding higher-order effects induced by biofilm formation are of ever-changing nature (Battin et al., 2016) mainly due to complex reciprocal interactions between flow, biofilm and sediment (Gerbersdorf and Wieprecht, 2015) and are also expected to change in a nontrivial way as a result of climate change (Piggott et al., 2015; Zeglin, 2015) and human alteration. However, our understanding of dynamic flow-biofilm-sediment processes nexus in natural water bodies which drive changes in ecosystem processes and functions remain still incomplete (Nikora, 2010; Packman, 2013; Paterson et al., 2018). In order to better manage our water bodies for the benefits of human society and ecosystem functioning as well as to support UN's Sustainable Development Goals, a better understanding of flow-biofilm-sediment interactions – that we call flow-biofilm-sediment triangle – is needed. Challenges include i) creating realistic experimental settings and utilizing a combination of tools and approaches to describe the reciprocal relationships between flow-biofilm-sediment and associated mass transfer, which alters microbial processes and vice-versa and ii) understanding the role of key microbial players (and processes) for biogeochemical and morphological processes (biostabilization) at the entire ecosystem level, and how organismal level functions can be linked to ecosystem functions. These challenges require acquisition of large bodies of information across various spatial scales

Fig. 1. How to investigate the interactions of flow-biofilm-sediment. Addressing various scales and applying appropriate techniques used in different disciplines. This figure is the result of a knowledge consolidation exercise through expert discussions during the joint workshop that was held between June 2018 and February 2019 in Stuttgart. Accordingly, the instruments reported in black font were employed in our pilot experiment as a contribution to this review paper.

by studying hydraulics, geomorphology and ecology as an integrated concept using advanced tools and approaches rather than viewing them as subordinately serving the other. The increasing needs for interdisciplinary approaches have been underlined by many recent studies (Battin et al., 2016; Palmer and Ruhi, 2019; Paterson et al., 2018; Rice et al., 2010; Roncoroni et al., 2019).

In this review coupled with an illustrative experiment, we summarize the current understanding of the flow-biofilm-sediment triangle and demonstrate how this three-way interaction and important ecosystem functions such as biostabilization can benefit from a co-application of measurement techniques from various disciplines. The intersection between scientific fields of hydrodynamics, biogeomorphology and microbiology is the theme of this paper. While we focus on flow-biofilm-sediment interactions with implications on fine sediment dynamics mainly in the benthic zone (first cm of the bed) of lotic and lentic environments, some examples from other environments (e.g., medicine) are also presented to provide a more comprehensive picture of the field.

2. Methodology

2.1. General approach

To address the flow-biofilm-sediment triangle and its effects on ecosystem processes with an emphasis on biostabilization (Fig. 1), a joint workshop (three-phase) was held in Stuttgart, Germany between June 2018 and February 2019, bringing together experts from Germany in the relevant areas of hydromechanics, microbial ecology, biochemistry and sedimentation engineering. The main goals of the workshop were i) to consolidate knowledge and identify knowledge gaps in understanding flow-biofilm-sediment interactions through expert discussions and pivotal papers and ii) to perform a pilot experiment to test and discuss how the identified knowledge gaps can be addressed by co-application of modern methods in the fields of hydraulics, sedimentation engineering, microbial ecology and biochemistry. The current knowledge and gaps to elucidate flow-biofilm-sediment interactions were discussed in the first phase together with the design of the pilot experiment,

and the second and third phases were focused on performance of experiments and review/discussion of the results, respectively.

2.2. Pilot experiment

During the pilot experiment, the capabilities of selected promising instruments and methods from different disciplines (shown in black font in Fig. 1) across various spatial scales were exemplarily demonstrated by their co-application on riverine biofilm samples that were quasi-naturally grown on fine sediment at contrasting (high bed shear stress ~0.04 Pa and low bed shear stress ~0.01 Pa) flow conditions in six recirculating flumes, each with dimensions of 3 m long and 0.15 m wide (Schmidt et al., 2015). The specific aims of this pilot experiment were (a) to test the applicability and limitations of the techniques applied and (b) to identify the spatial and temporal scales relevant to better understand the reciprocal interactions in the flow-biofilm-sediment triangle. For the latter, we summarize the various scales applied in different disciplines first (Fig. 1). Selected preliminary data from this pilot work focusing on young (21 days) and mature biofilms (90 days) were utilized in the context of current knowledge and methodological advances that exist in each of the relevant fields for this flow-biofilm-sediment triangle (Fig. 1).

2.3. Structure of the Review

This review article provides an update on current scientific knowledge, practices and methodological approaches related to flow-biofilm-sediment interactions, including fine sediment dynamics and outlines how future studies can benefit from an interdisciplinary approach in order to better understand the flow-biofilm-sediment processes nexus. The review is organized into three parts. The first starts from the initial colonization to mature microbial landscapes, thereby focusing on heterotrophic bacteria and microalgae (Section 3). The second describes the internal architecture, polymeric matrix, community biomass and composition of the biofilm as well as mass transfer (Section 4). The third discusses the mechanical properties of biofilm and biofilm-embedded sediments with specific regard to biostabilization (Section 5). In

each of these sections, selected data from the pilot experiment was used to support the challenges and benefits of a comprehensive interdisciplinary approach. Finally, in Section 6, we present research gaps and research challenges in the relevant disciplines based on the condensed knowledge and experience gained during the workshop. Section 7 concludes the review paper.

3. A view from above: mutual flow – sediment/biofilm interactions

3.1. Flow - Attachment - Colonization

In aquatic ecosystems, the mostly turbulent flow is generated by an external supply of energy (e.g., gravity, wind, waves) at the macroscale (bulk) (Kolmogorov, 1941) but gradually passed on to the microscale experienced by the aquatic microorganisms. The hydrodynamic forces affect many aspects of microbial movement, attachment and subsequent biofilm development for which adherence/remobilisation, nutrient supply and metabolic waste removal are of utmost importance. Therefore, understanding the reciprocal interaction between microbial assemblages and near-bed hydrodynamics has direct theoretical and practical implications. Living and moving at the microscale (herein referred as single-cell scale), microorganisms are directly exposed to a local viscous flow characterized by low Reynolds numbers ($Re \ll 1$), which in turn interacts with the larger turbulent scales (Tennekes, 1989). Overall, like non-motile macroorganisms, microbes are at the mercy of boundary conditions controlled by the turbulence. While macroorganisms experience flow as an intermittent and chaotic motion, rapid fluid fluctuations appear slower and smoother to microbes that are smaller than the size of the smallest eddies and thus, embedded within a single whirl of the flow (Wheeler et al., 2019). Nevertheless, most microorganisms are motile and thus, even at the microscale, self-propelling bacteria induce flow perturbations and create spatiotemporal chaos of the otherwise laminar flow. This swimming of a self-propelling bacterium can occur as a random walk, one of the mechanisms being "run-and-tumble" motion (e.g., for *Escherichia coli*). Apart from this individual locomotion, collective motion (e.g., chemotactic waves, swarming) of bacteria might take place (Lauga, 2016; Lauga and Powers, 2009). This behavior might lead to long-range motions to impact velocity speed and direction (Bratanov et al., 2015), meso–scale turbulence characterized by vortex length scale (Doostmohammadi et al., 2017) as well as collective oscillation as centimetre-scale travelling waves (Chen et al., 2017a, b). Thus, whether via passive (drift, downsweeps) or active (self-propulsion, buoyancy regulation) movements, macro- and microscale interactions between flow and microbes orchestrate together to influence the likelihood of surface contacts as well as detachment/attachment ratios (Characklis and Cooksey, 1983; Tuson and Weibel, 2013; Wey et al., 2009). For instance, it seems difficult for a microorganism to overcome the physical forcing when exposed to higher flow conditions (~0.08 Pa) resulting in delayed attachment as well as growth compared to low (~0.01 Pa) and medium (~0.04 Pa) flow (Schmidt et al., 2018). For further microbial colonization, flow again seems to be the most decisive factor since forcing may increase particle resuspension and light attenuation, limiting metabolic activity and establishment of photoautotrophs within the biofilm (Schmidt et al., 2018).

On the other hand, flow can be highly beneficial to biofilm development in order to maintain nutrient supply and the removal of waste-products. Decisive for these features is the so-called "diffusive benthic boundary layer" (DBBL), usually sub-millimeter in thickness. Along with surface roughness, the usually turbulent flow above dictates the thickness of this DBBL where viscous flow prevails (Gerbersdorf and Wieprecht, 2015). Accordingly, the DBBL represents the zone between zero velocity at the surface (no

slip condition) and turbulent conditions within the water column above. Within this viscous DBBL, molecules are transported by molecular diffusion, driven by a concentration gradient between the bulk fluid and the surface. The diffusion coefficients (Daq) are specific for the molecules of interest, and along with the thickness (L) of the DBBL determine the transfer velocity (kL). Along with the vertical concentration gradient, the external mass transfer towards the surface of the substratum or the developing biofilm (kL (m s^{-1}) = Daq (m^2 s^{-1}) / L (m)) is quantified. This external mass transfer is decisive for the replenishment of nutrients or other molecules essential for further biofilm colonization, and the term is used to distinguish it from internal diffusion limitations that might occur within the biofilm (Stewart, 2012). As seen above, the external mass transfer depends on the thickness of the DBBL, which again is controlled by near-bed turbulence and the surface roughness of the biofilm-bound sediment (Nikora, 2010), but difficult to determine experimentally due to its thinness and inherent proximity to the bed surface.

While a growing biofilm under fast local flow conditions, which leads to a relatively thin DBBL with a strong concentration gradient, might be in a favourable situation regarding nutrient replenishment, the risk of immediate detachment or sudden sloughing-off is also enhanced (Zhang et al., 2011). Consequently, the impact of the turbulence has been described as a trade-off between shear forces and nutrient supply to influence the overall lifecycle of microbial assemblages ranging from attachment, colonization, and ongoing growth to dispersal (McDougald et al., 2012).

3.2. Growth - Topography - Flow

When the biofilm grows horizontally and in height, it changes the topography of the colonized substratum, rendering the previous surface properties redundant. At first, the biofilm disseminates across the surface to be colonized and the resulting spatiotemporal pattern depends again largely on the flow above. While a hydraulically smooth and more constant flow seems to favor isotropic microcolonies, multidirectional, fluctuating and varying flow velocities allow higher degrees of freedom for colonization (Rossy et al., 2019; Stoodley et al., 1999; Thomas et al., 2013). Hence, growing clusters at a hydraulically rough environment (i.e., turbulent at the roughness-scale) result in anisotropic, star-like structures that may optimize the exploitation of space (Hodl et al., 2014). This is consistent with the data from the pilot experiment, where it was observed that young biofilm featured isotropic growth while more elevated matured biofilm exhibited a preferred growth orientation in alignment with the flow direction (Fig. 2a). While gaining height, the biofilm can either smoothen a formerly rough surface by accruing the "valleys" or enhance the roughness by growing on "hills" to accentuate small differences in surface structure (Picioreanu et al., 1998; Stewart, 2012). In the first scenario, growth in valleys might be favoured since the troughs act as a hideaway to protect from hydrodynamic forces (Barton et al., 2010). The second scenario, the "fingered" biofilm growth, has been proposed to be due to a competitive advantage at flow conditions that impede nutrient replenishment otherwise (Nikora et al., 2002). Generally, hydraulically smooth flow conditions seem to promote the formation of filamentous or stalk-like structures that protrude out of the biofilm and experience a compressed DBBL with a higher supply of nutrients. This is in line with our workshop results on freshwater biofilm where low bed shear stresses (~0.01 Pa) allowed the development of thicker and more heterogeneous biofilm, with elongated filaments (so-called streamers) moving with the flow. In contrast, medium stresses (~0.04 Pa) resulted in biofilm accumulating close to the surface and forming bungalow-type structures (Gerbersdorf and Wieprecht, 2015).

(A)
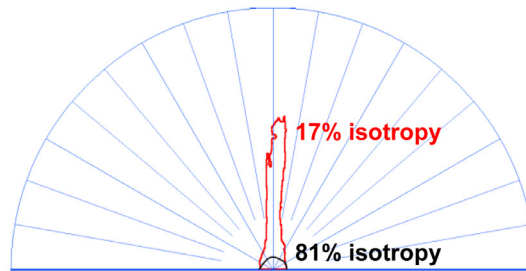
(B)

21-day biofilm
AR height: 0.53 mm
RMS height: 0.69 mm
Skewness = -0.03
Autocorrelation = 3.33 mm
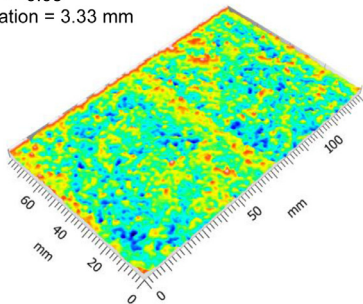
90-day biofilm
AR height: 0.63 mm
RMS height: 0.81 mm
Skewness = -0.14
Autocorrelation = 7.78 mm
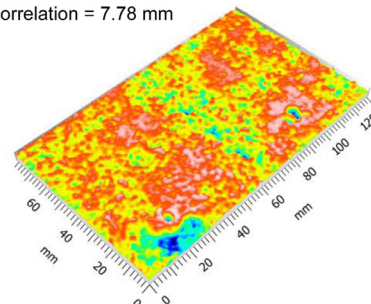
(C)
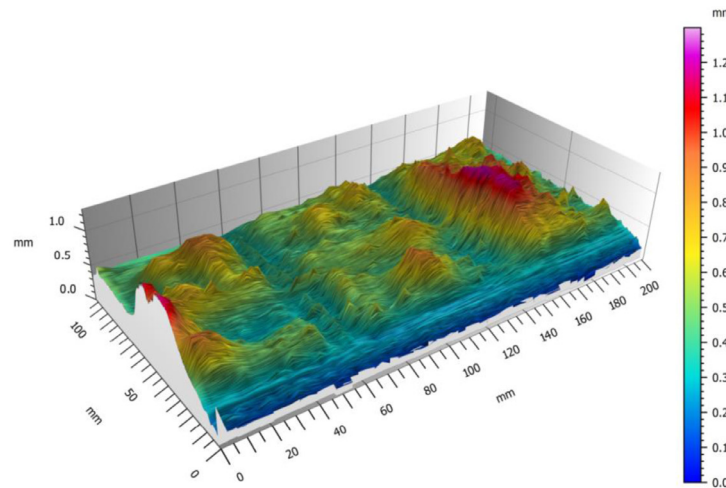
Fig. 2. Comparison of biofilm growth at different stages of development in the pilot experiment. (A) Young biofilm surface (black line) exhibits isotropic properties (81%) without any directional properties while mature biofilm surface (red line) shows anisotropic properties (17%) with a preferred orientation along with the flow direction. (B) Biofilm topography changes over the weeks followed by light microscopy (LM). (C) Mountainous appearance of mature biofilm after 4-week growth scanned by laser triangulation (LS) system.

Clearly, one way or the other, if given time, biofilm development changes the bed topography. In the pilot experiment, we measured bed topography by (a) scanning the area with microscope (Axio-Zoom 1.6) and (b) with laser triangulation system (e.g., Noss et al., 2018) where biofilm valleys and peaks are determined by measuring the reflected laser light that falls incidentally onto a receiving object and at a certain angle which depends on the distance of the object (here the biofilm). At the low flow conditions given above, increasing mean and RMS (root mean square) heights over the weeks of growth indicated a rougher topography, while increasing autocorrelation lengths (distance to a different structure) of the surface roughness reflected a more regular surface

structure of biofilm (Fig. 2b). Hence, the mature biofilm in week 4 has a remarkably mountainous appearance (Fig. 2c). As compared to the initial conditions, the average biofilm thickness (1.92 to 3.74 mm) as well as surface roughness (0.46 to 1.97 mm) increased significantly along with a reduced flow regime (0.04 to 0.01 Pa), as previously modelled by Head (2013). This increase in roughness appears to (a) reduce the DBBL thickness, (b) increase the surface area and/or (c) induce near-bed flow field fluctuations such as micro-eddies by the protruding structures (e.g., Bishop et al., 1997). Thereby, the effective roughness mediates the friction (=resistance) forces in a way, well beyond the expectation arising from the physical appearance of biofilm (Cowle et al., 2017). Measurements of

flow and biofilm growth across the 5 cm patch scale in our pilot experiment suggest a spatially heterogeneous distribution of the Reynolds stress (=total stress tensor in a fluid), which globally increases above the matured biofilm bed as compared to the initial bare sand bed. The enhanced and varying peaks in Reynolds stress might result in recirculating eddies, turbulent wakes or turbulent bursts (packets of energetic fluid) that penetrate deep into the DBBL to impinge transiently on the biofilm (de Beer et al., 1994a). This way, the mass transfer towards (sweeps to enhance food supply) and out of (ejections to boost waste removal) the biofilm is positively enhanced (Bishop et al., 1997; McDougald et al., 2012; Stewart, 2012) up to a point where detachment and abrasion occurs (Zhang et al., 2011). In the extreme, e.g., smooth flow conditions, the biofilm might become depleted in metabolic substrates and enriched in metabolic waste (Stewart, 2012), while the opposite is true for biofilm growth at rough flow conditions (Biggs et al., 1998); known as the eutrophic effect of the flow.

4. Entering the microbial city

4.1. Architecture and EPS matrix

Biologists developed an early interest in the architecture as well as in the chemical and biological composition of biofilms. Consequently, there are numerous papers dealing with flow-biofilm interactions from young to mature stages of biofilm development. In this context, it has been observed that biofilm matrix, architecture and species composition change significantly along with the hydrodynamics (Azeredo et al., 2017; Risse-Buhl et al., 2020; van Loosdrecht et al., 2002). Observations by several research groups congruently detail that biofilm thickness is inversely related to flow velocities (Graba et al., 2013; Paul et al., 2012; Pereira et al., 2002). Interestingly, biofilm mass follows this trend, but to a much lesser extent. For instance, Paul et al. (2012) reported for one biofilm type thickness reduction from 300 to 100 µm and mass reduction from 0.13 to 0.09 mg TOC cm^{-2} when exposed to increasing shear stress from 2 to 9 Pa. Dreszer et al. (2014) showed elastic sponge-like behavior of biofilm being exposed to varying flow conditions (first three days at 20 L m^{-2} h^{-1}, followed by an increase to 60 L m^{-2} h^{-1} and restoring back to the original flow). Their optical coherence tomography (OCT) measurements revealed that 50% decrease in biofilm thickness at higher velocity was largely due to the collapse of mushroom-like void spaces, while the biofilm mass remained the same (Dreszer et al., 2014). This not only proves the largely visco-elastic nature of biofilm, but also the variations in density of the biofilm matrix along with the flow conditions. By applying various levels of shear stress (from 0.09 to 13 Pa) on the surface of biofilm cultivation plates in an annular reactor, Paul et al. (2012) confirmed the significantly enhanced biofilm density (roughly about three times) with increasing shear stress. The investigations of Pereira et al. (2002) on single species *Pseudomonas* biofilm explained the possible mechanisms behind the observed changes in physiognomy: cells at stronger hydrodynamic conditions secreted more exopolymeric substances per unit volume while void spaces were reduced. The resulting thinner and denser biofilm seems to promote nutrient degradation rates and thus efficiency in wastewater treatment, but caution is warranted for the extrapolation to natural multispecies biofilm (Pereira et al., 2002). First studies in fluvial systems on epilithic biofilms confirmed these effects of turbulent flow on biofilm architecture; however, this was most pronounced at nutrient-rich conditions (Risse-Buhl et al., 2017). Furthermore, Fish et al. (2017) and Polst et al. (2018) attested as well significantly higher production of EPS carbohydrates and EPS proteins at a stronger hydrodynamic regime for biofilms in drinking water pipes and autotrophic stream biofilms, respectively. This was different com-
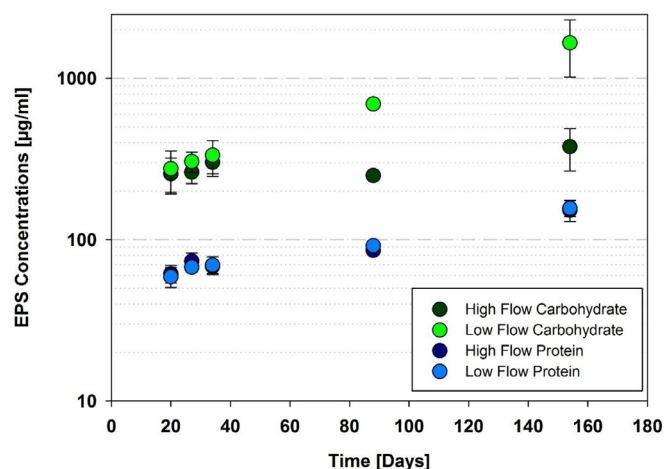
Fig. 3. Water-extractable (colloidal) extracellular polymeric substances (EPS) concentrations over time. Indicated are carbohydrates (green) and proteins (blue) at high (dark colours) and low (light colours) flow conditions.

pared to the results of our pilot experiment, which showed significantly higher carbohydrates content at the lower flow condition, but similar for proteins at both lower and higher flow regimes (Fig. 3). The studies are most likely incongruous since they address different biofilm communities (e.g., heterotrophic bacteria versus microalgae) with varying secretion pattern of polymeric substances (Pierre et al., 2012; Vu et al., 2009). Moreover, there are some uncertainties as to the broad range of extraction and determination methods used (Delattre et al., 2016). Furthermore, the composition of EPS is highly variable and complex, thus challenging to characterize (Flemming et al., 2016; Frølund et al., 1996; Jahn and Nielsen, 1995; Nielsen et al., 1997, 1996). To the best of our knowledge, there are currently no studies on shifts in EPS quality (e.g., monomer composition, functional groups, structural elucidation) according to various flow conditions although it is eminent that components for structural integrity (e.g., amyloids, Zeng et al., 2015) might be more prevalent at higher flow conditions. That again, will be most likely determined by the dominating microbial species that trigger EPS secretion highly differently depending on their adaptation – an uncharted territory.

4.2. Microbial biomass and multitrophic relations

The effect of flow on biofilm biomass is environment-dependent and still inconclusive. While most studies in drinking water distribution systems reported increasing bacterial biomass with increasing flow velocity (Fish et al., 2017; Simões et al., 2007; Torvinen et al., 2007), the others from stream ecosystems showed the opposite for both bacterial and microalgal biomass (Battin et al., 2003; Besemer et al., 2007). Yet, the effect of flow on biomass and diversity of biofilms in streams appears to be season-dependent (Risse-Buhl et al., 2020), suggesting a modulating effect of varying physicochemical parameters and synergistic multitrophic interactions. In our pilot experiment, hyperspectral imaging and quantification of absorption peaks was used to map photopigments across the surface of sedimentary biofilms (Chennu et al., 2013). This technique can be used to non-invasively monitor the distribution and dynamics of chlorophyll *a* and other pigments at very fine spatial scales (Chennu et al., 2015b) and flexible temporal resolution, providing a comprehensive view of the spatio-temporal evolution of photopigments in biofilms under various ecological interactions (Chennu et al., 2015a). The photopigment distributions in our measured biofilms of varying flow regimes, age and sedimentary grain structure (Fig. 4) indicated diversity in spatial
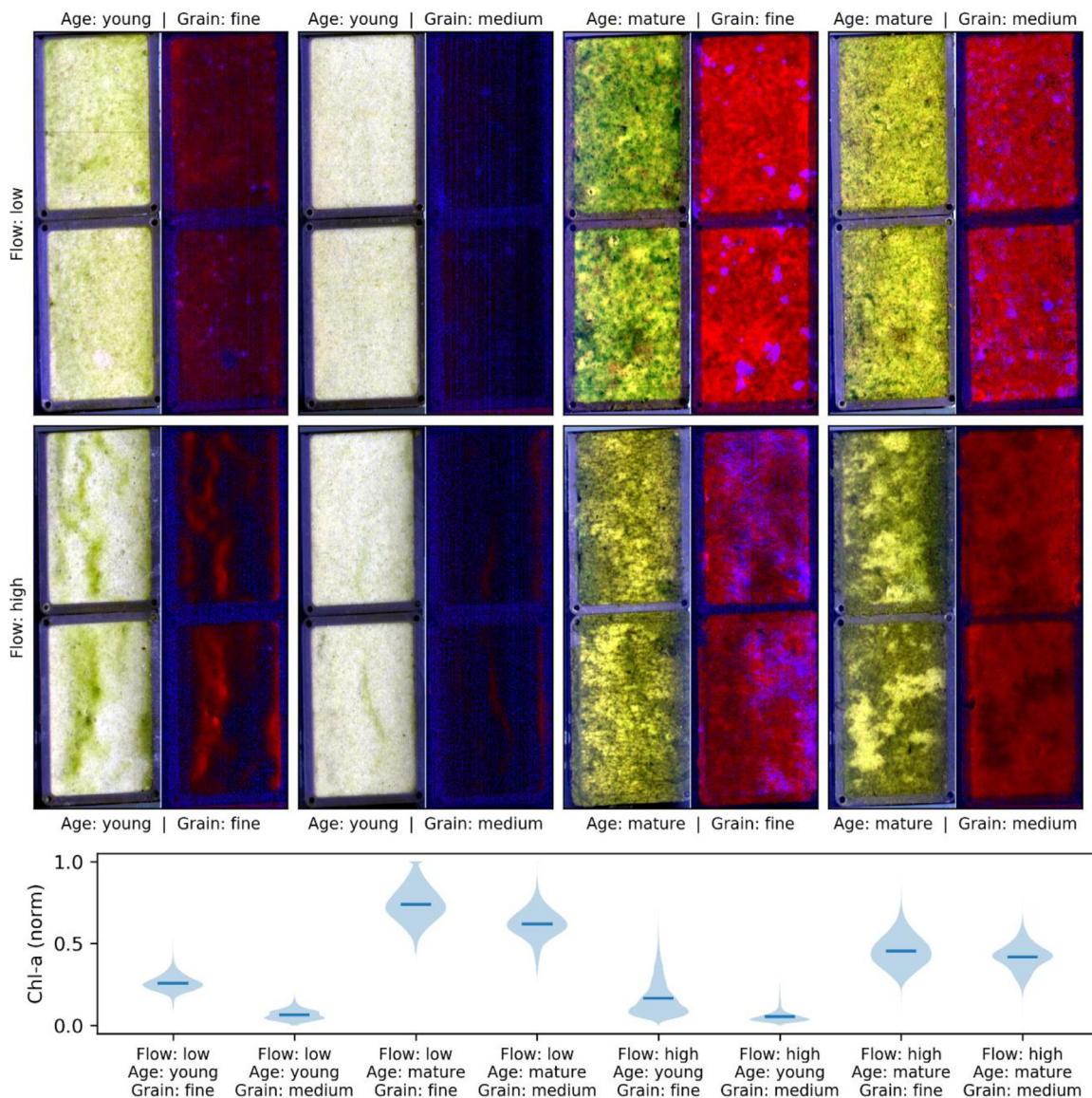
Fig. 4. Photopigment distributions derived from hyperspectral imaging. Monitored is the surface of sedimentary biofilms under various flow conditions, biofilm maturity (age) and sediment grain structure (see panel edge labels). Each condition shows the natural (true color) view of the surface alongside a false-color composite of the abundance of Chl a (in red) and Phycoerythrocyanin (in blue), with a common colormap scale for each pigment across all abundance maps. The Chl a abundance was calculated using the log-corrected MPBI centered at 675 nm (see reference in text: Chennu et al., 2013), and represents a proxy for photosynthetic biomass in the biofilm. Phycocyanin abundance was calculated using second derivative at 625 nm (see reference in text: Chennu et al., 2015a), but was not shown as it correlated completely with Chl-A map. The Phycoerythrocyanin abundance was calculated using second derivative at 575 nm, and was generally patchy across the surface but with higher values in the fine-grained sediment. The spatial patterns of Chl a was heterogeneous at mesoscales, but showed a directionality (perpendicular to flow) in young biofilms in medium-grained sediment under high flow velocities. The statistical distribution of the Chl a values from the ~1.2 million pixels in each abundance map is shown in the lower panel, indicating that age of the biofilm was the primary correlation to Chl a level, with values slightly lower for coarser sediments.

structure, succession of new functional groups in older biofilms and represent a generally robust proxy for photosynthetic potential. While studies on pure-cell biofilms have indicated discernibility for diatom-specific photopigments (Fucoxanthin, Jesus et al., 2014), we could not detect this in our studied biofilms embedded in a scattering sediment matrix. However, recent optical modeling work provides promising developments towards fine-tuned applications (Launeau et al., 2018). Besemer et al. (2007), by addressing the community successions of stream biofilms in flumes, gave evidence of higher bacterial species abundance and microalgal biomass within laminar to transitional flow as compared to fully turbulent conditions. Schmidt et al. (2018) verified reduced bacterial cell numbers as well as microalgal biomass at stronger flow conditions, where both flow scenarios (weak vs. strong) were turbulent. Nevertheless, the effects of flow on microbial cell num-

bers and biomass might be as well of indirect nature. For instance, negative effects on microbial grazer densities (e.g., flagellates, ciliates) by flow potentially generates positive effects in biofilm bacteria as the latter are released from grazing pressure (Risse-Buhl et al., 2020; Wey et al., 2008). Environmental biofilms are, in fact, multi-trophic consortia including also protistan and micro-metazoan grazers besides prokaryotes and algae (Weitere et al., 2018) and it is this complex microbial cosmos that finally determines biofilm functionality (Arndt et al., 2003; Besemer, 2015). Therefore, we could get revolutionary insights into the microbial world by including the whole microbial web. In this regard, Risse-Buhl et al. (2017) has done pioneering work to address the interaction between near bed turbulence, mean flow (ū) and biofilm composition, architecture as well as trophic structure in mountainous stream ecosystems. In this study, the abundance of filamentous

(A)
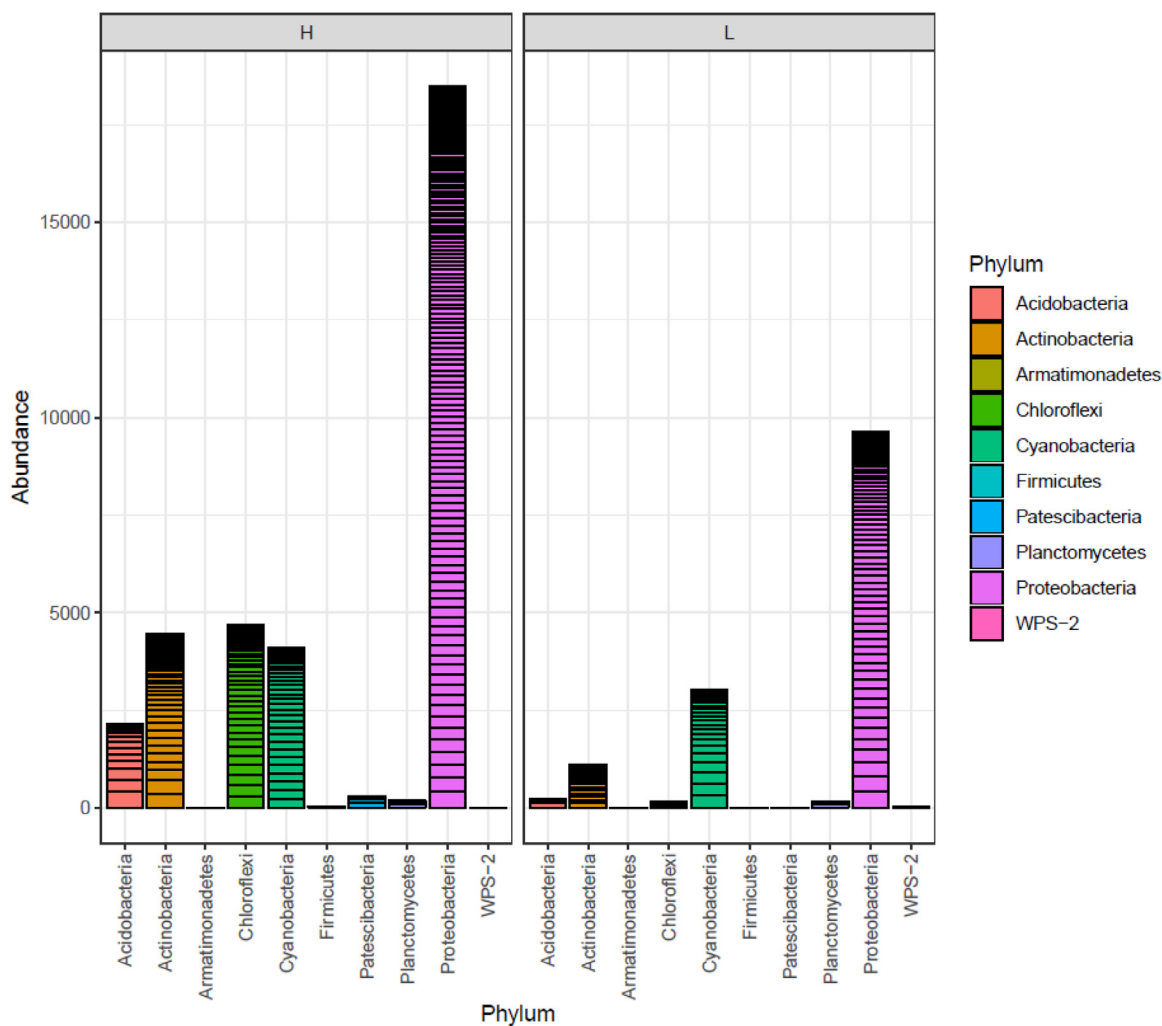
Fig. 5. Molecular fingerprinting of the community composition. Next generation sequencing (NGS) of 16S rRNA (prokaryotic organisms). Groups of individuals that are genetically closely related are organized in OTUs (operational taxonomic units) for the high (=H) flow conditions (left) and low (=L) flow conditions (right).

autotrophs increased with near-bed turbulent kinetic energy (TKE) which most likely offered shelter to bacteria that remained unaffected in numbers by the increasing flow velocities. Bacteria further benefited from a reduced grazing pressure at faster flowing, more turbulent sites, since the abundance of heterotrophic protists decreased with flow. Results by Risse-Buhl et al. (2017) suggested that near-bed flow might impact the magnitude and direction of matter fluxes through shifts in the microbial food web, thereby possibly affecting ecosystem functioning.

4.3. Microbial taxonomy (by microscope and molecular techniques)

Insights into the microbial community composition have been traditionally gained my microscopic evaluation of morphological, taxonomically unique features (Clark et al., 2018). This classical approach is for instance common for the determination of diatom species that – by their appearance and certain requirements – are excellent indicators of different water qualities or various hydrodynamics scenarios. Graba et al. (2013) reported that epilithic biofilms at smooth flow grew much thicker, developed thicker filaments and accommodated multicellular growth forms of diatoms while biofilm at rough conditions were more compact hosting smaller, mobile and unicellular diatoms. This seems to confirm the

progression of climax populations at low flow velocities that are subject to minor changes but undergo C-Selection (competition in terms of resources such as nutrients). In contrast, pioneer species dominate at high flow velocities where resources are available, but environmental forcing is strong to experience R-Selection (ruderal strategy to be adapted to disturbed habitats) (Biggs et al., 1998).

While these insights are very valuable on the microalgae level, addressing the occurrence of certain bacterial species requires metagenomics approaches. Nowadays, it has become possible to decipher the previously unprecedented diversity of biofilms using high-throughput technologies (referring to next-generation sequencing (NGS)). In terms of community composition, results of our pilot experiment of prokaryotic 16S ribosomal ribonucleic acid (rRNA) and eukaryotic 18S rRNA suggest varying responses of the prokaryotic (bacterial) and (micro-) eukaryotic ("higher" cells) species. Species diversity (number of species and number of individuals per species) was significantly higher at high flow condition (0.04 Pa) for the bacterial community while microalgal species flourished at the low flow (0.01 Pa). Additionally, bacterial species that are filamentous or well-known to have EPS-coding genes were more dominant at the mentioned high flow velocities (Fig. 5). This indicates clear shifts of the bacterial community as a response to the hydraulic regime. Few studies took it even further to the level

of gene expression in order to reveal microbial responses to mechanical stress by shear flow, but this is so far restricted to the single-cell level (Persat et al., 2015; Thomen et al., 2017)

4.4. Mass transfer (towards, out of and within the biofilm)

The above briefly discussed biofilm architecture, EPS quantity, biomass and community composition is decisive for the mass transfer towards and within the biofilm. Mass transfer has implications for both, the resupply of nutrients and the removal of waste-products as stated earlier and is largely influenced by the hydrodynamic features. To follow the transport of dissolved molecules into and within the biofilm, mainly microelectrodes have been used so far (Beyenal and Babauta, 2013; de Beer et al., 2018; Sønderholm et al., 2017). For instance, vertical profiles of oxygen microelectrodes allowed the calculation of the DBBL thickness for oxygen (depending on the flow conditions above) as well as metabolic activity (photosynthesis, respiration) and the resulting penetration depth and micro-niches within a biofilm or biofilm-inhabited sediment (de Beer et al., 1994b; Gerbersdorf et al., 2004; Jorgensen and Revsbech, 1985). Using oxygen microelectrodes in our pilot experiment, vertical profiles of oxygen concentration at the water-biofilm-sediment interface were recorded in the transition from light to dark (Fig. 6a). While oxygen peaks and concentrations within the first 5 mm of depth were clearly decreasing over darkness, the oxygen concentration below the photic zone never decreased to zero, indicating some advection. Based on the calculated photosynthetic and respiration rates, it could be stated that the metabolic activity was quite low in our system as compared to e.g., studies from intertidal flats (de Beer et al., 2005), microbial mats (Nübel et al., 2002) and alkaline lakes (Wieland and Kühl, 2000). The wide range of habitats tested proves the unbroken popularity of microsensors to determine physiological responses and essential functions of biofilms at high spatial and temporal resolution. Some investigations took it even one step further to address flow pattern *in situ* within cell clusters or voids of single-cell or multi-species bacterial biofilm by tracking the movement of microscopic fluorescent particles with the help of confocal microscopy (de Beer et al., 1994a; Thomen et al., 2017). Other studies directly determined local mass transfer coefficients applying modified limiting current techniques (LCT) within the biofilm (Yang and Lewandowski, 1995). As a result, the non-uniformity of local mass transfer processes within biofilms became apparent by their large fluctuations that were explained by irregularities in biofilm microstructures comprising channels, voids and cell clusters. While diffusion was prevailing in cell clusters, liquid flow (convection and diffusion) occurred within the biofilm voids (de Beer et al., 1994b, 1994a; Yang and Lewandowski, 1995). Moreover, the flux from the bulk water into the biofilm was enhanced by the elevated biofilm structure being twice as high as compared to a planar surface (de Beer et al., 1994b). With these valuable insights that can be gained at high spatial resolutions, it is not surprising that microsensor studies have skyrocketed in the last decades. Right now, mass transfer and local conversion rates of various molecules (e.g., N_2O, H_2S, NO_3^-, NO_2^-) can be determined by a large range of sensors to calculate the distribution of a suite of metabolic activities (de Beer, 2011). To give just one example, one of the more recent developments, the hydrogen peroxide (H_2O_2) microsensor, was applied in our pilot experiment. While photosynthesis produces H_2O_2 as damaging by-product, it is usually scavenged by catalase to avoid cell damage. However, bursts of H_2O_2 up to 100 – 200 μM were observed when the sensor tip touched a diatom colony – most likely a defense mechanism of these microalgae against predators that has not been noticed before (Fig. 6b). Again, this allows novel information on prey-predator relation and resulting functions at microscale level.

(A)

(B)
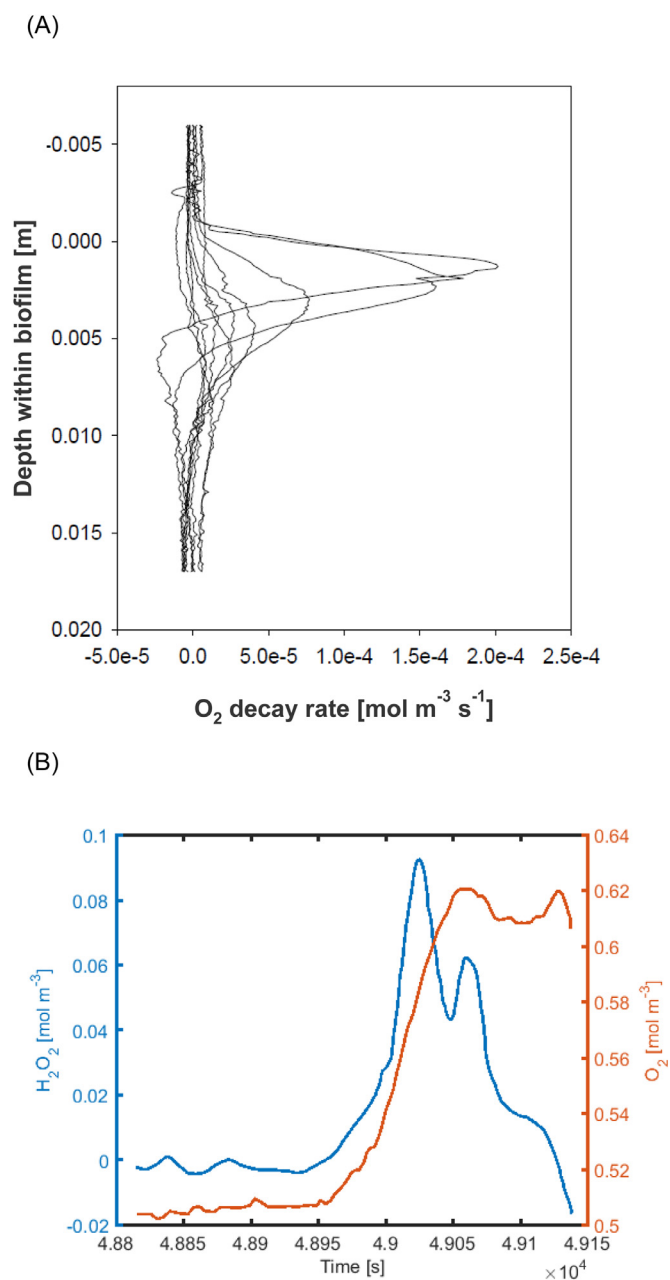
Fig. 6. Microsensor profiles. (A) Oxygen respiration rates determined by subsequent oxygen profiles in transition from light to dark. (B) Hydrogen peroxide burst after touching a diatom colony with the sensor tip.

In order to move on from the fragile micrometer-sized glass electrodes towards more robust sensors, macroelectrodes with sensing tips in centimetre range were developed and the simultaneous determination of molecules in two-dimensional arrays by optodes was pursued (Glud et al., 2000). These optodes based on luminescence quenching are superior to electrochemical sensors in many ways such as obstruction of the local flow field, hysteresis or cross-sensitivity (Kautsky, 1939; Tengberg et al., 2006). Still, there are new challenges associated like response time, drift, long-term stability in organic-rich environments and data processing (Bittig et al., 2018; Glud et al., 1994; Tengberg et al., 2006). Nowadays, both types, electrochemical and luminescent-based microsensors are pushed manifold. However, to particularly address biofilm-flow interaction is still rare (Glud et al., 1998; Kühl et al., 2007) but

has unbowed potential to unravel links between morphology and functionality of biofilms.

5. Mechanical stability of biofilm and its inhabited environment as one essential ecosystem function

5.1. Biofilm functions for its inhabitants and for the ecosystem

As opposed to a single planktonic lifestyle, the biofilm offers high survival, persistence and reproduction potential to the embedded microbes (Flemming and Wuertz, 2019). On one hand, there is co-metabolism and an enhanced availability of essential resources, resulting in significantly higher metabolic activity. This has attracted extensive attention since it links to the important microbial ecosystem functions such as biodegradation, self-purification or drinking water provision (see Introduction and the references therein). On the other hand, protection from environmental stressors is a key factor for biofilm members. The EPS matrix controls material fluxes largely by its internal porosity and permeability that determine fluid flow conduits and their connectivity (Flemming et al., 2016). Since slow diffusion processes prevail and adsorption occurs, toxicants such as antibiotics or disinfectants may be intercepted in the outer layers of a biofilm, which also represents a huge problem in medical treatment (Bjarnsholt et al., 2011). All of that is possible by the cohesive and adhesive forces binding microbes to each other as well as to their substratum and conferring their overall mechanical and structural integrity that is largely impacted by the predominant flow conditions. Thanks to this stability, biofilm eventually colonizes all kinds of interfaces whether unintentionally (e.g., biofouling in pipes and on ship-hulls) or encouraged (e.g., in waste-water treatment, on membranes). Therefore, understanding mechanical properties of aquatic biofilms and biostabilization potential of biofilm-bound sediment have important implications not limited to aquatic ecosystems.

5.2. The challenges with biofilm-induced mechanical stability

Characterizing the mechanical stability of biofilm and biofilm-enclosed environments is thus of broad and significant concern, but remains a challenging task despite a body of work. Part of the problem is that, traditionally, it was attempted to remove biological effects, while nowadays, biology is often brought to the laboratory with little consideration of natural settings (Paterson et al., 2018). In this regard, laboratory-grown biofilm are often based on distinct microbial strains growing at conditions that are difficult to compare and often lack natural relevance (e.g., single-species biofilm and nutrient supply that do not occur in natural rivers (Vignaga et al., 2012)). When testing for the biostabilization effect in the laboratory, a range of engineering devices are applied that act at different size scales while addressing different forces (e.g., vertical jets versus horizontal bed shear stress (Vardy et al., 2007; Widdows et al., 2007)). Moreover, examination of erosion thresholds are more complicated in biofilm-embedded sediments since they behave very differently compared to the traditionally used abiotic particle-size fractions (e.g., they erode in aggregates and chunks rather than in single-grain mode (Thom et al., 2015)). Last but not least, investigating development of biofilm over time requires non-destructive methods, but most approaches require bed failure to occur (Jonsson et al., 2006).

Overall, flow-microbe interactions and implications for mechanical stability of biofilm have received special attention since this process understanding might help to control (eradicating harmful or encouraging beneficial) biofilm by optimizing cleaning procedures (e.g., in drinking water pipes) or improving operational parameters (e.g., in rotating biological contactors). In the following, we will present a brief selection of such studies focusing on the mechanical strength of a biofilm in relation to flow from single-cell level to bulk biofilm measurements in the range from several millimeters to several centimeters (Wagner et al., 2010b).

5.3. Single-cell approaches to determine adhesive forces

Atomic force microscopy (AFM) has been widely used to determine the elasticity and adhesive capacity of single bacterial or microalgal cells linking the results to different cell surface biomolecules with implications to the initial stages of biofilm colonization (Wright et al., 2010). The AFM technique can be applied in a static or dynamic mode, measures in the range from piconewtons to several nanonewtons and allows 3D mapping of surfaces within a limited area (Boudarel et al., 2018). Since the technique has been widely used to study initial attachment, only few studies relate to reciprocal microbe-flow interactions that become most interesting in later stages of biofilm development. Lim et al. (2008) gave proof of the positive relation between morphological parameters such as surface coverage and roughness as well as flow rate in biofilms growing on glass beads within microfluidic cells. To shed light on the internal structure of biofilm, passive particle tracking microrheology (PTM) or active optical tweezer (OT) and magnetic tweezer (MT) techniques have been successfully implemented (see reviews by Ahmad Khalili and Ahmad, 2015; Azeredo et al., 2017). These approaches allow the determination of spatially and temporally varying adhesive strength as well as the quantification of shear stresses required for detachment while operating in the sub-piconewton (pN) to several hundreds of pN (<1 pN) range (Castelain et al., 2012; Picioreanu et al., 2018). Using MT as a more robust approach for actively moving cells, Galy et al. (2014) developed a 3D map of mechanical biofilm properties and demonstrated decreasing elastic compliance in *E. coli* biofilms being exposed to increasing shear stress. This research provided valuable insights of the heterogeneity of biofilm showing variations in shear compliance in the order of two magnitudes within close proximity (Galy et al., 2014). Again at microscale, microfluidics are an integral part in the study on mechanical properties of growing biofilms, often combined with microscopy to monitor biofilm formation during growth and biofilm deformation due to applied stress such as pressurized air or flow (see review by Karimi et al., 2015). Hohne et al. (2009) established such an approach to examine the Young modulus and relaxation time of two bacterial strains while imaging their deflection due to varying air pressure with confocal laser scanning microscopy (CLSM). Thomen et al. (2017) pursued the growth of *E.coli* to reveal the previously unknown bacterial strategy to settle in low shear stress regions before strategically expanding from these bases towards areas of high shear stress that were impossible to colonize before. Hou et al. (2018) applied attenuated total reflection Fourier transform infrared (ATR-FTIR) spectroscopy as well as CSLM to give evidence that the individual *Staphylococcos aureus* bacterium produced two to five times more EPS polysaccharides at high shear conditions as compared to low shear stress. That also extended to the entire biofilm as was shown by tribometrically measured coefficients of friction (CoF), confirming that EPS quantity is considered relevant for mechanical strength (Hou et al., 2018).

5.4. Structural visualization and mechanical strength at the mesoscale

While the microscale is certainly very important to learn about activities and functions of biofilms at high resolution, it remains difficult to extrapolate these insights to the dimensions of an entire biofilm (mm-cm range) which is of greater interest if it comes to flow-biofilm interaction and the resulting mechanical strength (Wagner and Horn, 2017). Knowledge on mechanical strength is

needed to re-think anti-biofouling measures, to manage biofilm growth in technical systems such as bioreactors, membranes or drinking water distribution pipes or simply to better understand the mode of action that is behind the effects recorded in biostabilization of sediments. Therefore, other techniques such as optical coherence tomography (OCT) or optical coherence elastography (OCE) (Larin and Sampson, 2017) which has a more holistic view on biofilm structure could be explored. OCT allows to work on this mesoscale in micrometer resolution and represents a fast, non-invasive, *in situ* imaging technique that gives depth-resolved structural information which does not require staining. Thus, employing near-infrared light allows deeper penetration into the biofilm in comparison to CLSM and does not need fluorophores that might interfere with local properties of the biofilm (Azeredo et al., 2017; Picioreanu et al., 2018). However, our own OCT measurements in the pilot experiment suggest that while surface topography is easy to image, it can be difficult to capture the internal structure as well as to differentiate between biofilm and sand particles. Still, OCT clearly visualized how the microbes filled the sand grain space with biofilm maturation (Fig. 7). In young biofilms, filaments were visible at the mentioned low flow conditions (0.01 Pa) while at high flow (0.04 Pa), the growth seems delayed again (Fig. 7). This influence of various flow scenarios in the initial stages of biofilm growth is expected to manifest later in variations in thickness, morphology as well as hydraulic resistance of the mature biofilm as has been revealed by other OCT measurements (Dreszer et al., 2014).

Exploring the usage of rotating disk electrodes (RDE), Boulêtreau et al. (2011) confirmed varying riverine biofilm thickness and elasticity that both were significantly higher at low flow conditions (0.1 versus 0.45 m s^{-1} over 21 days). In contrast to OCT, RDE examines the biofilm as homogenous bulk material which is similar to the application of rheometers that are commonly used for studying viscoelastic material although being destructive (Boudarel et al., 2018). Biofilm comprises both an elastic (or solid-like) and a viscous (or liquid-like) part that stores and dissipates energy during strain deformation. In our workshop, we also tested viscoelastic properties of young and mature biofilms using a rotational rheometer. Conducting dynamic tests in the oscillatory mode of the rheometer in our pilot experiment documented clearly the viscoelastic behavior of the biofilms at varying stages of maturity. Beforehand, some biofilm samples (young biofilm) were cultivated *in situ* on rheometer disks with the same substrate tested simultaneously with other devices, while other samples (mature biofilm) were transferred later onto those disks at termination of the experiment. Due to the roughness of the substrate, both sample preparation methods showed similar results even though the *in situ* growth has a clear advantage of ensuring an overall structural integrity. The recorded phase angle highlighted the strong dependence of the viscoelastic properties on the maturity of the biofilm. The results showed a low phase angle of tanδ = 0.16 for the matured biofilm, indicating less viscous and more elastic behavior, while this value increased for the young biofilm to tanδ = 0.28 (Fig. 8). However, no clear relation could be detected between the phase angle and the prevailing flow conditions, although the margin of the phase angle has been slightly larger for biofilms exposed to lower flow conditions (Fig. 8). For a more comprehensive interpretation however, it is necessary to link the results on rheological properties to structural features (e.g., streamers or flat biofilm) and chemical composition (polymer type) in future studies. Then it would also be possible to structurally explain stronger adhesion and lower detachment rates at higher shear stresses as it has been previously observed by recording stress-strain tests and creep-compliance curves in *Pseudomonas aeruginosa* biofilm samples (Stoodley et al., 2002).
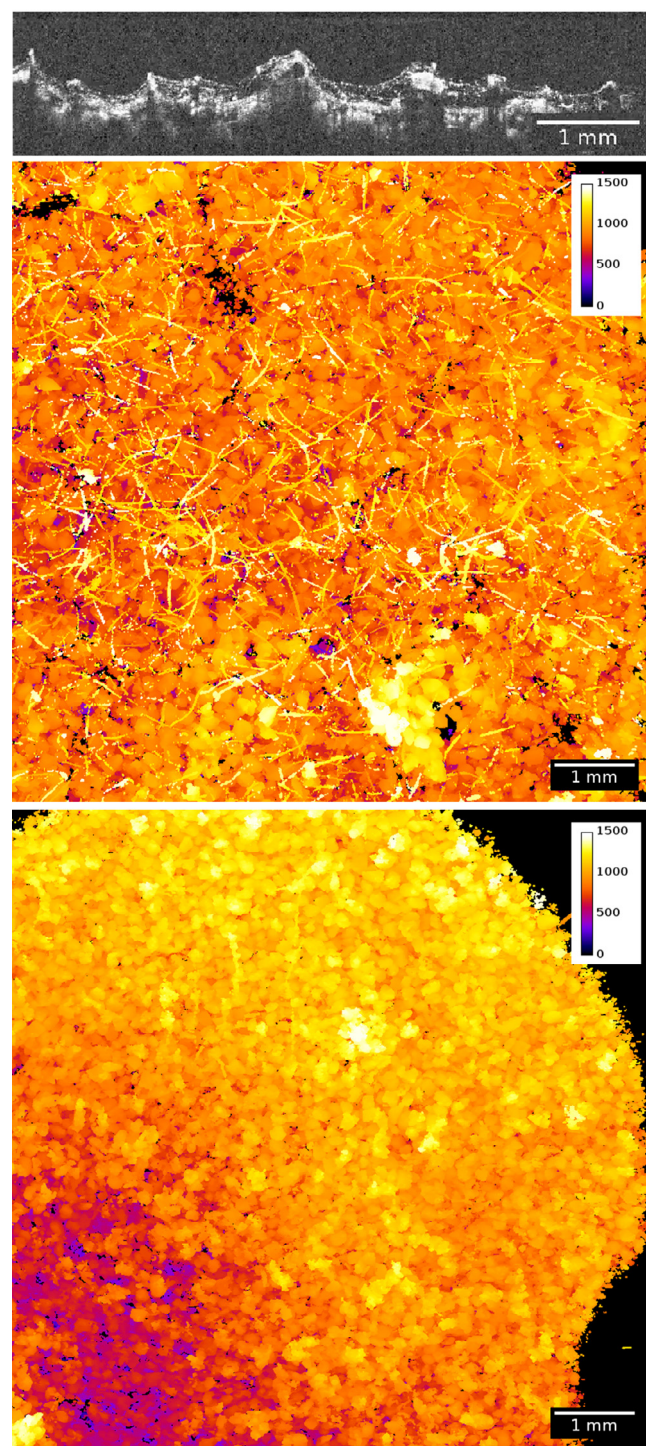
Fig. 7. Optical coherence tomography (OCT) images. Sand grains embedded by biofilm showing young growing biofilm with filamentous structure at low flow (above) and delayed attachment at high flow (below).

5.5. Erosion vulnerability and adhesive capacity in sediment research

As we can see from Sections 5.1–5.4, there exists promising studies highlighting mechanical properties of biofilm in interaction with the flow at various scales (see also review by Araújo et al., 2019). However, none of the research includes the substratum, except for our presented OCT (Fig. 7) and rheometer measurements (Fig. 8) where biofilm grew on fine sand. This is, of course, different in sedimentation engineering where the erosive response
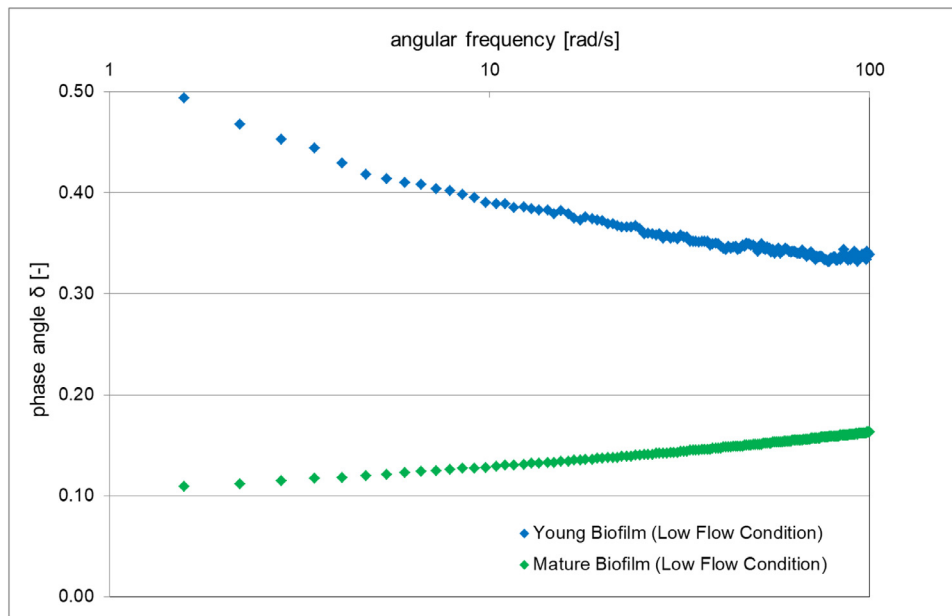
Fig. 8. Rheometer Measurements. Phase angles of the mature and young biofilm samples measured by rheometer under low flow conditions.

of the substratum towards hydrodynamic forcing is central. However, biofilms were and sometimes still are neglected in this research field (Paterson et al., 2018; Righetti and Lucarelli, 2007). That changed some decades ago when it was increasingly recognized that biofilms are ubiquitously distributed and impact significantly the dynamics of the ETDC (erosion – transport – deposition – consolidation) sediment cycle (Black et al., 2002). With the consensus on the importance of biostabilization, the portfolio of methods to address sediment stability has broadened. The classical approach in hydraulic research and engineering utilizes erosion flumes or chambers in which the flowing water eventually causes bed failure to occur (Aberle et al., 2003; Jonsson et al., 2006; Noack et al., 2015; Widdows et al., 2007). With growing interest in the biology mediating the erosive response, devices with smaller footprints capable for usage in the field were developed to pursue mechanical failure and sloughing-off at higher temporal and spatial resolution (Vardy et al., 2007). However, to follow-up gradual changes in the attachment and increasing cohesion of substratum by young biofilms, non-destructive methods with higher sensitivity were needed. Magnetic particle induction (MagPI) system has been developed to determine the adhesive capacity of growing biofilm at the patch scale with a small footprint, but large enough to get meaningful results on biofilm-embedded sediment stability (Gerbersdorf et al., 2018; Larson et al., 2009). Using 50% particle clearance, the MagPI indicated significantly lower adhesiveness at low flow condition (834 ± 59 mA) as compared to high flow condition (1241 ± 97 mA) in our pilot experiment. This is in line with the results of Graba et al. (2013) who performed a sloughing test on 40-day-old biofilms and showed an inverse relation between the proportion of detached biomass and the average value of friction velocity during growth. The higher stability might be related to enhanced secretion of extracellular polymeric substances at high shear stresses as stated earlier (Brading et al., 1995; Fish et al., 2017). Whether or not this translates into a higher biostabilization capacity of the biofilm within the sediment at high flow regimes, is currently unknown (Gerbersdorf and Wieprecht, 2015). In our pilot experiment, by investigating the erosion failure of the samples within the SETEG-flume (Noack et al., 2015), the critical shear stress necessary to erode the biofilm-sediment complex was 40-fold higher as compared to the bare sand (Fig. 9). However, there was no statistically significant difference between the two con-

trasting flow scenarios. This might be explained by the growing mode of these samples where the biofilm covered the underlying substratum like a carpet. Erosion often occurred suddenly at the edges of our sample holders, followed by a severe resuspension of the bare, unprotected sediment beneath the biofilm carpet, rather than indicating a true failure of the biofilm-sediment surface (see S1 and S2 for videos). The starting position of the erosion at the edges of the cartridges can be attributed to a sudden change in surface roughness upstream and downstream of the measurement location. Hence, while cultivating biofilms in special cartridges (Schmidt et al., 2015) or coupons (Singer et al., 2010, 2006) facilitates *in situ* and easier measurements using a multitude of instruments, it is critical for erosion tests to exclude unwanted effects of sudden roughness change. It is further deemed advisable to adapt Shield's-like erosion schemes to biofilm-embedded material (Shields, 1936; Thom et al., 2015).

6. The gaps in hydromechanics, biofilm and sediment research and lessons to learn

In biofilm research, the single-cell scale has been naturally favoured to decipher details on biofilm attachment, quorum sensing, morphology and/or detachment (Kim et al., 2016; Mukherjee and Bassler, 2019; Wheeler et al., 2019). As we have reported above, reciprocal flow-biofilm interactions have been experimentally explored within micro-fabricated channels that mostly range from micrometres to millimetres and analysed mainly by microsensors (de Beer et al., 1994a; Yang and Lewandowski, 1995) and/or imaging techniques. For the latter, Thomen et al. (2017) visualized the trail lengths of 1-μm fluorescent particles via microscopically derived z-stack images in millifluidic channels. Magnetic resonance microscopy (MRM) is another promising method for the investigation of transport phenomena, which is capable of simultaneously imaging the development of flow field and biofilm structure in a non-invasive, less time-consuming way while covering quantitatively relevant areas (Gjersing et al., 2005; Manz et al., 2005, 2003). For instance, Wagner et al. (2010a) addressed the response of biofilm to various flow gradients and shear rates by scanning the flow field with MRM. Herrling et al. (2017) successfully elucidated water diffusion within five different types of biofilm structures by pulsed field gradient-nuclear magnetic res-

Fig. 9. Erodibility tests. Biofilm-sediment complex is exposed to increasing shear stress in the erosion flume SETEG (Strömungskanal zur Ermittlung der tiefenabhängigen Erosionsstabilität von Gewässersedimenten). Left is the bare sand that acts as the control (critical shear stress: 0.3 Pa), right is the mature biofilm after 6 weeks of growth (critical shear stress: 12 Pa after failure at the edges). Please also see S1 and S2 videos in the supplementary material.

onance (PFG-NMR). As Morgenroth and Milferstedt (2009) stated, "…a biofilm with a total area of 1 m^2 is not simply the sum of biofilm grown in 1000 flow channels, even though the total areas roughly correspond." Consequently, in their study, Morgenroth and Milferstedt (2009) went up to the patch scale to address the effect of laminar, transient and fully turbulent conditions on biofilm in the range of several millimetres to centimetres. Collectively, these experiments gave essential insights into detailed processes of biofilm development at various hydrodynamic settings. However, their relevance for aquatic environments is still largely debatable due to difficulties in reproducing natural conditions in the laboratory. Challenges include representing natural temporal and spatial variability of flow (single-cell scale to ecosystem scale) and biofilm (multitaxa and multispecies communities) or generating fully-developed turbulent flow conditions and irregular surfaces (e.g., mixed sediments, spatial heterogeneity of roughness) at the measurement section.

Ideally, biofilm should be grown in a most natural-like setting to allow a typical community composition and matrix structure at environmentally relevant flow patterns. Obviously, this might differ severely in simulating technical or natural habitats but in both cases, this requires experimental facilities that are beyond the small scale of the microfluidic channels. Despite increasing number of mesocosm studies, our understanding of near-bed flow dynamics is currently hampered by the lack of velocity measurements at the flow-biofilm-sediment interface (e.g., Nuy et al., 2018; Risse-Buhl et al., 2017). While the interactions between flow and biofilm occur predominantly at mesoscale (100 μm to 10 cm in vertical length), most studies concerning flow-biofilm reciprocity usually represent flow with a single (bulk) value for the entire channel either as a depth-averaged or cross-sectional average velocity (and discharge) (Moulin and Eiff, 2012 and references therein) or temporally-averaged flow and turbulence parameters far above the bed (Risse-Buhl et al., 2017, 2020; Singer et al., 2010), ignoring the heterogenous characteristics of the flow at local biofilm scale (μm to cm) and its dispersive contribution to mass flux. This can mainly be attributed to frequent use of acoustic-based (e.g., acoustic Doppler velocimeter or ADV) or magnetic field based (e.g., electromagnetic current meter or ECM) instruments in both laboratory and field studies, which have difficulties in measuring near-bed mean flow (<5 mm) and turbulence (<10 mm) due to acoustic interference of the bed (Koca et al., 2017; Voulgaris and Trowbridge, 1998) and/or sensor size. On the other hand, applying hot-film anemometers, Biggs et al. (1998) demonstrated clearly the influence that the biofilm has on the close-by flow pattern 2 mm above its surface while there was no measurable effect to the far more uniform mean velocity of the mid-water column. Hydrodynamic fluctuations with local shear stress peaks are critical to mass transfer (Stoodley et al., 1999; Voermans et al., 2017),

with important consequences for biofilm to modulate ecosystem health and services. This is particularly important for biofilms with streamers which oscillate with the flow and modulate mass transfer (Nikora, 2010; Larned et al., 2011). Ultimately, only local flow conditions are relevant to describe the forcing at microscale and are not easily inferred from mean bulk velocities (Graba et al., 2013). The introduction of modern, optical and non-intrusive techniques such as particle image velocimetry (PIV) allows high resolution measurements of flow patterns close to the biofilm (~1–2 mm) in standard configurations. PIV is based on visualization and computation of the displacement of small tracer particles in a flow, captured by two subsequent images (see reviews by Adrian et al., 2011; Westerweel et al., 2013). Since it allows for both quantitative measurements at larger areas (few dm^2) and visualization of flow structures, PIV provides physical insights into the behavior of flow and biofilm interactions, thereby offering various advantages over traditional methods (i.e., ADV, ECM). Despite its costly and complicated setup, low-cost PIV systems have recently been developed for use in the laboratory (Cierpka et al., 2016) and in the field (Cameron et al., 2013; Koca et al., 'Unpublished results'). Thus, instead of following traditional single-point or vertical profile measurements, it is now possible and timely to characterize flow pattern near biofilm at high resolution (Koca et al., 2016). Nevertheless, the challenge remains to measure this at sub-millimeter scales in fully-turbulent, fully-rough and fully-developed environments, which, unavoidably, must be performed in relatively large flow facilities on the several-meter scale for a variety of controlled flow and environmental conditions (Packman, 2013; Vignaga et al., 2013). Indeed, it would be desirable to describe scales small enough to include the viscous sublayer on the biofilm and grains while simultaneously capturing the full turbulent spectrum. Only then can the mechanisms behind biofilm growth as well as mass and momentum flux exchanges between biofilm and the water be elucidated.

Research on flow-sediment interaction has a long tradition in engineering science which is motivated *inter alia* by the huge economical aspect to maintain waterways and harbours for shipping as well as flood control measures (Voermans et al., 2017). Sediment dynamics from bedload such as rolling gravel to suspended load of fine particles is of uttermost importance for the hydrological, geomorphological and ecological functioning of aquatic systems including rivers, lakes, reservoirs, estuaries and coastal zones (Forstner and Westrich, 2005). Along with sediment properties, the hydrodynamic regime is decisive for the transport, deposition and finally spatial distribution of sediments. Hence, fine-grained particles such as silt and clay usually settle in low energetic habitat while coarser sediment deposit in areas of high energy impact where frequent collisions of sand particles ("rolling") occur (Van Rijn, 1993). This in turn impacts the settlement of microbes

with a higher likelihood to develop in fine sediments since these small particles feature (a) a high surface to volume ratio, (b) offer plenty of binding sites to trap nutrients and (c) offer more protection for sensible shells such as diatom frustules that might be destroyed in rolling (Delgado et al., 1991; Gerbersdorf and Wieprecht, 2015). Mediation of fine sediment characteristics by the developing microbial assemblages then changes their erosive response to hydraulic forcing as described in Sections 1 and 5.5. While the onset of motion of non-cohesive sediment particles such as sand or gravel is generally predicted by using the Shields diagram (Shields, 1936), there is no valid approach for fine cohesive sediment because of the biological features inhabited (Black et al., 2002). In order to better predict the behavior of fine sediment and the often-associated pollutants at extreme (e.g., 100-year flood) or management scenarios (e.g., flushing), experiments have been largely performed in laboratory flumes with sediments that were retrieved and transferred from the field (Forstner and Salomons, 2008; Gerbersdorf et al., 2007; Haag et al., 2001). However, there are increasing efforts towards *in situ* measurements in order to avoid unwanted changes due to transport of sediment from field to flume and sediment aging (Aberle et al., 2003; Noack et al., 2015; Witt and Westrich, 2003).

Overall, although fine sediments and their erosional behavior have thus received increasing attention over the last decades with or without the consideration of biofilm, their link to the temporally and spatially highly varying pattern of hydrodynamics (e.g., TKE) and bed topography co-evolving with biofilm growth have not been studied yet (Gerbersdorf and Wieprecht, 2015; Hannah et al., 2004; Rice et al., 2010). On a much smaller scale, some studies addressed the sloughing-off phenomena of biofilm at varying shear stresses by measuring biofilm weight losses or the amount of eroded sand/biofilm mixtures (Grün et al., 2016; Pique et al., 2016). Consequently, future studies should further explore the flow-biofilm-sediment processes nexus in order to better understand biostabilization and sediment dynamics which have key implications for morphodynamics, aquatic habitat, water quality and beyond. This requires integrated investigations of hydrodynamics, biogeomorphology and microbiology. An example of such integrated approach was illustrated in this review paper combined with a pilot experiment. Based on the co-application of state-of-the-art methods from different disciplines (black font in Fig. 1) on quasi-naturally grown biofilm-bound sediment developed at contrasting flow conditions, we have made following observations about advantages and challenges associated with the tested methods:

- Flow affected time of settlement, growth direction and subsequent topography of biofilm-bound sediment (Fig. 2). In turn, the biofilm growth increased considerably the magnitude and heterogeneity of Reynolds shear stress (not shown here). While the measurements of spatially and temporally varying flow in combination with motion of streamers are still challenging, PIV may become a key method in studying natural flow-biofilm interactions at high resolution.
- Obtaining topography by scanning microscopy (Fig. 2a-b) was far too time-consuming for larger areas, instead laser triangulation system showed similar results (Fig. 2c) in a fraction of the time previously needed and is thus an excellent choice for characterizing topography at patch scale (cm^2– dm^2). Microscopy is needed for higher resolutions at spatially limited spots in order to e.g., visualize key components of the biofilm (members and EPS moieties) by fluorescence signals.
- With application of microsensors, we have observed bursts of H_2O_2 when touching a diatom colony, suggesting a likely defense mechanism of these microalgae against predators. Therefore, using microsensors, one can also gain insights into how

microbes cope with friendly and unfriendly neighbours in their close surrounding (Fig. 6).
- Microsensor measurements could be used together with PIV measurements and OCT images for analyzing the external and internal mass as well as momentum transfer by combining substrate distribution, flow dynamics and biofilm structure. Even though it is not tested here, the application of MRM holds promise for studying internal and external diffusion and flow patterns.
- OCT is a beneficial imaging technique for characterizing internal structure of biofilm without disturbing or damaging the samples. However, since the probe depth is limited, it remains to be tested how suitable this technique is for analyzing biofilm-embedded sediment over depths larger than 2 mm (Fig. 7).
- Performing biochemical and microbiological analyses, it was observed that quantities of polymeric substances and cell numbers play a minor role in explaining the mechanisms of binding within the biofilm and beyond (Fig. 3), suggesting the significant role of various EPS moieties and key microbial players to translate into functionality, herein biostabilization.
- Applying molecular techniques, we have observed significant shifts in species composition and diversity at both prokaryotic and eukaryotic levels according to temporal and environmental changes (Fig. 5). The link between functionality and diversity of key players is a matter of an ongoing debate in ecology (Besemer, 2015; Dang and Lovell, 2016; Leibold et al., 2004). To introduce this idea into biofilm science would be a great research concept for hypothesis building.
- Microalgae seem to play a dominant role in biostabilizing the sediment with impact according to the particular groups or species involved. Thus, the possibility to monitor by hyperspectral imaging the density, composition and distribution of phototrophic biofilms (Fig. 4) creates a strong predictor for metabolic activity and sediment stability.
- While the magnetic particle induction technique is highly sensitive for measuring adhesiveness of biofilm-bound sediment at high temporal and spatial resolution (< 5 mm, not shown here), it is restricted to measurements at the sediment surface. Furthermore, measurements are challenging if streamers are abundant.
- Until now, determination of the stability of deeper layers has been limited to erosion flumes, with the known methodological limitations (Fig. 9). Like with the erosion flumes, the rheometer approach does not allow ongoing measurements for the same sample over time, but could structurally explain varying adhesiveness and detachment rates of biofilm at different environmental scenarios (Fig. 8)

7. Conclusions

Recent advances in measurement techniques have provided a wealth of knowledge regarding individual domains of biofilm research, yet the understanding of flow-biofilm-sediment processes is still at its infancy. Studying flow-biofilm-sediment interactions are of importance to better understand ecological functions and engineering processes and to help establish healthy aquatic ecosystems. Most of the insights on the sediment-ecology relation derive from investigations on macroorganisms and macrophytes. This is surprising since microbes are the first colonizers to dictate subsequent colonization by higher trophic levels and they e.g., predominately affect the flux of matter on larger scales. Moreover, the link to the substratum in which microorganisms settle is mostly missing. Therefore, integrative and interdisciplinary approaches are needed that simultaneously and equally address the complex and non-linear ways in which sediment properties and biofilm interact with the hydrodynamics at a scale of μm to cm (single-

cell and patch scale) before extrapolating the theoretical knowledge to the larger scales for environmental management purposes. While field studies are essential, process understanding comes from controllable and repeatable conditions addressed in laboratory experiments which should cross disciplinary boundaries to avoid oversimplification and unrealistic settings (e.g., use of isolated species, inappropriate physical conditions, unconsidered wall effects or short test sections).

In this Review, we summarized the current state of the knowledge and methodological approaches in the flow-biofilm-sediment research with an emphasis on biostabilization and fine sediment dynamics mainly in the benthic zone of lotic and lentic environments. Specifically, we combined a literature review with the results of a pilot experiment that was conducted in the framework of a joint workshop, with the aims of i) consolidating expert knowledge from different scientific fields, but all with the same goal directed towards flow-biofilm-sediment triangle, ii) identifying knowledge gaps and iii) exploring the feasibility of different instruments to address these gaps. In the pilot experiment, co-application of advanced methods with capabilities to visualize at cell-, patch- and reach scales at high spatial resolution in controllable laboratory conditions has facilitated investigations into flow dynamics (particle image velocimetry), bed topography (laser triangulation system and light microscopy), biofilm structure (optical coherence tomography), mass transfer (microsensors), microbial community (16S and 18S rRNA gene sequencing) as well as mechanical characteristics (rheometer) and biostabilization potential (magnetic particle induction and erosion flumes). Based on the evaluation of feasibility of these techniques, we also provided research insights, methodological limitations, existing research gaps and future research directions that have potential to make important contribution to the field of biostabilization.

Declaration of Competing Interest

The authors declare that they have no known competing financial interests or personal relationships that could have appeared to influence the work reported in this paper.

Acknowledgement

Supplementary materials

Supplementary material associated with this article can be found, in the online version, at doi:10.1016/j.watres.2020.116182.

References

Aberle, J., Nikora, V., McLean, S., Doscher, C., McEwan, I., Green, M., Goring, D., Wash, J., 2003. Straight benthic flow-through flume for in situ measurement of cohesive sediment dynamics. J. Hydraul. Eng.-Asce 129, 63–67. doi:10.1061/(asce)0733-9429(2003)129:1(63).

Adrian, L., Adrian, R.J., Westerweel, J., 2011. Particle Image Velocimetry. Cambridge University Press.

Ahmad Khalili, A., Ahmad, M.R., 2015. A review of cell adhesion studies for biomedical and biological applications. Int. J. Mol. Sci. 16, 18149–18184. doi:10.3390/ijms160818149.

Allan, D.J., Castillo, M.M., 2007. Stream Ecology - Structure and Function of Running Waters, Second. ed.. Springer, Dordrecht, The Netherlands.

Araújo, G.R., de, S., Viana, N.B., Gómez, F., Pontes, B., Frases, S., 2019. The mechanical properties of microbial surfaces and biofilms. Cell Surf. 5, 100028. doi:10.1016/j.tcsw.2019.100028.

Arndt, H., Schmidt-Denter, K., Auer, B., Weitere, M., 2003. Protozoans and Biofilms. In: Krumbein, W.E., Paterson, D.M., Zavarzin, G.A. (Eds.), Fossil and Recent Biofilms: A Natural History of Life on Earth. Springer, Netherlands, Dordrecht, pp. 161–179. doi:10.1007/978-94-017-0193-8_10.

Azeredo, J., Azevedo, N.F., Briandet, R., Cerca, N., Coenye, T., Costa, A.R., Desvaux, M., Di Bonaventura, G., Hébraud, M., Jaglic, Z., Kačániová, M., Knøchel, S., Lourenço, A., Mergulhão, F., Meyer, R.L., Nychas, G., Simões, M., Tresse, O., Sternberg, C., 2017. Critical review on biofilm methods. Crit. Rev. Microbiol. 43, 313–351. doi:10.1080/1040841X.2016.1208146.

Banasiak, R., Verhoeven, R., De Sutter, R., Tait, S., 2005. The erosion behaviour of biologically active sewer sediment deposits: observations from a laboratory study. Water Res. 39, 5221–5231. doi:10.1016/j.watres.2005.10.011.

Barton, A.F., Sargison, J.E., Osborn, J.E., Perkins, K., Hallegraeff, G., 2010. Characterizing the roughness of freshwater biofilms using a photogrammetric methodology. Biofouling 26, 439–448. doi:10.1080/08927011003699733.

Battin, T.J., 2000. Hydrodynamics is a major determinant of streambed biofilm activity: from the sediment to the reach scale. Limnol. Oceanogr. 45, 1308–1319. doi:10.4319/lo.2000.45.6.1308.

Battin, T.J., Besemer, K., Bengtsson, M.M., Romani, A.M., Packmann, A.I., 2016. The ecology and biogeochemistry of stream biofilms. Nat. Rev. Microbiol. 14, 251–263. doi:10.1038/nrmicro.2016.15.

Battin, T.J., Kaplan, L.A., Findlay, S., Hopkinson, C.S., Marti, E., Packman, A.I., Newbold, J.D., Sabater, F., 2008. Biophysical controls on organic carbon fluxes in fluvial networks. Nat. Geosci. 1, 95–100. doi:10.1038/ngeo101.

Battin, T.J., Kaplan, L.A., Newbold, J.D., Cheng, X., Hansen, C., 2003. Effects of current velocity on the nascent architecture of stream microbial biofilms. Appl. Environ. Microbiol. 69, 5443–5452. doi:10.1128/AEM.69.9.5443-5452.2003.

Berke, A.P., Turner, L., Berg, H.C., Lauga, E., 2008. Hydrodynamic attraction of swimming microorganisms by surfaces. Phys. Rev. Lett. 101, 038102. doi:10.1103/PhysRevLett.101.038102.

Berne, C., Ellison, C.K., Ducret, A., Brun, Y.V., 2018. Bacterial adhesion at the single-cell level. Nat. Rev. Microbiol. 16, 616–627. doi:10.1038/s41579-018-0057-5.

Besemer, K., 2015. Biodiversity, community structure and function of biofilms in stream ecosystems. Res. Microbiol. 166, 774–781. doi:10.1016/j.resmic.2015.05.006.

Besemer, K., Singer, G., Limberger, R., Chlup, A.-K., Hochedlinger, G., Hödl, I., Baranyi, C., Battin, T.J., 2007. Biophysical controls on community succession in stream biofilms. Appl. Environ. Microbiol. 73, 4966–4974. doi:10.1128/AEM.00588-07.

Beyenal, H., Babauta, J., 2013. Microsensors and microscale gradients in biofilms. Product. Biofilms 235–256. doi:10.1007/10_2013_247.

Biggs, B.J.F., Goring, D.G., Nikora, V.I., 1998. Subsidy and stress responses of stream periphyton to gradients in water velocity as a function of community growth form. J. Phycol. 34, 598–607. doi:10.1046/j.1529-8817.1998.340598.x.

Bishop, P.L., Gibbs, J.T., Cunningham, B.E., 1997. Relationship between concentration and hydrodynamic boundary layers over biofilms. Environ. Technol. 18, 375–385. doi:10.1080/09593331808616551.

Bittig, H.C., Körtzinger, A., Neill, C., van Ooijen, E., Plant, J.N., Hahn, J., Johnson, K.S., Yang, B., Emerson, S.R., 2018. Oxygen optode sensors: principle, characterization, calibration, and application in the ocean. Front. Mar. Sci. 4, 429. doi:10.3389/fmars.2017.00429.

Bjarnsholt, T., Jensen, P.Ø., Moser, C., Høiby, N. (Eds.), 2011. Biofilm Infections. Springer-Verlag, New York doi:10.1007/978-1-4419-6084-9.

Black, K.S., Tolhurst, T.J., Paterson, D.M., Hagerthey, S.E., 2002. Working with natural cohesive sediments. J. Hydraul. Eng.-Asce 128, 2–8.

Boudarel, H., Mathias, J.-.D., Blaysat, B., Grédiac, M., 2018. Towards standardized mechanical characterization of microbial biofilms: analysis and critical review. NPJ Biofilms Microb. 4, 1–15. doi:10.1038/s41522-018-0062-5.

Boulêtreau, S., Charcosset, J.-.Y., Gamby, J., Lyautey, E., Mastrorillo, S., Azémar, F., Moulin, F., Tribollet, B., Garabetian, F., 2011. Rotating disk electrodes to assess river biofilm thickness and elasticity. Water Res. 45, 1347–1357. doi:10.1016/j.watres.2010.10.016.

Brading, M.G., Boyle, J., Lappinscott, H.M., 1995. Biofilm formation in laminar-flow using pseudomonas-florescens EX101. J. Ind. Microbiol. 15, 297–304. doi:10.1007/bf01569983.

Bratanov, V., Jenko, F., Frey, E., 2015. New class of turbulence in active fluids. Proc. Natl. Acad. Sci. U.S.A. 112, 15048. doi:10.1073/pnas.1509304112.

Burns, A., Ryder, D.S., 2001. Potential for biofilms as biological indicators in Australian riverine systems. Ecol. Manag. Restor. 2, 53–64. doi:10.1046/j.1442-8903.2001.00069.x.

Cameron, S.M., Nikora, V.I., Albayrak, I., Miler, O., Stewart, M., Siniscalchi, F., 2013. Interactions between aquatic plants and turbulent flow: a field study using stereoscopic PIV. J. Fluid Mech. 732, 345–372. doi:10.1017/jfm.2013.406.

Castelain, M., Rouxhet, P.G., Pignon, F., Magnin, A., Piau, J.-.M., 2012. Single-cell adhesion probed in-situ using optical tweezers: a case study with Saccharomyces cerevisiae. J. Appl. Phys. 111, 114701. doi:10.1063/1.4723566.

Chan, S., Pullerits, K., Keucken, A., Persson, K.M., Paul, C.J., Rådström, P., 2019. Bacterial release from pipe biofilm in a full-scale drinking water distribution system. NPJ Biofilms Microb. 5, 1–8. doi:10.1038/s41522-019-0082-9.

Characklis, W.G., Cooksey, K.E., 1983. Biofilms and microbial fouling. In: Laskin, A.I. (Ed.), Advances in Applied Microbiology. Academic Press, pp. 93–138. doi:10.1016/S0065-2164(08)70355-1.

Chen, C., Liu, S., Shi, X., Chaté, H., Wu, Y., 2017a. Weak synchronization and large-scale collective oscillation in dense bacterial suspensions. Nature 542, 210–214. doi:10.1038/nature20817.

Chen, X.D., Zhang, C.K., Zhou, Z., Gong, Z., Zhou, J.J., Tao, J.F., Paterson, D.M., Feng, Q., 2017b. Stabilizing effects of bacterial biofilms: EPS penetration and redistribution of bed stability down the sediment profile. J. Geophys. Res. 122, 3113–3125. doi:10.1002/2017JG004050.

Chennu, A., Färber, P., Volkenborn, N., Al-Najjar, M.A.A., Janssen, F., de Beer, D., Polerecky, L., 2013. Hyperspectral imaging of the microscale distribution and

dynamics of microphytobenthos in intertidal sediments. Limnol. Oceanogr. 11, 511–528. doi:10.4319/lom.2013.11.511.

Chennu, A., Grinham, A., Polerecky, L., de Beer, D., Al-Najjar, M.A.A., 2015a. Rapid reactivation of cyanobacterial photosynthesis and migration upon rehydration of desiccated marine microbial mats. Front. Microbiol. 6, 1472. doi:10.3389/fmicb.2015.01472.

Chennu, A., Volkenborn, N., de Beer, D., Wethey, D.S., Woodin, S.A., Polerecky, L., 2015b. Effects of bioadvection by arenicola marina on microphytobenthos in permeable sediments. PLoS ONE 10, e0134236. doi:10.1371/journal.pone.0134236.

Cierpka, C., Hain, R., Buchmann, N.A., 2016. Flow visualization by mobile phone cameras. Exp. Fluids 57, 108. doi:10.1007/s00348-016-2192-y.

Clark, D.R., Ferguson, R.M.W., Harris, D.N., Nicholass, K.J.M., Prentice, H.J., Randall, K.C., Randell, L., Warren, S.L., Dumbrell, A.J., 2018. Streams of data from drops of water: 21st century molecular microbial ecology. WIREs Water 5, e1280. doi:10.1002/wat2.1280.

Cowle, M.W., Babatunde, A.O., Bockelmann-Evans, B.N., 2017. The frictional resistance induced by bacterial based biofouling in drainage pipelines. J. Hydraul. Res. 55, 269–283. doi:10.1080/00221686.2016.1212411.

Dang, H., Lovell, C.R., 2016. Microbial surface colonization and biofilm development in marine environments. Microbiol. Mol. Biol. Rev. 80, 91–138. doi:10.1128/MMBR.00037-15.

de Beer, D., Stoodley, P., Lewandowski, Z., 1994a. Liquid flow in heterogeneous biofilms. Biotechnol. Bioeng. 44, 636–641. doi:10.1002/bit.260440510.

de Beer, D., Stoodley, P., Roe, F., Lewandowski, Z., 1994b. Effects of biofilm structures on oxygen distribution and mass transport. Biotechnol. Bioeng. 43, 1131–1138. doi:10.1002/bit.260431118.

de Beer, D., 2011. Microsensors for sediments, microbial mats, and biofilms. Encycl. Geobiol. 658–662. doi:10.1007/978-1-4020-9212-1_149.

de Beer, D., Wenzhöfer, F., Ferdelman, T.G., Boehme, S.E., Huettel, M., van Beusekom, J.E.E., Böttcher, M.E., Musat, N., Dubilier, N., 2005. Transport and mineralization rates in North Sea sandy intertidal sediments, Sylt-Rømø Basin, Wadden Sea. Limnol. Oceanogr. 50, 113–127. doi:10.4319/lo.2005.50.1.0113.

de Beer, D., Meyer, V., Klatt, J., Li, T., 2018. Photosynthesis under very high oxygen concentrations in dense microbial mats and biofilms. bioRxiv 335299. 10.1101/335299.

de Brouwer, J.F.C., Wolfstein, K., Ruddy, G.K., Jones, T.E.R., Stal, L.J., 2005. Biogenic stabilization of intertidal sediments: the importance of extracellular polymeric substances produced by benthic diatoms. Microb. Ecol. 49, 501–512. doi:10.1007/s00248-004-0020-z.

Delattre, C., Pierre, G., Laroche, C., Michaud, P., 2016. Production, extraction and characterization of microalgal and cyanobacterial exopolysaccharides. Biotechnol. Adv. 34, 1159–1179. doi:10.1016/j.biotechadv.2016.08.001.

Delgado, M., De Jonge, V.N., Peletier, H., 1991. Effect of sand movement on the growth of benthic diatoms. J. Exp. Mar. Biol. Ecol. 145, 221–231. doi:10.1016/0022-0981(91)90177-X.

Demars, B.O.L., 2019. Hydrological pulses and burning of dissolved organic carbon by stream respiration. Limnol. Oceanogr. 64, 406–421. doi:10.1002/lno.11048.

Doostmohammadi, A., Shendruk, T.N., Thijssen, K., Yeomans, J.M., 2017. Onset of meso-scale turbulence in active nematics. Nat. Commun. 8, 1–7. doi:10.1038/ncomms15326.

Douterelo, I., Sharpe, R.L., Husband, S., Fish, K.E., Boxall, J.B., 2019. Understanding microbial ecology to improve management of drinking water distribution systems. Wiley Interdiscip. Rev. 6, e01325. doi:10.1002/wat2.1325.

Dreszer, C., Wexler, A.D., Drusová, S., Overdijk, T., Zwijnenburg, A., Flemming, H.-.C., Kruithof, J.C., Vrouwenvelder, J.S., 2014. In-situ biofilm characterization in membrane systems using Optical Coherence Tomography: formation, structure, detachment and impact of flux change. Water Res. 67, 243–254. doi:10.1016/j.watres.2014.09.006.

Droppo, I.G., D'Andrea, L., Krishnappan, B.G., Jaskot, C., Trapp, B., Basuvaraj, M., Liss, S.N., 2015. Fine-sediment dynamics: towards an improved understanding of sediment erosion and transport. J. Soils Sediments 15, 467–479. doi:10.1007/s11368-014-1004-3.

Falkowski, P.G., Fenchel, T., Delong, E.F., 2008. The microbial engines that drive Earth's biogeochemical cycles. Science 320, 1034–1039. doi:10.1126/science.1153213.

Fang, H., Zhao, H., Shang, Q., Chen, M., 2012. Effect of biofilm on the rheological properties of cohesive sediment. Hydrobiologia 694, 171–181. doi:10.1007/s10750-012-1140-y.

Fang, H.W., Lai, H.J., Cheng, W., Huang, L., He, G.J., 2017. Modeling sediment transport with an integrated view of the biofilm effects. Water Resour. Res. 53, 7536–7557. doi:10.1002/2017WR020628.

Fish, K., Osborn, A.M., Boxall, J.B., 2017. Biofilm structures (EPS and bacterial communities) in drinking water distribution systems are conditioned by hydraulics and influence discolouration. Sci. Total Environ. 593–594, 571–580. doi:10.1016/j.scitotenv.2017.03.176.

Flemming, H.-.C., Neu, D.T.R., Wingender, D.J., 2016. The Perfect Slime: Microbial Extracellular Polymeric Substances (EPS). IWA Publishing.

Flemming, H.-.C., Wingender, J., 2010. The biofilm matrix. Nat. Rev. Microbiol. 8, 623–633. doi:10.1038/nrmicro2415.

Flemming, H.-.C., Wuertz, S., 2019. Bacteria and archaea on Earth and their abundance in biofilms. Nat. Rev. Microbiol. 17, 247–260. doi:10.1038/s41579-019-0158-9.

Förstner, U., Heise, S., Schwartz, R., Westrich, B., Ahlf, W., 2004. Historical contaminated sediments and soils at the river basin scale - Examples from the Elbe river catchment area. J. Soils Sediments 4, 247–260.

Forstner, U., Salomons, W., 2008. Trends and challenges in sediment research 2008: the role of sediments in river basin management. J. Soils Sediments 8, 281–283. doi:10.1007/s11368-008-0033-1.

Forstner, U., Westrich, B., 2005. BMBF coordinated research project SEDYMO (2002-2006) - sediment dynamics and pollutant mobility in river basins. J. Soils Sediments 5, 134–138. doi:10.1065/jss2005.08.002.

Frølund, B., Palmgren, R., Keiding, K., Nielsen, P.H., 1996. Extraction of extracellular polymers from activated sludge using a cation exchange resin. Water Res. 30, 1749–1758. doi:10.1016/0043-1354(95)00323-1.

Galy, O., Zrelli, K., Latour-Lambert, P., Kirwan, L., Henry, N., 2014. Remote magnetic actuation of micrometric probes for in situ 3D mapping of bacterial biofilm physical properties. J. Vis. Exp. doi:10.3791/50857.

Gerbersdorf, S.U., Jancke, T., Westrich, B., 2007. Sediment properties for assessing the erosion risk of contaminated riverine sites. An approach to evaluate sediment properties and their covariance patterns over depth in relation to erosion resistance. First investigations in natural sediments (11 pp). J. Soils Sediments 7, 25–35. doi:10.1065/jss2006.11.190.

Gerbersdorf, S.U., Manz, W., Paterson, D.M., 2008. The engineering potential of natural benthic bacterial assemblages in terms of the erosion resistance of sediments. FEMS Microbiol. Ecol. 66, 282–294. doi:10.1111/j.1574-6941.2008.00586.x.

Gerbersdorf, S.U., Meyercordt, J., Meyer-Reil, L.-.A., 2004. Microphytobenthic primary production within the flocculent layer, its fractions and aggregates, studied in two shallow Baltic estuaries of different eutrophic status. J. Exp. Mar. Biol. Ecol. 307, 47–72. doi:10.1016/j.jembe.2004.01.020.

Gerbersdorf, S.U., Wieprecht, S., 2015. Biostabilization of cohesive sediments: revisiting the role of abiotic conditions, physiology and diversity of microbes, polymeric secretion, and biofilm architecture. Geobiology 13, 68–97. doi:10.1111/gbi.12115.

Gerbersdorf, S.U., Wieprecht, S., Thom, M., Paterson, D.M., Scheffler, M., 2018. New insights into MagPI: a promising tool to determine the adhesive capacity of biofilm on the mesoscale. Biofouling 34, 618–629. doi:10.1080/08927014.2018.1476971.

Gibbs, R.J., 1983. Effect of natural organic coatings on the coagulation of particles. Environ. Sci. Technol. 17, 237–240. doi:10.1021/es00110a011.

Gjersing, E.L., Codd, S.L., Seymour, J.D., Stewart, P.S., 2005. Magnetic resonance microscopy analysis of advective transport in a biofilm reactor. Biotechnol. Bioeng. 89, 822–834. doi:10.1002/bit.20400.

Glud, R.N., Gundersen, J.K., Ramsing, N.B., 2000. Electrochemical and optical oxygen microsensors for in situ measurements. In: In Situ Monitoring of Aquatic Systems: Chemical Analysis and Speciation, pp. 20–73.

Glud, R.N., Gundersen, J.K., Revsbech, N.P., Jørgensen, B.B., 1994. Effects on the benthic diffusive boundary layer imposed by microelectrodes. Limnol. Oceanogr. 39, 462–467. doi:10.4319/lo.1994.39.2.0462.

Glud, R.N., Santegoeds, C.M., Beer, D.D., Kohls, O., Ramsing, N.B., 1998. Oxygen dynamics at the base of a biofilm studied with planar optodes. Aquat. Microb. Ecol. 14, 223–233. doi:10.3354/ame014223.

Graba, M., Moulin, F.Y., Boulêtreau, S., Garabétian, F., Kettab, A., Eiff, O., Sánchez-Pérez, J.M., Sauvage, S., 2010. Effect of near-bed turbulence on chronic detachment of epilithic biofilm: experimental and modeling approaches. Water Resour. Res. 46. doi:10.1029/2009WR008679.

Graba, M., Sauvage, S., Moulin, F.Y., Urrea, G., Sabater, S., Sanchez-Pérez, J.M., 2013. Interaction between local hydrodynamics and algal community in epilithic biofilm. Water Res. 47, 2153–2163. doi:10.1016/j.watres.2013.01.011.

Grün, A.Y., Meier, J., Metreveli, G., Schaumann, G.E., Manz, W., 2016. Sublethal concentrations of silver nanoparticles affect the mechanical stability of biofilms. Environ. Sci. Pollut. Res. 23, 24277–24288. doi:10.1007/s11356-016-7691-0.

Haag, I., Kern, U., Westrich, B., 2001. Erosion investigation and sediment quality measurements for a comprehensive risk assessment of contaminated aquatic sediments. Sci. Tot. Environ. 266, 249–257.

Hannah, D.M., Wood, P.J., Sadler, J.P., 2004. Ecohydrology and hydroecology: a new paradigm? Hydrol. Process 18, 3439–3445. doi:10.1002/hyp.5761.

Head, D.A., 2013. Linear surface roughness growth and flow smoothening in a three-dimensional biofilm model. Phys. Rev. E 88, 032702. doi:10.1103/PhysRevE.88.032702.

Herrling, M.P., Weisbrodt, J., Kirkland, C.M., Williamson, N.H., Lackner, S., Codd, S.L., Seymour, J.D., Guthausen, G., Horn, H., 2017. NMR investigation of water diffusion in different biofilm structures. Biotechnol. Bioeng. 114, 2857–2867. doi:10.1002/bit.26392.

Hodl, I., Mari, L., Bertuzzo, E., Suweis, S., Besemer, K., Rinaldo, A., Battin, T.J., 2014. Biophysical controls on cluster dynamics and architectural differentiation of microbial biofilms in contrasting flow environments. Environ. Microbiol. 16, 802–812. doi:10.1111/1462-2920.12205.

Hohne, D.N., Younger, J.G., Solomon, M.J., 2009. Flexible microfluidic device for mechanical property characterization of soft viscoelastic solids such as bacterial biofilms. Langmuir 25, 7743–7751. doi:10.1021/la803413x.

Hou, J., Veeregowda, D.H., van de Belt-Gritter, B., Busscher, H.J., van der Mei, H.C., 2018. Extracellular polymeric matrix production and relaxation under fluid shear and mechanical pressure in staphylococcus aureus biofilms. Appl. Environ. Microbiol 84. doi:10.1128/AEM.01516-17.

Huiming, Z., Hongwei, F., Minghong, C., 2011. Floc architecture of bioflocculation sediment by ESEM and CLSM. Scanning 33, 437–445. doi:10.1002/sca.20247.

Jahn, A., Nielsen, P.H., 1995. Extraction of extracellular polymeric substances from biofilms using a cation exchange resin. Water Sci. Technol. 32, 157–164.

Jesus, B., Rosa, P., Mouget, J.-.L., Méléder, V., Launeau, P., Barillé, L., 2014. Spectral-radiometric analysis of taxonomically mixed microphytobenthic biofilms. Remote Sens. Environ. 140, 196–205. doi:10.1016/j.rse.2013.08.040.

Jones, S., 2017. Goo, glue, and grain binding: importance of biofilms for diagenesis in sandstones. Geology 45, 959–960. doi:10.1130/focus102017.1.

Jonsson, P.R., van Duren, L.A., Amielh, M., Asmus, R., Aspden, R.J., Daunys, D., Friedrichs, M., Friend, P.L., Olivier, F., Pope, N., Precht, E., Sauriau, P.-G., Schaaff, E., 2006. Making water flow: a comparison of the hydrodynamic characteristics of 12 different benthic biological flumes. Aquat. Ecol. 40, 409–438. doi:10.1007/s10452-006-9049-z.

Jorgensen, B.B., Revsbech, N.P., 1985. Diffusive boundary layers and the oxygen uptake of sediments and detritus. Limnol. Oceanogr. 30, 111–122.

Karimi, A., Karig, D., Kumar, A., Ardekani, A.M., 2015. Interplay of physical mechanisms and biofilm processes: review of microfluidic methods. Lab. Chip 15, 23–42. doi:10.1039/c4lc01095g.

Kautsky, H., 1939. Quenching of luminescence by oxygen. Trans. Faraday Soc. 35, 216–219. doi:10.1039/TF9393500216.

Koca, K., Lorke, A., Noss, C., 2016. Field-deployable particle image velocimetry with a consumer-grade digital camera applicable for shallow flows.

Kim, M.K., Ingremeau, F., Zhao, A., Bassler, B.L., Stone, H.A., 2016. Local and global consequences of flow on bacterial quorum sensing. Nat. Microbiol. 1, 15005. doi:10.1038/nmicrobiol.2015.5.

Koca, K., Noss, C., Anlanger, C., Brand, A., Lorke, A., 2017. Performance of the Vectrino Profiler at the sediment–water interface. J. Hydraul. Res. 1–9. doi:10.1080/00221686.2016.1275049.

Kolmogorov, A.N., 1941. The local structure of turbulence in incompressible viscous fluid for very large Reynolds' numbers, in: Dokl. Akad. Nauk SSSR. pp. 301–305.

Kühl, M., Rickelt, L.F., Thar, R., 2007. Combined imaging of bacteria and oxygen in biofilms. Appl. Environ. Microbiol. 73, 6289–6295. doi:10.1128/AEM.01574-07.

Larin, K.V., Sampson, D.D., 2017. Optical coherence elastography – OCT at work in tissue biomechanics [Invited]. Biomed. Opt. Express 8, 1172–1202. doi:10.1364/BOE.8.001172.

Larned, S.T., Packman, A.I., Plew, D.R., Vopel, K., 2011. Interactions between the mat-forming alga Didymosphenia geminata and its hydrodynamic environment. Limnol. Oceanogr. 1, 4–22. doi:10.1215/21573698-1152081.

Larson, F., Lubarsky, H., Gerbersdorf, S.U., Paterson, D.M., 2009. Surface adhesion measurements in aquatic biofilms using magnetic particle induction: MagPI. Limnol. Oceanogr. Methods 7, 490–497. doi:10.4319/lom.2009.7.490.

Lauga, E., 2016. Bacterial hydrodynamics. Annu. Rev. Fluid Mech 48, 105–130. doi:10.1146/annurev-fluid-122414-034606.

Lauga, E., Powers, T.R., 2009. The hydrodynamics of swimming microorganisms. Rep. Prog. Phys. 72, 096601. doi:10.1088/0034-4885/72/9/096601.

Launeau, P., Méléder, V., Verpoorter, C., Barillé, L., Kazemipour-Ricci, F., Giraud, M., Jesus, B., Le Menn, E., 2018. Microphytobenthos biomass and diversity mapping at different spatial scales with a hyperspectral optical model. Remote Sens. 10, 716. doi:10.3390/rs10050716.

Leibold, M.A., Holyoak, M., Mouquet, N., Amarasekare, P., Chase, J.M., Hoopes, M.F., Holt, R.D., Shurin, J.B., Law, R., Tilman, D., Loreau, M., Gonzalez, A., 2004. The metacommunity concept: a framework for multi-scale community ecology. Ecol. Lett. 7, 601–613. doi:10.1111/j.1461-0248.2004.00608.x.

Lim, J., Lee, K.M., So, H.K., Nam, S.W., Yoo, J.O., Hyun, S.Y., Jo, W., Oh, S., Kim, S.H., Park, S., 2008. Nanoscale characterization of Escherichia coli biofilm formed under laminar flow using atomic force microscopy (AFM) and scanning electron microscopy (SEM). Bull. Korean Chem. Soc. 29, 2114–2118. doi:10.5012/bkcs.2008.29.11.2114.

Loreau, M., Naeem, S., Inchausti, P., Bengtsson, J., Grime, J.P., Hector, A., Hooper, D.U., Huston, M.A., Raffaelli, D., Schmid, B., Tilman, D., Wardle, D.A., 2001. Biodiversity and ecosystem functioning: current knowledge and future challenges. Science 294, 804. doi:10.1126/science.1064088.

Madsen, E.L., 2011. Microorganisms and their roles in fundamental biogeochemical cycles. Curr. Opin. Biotechnol. 22, 456–464. doi:10.1016/j.copbio.2011.01.008.

Malarkey, J., Baas, J.H., Hope, J.A., Aspden, R.J., Parsons, D.R., Peakall, J., Paterson, D.M., Schindler, R.J., Ye, L., Lichtman, I.D., Bass, S.J., Davies, A.G., Manning, A.J., Thorne, P.D., 2015. The pervasive role of biological cohesion in bedform development. Nat. Commun. 6. doi:10.1038/ncomms7257.

Manz, B., Volke, F., Goll, D., Horn, H., 2005. Investigation of biofilm structure, flow patterns and detachment with magnetic resonance imaging. Water Sci. Technol. 52, 1–6. doi:10.2166/wst.2005.0173.

Manz, B., Volke, F., Goll, D., Horn, H., 2003. Measuring local flow velocities and biofilm structure in biofilm systems with magnetic resonance imaging (MRI). Biotechnol. Bioeng. 84, 424–432. doi:10.1002/bit.10782.

McDougald, D., Rice, S.A., Barraud, N., Steinberg, P.D., Kjelleberg, S., 2012. Should we stay or should we go: mechanisms and ecological consequences for biofilm dispersal. Nat. Rev. Microbiol. 10, 39–50. doi:10.1038/nrmicro2695.

Morgenroth, E., Milferstedt, K., 2009. Biofilm engineering: linking biofilm development at different length and time scales. Rev. Environ. Sci. Biotechnol. 8, 203–208. doi:10.1007/s11157-009-9163-1.

Moulin, F.Y., Eiff, O., 2012. Biofilms, hydraulics and sediment dynamics. Critical Review of Ecohydraulic Experiments. HYDRALAB-IV Deliverable D7.1 EC contract no. 261520.

Mukherjee, S., Bassler, B.L., 2019. Bacterial quorum sensing in complex and dynamically changing environments. Nat. Rev. Microbiol. 17, 371–382. doi:10.1038/s41579-019-0186-5.

Nielsen, P.H., Frølund, B., Keiding, K., 1996. Changes in the composition of extracellular polymeric substances in activated sludge during anaerobic storage. Appl. Microbiol. Biotechnol. 44, 823–830. doi:10.1007/BF00178625.

Nielsen, P.H., Jahn, A., Palmgren, R., 1997. Conceptual model for production and composition of exopolymers in biofilms. Water Sci. Technol. Biofilm Syst. III 36, 11–19. doi:10.1016/S0273-1223(97)00318-1.

Nikora, V., 2010. Hydrodynamics of aquatic ecosystems: an interface between ecology, biomechanics and environmental fluid mechanics. River Res. Appl. 26, 367–384. doi:10.1002/rra.1291.

Nikora, V.I., Goring, D.G., Biggs, B.J.F., 2002. Some observations of the effects of micro-organisms growing on the bed of an open channel on the turbulence properties. J. Fluid Mech. 450, 317–341. doi:10.1017/S0022112001006486.

Noack, M., Gerbersdorf, S.U., Hillebrand, G., Wieprecht, S., 2015. Combining field and laboratory measurements to determine the erosion risk of cohesive sediments best. Water (Basel) 7, 5061–5077. doi:10.3390/w7095061.

Noss, C., Wilkinson, J., Lorke, A., 2018. Triangulation hand-held laser-scanning (Tri-HaLaS) for micro- and meso-habitat surveys in streams. Earth Surf. Process. Landf. 43, 1241–1251. doi:10.1002/esp.4310.

Nübel, U., Bateson, M.M., Vandieken, V., Wieland, A., Kühl, M., Ward, D.M., 2002. Microscopic examination of distribution and phenotypic properties of phylogenetically diverse Chloroflexaceae-related bacteria in hot spring microbial mats. Appl. Environ. Microbiol. 68, 4593–4603. doi:10.1128/aem.68.9.4593-4603.2002.

Nuy, J.K., Lange, A., Beermann, A.J., Jensen, M., Elbrecht, V., Röhl, O., Peršoh, D., Begerow, D., Leese, F., Boenigk, J., 2018. Responses of stream microbes to multiple anthropogenic stressors in a mesocosm study. Sci. Total Environ. 633, 1287–1301. doi:10.1016/j.scitotenv.2018.03.077.

Packman, A., 2013. Building bacterial bridges. Nat. Geosci. 6, 682–683. doi:10.1038/ngeo1938.

Palmer, M., Ruhi, A., 2019. Linkages between flow regime, biota, and ecosystem processes: implications for river restoration. Science 365, eaaw2087. doi:10.1126/science.aaw2087.

Passarelli, C., Olivier, F., Paterson, D.M., Meziane, T., Hubas, C., 2014. Organisms as cooperative ecosystem engineers in intertidal flats. J. Sea Res. 92, 92–101. doi:10.1016/j.seares.2013.07.010.

Paterson, D.M., Hope, J.A., Kenworthy, J., Biles, C.L., Gerbersdorf, S.U., 2018. Form, function and physics: the ecology of biogenic stabilisation. J. Soils Sediments 18, 3044–3054. doi:10.1007/s11368-018-2005-4.

Paul, E., Ochoa, J.C., Pechaud, Y., Liu, Y., Liné, A., 2012. Effect of shear stress and growth conditions on detachment and physical properties of biofilms. Water Res. 46, 5499–5508. doi:10.1016/j.watres.2012.07.029.

Pereira, M.O., Kuehn, M., Wuertz, S., Neu, T., Melo, L.F., 2002. Effect of flow regime on the architecture of a Pseudomonas fluorescens biofilm. Biotechnol. Bioeng. 78, 164–171. doi:10.1002/bit.10189.

Persat, A., Inclan, Y.F., Engel, J.N., Stone, H.A., Gitai, Z., 2015. Type IV pili mechanochemically regulate virulence factors in Pseudomonas aeruginosa. Proc. Natl. Acad. Sci. U.S.A. 112, 7563. doi:10.1073/pnas.1502025112.

Picioreanu, C., Blauert, F., Horn, H., Wagner, M., 2018. Determination of mechanical properties of biofilms by modelling the deformation measured using optical coherence tomography. Water Res. 145, 588–598. doi:10.1016/j.watres.2018.08.070.

Picioreanu, C., van Loosdrecht, M.C.M., Heijnen, J.J., 1998. Mathematical modeling of biofilm structure with a hybrid differential-discrete cellular automaton approach. Biotechnol. Bioeng. 58, 101–116. doi:10.1002/(SICI)1097-0290(19980405)58:1⟨101::AID-BIT11⟩3.0.CO;2-M.

Pierre, G., Graber, M., Rafiliposon, B.A., Dupuy, C., Orvain, F., De Crignis, M., Maugard, T., 2012. Biochemical composition and changes of extracellular polysaccharides (ECPS) produced during microphytobenthic biofilm development (Marennes-Oléron, France). Microb. Ecol. 63, 157–169. doi:10.1007/s00248-011-9959-8.

Piggott, J.J., Niyogi, D.K., Townsend, C.R., Matthaei, C.D., 2015. Multiple stressors and stream ecosystem functioning: climate warming and agricultural stressors interact to affect processing of organic matter. J. Appl. Ecol. 52, 1126–1134. doi:10.1111/1365-2664.12480.

Pique, G., Vericat, D., Sabater, S., Batalla, R.J., 2016. Effects of biofilm on river-bed scour. Sci. Total Environ. 572, 1033–1046. doi:10.1016/j.scitotenv.2016.08.009.

Polst, B.H., Anlanger, C., Risse-Buhl, U., Larras, F., Hein, T., Weitere, M., Schmitt-Jansen, M., 2018. Hydrodynamics alter the tolerance of autotrophic biofilm communities toward herbicides. Front. Microbiol 9. doi:10.3389/fmicb.2018.02884.

Rice, S.P., Lancaster, J., Kemp, P., 2010. Experimentation at the interface of fluvial geomorphology, stream ecology and hydraulic engineering and the development of an effective, interdisciplinary river science. Earth Surf. Process. Landf. 35, 64–77. doi:10.1002/esp.1838.

Righetti, M., Lucarelli, C., 2010. Resuspension phenomena of benthic sediments: the role of cohesion and biological adhesion. River Res. Appl. 26, 404–413. doi:10.1002/rra.1296.

Righetti, M., Lucarelli, C., 2007. May the Shields theory be extended to cohesive and adhesive benthic sediments? J. Geophys. Res. 112. doi:10.1029/2006JC003669.

Risse-Buhl, U., Anlanger, C., Chatzinotas, A., Noss, C., Lorke, A., Weitere, M., 2020. Near streambed flow shapes microbial guilds within and across trophic levels in fluvial biofilms. Limnol. Oceanogr. doi:10.1002/lno.11451.

Risse-Buhl, U., Anlanger, C., Kalla, K., Neu, T.R., Noss, C., Lorke, A., Weitere, M., 2017. The role of hydrodynamics in shaping the composition and architecture of epilithic biofilms in fluvial ecosystems. Water Res. 127, 211–222. doi:10.1016/j.watres.2017.09.054.

Roncoroni, M., Brandani, J., Battin, T.I., Lane, S.N., 2019. Ecosystem engineers: biofilms and the ontogeny of glacier floodplain ecosystems. Wiley Interdiscip. Rev. 6, e1390. doi:10.1002/wat2.1390.

Rossy, T., Nadell, C.D., Persat, A., 2019. Cellular advective-diffusion drives the emergence of bacterial surface colonization patterns and heterogeneity. Nat. Commun. 10, 2471. doi:10.1038/s41467-019-10469-6.

Rusconi, R., Guasto, J.S., Stocker, R., 2014. Bacterial transport suppressed by fluid shear. Nat. Phys. 10, 212–217. doi:10.1038/nphys2883.

Salta, M., Wharton, J.A., Blache, Y., Stokes, K.R., Briand, J.-F., 2013. Marine biofilms

on artificial surfaces: structure and dynamics. Environ. Microbiol. 15, 2879–2893. doi:10.1111/1462-2920.12186.

Schiller, D.V., Martí, E., Riera, J.L., Sabater, F., 2007. Effects of nutrients and light on periphyton biomass and nitrogen uptake in Mediterranean streams with contrasting land uses. Freshw. Biol. 52, 891–906. doi:10.1111/j.1365-2427.2007.01742.x.

Schmidt, H., Thom, M., Matthies, K., Behrens, S., Obst, U., Wieprecht, S., Gerbersdorf, S.U., 2015. A multi-disciplinarily designed mesocosm to address the complex flow-sediment-ecology tripartite relationship on the microscale. Environ. Sci. Eur. 27, 2. doi:10.1186/s12302-014-0037-y.

Schmidt, H., Thom, M., Wieprecht, S., Manz, W., Gerbersdorf, S.U., 2018. The effect of light intensity and shear stress on microbial biostabilization and the community composition of natural biofilms. Res. Rep. Biol. 8, 1–16.

Shang, Q., Fang, H., Zhao, H., He, G., Cui, Z., 2014. Biofilm effects on size gradation, drag coefficient and settling velocity of sediment particles. Int. J. Sediment Res. 29, 471–480. doi:10.1016/S1001-6279(14)60060-3.

Shannon, M.A., Bohn, P.W., Elimelech, M., Georgiadis, J.G., Mariñas, B.J., Mayes, A.M., 2008. Science and technology for water purification in the coming decades. Nature 452, 301–310. doi:10.1038/nature06599.

Shields, A., 1936. Anwendung Der Ähnlichkeitsmechanik und Der Turbulenzforschung auf Die Geschiebebewegung. Preussischen Versuchsanstalt für Wasserbau, Berlin.

Simões, M., Pereira, M.O., Sillankorva, S., Azeredo, J., Vieira, M.J., 2007. The effect of hydrodynamic conditions on the phenotype of Pseudomonas fluorescens biofilms. Biofouling 23, 249–258. doi:10.1080/08927010701368476.

Singer, G., Besemer, K., Hödl, I., Chlup, A., Hochedlinger, G., Stadler, P., Battin, T.J., 2006. Microcosm design and evaluation to study stream microbial biofilms. Limnol. Oceanogr. 4, 436–447. doi:10.4319/lom.2006.4.436.

Singer, G., Besemer, K., Schmitt-Kopplin, P., Hödl, I., Battin, T.J., 2010. Physical heterogeneity increases biofilm resource use and its molecular diversity in stream mesocosms. PLoS ONE 5, e9988. doi:10.1371/journal.pone.0009988.

Sønderholm, M., Kragh, K.N., Koren, K., Jakobsen, T.H., Darch, S.E., Alhede, M., Jensen, P.Ø., Whiteley, M., Kühl, M., Bjarnsholt, T., 2017. Pseudomonas aeruginosa aggregate formation in an alginate bead model system exhibits in vivo-like characteristics. Appl. Environ. Microbiol. 83. doi:10.1128/AEM.00113-17.

Statzner, B., Arens, M.-.F., Champagne, J.-.Y., Morel, R., Herouin, E., 1999. Silkproducing stream insects and gravel erosion: significant biological effects on critical shear stress. Water Resour. Res. 35, 3495–3506. doi:10.1029/1999WR900196.

Stevenson, R.J., Bothwell, M.L., Lowe, R.L., 1996. Algal Ecology: Freshwater Benthic Ecosystems. Academic Press, San Diego.

Stewart, P.S., 2012. Mini-review: convection around biofilms. Biofouling 28, 187–198. doi:10.1080/08927014.2012.662641.

Stoodley, P., Cargo, R., Rupp, C.J., Wilson, S., Klapper, I., 2002. Biofilm material properties as related to shear-induced deformation and detachment phenomena. J. Ind. Microbiol. Biotechnol. 29, 361–367. doi:10.1038/sj.jim.7000282.

Stoodley, P., Lewandowski, Z., Boyle, J.D., Lappin-Scott, H.M., 1999. The formation of migratory ripples in a mixed species bacterial biofilm growing in turbulent flow. Environ. Microbiol. 1, 447–455. doi:10.1046/j.1462-2920.1999.00055.x.

Tengberg, A., Hovdenes, J., Andersson, H.J., Brocandel, O., Diaz, R., Hebert, D., Arnerich, T., Huber, C., Körtzinger, A., Khripounoff, A., Rey, F., Rönning, C., Schimanski, J., Sommer, S., Stangelmayer, A., 2006. Evaluation of a lifetime-based optode to measure oxygen in aquatic systems. Limnol. Oceanogr. 4, 7–17. doi:10.4319/lom.2006.4.7.

Tennekes, H., 1989. A First Course in Turbulence. Butterworth.

Thom, M., Schmidt, H., Gerbersdorf, S.U., Wieprecht, S., 2015. Seasonal biostabilization and erosion behavior of fluvial biofilms under different hydrodynamic and light conditions. Int. J. Sediment Res. 30, 273–284. doi:10.1016/j.ijsrc.2015.03.015.

Thomas, K., Herminghaus, S., Porada, H., Goehring, L., 2013. Formation of Kinneyia via shear-induced instabilities in microbial mats. Philos. Trans. R. Soc. A 371, 20120362. doi:10.1098/rsta.2012.0362.

Thomen, P., Robert, J., Monmeyran, A., Bitbol, A.-.F., Douarche, C., Henry, N., 2017. Bacterial biofilm under flow: first a physical struggle to stay, then a matter of breathing. PLoS ONE 12, e0175197. doi:10.1371/journal.pone.0175197.

Tolker-Nielsen, T., 2015. Biofilm development. Microbiol. Spectr. 3. doi:10.1128/microbiolspec.MB-0001-2014.

Torvinen, E., Lehtola, M.J., Martikainen, P.J., Miettinen, I.T., 2007. Survival of mycobacterium avium in drinking water biofilms as affected by water flow velocity, availability of phosphorus, and temperature. Appl. Environ. Microbiol. 73, 6201–6207. doi:10.1128/AEM.00828-07.

Tuson, H.H., Weibel, D.B., 2013. Bacteria–surface interactions. Soft Matter 9, 4368–4380. doi:10.1039/C3SM27705D.

van Loosdrecht, M.C.M., Heijnen, J.J., Eberl, H., Kreft, J., Picioreanu, C., 2002. Mathematical modelling of biofilm structures. Antonie Van Leeuwenhoek 81, 245–256. doi:10.1023/A:1020527020464.

Van Rijn, L.C., 1993. Principles of sediment transport in rivers, estuaries and coastal seas. Delft Hydraulics. Universiteit Utrecht, Aqua Publications.

Vardy, S., Saunders, J.E., Tolhurst, T.J., Davies, P.A., Paterson, D.M., 2007. Calibration of the high-pressure cohesive strength meter (CSM). Cont. Shelf Res. 27, 1190–1199. doi:10.1016/j.csr.2006.01.022.

Vignaga, E., Haynes, H., Sloan, W.T., 2012. Quantifying the tensile strength of microbial mats grown over noncohesive sediments. Biotechnol. Bioeng. 109, 1155–1164. doi:10.1002/bit.24401.

Vignaga, E., Sloan, D.M., Luo, X., Haynes, H., Phoenix, V.R., Sloan, W.T., 2013. Erosion of biofilm-bound fluvial sediments. Nat. Geosci. 6, 770–774. doi:10.1038/ngeo1891.

van de Vijsel, R.C., van Belzen, J., Bouma, T.J., van der Wal, D., Cusseddu, V., Purkis, S.J., Rietkerk, M., van de Koppel, J., 2020. Estuarine biofilm patterns: modern analogues for Precambrian self-organization. Earth Surfa. Process. Landf. 45, 1141–1154. doi:10.1002/esp.4783.

Voermans, J.J., Ghisalberti, M., Ivey, G.N., 2017. The variation of flow and turbulence across the sediment–water interface. J. Fluid Mech. 824, 413–437. doi:10.1017/jfm.2017.345.

Voulgaris, G., Trowbridge, J.H., 1998. Evaluation of the acoustic doppler velocimeter (ADV) for turbulence measurements*. J. Atmos. Oceanic Technol. 15, 272–289. doi:10.1175/1520-0426(1998)015⟨0272:EOTADV⟩2.0.CO;2.

Vu, B., Chen, M., Crawford, R.J., Ivanova, E.P., 2009. Bacterial extracellular polysaccharides involved in biofilm formation. Molecules 14, 2535–2554. doi:10.3390/molecules14072535.

Wagner, M., Horn, H., 2017. Optical coherence tomography in biofilm research: a comprehensive review. Biotechnol. Bioeng. 114, 1386–1402. doi:10.1002/bit.26283.

Wagner, M., Manz, B., Volke, F., Neu, T.R., Horn, H., 2010a. Online assessment of biofilm development, sloughing and forced detachment in tube reactor by means of magnetic resonance microscopy. Biotechnol. Bioeng. 107, 172–181. doi:10.1002/bit.22784.

Wagner, M., Taherzadeh, D., Haisch, C., Horn, H., 2010b. Investigation of the mesoscale structure and volumetric features of biofilms using optical coherence tomography. Biotechnol. Bioeng. 107, 844–853. doi:10.1002/bit.22864.

Weitere, M., Erken, M., Majdi, N., Arndt, H., Norf, H., Reinshagen, M., Traunspurger, W., Walterscheid, A., Wey, J.K., 2018. The food web perspective on aquatic biofilms. Ecol. Monogr. 88, 543–559. doi:10.1002/ecm.1315.

West, S.A., Diggle, S.P., Buckling, A., Gardner, A., Griffin, A.S., 2007. The social lives of microbes. Annu. Rev. Ecol. Evol. Syst. 38, 53–77. doi:10.1146/annurev.ecolsys.38.091206.095740.

Westerweel, J., Elsinga, G.E., Adrian, R.J., 2013. Particle image velocimetry for complex and turbulent flows. Annu. Rev. Fluid Mech. 45, 409–436. doi:10.1146/annurev-fluid-120710-101204.

Wey, J.K., Norf, H., Arndt, H., Weitere, M., 2009. Role of dispersal in shaping communities of ciliates and heterotrophic flagellates within riverine biofilms. Limnol. Oceanogr. 54, 1615–1626. doi:10.4319/lo.2009.54.5.1615.

Wey, J.K., Scherwass, A., Norf, H., Arndt, H., Weitere, M., 2008. Effects of protozoan grazing within river biofilms under semi-natural conditions. Aquat. Microb. Ecol. 52, 283–296. doi:10.3354/ame01236.

Wheeler, J.D., Secchi, E., Rusconi, R., Stocker, R., 2019. Not just going with the flow: the effects of fluid flow on bacteria and plankton. Annu. Rev. Cell Dev. Biol. 35, 213–237. doi:10.1146/annurev-cellbio-100818-125119.

Widdows, J., Friend, P.L., Bale, A.J., Brinsley, M.D., Pope, N.D., Thompson, C.E.L., 2007. Inter-comparison between five devices for determining erodability of intertidal sediments. Con. Shelf Res. 27, 1174–1189. doi:10.1016/j.csr.2005.10.006.

Wieland, A., Kühl, M., 2000. Irradiance and temperature regulation of oxygenic photosynthesis and O_2 consumption in a hypersaline cyanobacterial mat (Solar Lake, Egypt). Mar. Biol. 137, 71–85. doi:10.1007/s002270000331.

Wilhelm, L., Besemer, K., Fasching, C., Urich, T., Singer, G.A., Quince, C., Battin, T.J., 2014. Rare but active taxa contribute to community dynamics of benthic biofilms in glacier-fed streams. Environ. Microbiol. 16, 2514–2524. doi:10.1111/1462-2920.12392.

Witt, O., Westrich, B., 2003. Quantification of erosion rates for undisturbed contaminated cohesive sediment cores by image analysis. Hydrobiologia 494, 271–276. doi:10.1023/A:1025495122246.

Woodcock, S., Besemer, K., Battin, T.J., Curtis, T.P., Sloan, W.T., 2013. Modelling the effects of dispersal mechanisms and hydrodynamic regimes upon the structure of microbial communities within fluvial biofilms. Environ. Microbiol. 15, 1216–1225. doi:10.1111/1462-2920.12055.

Wright, C.J., Shah, M.K., Powell, L.C., Armstrong, I., 2010. Application of AFM from microbial cell to biofilm. Scanning 32, 134–149. doi:10.1002/sca.20193.

Yallop, M.L., de Winder, B., Paterson, D.M., Stal, L.J., 1994. Comparative structure, primary production and biogenic stabilization of cohesive and non-cohesive marine sediments inhabited by microphytobenthos. Estuar. Coast. Shelf Sci. 39, 565–582. doi:10.1016/S0272-7714(06)80010-7.

Yang, S., Lewandowski, Z., 1995. Measurement of local mass transfer coefficient in biofilms. Biotechnol. Bioeng. 48, 737–744. doi:10.1002/bit.260480623.

Zeglin, L.H., 2015. Stream microbial diversity in response to environmental changes: review and synthesis of existing research. Front. Microbiol. 6. doi:10.3389/fmicb.2015.00454.

Zeng, G., Vad, B.S., Dueholm, M.S., Christiansen, G., Nilsson, M., Tolker-Nielsen, T., Nielsen, P.H., Meyer, R.L., Otzen, D.E., 2015. Functional bacterial amyloid increases Pseudomonas biofilm hydrophobicity and stiffness. Front. Microbiol. 6. doi:10.3389/fmicb.2015.01099.

Zhang, L., Shen, T., Cheng, Y., Zhao, T., Li, L., Qi, P., 2020. Temporal and spatial variations in the bacterial community composition in Lake Bosten, a large, brackish lake in China. Sci. Rep. 10, 304. doi:10.1038/s41598-019-57238-5.

Zhang, W., Sileika, T.S., Chen, C., Liu, Y., Lee, J., Packman, A.I., 2011. A novel planar flow cell for studies of biofilm heterogeneity and flow-biofilm interactions. Biotechnol. Bioeng. 108, 2571–2582. doi:10.1002/bit.23234.

Appendix III

Functional relationships between critical erosion thresholds of fine reservoir sediments and their sedimentological characteristics[iii]

FUNCTIONAL RELATIONSHIPS BETWEEN CRITICAL EROSION THRESHOLDS OF FINE RESERVOIR SEDIMENTS AND THEIR SEDIMENTOLOGICAL CHARACTERISTICS

Felix Beckers*[1,2], Kaan Koca*[1], Stefan Haun[1], Markus Noack[3], Sabine U. Gerbersdorf[4], and Silke Wieprecht[1]

[1]Institute for Modelling Hydraulic and Environmental Systems, Department of Hydraulic Engineering and Water Resources Management, University of Stuttgart, Stuttgart, Germany. Email: felix.beckers@iws.uni-stuttgart.de

[2]Ministry of the Environment, Climate Protection and the Energy Sector Baden-Württemberg, Stuttgart, Germany

[3]Faculty of Architecture and Civil Engineering, Karlsruhe University of Applied Science, Karlsruhe, Germany

[4]Ministry of Science, Research and Arts Baden-Württemberg, Stuttgart, Germany

*Equally contributing authors.

ABSTRACT

The present study investigated multivariate relationships between critical erosion thresholds of reservoir sediments and their physico-chemical and biological characteristics to unravel the effect of sedimentological parameters on fine sediment erosion. We collected 22 sediment cores from the deposits of two reservoirs located in southern Germany (Großer Brombachsee = GBS; Schwarzenbachtalsperre = SBT). An erosion flume and an advanced photogrammetric method were used to quantify critical erosion thresholds for a succession of vertical layers over sediment depth. The functional relationships between the critical erosion thresholds and a collection of sediment parameters, including bulk density, sediment composition, percentiles, cation exchange

1

capacity, organic content, extracellular polymeric substances (EPS proteins and carbohydrates), and chlorophyll-a were examined. The clay-dominated sediments of the GBS with comparatively low total organic carbon and sand content were on average 10 times more stable compared to the sandy sediments of the SBT. Consequently, for the clay-dominated sediments, strong positive correlations were found between the erosion thresholds and clay content. In contrast, the sandy sediment layers experienced strong positive correlations with the sand content and percentiles. The bulk density was mainly positively and the total organic carbon content was mainly negatively correlated with the erosion thresholds. Furthermore, EPS and chlorophyll-a were not good indicators for the erosion thresholds, suggesting an ambiguous influence of biology. Generally, the strength of the relations decreased for sediment layers deeper than 10 cm. Overall, our results underline the need to investigate the influence of sediment characteristics on fine sediment erodibility from varying natural environments.

INTRODUCTION

Understanding fine sediment erosion is of particular importance in various water-related fields in engineering and natural sciences. For instance, detailed process knowledge is inevitable to reliably predict morphodynamic changes in order to establish sustainable sediment management strategies (Annandale 1987; Aberle 2008). Numerous studies have investigated the erodibility of fine sediments with cohesive properties in riverine (Noack et al. 2015; Schäfer Rodrigues Silva et al. 2018), lacustrine (Righetti and Lucarelli 2007), and marine (Yang et al. 2019; Zhu et al. 2019) environments. In spite of their global importance for sustainability of future water supplies and ecological quality of downstream channels (Kondolf et al. 2014), studies focusing on the erosion stability of reservoir deposits are limited (Annandale et al. 2016; Morris 2016; Peteuil et al. 2018). In this context, two main scenarios are crucial: i) the certainty that sediment deposits are remobilized (e.g., by management strategies such as reservoir flushing) and ii) the certainty that sediment deposits remain at the same position (in case of contaminated sediments, e.g., Gerbersdorf et al. 2007.) Generally, erosion is controlled by the balance between bed shear stress exerted by hydrodynamic forces and internal resistance forces of sediment particles. Consequently, one of the

2

most important parameters in experimental erosion studies is the threshold indicating the initiation of motion (Briaud 2008), that is, the critical bed shear stress (τ_{cr}). The incipient motion of non-cohesive sediments mainly depends on the submerged weight of the particles. It can be described by the Shields (1936) curve or its adaptations, which account to a certain extent for uncertainty induced by, e.g., varying experimental methods and protocols despite the data scatter around the mean Shields curve (see Buffington and Montgomery 1997). In turn, the shear strength (resistance) of cohesive sediments against the flow induced shear stress is mainly caused by inter-particular forces between the particles (e.g., Kothyari and Jain 2008; Briaud 2008; Zhu et al. 2019) and no generally accepted relationships for the prediction of critical bed shear stresses are available for these kind of sediments (van Rijn 2020). The reason is that various physical, chemical, and biological sediment characteristics influence the inter-particular forces, and thus, making the the measurement of the cohesive shear strength a more complex undertaking compared to non-cohesive sediments (e.g., Berlamont et al. 1993; Burt et al. 1997; Grabowski et al. 2011; Kimiaghalam et al. 2016).

To underline this fact and as motivation for our research, Figure 1 presents ranges of critical erosion thresholds and their median particle size diameters (d_{50}) from previously conducted erosion studies in diverse environments, plotted together with those of the present study (GBS and SBT, see chapter 3). The figure also contains the Shields (1936) curve as a reference for coarse grains, empirical equations derived by Briaud (2008) and Briaud et al. (2017) to create upper and lower limits for the erosion thresholds of fine grained soils with a d_{50} <0.1 mm, and a refined upper limit based on our data ($\tau_{cr} = 0.001d_{50}^{-2}$). Figure 1 reveals that a high range of variability exists for erosion threshold data that cannot be accounted for by the d_{50} only and additional parametric effects beyond the d_{50} must influence the erosion threshold data (e.g., Briaud et al. 2017).

Generally, cohesiveness forms for fine grained sediments in the clay ($\leq 2\mu$m) and silt size ($\leq 63\mu$m), although the clay concentration is primarily responsible for cohesion (Grabowski et al. 2011). Therefore, clay and silt are often combined and referred to as the 'mud' content of a mixture, where mud $\leq 63\mu$m (e.g., Mitchener and Torfs 1995; van Rijn 2020). Non-cohesive/cohesive

3

sediment mixtures experience a cohesive erosion behavior once the mud content exceeds a certain threshold. This threshold is reported to be between 10% to 15% (Mitchener and Torfs 1995; Panagiotopoulos et al. 1997; Debnath et al. 2007; Perera et al. 2020). Furthermore, the shear strength of a non-cohesive/cohesive sediment mixture is influenced by different sediment compositions, consolidation/compaction, ion-exchange capacity, organic content, and biological activity (such as by a biofilm) (e.g., Berlamont et al. 1993). Therefore, exploring critical erosion thresholds of sediment mixtures exceeding a mud content of >5% becomes challenging.

Another challenge is the limited transferability of results to natural sediment conditions. The reason is that process understanding and existing erosion models have been mainly derived from laboratory experiments, conducted with non-cohesive/cohesive sediment mixtures or remolded sediments (e.g., Panagiotopoulos et al. 1997; Kothyari and Jain 2008; Zhang and Yu 2017). However, natural sediments are much more complex as they are graded and heterogeneous mixtures (Van Ledden 2003; Winterwerp et al. 2012; Schäfer Rodrigues Silva et al. 2018) with stratified bed properties (Lau et al. 2001), resulting in variable bed shear strengths in all directions of space (e.g., Tolhurst et al. 2006; Zhu et al. 2019; Beckers et al. 2020).

Additionally, the capability of microbial aggregates (biofilm) to adhere to sediment particles or organic matter and bind them together have gained increasing attention recently (e.g., Paterson 1997; Valentine et al. 2014; Paterson et al. 2018; Koca and Gerbersdorf 2019; Gu et al. 2020, among others). When growing on fine sediment, biofilm alters sediment properties and dynamics, leading to biostabilization (Black et al. 2002; Righetti and Lucarelli 2007; Gerbersdorf et al. 2020). For instance, Thom et al. (2015) described the erosion pattern of bio-inhabited sediment as crust or carpet-like, which was clearly different from pure sediment erosion. Despite the importance of biological sediment properties, most studies focus on physico-chemical sediment characteristics.

These multi-parametric effects can hardly be simulated with artificial non-cohesive/cohesive sediment mixtures, thus, experimental investigations with natural sediments are required. In this context, the currently available *in-situ* devices to measure cohesive erosion are limited in terms of the measurement technology and depth of operation. Therefore, *ex-situ* investigations of

4

natural sediments under controlled hydraulic conditions using an advanced measurement technology represent a possibility to meet the needs of cohesive sediment erosion research (e.g., McNeil et al. 1996; Briaud et al. 2001; Roberts et al. 2003; Le Hir et al. 2008).

Erosion Thresholds Concepts for Cohesive Sediments

Debnath and Chaudhuri (2010) reviewed and evaluated five erosion threshold definitions reported in the literature (see also Sanford and Maa 2001). These thresholds are defined by (i) the initial occurring sediment motion, (ii) significant occurring erosion, (iii) the intersect with the x-axis of a back extrapolated line from the plotted erosion rate, (iv) a sediment depth sequence of increasing critical bed shear stress, and (v) an occurring burst in sediment motion (Sanford and Maa 2001; Debnath and Chaudhuri 2010). Additional threshold concepts can be found, which are often supplemented by describing the erosion behavior. Righetti and Lucarelli (2007) observed a multistep entrainment phenomenon by studying entrained particles and flocs (aggregates) in suspension using image analyses techniques. They defined a criterion to distinguish between the incipient motion of single particles and flocs or aggregates. Wu et al. (2018) considered the incipient surface erosion in their study and emphasized the effect of varying mud contents (low, moderate, high, and pure mud) on the erosion threshold. van Rijn (2020) reported thresholds of critical bed shear stresses for particle, surface, and mass erosion which were visually determined from flume experiments. Beckers et al. (2020) measured emerging erosion spots caused by surface erosion and large holes torn open by detached aggregate chunks. Such specific erosion forms have also been visually observed by other researchers (e.g., McNeil et al. 1996; Roberts et al. 2003; Debnath et al. 2007), and their occurrence may also serve as threshold definition.

In summary, the multiple existing threshold definitions underline the complexity in identifying one universal critical erosion threshold for cohesive sediments and non-cohesive/cohesive sediment mixtures. Moreover, the existing definitions might describe different erosion and transport modes or different erosion types which are not always evident from the data (van Rijn 2020) and make the comparison additionally difficult (e.g., Aberle et al. 2006). Thus, it is deemed advisable to work with more than one threshold value to investigate multivariate relationships between critical

5

erosion thresholds and sediment characteristics (e.g., Le Hir et al. 2007; Righetti and Lucarelli 2007; Briaud et al. 2017; van Rijn 2020).

The main objective of this study is to explore the functional relationships between critical erosion thresholds and sediment characteristics for the deposits of two reservoirs located in southern Germany. For this purpose, we removed sediment cores from deep reservoir regions and investigate their erodibility in a multitude of erosion experiments using an advanced photogrammetric method. We present a slope-criterion to identify the incipient particle erosion (surface erosion) and the maximum occurring erosion from the cumulative erosion volume, which enables a robust assessment of the erosion data to obtain confident erosion thresholds. From a set of adjacent sediment cores, we analyze physico-chemical and biological sediment characteristics (bulk density, sediment composition, percentiles, total organic carbon, cation exchange capacity, chlorophyll-a, extracellular polymeric substances). Based on the collected data, we explore the multivariate relationships between the erosion thresholds and the sedimentological characteristics in vertical layers over sediment depth. Ultimately, we reveal the key sediment parameters that govern the erosion stability of the investigated reservoir deposits and provide a set of limitations and recommendations for future experimental erosion studies.

MATERIALS AND METHODS

Study Sites and Sediment Core Extraction

Two reservoirs with different sediment characteristics were investigated: i) The reservoir *Großer Brombachsee* (GBS) is the largest reservoir of the Franconian Lake district in Bavaria, Germany (49°07'47.6"N 10°55'60.0"E). It was built during 1983-1992 for the purpose of low water regulation of the Regnitz-Main catchment. In addition, it is used for recreation (Daus et al. 2019). At the maximum operation level (410.5 m.a.s.l.), the GBS has a water surface of 8.63 km^2 and a total storage volume of 143.73×10^6 m^3 (Deutsches TalsperrenKomitee e. V. 2013). ii) The reservoir of the *Schwarzenbachtalsperre* (SBT) is located in the Northern Black Forest, Germany (48°39'25.6"N 8°19'28.9"E). It was built between 1922-1926 and is the upper reservoir in a pump-storage system. At the maximum operation level (668.5 m.a.s.l.), the Schwarzenbach reservoir has a water surface

6

of 0.66 km^2 and provides a total storage volume of 14.42×10^6 m^3 with a maximum length of 2.2 km, width of 600 m, and depth of 47 m (Deutsches TalsperrenKomitee e. V. 2013; Mouris et al. 2018). Two inflows, one transition tunnel, and the pumped water feed the reservoir.

In order to explore the sediment deposits, 9 and 13 sediment cores were removed from GBS and SBT, respectively (22 cores in total, Table 1). In each reservoir, the cores were removed from three previously explored regions of the reservoir bed. For this purpose we employed a Frahm-Sediment Sampler (see Beckers et al. 2018). With this device, relatively undisturbed sediment cores can be removed from deposits (maximum depth of operation is 100 m). This is ensured by using customized PVC-tubes to mitigate possible shearing effects during penetration. The tubes had a length of 1 m and a diameter of 0.1 m. Their lower opening was cut off diagonally at an angle of 5° and the wall was bevelled all around. Furthermore, the transparent PVC-tubes enabled a visual *in-situ* assessment of the sediment cores directly after the removal. In case of any signs of disturbance, e.g., cracks or an oblique surface, the retrieved core was immediately rejected and not used further (see also Beckers et al. 2019).

Experimental Measurement Procedure

The removed sediment cores were analyzed in several layers over core depth. First, the depth distribution of bulk density (BD) was measured for all 22 sediment cores with a vertical resolution of 2 cm. Based on the similarity of the bulk density, sediment cores from an investigated reservoir region (Table 1) were, first, assigned to each other and, second, assigned to further destructive analyses. From the assignments made, a set of vertical layers was analyzed in terms of their physical and partly chemical and biological sediment characteristics. The remaining sediment layers were analyzed in terms of their erodibility using the SETEG/PHOTOSED-system within the equivalent depths. Due to assignment of two sediment cores to each other, a certain degree of uncertainty was naturally involved in the analysis. To quantify this uncertainty, the percentage error from the matched sediment layers of similar bulk densities was calculated. Special care was taken to ensure a maximum deviation of 7.5 % between two vertical layers. This resulted in a correlation matrix containing 92 elements (GBS: 42 and SBT: 50; see Beckers et al. 2021).

7

Analysis of Physico-Chemical and Biological Sediment Parameters

Bulk Density

The (wet) bulk density (BD) of each sediment core was measured non-destructively and prior to any further analysis using a bulk densitometer (source: ^{137}CS with a decay energy 662 keV; scintillator: NaI(TI)) (e.g., Mayar et al. 2019; Mayar et al. 2020). For the analysis, the sediment core was placed between a traverse system that automatically moves down the core to measure the BD at a predefined vertical spacing, here at 2 cm steps, to collect the BD profile over depth (Beckers et al. 2018; Beckers et al. 2019).

Sediment Composition and Percentiles

The particle size distribution (PSD) was determined by laser diffraction with a Malvern Mastersizer 2000 (Malvern Instruments Ltd, Malvern, UK). The instrument enables to measure particle sizes in the milli-, micro- and nanometer range (0.02-2,000 μm) (Malvern Instruments 2007). Each measurement was conducted in triplicates, whereas each triplicate comprised seven measurement runs. During the measurements, the flocs (or aggregates) were broken by ultrasound treatment. Finally, the particle sizes were obtained by averaging over the triplicate measurements in order to minimize reported uncertainty from laser diffraction methods (Lepage et al. 2019). From the measured particle sizes, the sediment composition (SC) was derived according to ISO 14688-1:2017 (2017) (clay: $\leq$2 μm, silt: $>2 \leq 63$ μm , sand: $>63 \leq 2,000$ μm). For the characterization of the deposits, we differentiated between clay, silt, and sand. Furthermore, the 10th-, 50th-, and 90th-percentiles (d_{10}, d_{50}, and d_{90}) were derived from the particle size distribution.

Total Organic Carbon and Cation Exchange Capacity

The Total Organic Carbon (TOC) was determined by loss on ignition (in percent) of dried sediment according to the European standard DIN EN 13137 (2001). The sediment loss on ignition is the most common way of measuring organic content (Grabowski et al. 2011).

The effective Cation Exchange Capacity (CEC) was determined using hexamminecobalt(III)chloride as extracting solution to quantify the exchangeable cations using a spectrophotometric method according to the international standard ISO 23470:2018 (2018).

8

Extracellular Polymeric Substances and Chlorophyll-a

Extracellular Polymeric Substances (EPS) are secreted by microorganisms and mainly composed of proteins and carbohydrates (Gerbersdorf et al. 2020), accounting for 75-90% of the EPS-matrix (Tsuneda et al. 2003). The modified Lowry method (Raunkjær et al. 1994) and the phenol-sulfuric acid method by DuBois et al. (1956) were used to determine the water-extracable fraction of EPS-proteins (EPS-p) and EPS-carbohydrates (EPS-c), respectively.

Chlorophyll-a (CHL-a), a proxy for autotrophic biomass of biofilm, was extracted and quantified before and after acidification using a photometric analysis (DIN 38412-16:1985-12 1985).

Experiments for Investigating the Erosion Potential

Erosion experiments were conducted using the SETEG/PHOTOSED-system (Figure 2). The system consists of the SETEG erosion flume (Kern et al. 1999), whose general construction resembles different laboratory erosion flumes exploring the erosion potential of cohesive sediments and non-cohesive/cohesive sediment mixtures (e.g., McNeil et al. 1996; Briaud et al. 2001; Roberts et al. 2003). The flume is constructed as a straight, rectangular, transparent, and closed flume that is operated under pressurized flow. It has a length of 8.00 m, a width of 0.142 m, and a height of 0.10 m (inner dimensions). The upper part below the inlet is made of stainless steel (6.00 m). The lower part, where the measurements are conducted, is made of glass (2.00 m) to allow for optical access. The flume allows to investigate flow rates from 1 to 65 L s^{-1}. The corresponding bed shear stresses ($\tau \approx 0.04$ - 32 Pa) were obtained from a *priori* calibrated function of flow using 2D laser Doppler velocimetry (LDV) measurements (Beckers et al. 2020). The measuring section consists of a circular opening at the bottom of the flume, where sediment cores with diameters between 0.1 and 0.135 m can be locked in position. The center of the measuring section is located 7.64 m downstream of the inflow to ensure a fully developed turbulent flow field. The SETEG erosion flume is complemented by PHOTOSED, a versatile photogrammetric method to detect sediment erosion (Noack et al. 2018) at high resolution (detection limit: Δz_{min}=0.1 mm on approximately 10 mm^2).

During an erosion experiment, sediment cores were locked in position at the flume bottom

from below (see Figure 2). By means of a mechanical lifting apparatus, (pre-)selected sediment layers were vertically elevated and positioned for erosion tests. When a desired sediment layer was reached, the protruding sediment was cut off by a wire, leaving the sediment layer flush with the flume bottom (see Figure 46 in Beckers et al. 2019). Next, the sediment response against a set of incrementally increasing bed shear stresses (t_τ=600s) was explored until sediment failure was observed. Caution was taken to start each experiment at a bed shear stress below the threshold for incipient motion.

During the experiments, a semiconductor laser with a diffraction optic was projected onto the sediment surface, resulting in a structured light pattern of approximately 24,000 points (on a surface area of 143 cm^2). The changes of the sediment surface were continuously monitored by a CMOS camera (2 MP, 10 Hz, Imaging Development Systems GmbH, Obersulm, Germany). In a post-processing routine, the volumetric change of the sediment layer between consecutive frames (here: $\Delta t = 60$ s) was computed within a user-specified region of interest (ROI with area of 2456 mm^2) using Farnebaeck's Dense Optical Flow algorithm (Farnebäck 2003). This provides the volumetric change of the sediment surface as a function of the applied bed shear stress over time. Consequently, the method accounts for both, eroded material being transported in suspension and along the bed. Furthermore, selecting a ROI with sufficient distance from the core edge, allows to mitigate potential boundary effects impacting on the erosion data. This provides reliable data and the means to distinguish between fundamental erosion processes and specific erosion forms (see Beckers et al. 2020).

Identification of Critical Erosion Thresholds

The measurements with the SETEG/PHOTOSED-system provide the means to identify critical erosion thresholds (τ_c) from the time-series of the recorded erosion volumes. To address existing uncertainties in data analysis and interpretation (e.g., Aberle et al. 2006), we followed a pseudo-automatic approach to identify confident erosion threshold values. After plotting the cumulative erosion volume V_e (aggregated over the ROI) over the entire duration of an erosion experiment (investigated sediment layer at a certain core depth), we applied a slope-criterion (see also Gularte

10

et al. 1980; Mehta and Partheniades 1982; Righetti and Lucarelli 2007) that identifies change points based on the derivative of the data (acceleration points) (Figure 3). The initial continuous rise of the curve (Figure 3 A, τ=0.5 Pa) can be attributed to particle and surface erosion. The shear stress at this point is denoted as $\tau_{c,0}$ and often defined as the critical bed shear stress for incipient motion (e.g., Young and Southard 1978; Wu et al. 2018).

Furthermore, we consider the evidence of Righetti and Lucarelli (2007) who reported a multistep entrainment phenomenon with changing erosion regimes for cohesive sediment erosion. This change in the erosion regime (or in the erosion behavior) is the response of the sediment to an exceedance of the bed shear stress, which exhibits a distinct rise in the cumulative erosion volume due to a significant increase of the erosion (see also Beckers et al. 2020). It is represented by the maximum change in slope (maximum acceleration) of the erosion data (Figure 3 A, τ=1.61 Pa). The bed shear stress applied at this threshold was also considered in our study and denoted as $\tau_{c,S}$.

It must be noted that for some cases $\tau_{c,0}$ coincides with $\tau_{c,S}$. This is particularly the case for fully consolidated and uniform sediments, because they erode at a constant rate once the erosion is initiated, which is often referred to as Type II (steady-state or unlimited) erosion (Mehta and Partheniades 1982; Sanford and Maa 2001; Aberle 2008). Consequently, no clear distinction between different erosion regimes can be made when the erosion progresses continuously over time (see Figure 3 B; $\tau_{c,0}$=$\tau_{c,S}$=1.61 Pa).

Statistical Analysis

The statistical analyses between the sediment characteristics and the critical erosion thresholds were conducted using *R* (v.3.5.1) (R Core Team 2017). The degree of potential relationships among the sediment characteristics and the critical erosion thresholds was conducted using a Pearson correlation analysis with the *Hmisc* package (Harrell Jr et al. 2020). Prior to an analysis, univariate and multivariate normality was tested using the test of Shapiro and Wilk (1965), followed by log- and arcsine square-root-transformations as needed. Transformation of data frames were performed using the *dplyr* package (Wickham et al. 2020). Pearson correlation coefficients at a significance level (p-value ≤ 0.05) between the selected variables indicating functional relationships

were plotted by means of correlograms using the *Corrplot* package (Wei and Simko 2017).

Furthermore, the data was categorized into two groups of sediment depth to explore depth-dependency of the correlations. These groups were A (0-10 cm) and B (>10 cm). Draftsman plots were generated to visualize depth-dependent correlations using the *Performance Analytics* package (Peterson and Carl 2020). Next, the variations of the correlation coefficients were explored for the evaluated sediment parameters in the depth-dependent layers. In the correlation graphs, "+1" represents a perfect positive correlation and "-1" represents a perfect negative correlation, whereas "0" represents no relationship. The statistical significance of the relationships was evaluated at various significance levels, which are indicated in the results.

RESULTS AND DISCUSSION

Synthesis of Sediment Characteristics and Critical Erosion Thresholds

Table 2 provides the summary of the minimum, mean, and maximum values for all measured sediment parameters. The complete data set is freely available online (Beckers et al. 2021).

In general, the measured critical erosion thresholds $\tau_{c,0}$ and $\tau_{c,S}$ in the GBS are on average approximately 10 times higher than those in the SBT. While the lower limit of the measured values of $\tau_{c,0}$ and $\tau_{c,S}$ is of similar range, the maximum values differ by an order of magnitude (see Table 2). The high erosion thresholds of the GBS deposits can be attributed to larger BD, mud, and clay contents. An increase of these parameters are generally associated with a higher erosion stability (e.g., Mitchener and Torfs 1995; Panagiotopoulos et al. 1997; Van Ledden 2003; Kothyari and Jain 2008; Wu et al. 2018). Along with an increase in clay content, the CEC increases since it is a proxy for the electro-chemical activity of clay minerals (Partheniades 2007). Accordingly, a high CEC suggests a high cohesive strength of a sediment mixture, and thus, results in a higher erosion stability (e.g., Gerbersdorf et al. 2007). Moreover, the GBS sediments are characterized by comparatively low TOC ($\leq$3.70%), which is indicative of high erosion stability as an increased TOC accumulation could increase the erodibility of sediment deposits (e.g., Mehta 1991).

The lower erosion stability of the SBT deposits can be explained by an overall lower BD due to the presence of organic-rich sediments (TOC$\geq$8.38%) and little consolidation (as indicated by

12

the low BDs), which suggests a high water content (Fukuda and Lick 1980). Furthermore, the sand content is substantially larger (see Table 2). These sediment characteristics are generally associated with low erosion stability (see Grabowski et al. 2011) and confirm previous findings (e.g., Mitchener and Torfs 1995; Panagiotopoulos et al. 1997; Zhang and Yu 2017). It is worth mentioning that Krishnappan et al. (2020) observed similar critical thresholds (τ_c = 0.09 Pa) for fine-grained cohesive river sediment. They observed the sediment particles were interconnected through loose fibril material, which is an effect of microbial secretion or of the present organic material.

Noticeable in the SBT data are low BD values (<1 g cm^{-3}). This indicates the presence of air or gas in the sediment (Grabowski et al. 2011). The formation of carbon dioxide and methane mainly results from anaerobic carbon mineralization in anoxic sediments (Segers 1998). Given the sediment composition and organic content of the SBT deposits, gas formation in the SBT sediment occurs (see Peeters et al. 2019), and gas fluxes to the atmosphere have been reported (see Encinas Fernández et al. 2020). Generally, the presence of gas decreases the stability (Jepsen et al. 2000), which additionally supports the lower critical bed shear stresses measured for the SBT deposits.

Given the SC, low BDs (≤1.11 %), and the amount of TOC (≥8.38 %), we expected high biological activity in the sediments of the SBT. Thus, we analyzed a set of biological parameters to consider their influence on the sediment stability. The microalgae biomass indicated by the CHL-a content (41-413 μg g^{-1}) confirms this hypothesis, since the present range corresponds to and exceeds values of biologically active sediments (e.g., de Brouwer et al. (2003) found a range of 1.0-10.3 μg g^{-1} in the top 0.5 cm for three intertidal mudflats located in different geographical areas in Northwest Europe; Gerbersdorf et al. (2007) found a range of 35-197 μg g^{-1} in the river Neckar in the top 2.0 cm of the sediment). Similarly, the EPS contents found in the SBT sediments confirm the hypothesis of biologically active sediment. For instance, Morelle et al. (2020) observed highly productive sediments in the intertidal areas downstream of Seine estuary (Normandy, France), with EPS-c and EPS-p contents being larger than 70 μg g^{-1} in autumn and 35 μg g^{-1} in spring samples

due to the higher percentage of fine particles in summer. While underlying the importance of fine sediments for biofilm production, the range of EPS contents observed by Morelle et al. (2020) is at least 10 times lower compared to those in the SBT.

Functional Relationships between Critical Erosion Thresholds and Sediment Characteristics of the GBS Deposits

Positive correlations were observed for the GBS sediments between the critical erosion thresholds and the sediment depth, bulk density, and clay content, whereas negative correlations were found with the TOC content, d_{10}, silt content, and d_{50} (Figure 4). These correlations follow typical findings of parametric dependencies with cohesive erosion thresholds. Particularly, bulk density was most closely and positively associated with the critical erosion thresholds, which is also reported from other studies (e.g., McNeil et al. 1996; Gerbersdorf et al. 2007; van Rijn 2020).

Although the silt content is negatively correlated with the critical erosion thresholds, this is outweighed by the positive correlation of the clay content (Figure 4). This highlights the role of clay content (not the silt or mud content) on the cohesive erosion resistance, supporting previous findings (e.g., Schäfer Rodrigues Silva et al. 2018; van Rijn 2020). Similar to the findings of Mehta (1991), we also observed negative correlations between the critical erosion thresholds and the TOC content. Despite the impact of TOC on the erodibility of cohesive sediments is widely recognized (Grabowski et al. 2011), the effect on sediment stability is still ambiguous. Additionally, the erosion resistance increased with sediment depth, which confirms results obtained from experiments investigating depth-dependent erosion of natural cohesive sediments (e.g., McNeil et al. 1996; Lick and McNeil 2001) and supports the general understanding of depth-limited erosion (Mehta and Partheniades 1982).

To study a variation of functional relationships over sediment depth, we divided the results into two depth regions. Region A represents depths of 0-10 cm and B represents depths of >10 cm. The trend of the depth-sequenced correlations is mainly consistent for region A and B (Table 3 and Figure S1). The erosion resistance increases with BD and clay content and decreases with d_{10} and TOC content through regions A and B. Interestingly, d_{50} and d_{90} are negatively

14

associated with the erosion resistance in the region A, but positively associated in the region B, which is not reflected in Figure 4. Since the average particle sizes are only slightly different, this demonstrates the complexity in identifying functional relationships and highlights the necessity to consider parametric relationships in various depth-sequences. Moreover, an increase in silt content suggests a decrease in the erosion resistance. However, the significance levels of the correlations are in the range of $p = 0.06$-0.15, and thus, caution must be taken. Since the sand content in the GBS deposits is overall small (≤ 6.72 %), no significant correlations were found. Furthermore, it becomes evident that the different types of critical erosion thresholds ($\tau_{c,0}$ and $\tau_{c,S}$) yield different functional relationships with the sediment characteristics. The correlations between the sediment characteristics and $\tau_{c,S}$ are stronger compared to $\tau_{c,0}$ for the depth regions A (0-10 cm) and B (>10 cm). We attribute this to the fact that the identification of initial surface erosion, reflected by $\tau_{c,0}$, is difficult for sediments with a "strong cohesive erosion behavior" since tearing of flocs is highly variable due to stochastic nature of flow. In turn, the detection of a change in the erosion regime, indicated by $\tau_{c,S}$, is more robust for this type of sediments, thus, yielding stronger correlations with sediment characteristics.

Functional Relationships between Critical Erosion Thresholds and Sediment Characteristics of the SBT Deposits

For the SBT deposits, significant positive correlations were observed between the critical erosion thresholds and the d_{50} as well as the sand content, whereas significant negative correlations were observed with the clay and silt content as well as sediment depth (Figure 5).

The observed relationships seem contradictory at first, since one would rather expect positive relationships between the erosion thresholds and mud (clay and silt) content instead of the sand content. This effect was also reflected by the positive correlations between the critical erosion thresholds and d_{50}, since a positive correlation indicates an increasing erosion stability with an increasing median particle size diameter. It is interesting to note that a negative correlation between sediment stability and silt content was also observed for the GBS deposits (Figure 4). It has been reported that the highest erosion resistance of non-cohesive/cohesive sediment mixtures emerges

15

at a certain mud/sand ratio. Mitchener and Torfs (1995) found this ratio to be 30-50% mud added to sand by weight while Perkey et al. (2020) reported the maximum critical bed shear stress at a mud content of 30-40% for homogeneously mixed non-cohesive/cohesive sediments. The SBT sediments showed a mud content of 71.71-85.58% and a sand content of 14.42-28.30% (Table 2). Therefore, it is conceivable that the SBT sediments with a higher sand content are closer to the optimal mud/sand ratio, and thus, leading to higher shear strength and to a positive correlation between the critical erosion thresholds and sand content and (d_{50}). The negative correlation between the erosion thresholds and the sediment depth suggests that there is no uniform vertical trend of the sediment characteristics. For example, Figure 5 indicates a negative correlation between BD and sediment depth. This implies that the SBT deposits do not show a classical trend with an increasing consolidation level over the depth. Such trends have been reported for natural sediments due to intermediate layers of differently composed sediment (e.g., Gerbersdorf et al. 2007). The SBT deposits were further weakly consolidated with low mean and minimum BDs (Table 2). This results from the organic matter content and biologically active sediment, which likely leads to gas production as reflected in the low BDs in some layers (see Beckers et al. 2021). In freshwater lakes, the highest gas concentrations are usually found below a certain sediment depth (e.g., Kuivila et al. 1989; Thebrath et al. 1993). Thus, the presence of gas explains low BDs in the deeper located sediment layers and the negative correlation between BD and sediment depth.

By evaluating the variation of correlations over the two depth regions, multiple significant correlations with $\tau_{c,0}$ can be observed for the region A (0-10 cm) (Table 4 and Figure S2). The statistical analysis indicates that the erosion resistance of the SBT deposits significantly increases with sand content and the percentage values (d_{10}, d_{50}, and d_{90}) and decreases with contents of clay, silt, and TOC. These relationships resemble the erosion behavior of non-cohesive sediment despite the fact that the sediment of the SBT are composed of sufficient fine material to expect cohesion (Table 2). Thus, the erosion behavior can be explained by the mud/sand ratio, low BDs due to higher TOC and biologically active sediment, as well as by the weakly consolidated material in the SBT sediments (see Beckers et al. 2021). In the depth region B (>10 cm), a significant

16

positive correlation was only found between the critical erosion threshold $\tau_{c,s}$ and BD ($R = 0.54$; $p < 0.01$), further suggesting that the erosion stability increases with BD. However, since the BD ranges between 0.91-1.11 g cm^{-3}, as result of organic matter, little consolidation, and the presence of gas, it is difficult to make any concluding statement. Rather, the findings for the SBT underline the importance of considering different depth-sequences for weakly consolidated reservoir deposits since sediment parameters change over depth in a complex and nontrivial way.

Comparison of Functional Relationships between the GBS and SBT Deposits

The overall variation of Pearson's correlation coefficients (Figure 6) indicates that the functional relationships between the critical erosion thresholds and the sediment characteristics were stronger for the region A (0-10 cm) for both, GBS and SBT deposits. The correlations decreased at deeper sediment layers represented by region B (>10 cm). Furthermore, the SBT sediments showed less significant and weaker correlations, particularly for the deeper sediment layers (region B >10 cm) (compare with Table 3 and 4). As a whole, this highlights the complexity in identifying functional relationships for strongly heterogeneous and biologically active natural sediments, such as from the SBT, compared to deposits of moderate heterogeneity, such as from the GBS.

In general, the strongest parameter-specific functional relationship with the critical erosion thresholds was found for the BD. Averaged over all depth regions, the BD yielded the correlation coefficients of $R_{\tau_{c,0}}$=0.61 and $R_{\tau_{c,S}}$=0.79. Moreover, the clay content ($R_{\tau_{c,0}}$=0.57 and $R_{\tau_{c,S}}$=0.77) and d_{10} ($R_{\tau_{c,0}}$=-0.55 and $R_{\tau_{c,S}}$=-0.76) indicated strong correlations with the erosion thresholds. The weakest relationship was found for the silt content through all regions, however, the correlation was still high ($R_{\tau_{c,0}}$=0.47 and $R_{\tau_{c,S}}$=0.67). These results support various findings reported in previous studies (Mitchener and Torfs 1995; Panagiotopoulos et al. 1997; Schäfer Rodrigues Silva et al. 2018; van Rijn 2020).

LIMITATIONS AND RECOMMENDATIONS

The use of sediment cores for depth-dependent erosion tests is a common practice (e.g., McNeil et al. 1996; Briaud et al. 2001; Righetti and Lucarelli 2007; Schäfer Rodrigues Silva et al. 2018).

However, the removal of sediment cores from sediment deposits may cause certain types of distur-bance (see Dück et al. 2019). Through technical measures, coring disturbances can be mitigated but never fully avoided. For instance, McIntyre (1971) reported on the necessity to use coring tubes with a diameter of ≥0.1 m to overcome sampling problems at the sediment-water interface. In particular, the escape of gas bubbles from the sediment during coring or core transportation may disturb the sediment structure. Although, technical methods such as freeze coring preserve the gas bubbles in the sediment (Dück et al. 2019), freezing and thawing may also alter the sediment struc-ture, making this method unsuitable for erosion studies. Yet, we are aware that a non-quantifiable error from core removal and transportation exists in all erosion studies where sediment cores are employed.

Potential uncertainties arise from the SETEG erosion flume, such as sudden roughness transition from the smooth bed to the sediment surface, which does not accurately resemble natural conditions and might affect the flow field. However, similar studies concluded that sudden roughness change contributes minimally to the overall experimental results (Roberts et al. 2003). In this paper, we addressed this by selecting a ROI distant from the boundaries through our photogrammetric approach in order to minimize the boundary effect (also see Beckers et al. 2020). It is, nevertheless, advisable to technically address this limitation in the future (see, e.g., Le Hir et al. 2008).

Regarding the method of core allocation and data analysis, four limitations must be mentioned: First, we assume that the BD is as a representative bulk parameter for sediment characteristics to assign sediment layers to each other for subsequent analyses. We allowed a maximum deviation of 7.5% between two layers when assigning them to each other. In doing so, we quantified the error from this frequently used method in sediment research (e.g., Gerbersdorf et al. 2007; Righetti and Lucarelli 2007). Consequently, a maximum uncertainty interval of ±7.5% can exist. This may also explain the scatter in the data, particularly in the case of the SBT sediments (see Beckers et al. 2021). As described previously, some sediment samples could be collected for characterizing analyses prior to the start of an erosion experiment directly from the SETEG flume. This procedure should be preferred in principle, but it depends strongly on the sediment characteristics and the

18

possibilities to obtain representative samples from the erosion flume. However, in this case, the sediment characteristics directly correspond to the measured erosion thresholds and no error from assigning different layers to each other exist (see Beckers et al. 2021).

Second, the procedure to analyze the erosion data for detecting critical erosion thresholds offers advantages over a visual determination since it works analytically and is thus not biased by different user opinions. Potential problems arise from the fact that a small flaw in the surface, maybe due to the vertical slicing (see Beckers et al. 2019), might lead to local sediment movement at the beginning of an erosion experiment. Since PHOTOSED is very sensitive and detects even small erosion events (Beckers et al. 2020), this could result in an initial rise of the erosion volume. We overcome this challenge by applying a pseudo-automatic routine, which requires confirmation by the operator before a threshold is finally stored, allowing to cross-check the individual frames in case of ambiguity. Furthermore, we consider two erosion thresholds to consider the multiple different threshold concepts employed by various authors (see Sanford and Maa 2001; Debnath and Chaudhuri 2010).

Third, we focused on a collection of promising parameters to describe the sediment characteristics. Although they encompass physical, chemical, and biological parameters, we do not claim to have included all relevant parameters (e.g., Berlamont et al. 1993; Grabowski et al. 2011). As mentioned, parameters such as gas content in the sediment were not considered although it may affect the erodibility (Jepsen et al. 2000; Lick and McNeil 2001) and must be considered in future studies on the erodibility of natural reservoir sediments.

Fourth, although our data set was comparably large (see Beckers et al. 2021), it was not large enough to ensure statistical significance for all considered parametric functional relationships (Table 3 and 4, Figure 4 and 5).

It is worth noting that we did not intend to provide new equations based on the multi-correlation analysis conducted for the studied reservoirs. As discussed in the introduction, a considerable degree of uncertainty exists regarding accuracy and comparability of fitted equations to data in sediment erodibility estimates, which is due to site-specific sediment properties as well as utilization of

19

varying experimental methods and data collection protocols (Sanford 2006). Whilst data sharing is still minimal within the hydraulic engineering community, it is expected to facilitate controlled testing and benchmarking of standardized approaches for data analysis and new hypotheses about cohesive sediment erosion. In this respect, our data includes not only physico-chemical and biological sediment properties, but also erosion thresholds based on a robust analytical rather than on a visual determination approach. Several such high quality laboratory and field data are required for further development of accurate and widely applicable sediment transport models (Bhattacharya et al. 2005). As suggested by Sanford (2006), it is therefore advisable to increase the data pool and we welcome if other researchers utilize our data in their work.

SUMMARY AND CONCLUSIONS

In this study, we presented critical erosion thresholds as well as a collection of physico-chemical and biological sediment characteristics for the deposits of two reservoirs located in southern Germany, namely Großer Brombachsee (GBS) and Schwarzenbach reservoir (SBT). Critical erosion thresholds were evaluated from experimental data obtained with an erosion flume and an advanced photogrammetric system that can detect and quantify erosion events at high spatial and temporal resolution. We considered two erosion thresholds (expressed as critical bed shear stresses) by using a slope criterion applied to the cumulative erosion volume: i) the threshold for incipient particle (surface) erosion and ii) the threshold indicating a change in the erosion behavior/regime. Based on a large data set measured at various depth-dependent sediment layers (Beckers et al. 2021), we explored the functional relationships between the erosion thresholds and the evaluated sediment parameters. Based on the presented results, the following conclusions can be summarized:

1. The GBS sediments were characterized by an increasing bulk density, clay and silt content, and cation exchange capacity as well as by decreasing contents of sand and total organic carbon over the sediment depth.

2. The SBT sediments were characterized by a comparatively low bulk density (1.02 g cm^{-3}

20

on average), with no clear trend of sedimentological characteristics over sediment depth. Furthermore, the SBT sediments were, in comparison to the GBS sediments, characterized by lower clay and silt contents and a lower cation exchange capacity, but by higher sand and total organic carbon contents. In general, the SBT sediments were characterized by high biological activity.

3. The sediment deposits of the GBS were on average 10 times more resistant against erosion compared to those of the SBT.

4. For the GBS deposits, strong positive correlations were observed between critical erosion thresholds and clay content, and to a less extent with bulk density. Strong negative correlations were observed between erosion thresholds and total organic carbon content. The correlations of erosion thresholds and sediment characteristics consistently decreased over depth.

5. In contrast, for the SBT sediments, strong negative correlations were found between the erosion thresholds and the clay content, which can be attributed to the comparatively higher sand content (by approx. a factor of 6). The increased sand content was strongly associated with increasing erosion thresholds in the first 10 cm of the sediment core, but this relation diminished in deeper layers. We attributed this effect to high biological activity in deeper layers, which complicated the elucidation of clear functional relationships for the SBT deposits.

Future experimental erosion studies are required to consider more physico-chemical and biological sediment parameters from different reservoir deposits consisting of various fine sediment mixtures. This will help to increase the data pool for statistical analysis in pursuit of better understanding of the functional relationships between sediment stability and sediment characteristics. To foster a standardized approach and facilitate the comparison between different studies, multiple critical erosion thresholds using advanced quantitative methods should be considered, an example of which was presented in this paper.

Conflict of Interest

The authors have no conflict of interest to declare.

Supplemental Materials

Figs. S1 and S2 are available online in the ASCE Library (ascelibrary.org)

REFERENCES

Aberle, J. (2008). *Measurement techniques for the estimation of cohesive sediment erosion*. Hydraulic Methods for Catastrophes: Floods, Droughts, Environmental Disasters. Publications of the Institute of Geophysics, Polish Academy of Sciences.

Aberle, J., Nikora, V., and Walters, R. (2006). "Data interpretation for in situ measurements of cohesive sediment erosion." *Journal of Hydraulic Engineering*, 132(6), 581–588.

Annandale, G. (1987). *Reservoir Sedimentation*. Elsevier Science, Burlington OCLC: 1162022726.

Annandale, G. W., Karki, P., and Morris, G. L. (2016). *Extending the Life of Reservoirs: Sustainable Sediment Management for Dams and Run-of-river Hydropower*. World Bank Google-Books-ID: TRe7jwEACAAJ.

Beckers, F., Biserov, R., and Wieprecht, S. (2019). "Experimental investigation of sediment stability at reservoirs on the Rhône River." *Technical Report 09/2019*, Institute for Modelling Hydraulic and Environmental Systems (IWS), Stuttgart, Germany.

Beckers, F., Haun, S., and Noack, M. (2018). "Experimental investigation of reservoir sediments." *In Proc. River Flow Conference, Lyon, France*, 40, 03030.

Beckers, F., Inskeep, C., Haun, S., Schmid, G., Wieprecht, S., and Noack, M. (2020). "High spatio-temporal resolution measurements of cohesive sediment erosion." *Earth Surface Processes and Landforms*, esp.4889.

Beckers, F., Koca, K., Haun, S., Noack, M., Gerbersdorf, S. U., and Wieprecht, S. (2021). "Data related to the manuscript "Functional relationships between critical erosion thresholds of fine reservoir sediments and their sedimentological characteristics"." *Zenodo*, Data set (Version 1).

Berlamont, J., Ockenden, M., Toorman, E., and Winterwerp, J. (1993). "The characterisation of cohesive sediment properties." *Coastal Engineering*, 21, 105 – 128.

Bhattacharya, B., Price, R., and Solomatine, D. (2005). "Data-driven modelling in the context of sediment transport." *Physics and Chemistry of the Earth, Parts A/B/C*, 30(4), 297–302 Dealing with Floods within Constraints.

Black, K. S., Tolhurst, T. J., Paterson, D. M., and Hagerthey, S. E. (2002). "Working with natural cohesive sediments." *Journal of Hydraulic Engineering*, 128(1), 2–8.

Briaud, J.-L. (2008). "Case histories in soil and rock erosion: Woodrow Wilson Bridge, Brazos River Meander, Normandy Cliffs, and New Orleans Levees." *Journal of Geotechnical and Geoenvironmental Engineering*, 134(10), 1425–1447.

Briaud, J.-L., Govindasamy, A. V., and Shafii, I. (2017). "Erosion charts for selected geomaterials." *Journal of Geotechnical and Geoenvironmental Engineering*, 143(10), 04017072.

Briaud, J. L., Ting, F. C. K., Chen, H. C., Cao, Y., Han, S. W., and Kwak, K. W. (2001). "Erosion function apparatus for scour rate predictions." *Journal of Geotechnical and Geoenvironmental Engineering*, 127(2), 105–113.

Buffington, J. M. and Montgomery, D. R. (1997). "A systematic analysis of eight decades of incipient

motion studies, with special reference to gravel-bedded rivers." *Water Resources Research*, 33(8), 1993–2029.

Burt, N., Parker, R., and Watts, J. H. (1997). *Cohesive Sediments*. John Wiley, Chichester, UK.

Daus, M., Koberger, K., Gnutzmann, N., Hertrich, T., and Glaser, R. (2019). "Transferring water while transforming landscape: New societal implications, perceptions and challenges of management in the reservoir system Franconian Lake District." *Water*, 11(12), 2469.

de Brouwer, J., de Deckere, E., and Stal, L. (2003). "Distribution of extracellular carbohydrates in three intertidal mudflats in Western Europe." *Estuarine, Coastal and Shelf Science*, 56(2), 313–324.

Debnath, K. and Chaudhuri, S. (2010). "Cohesive sediment erosion threshold: a review." *ISH Journal of Hydraulic Engineering*, 16(1), 36–56.

Debnath, K., Nikora, V., Aberle, J., Westrich, B., and Muste, M. (2007). "Erosion of cohesive sediments: Resuspension, bed load, and erosion patterns from field experiments." *Journal of Hydraulic Engineering*, 133(5), 508–520.

Deutsches TalsperrenKomitee e. V., ed. (2013). *Talsperren in Deutschland [Dams and reservoirs (in German)]*. Springer Fachmedien Wiesbaden, Wiesbaden.

DIN 38412-16:1985-12 (1985). *German standard methods for the examination of water, waste water and sludge; test methods using water organisms (group L); determination of chlorophyll-a in surface water (L 16)*.

DIN EN 13137 (2001). *Characterization of waste - Determination of total organic carbon (TOC) in waste, sludges and sediments* (December).

DuBois, M., Gilles, K. A., Hamilton, J. K., Rebers, P. A., and Smith, F. (1956). "Colorimetric method for determination of sugars and related substances." *Analytical chemistry*, 28(3), 350–356.

Dück, Y., Lorke, A., Jokiel, C., and Gierse, J. (2019). "Laboratory and field investigations on freeze and gravity core sampling and assessment of coring disturbances with implications on gas bubble characterization." *Limnology and Oceanography: Methods*, lom3.10335.

24

Encinas Fernández, J., Hofmann, H., and Peeters, F. (2020). "Diurnal pumped-storage operation minimizes methane ebullition fluxes from hydropower reservoirs." *Water Resources Research*, 56(12).

Farnebäck, G. (2003). "Two-frame motion estimation based on polynomial expansion." *Image Analysis*, G. Goos, J. Hartmanis, J. vanLeeuwen, J. Bigun, and T. Gustavsson, eds., Vol. 2749, Springer Berlin Heidelberg, Berlin, Heidelberg, 363–370.

Fukuda, M. K. and Lick, W. (1980). "The entrainment of cohesive sediments in freshwater." *Journal of Geophysical Research*, 85(C5), 2813.

Gerbersdorf, S. U., Jancke, T., and Westrich, B. (2007). "Sediment properties for assessing the erosion risk of contaminated riverine sites. An approach to evaluate sediment properties and their covariance patterns over depth in relation to erosion resistance. First investigations in natural sediments (11 pp)." *Journal of Soils and Sediments*, 7(1), 25–35.

Gerbersdorf, S. U., Koca, K., de Beer, D., Chennu, A., Noss, C., Risse-Buhl, U., Weitere, M., Eiff, O., Wagner, M., Aberle, J., Schweikert, M., and Terheiden, K. (2020). "Exploring flow-biofilm-sediment interactions: Assessment of current status and future challenges." *Water Research*, 185, 116182.

Grabowski, R. C., Droppo, I. G., and Wharton, G. (2011). "Erodibility of cohesive sediment: The importance of sediment properties." *Earth-Science Reviews*, 105(3-4), 101–120.

Gu, Y., Zhang, Y., Qian, D., Tang, Y., Zhou, Y., and Zhu, D. Z. (2020). "Effects of microbial activity on incipient motion and erosion of sediment." *Environmental Fluid Mechanics*, 20(1), 175–188.

Gularte, R., Kelly, W., and Nacci, V. (1980). "Erosion of cohesive sediments as a rate process." *Ocean Engineering*, 7(4), 539–551.

Harrell Jr, F. E., with contributions from Charles Dupont, and many others (2020). *Hmisc: Harrell Miscellaneous*, <https://CRAN.R-project.org/package=Hmisc>.

ISO 14688-1:2017 (2017). *Geotechnical investigation and testing – Identification and classification of soil – Part 1: Identification and description (ISO 14688-1:2017)*.

ISO 23470:2018 (2018). *DIN EN ISO 23470, Soil quality – Determination of effective cation exchange capacity (CEC) and exchangeable cations using a hexamminecobalttrichloride solution (ISO 23470:2018)* (December).

Jepsen, R., McNeil, J., and Lick, W. (2000). "Effects of gas generation on the density and erosion of sediments from the Grand River." *Journal of Great Lakes Research*, 26(2), 209–219.

Kern, U., Haag, I., Schürlein, V., Holzwarth, M., and Westrich, B. (1999). "Ein Strömungskanal zur Ermittlung der tiefenabhängigen Erosionsstabilität von Gewässersedimenten: das SETEG-System (in German)." *Wasserwirtschaft*, 89, 72–77.

Kimiaghalam, N., Clark, S. P., and Ahmari, H. (2016). "An experimental study on the effects of physical, mechanical, and electrochemical properties of natural cohesive soils on critical shear stress and erosion rate." *International Journal of Sediment Research*, 31(1), 1–15.

Koca, K. and Gerbersdorf, S. U. (2019). "Biofilms stabilize fine sediment in reservoirs: Dynamic interactions between flow, substrate and community." *Proc. of the 10th EcomeetIng*, Stuttgart, Germany, 21-22.02.2019.

Kondolf, G. M., Gao, Y., Annandale, G. W., Morris, G. L., Jiang, E., Zhang, J., Cao, Y., Carling, P., Fu, K., Guo, Q., Hotchkiss, R., Peteuil, C., Sumi, T., Wang, H.-W., Wang, Z., Wei, Z., Wu, B., Wu, C., and Yang, C. T. (2014). "Sustainable sediment management in reservoirs and regulated rivers: Experiences from five continents." *Earth's Future*, 2(5), 256–280.

Kothyari, U. C. and Jain, R. K. (2008). "Influence of cohesion on the incipient motion condition of sediment mixtures." *Water Resources Research*, 44(4).

Krishnappan, B. G., Stone, M., Granger, S. J., Upadhayay, H. R., Tang, Q., Zhang, Y., and Collins, A. L. (2020). "Experimental investigation of erosion characteristics of fine-grained cohesive sediments." *Water*, 12(5), 1511.

Kuivila, K., Murray, J., Devol, A., and Novelli, P. (1989). "Methane production, sulfate reduction and competition for substrates in the sediments of Lake Washington." *Geochimica et Cosmochimica Acta*, 53(2), 409–416.

Lau, Y. L., Droppo, I. G., and Krishnappan, B. G. (2001). "Sequential erosion/deposition experi-

ments - demonstrating the effects of depositional history on sediment erosion." *Water Research*, 35(11), 2767–2773.

Le Hir, P., Cann, P., Waeles, B., Jestin, H., and Bassoullet, P. (2008). "Erodibility of natural sediments: experiments on sand/mud mixtures from laboratory and field erosion tests." *Sediment and Ecohydraulics*, T. Kusuda, H. Yamanishi, J. Spearman, and J. Z. Gailani, eds., Vol. 9 of *Proceedings in Marine Science*, Elsevier, chap.11, 137–153.

Le Hir, P., Monbet, Y., and Orvain, F. (2007). "Sediment erodability in sediment transport modelling: Can we account for biota effects?." *Continental Shelf Research*, 27(8), 1116–1142.

Lepage, H., Masson, M., Delanghe, D., and Le Bescond, C. (2019). "Grain size analyzers: results of an intercomparison study." *SN Applied Sciences*, 1(9), 1100.

Lick, W. and McNeil, J. (2001). "Effects of sediment bulk properties on erosion rates." *The Science of The Total Environment*, 266(1-3), 41–48.

Malvern Instruments (2007). *Mastersizer 2000 - User Manual*, Vol. MAN0384-1.0. Malvern Instruments Ltd., Worcestershire, United Kingdom, man0384-1.0 edition.

Mayar, M. A., Schmid, G., Wieprecht, S., and Noack, M. (2019). "Optimizing vertical profile measurements setup of gamma ray attenuation." *Radiation Physics and Chemistry*, 164, 108376.

Mayar, M. A., Schmid, G., Wieprecht, S., and Noack, M. (2020). "Proof-of-concept for nonintrusive and undisturbed measurement of sediment infiltration masses using gamma-ray attenuation." *Journal of Hydraulic Engineering*, 146(5), 11.

McIntyre, A. D. (1971). "Deficiency of gravity corers for sampling meiobenthos and sediments." *Nature*, 231(5300), 260–260.

McNeil, J., Taylor, C., and Lick, W. (1996). "Measurements of erosion of undisturbed bottom sediments with depth." *Journal of Hydraulic Engineering*, 122(6), 316–324.

Mehta, A. (1991). *Characterization of cohesive soil bed surface erosion, with special reference to the relationship between erosion shear strength and bed density*. Coastal and Oceanographic Engineering Department, University of Florida, Gainesville, Florida.

Mehta, A. J. and Partheniades, E. (1982). "Resuspension of deposited cohesive sediment beds."

Cape Town, South Africa, Coastal Engineering Research Council, 1569–1588.

Mitchener, H. and Torfs, H. (1995). "Erosion of mud-sand mixtures." *Coastal Engineering 29 (1996) 1-25*.

Morelle, J., Claquin, P., and Orvain, F. (2020). "Evidence for better microphytobenthos dynamics in mixed sand/mud zones than in pure sand or mud intertidal flats (Seine estuary, Normandy, France)." *PLOS ONE*, 15(8), e0237211.

Morris, G. L. (2016). *Reservoir Sustainability Best Practices Guidance*. 149–159.

Mouris, K., Beckers, F., and Haun, S. (2018). "Three-dimensional numerical modeling of hydraulics and morphodynamics of the Schwarzenbach reservoir." *In Proc. River Flow Conference, Lyon, France*, 40, 03005.

Noack, M., Gerbersdorf, S., Hillebrand, G., and Wieprecht, S. (2015). "Combining field and laboratory measurements to determine the erosion risk of cohesive sediments best." *Water*, 7(9), 5061–5077.

Noack, M., Schmid, G., Beckers, F., Haun, S., and Wieprecht, S. (2018). "PHOTO-SED—PHOTOgrammetric Sediment Erosion Detection." *Geosciences*, 8(7), 243.

Panagiotopoulos, I., Voulgaris, G., and Collins, M. (1997). "The influence of clay on the threshold of movement of fine sandy beds." *Coastal Engineering 32 (1997) 19-43*.

Partheniades, E. (2007). *Engineering properties and hydraulic behavior of cohesive sediments*. CRC, Boca Raton, Fla.; London.

Paterson, D. M. (1997). "Biological mediation of sediment erodibility: Ecology and physical dynamics." *Cohesive Sediments*, John Wiley and Sons, n. burt, r. parker, and j. watts (eds.) edition, 215–229.

Paterson, D. M., Hope, J. A., Kenworthy, J., Biles, C. L., and Gerbersdorf, S. U. (2018). "Form, function and physics: the ecology of biogenic stabilisation." *Journal of Soils and Sediments*, 18(10), 3044–3054.

Peeters, F., Encinas Fernandez, J., and Hofmann, H. (2019). "Sediment fluxes rather than oxic methanogenesis explain diffusive CH4 emissions from lakes and reservoirs." *Scientific Reports*,

9(1), 243.

Perera, C., Smith, J., Wu, W., Perkey, D., and Priestas, A. (2020). "Erosion rate of sand and mud mixtures." *International Journal of Sediment Research*, 35(6), 563–575.

Perkey, D. W., Smith, S. J., and Priestas, A. M. (2020). "Erosion thresholds and rates for sand-mud mixtures." *TR-20-13*, The U.S. Army Engineer Research and Development Center (ERDC), Vicksburg, Mississippi (July).

Peterson, B. G. and Carl, P. (2020). *PerformanceAnalytics: Econometric Tools for Performance and Risk Analysis*, <https://CRAN.R-project.org/package=PerformanceAnalytics>.

Peteuil, C., Jodeau, M., De Linares, M., Valette, E., Alliau, D., Wirz, C., Fretaud, T., Antoine, G., and Sécher, M. (2018). "Toward an operational approach for the characterization and modelling of fine sediments dynamics in reservoirs." *In Proc. River Flow Conference, Lyon, France*, 40, 03028.

R Core Team (2017). *R: A Language and Environment for Statistical Computing*. R Foundation for Statistical Computing, Vienna, Austria, <https://www.R-project.org/>.

Raunkjær, K., Hvitved-Jacobsen, T., and Nielsen, P. H. (1994). "Measurement of pools of protein, carbohydrate and lipid in domestic wastewater." *Water Research*, 28(2), 251–262.

Righetti, M. and Lucarelli, C. (2007). "May the Shields theory be extended to cohesive and adhesive benthic sediments?." *Journal of Geophysical Research*, 112(C05039).

Roberts, J. D., Jepsen, R. A., and James, S. C. (2003). "Measurements of sediment erosion and transport with the Adjustable Shear Stress Erosion and Transport Flume." *Journal of Hydraulic Engineering*, 129(11), 862–871.

Sanford, L. P. (2006). "Uncertainties in sediment erodibility estimates due to a lack of standards for experimental protocols and data interpretation: Standards and Erodibility Uncertainties." *Integrated Environmental Assessment and Management*, 2(1), 29–34.

Sanford, L. P. and Maa, J. P.-Y. (2001). "A unified erosion formulation for fine sediments." *Marine Geology*, 179(1-2), 9–23.

Schäfer Rodrigues Silva, A., Noack, M., Schlabing, D., and Wieprecht, S. (2018). "A data-driven

fuzzy approach to simulate the critical shear stress of mixed cohesive/non-cohesive sediments."
Journal of Soils and Sediments, 18(10), 3070–3081.

Segers, R. (1998). "Methane production and methane consumption: a review of processes underlying wetland methane fluxes." *Biogeochemistry*, 41(1), 23–51.

Shapiro, S. S. and Wilk, M. B. (1965). "An analysis of variance test for normality (complete samples)." *Biometrika*, 52(3/4), 591–611.

Shields, A. (1936). "Anwendung der Ähnlichkeitsmechanik und der Turbulenzforschung auf die Geschiebebewegung [Application of mechanical similarity and turbulence research to bedload motion (in German)]." Ph.D. thesis, Preussischen Versuchsanstalt für Wasserbau, Berlin.

Thebrath, B., Rothfuss, F., Whiticar, M., and Conrad, R. (1993). "Methane production in littoral sediment of Lake Constance." *FEMS Microbiology Letters*, 102(3-4), 279–289.

Thom, M., Schmidt, H., Gerbersdorf, S. U., and Wieprecht, S. (2015). "Seasonal biostabilization and erosion behavior of fluvial biofilms under different hydrodynamic and light conditions." *International Journal of Sediment Research*, 30(4), 273–284.

Tolhurst, T., Defew, E., de Brouwer, J., Wolfstein, K., Stal, L., and Paterson, D. (2006). "Small-scale temporal and spatial variability in the erosion threshold and properties of cohesive intertidal sediments." *Continental Shelf Research*, 26(3), 351–362.

Tsuneda, S., Aikawa, H., Hayashi, H., Yuasa, A., and Hirata, A. (2003). "Extracellular polymeric substances responsible for bacterial adhesion onto solid surface." *FEMS Microbiology Letters*, 223(2), 287–292.

Valentine, K., Mariotti, G., and Fagherazzi, S. (2014). "Repeated erosion of cohesive sediments with biofilms." *Advances in Geosciences*, 39, 9–14.

Van Ledden, M. (2003). "Sand-mud segregation in estuaries and tidal basins." Ph.D. thesis, Delft.

van Rijn, L. C. (2020). "Erodibility of mud–sand bed mixtures." *Journal of Hydraulic Engineering*, 146(1), 04019050.

Wei, T. and Simko, V. (2017). *R package "corrplot": Visualization of a Correlation Matrix*, <https://github.com/taiyun/corrplot>.

Wickham, H., François, R., Henry, L., and Müller, K. (2020). *dplyr: A Grammar of Data Manipulation*, <https://CRAN.R-project.org/package=dplyr>.

Winterwerp, J. C., van Kesteren, W. G. M., van Prooijen, B., and Jacobs, W. (2012). "A conceptual framework for shear flow-induced erosion of soft cohesive sediment beds." *Journal of Geophysical Research: Oceans*, 117(C10), 1–17.

Wu, W., Perera, C., Smith, J., and Sanchez, A. (2018). "Critical shear stress for erosion of sand and mud mixtures." *Journal of Hydraulic Research*, 56(1), 96–110.

Yang, Y., Gao, S., Wang, Y. P., Jia, J., Xiong, J., and Zhou, L. (2019). "Revisiting the problem of sediment motion threshold." *Continental Shelf Research*, 187, 103960.

Young, R. N. and Southard, J. B. (1978). "Erosion of fine-grained marine sediments: Sea-floor and laboratory experiments." *Geological Society of American Bulletin*, 89, 10.

Zhang, M. and Yu, G. (2017). "Critical conditions of incipient motion of cohesive sediments." *Water Resources Research*, 53(9), 7798–7815.

Zhu, Q., van Prooijen, B., Maan, D., Wang, Z., Yao, P., Daggers, T., and Yang, S. (2019). "The heterogeneity of mudflat erodibility." *Geomorphology*, 345, 106834.

List of Tables

32

TABLE 1. Overview of removed and analyzed sediment cores

Reservoir	No. of Cores	Sediment Length (Min-Max) [m]	Explored Regions	Removal Date
GBS	9	0.49-0.64	3	25-26.09.2017
SBT	13	0.25-0.56	3	06-07.08.2018
SBT = *Schwarzenbachtalsperre*; GBS = *Großer Brombachsee*				

TABLE 2. Overview of main results including critical erosion thresholds and sediment characteristics of the GBS and SBT deposits. Note: NA denotes "not applicable".

Reservoir	GBS			SBT		
Parameter	MIN	MEAN	MAX	MIN	MEAN	MAX
$\tau_{c,0}$ [Pa]	0.10	2.43	11.34	0.07	0.28	0.81
$\tau_{c,S}$ [Pa]	0.32	3.84	12.48	0.17	0.38	0.99
BD [g cm^{-3}]	1.06	1.20	1.46	0.91	1.02	1.11
Clay [%]	4.58	8.12	12.52	2.10	2.94	3.93
Silt [%]	82.30	88.52	93.09	69.35	76.51	82.18
Mud [%]	93.27	96.65	98.65	71.71	79.45	85.58
Sand [%]	1.35	3.35	6.72	14.42	20.55	28.30
d_{10} [μm]	1.38	1.99	2.92	3.36	4.20	5.34
d_{50} [μm]	6.28	8.37	11.38	17.41	20.83	25.79
d_{90} [μm]	21.96	30.92	40.30	64.95	95.09	147.93
TOC [%]	0.71	2.11	3.70	8.38	11.66	14.73
CEC [cmol kg^{-1}]	71.80	102.96	190.96	46.78	79.39	105.29
CHL-a [μg g^{-1}]	NA	NA	NA	40.68	154.05	412.71
EPS-p [μg g^{-1}]	NA	NA	NA	406.06	758.10	1124.39
EPS-c [μg g^{-1}]	NA	NA	NA	266.33	455.65	739.89

TABLE 3. Correlation coefficients between critical erosion thresholds and sediment characteristics for the GBS deposits separated into depth regions A (0-10 cm) and B (>10 cm). The significance levels are indicated by $*p \leq 0.05$, $**p \leq 0.01$, and $***p \leq 0.001$.

GBS	A (0-10cm)		B (>10cm)	
	$\tau_{c,0}$	$\tau_{c,S}$	$\tau_{c,0}$	$\tau_{c,S}$
BD [g cm^{-3}]	0.37	**0.66****	0.28	**0.54***
Clay [%]	**0.50***	**0.72****	**0.48***	0.38
Silt [%]	-0.32	**-0.40**	-0.40	-0.39
Sand [%]	0	-0.07	0.11	0.20
d_{10} [μm]	**-0.46***	**-0.70****	**-0.45***	-0.36
d_{50} [μm]	**-0.44***	**-0.66****	0.29	**0.49***
d_{90} [μm]	-0.16	-0.26	0.29	**0.45***
TOC [%]	-0.49	**-0.73***	-0.38	**-0.51***

TABLE 4. Correlation coefficients between critical erosion thresholds and sediment characteristics for the SBT deposits separated into depth regions A (0-10 cm) and B (>10 cm). The significance levels are indicated by $*p \leq 0.05$, $**p \leq 0.01$, and $***p \leq 0.001$.

SBT	A (0-10cm)		B (>10cm)	
	$\tau_{c,0}$	$\tau_{c,S}$	$\tau_{c,0}$	$\tau_{c,S}$
BD [g cm^{-3}]	0.03	-0.19	0.31	**0.41***
Clay [%]	**-0.82***	**-0.71**	-0.13	-0.14
Silt [%]	**-0.71**	-0.46	-0.23	-0.19
Sand [%]	**0.72**	0.47	0.23	0.19
d_{10} [μm]	**0.74**	**0.66***	0.16	0.15
d_{50} [μm]	**0.79***	**0.61***	0.31	0.22
d_{90} [μm]	**0.62***	0.35	0.16	0.12
TOC [%]	**-0.70**	-0.47	0.26	0
CEC [cmol kg^{-}1]	-0.26	0.06	0.20	-0.07

List of Figures

37

Fig. 1. Erosion data from literature plotted over d_{50} including the limits (upper and lower) suggested by Briaud (2008) and Briaud et al. (2017) and a refined upper limit based on our presented erosion data.
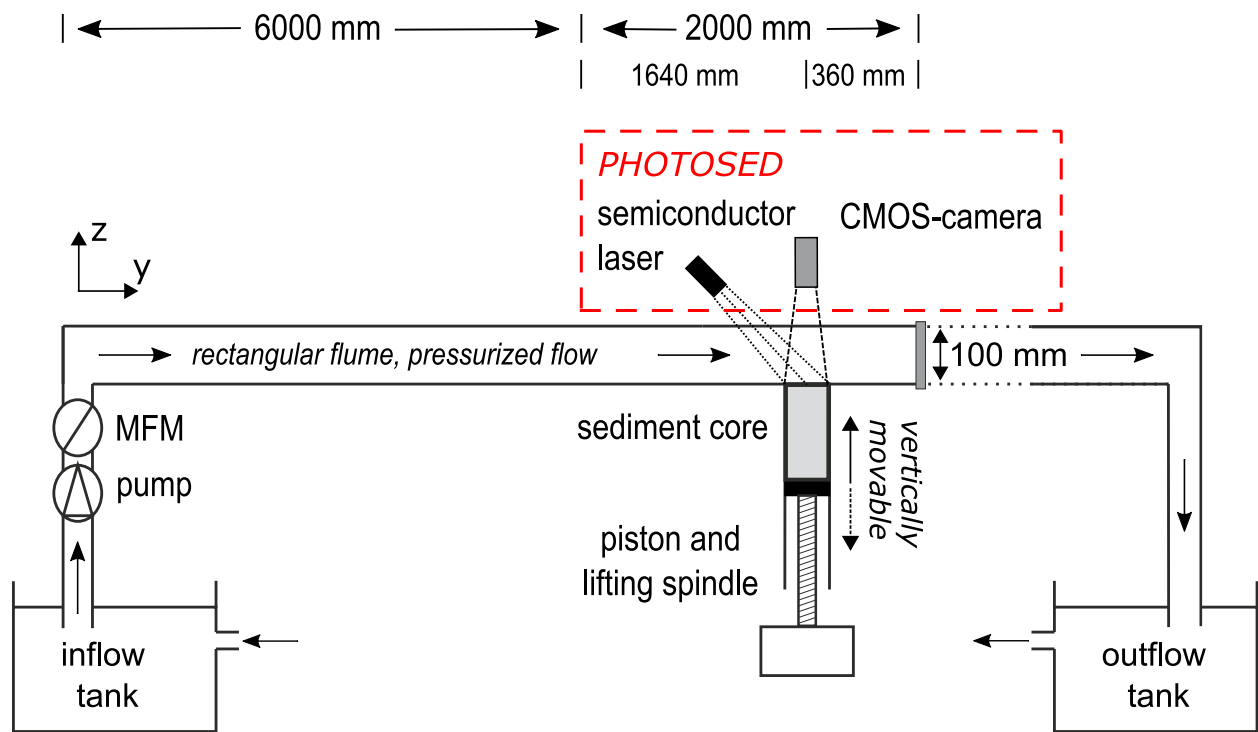
Fig. 2. Schematic side view of the SETEG/PHOTOSED-system, which is used to measure the depth-dependent erosion potential of cohesive sediments and non-cohesive/cohesive sediment mixtures

(Beckers et al. 2019).
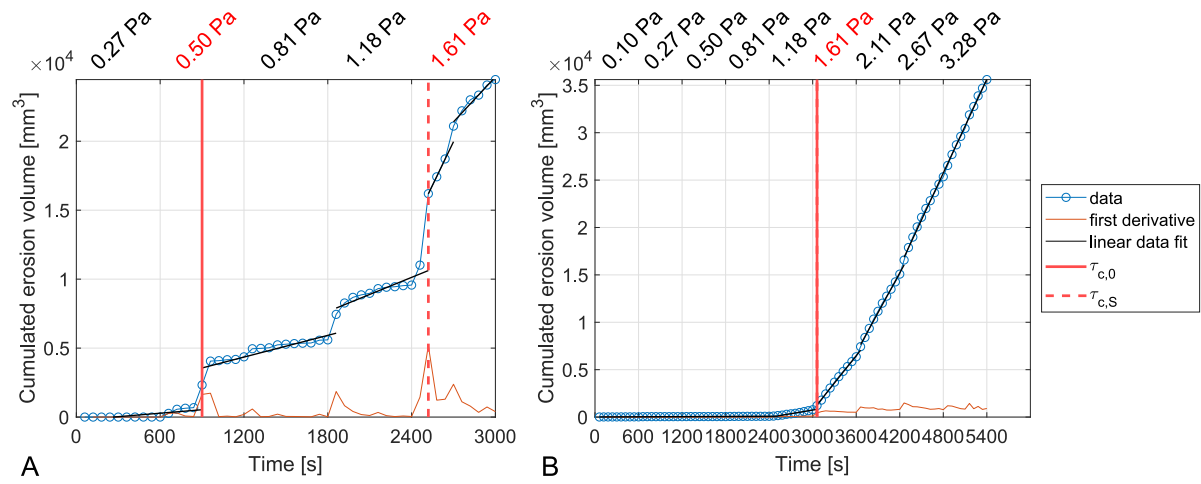
Fig. 3. Examples of critical erosion thresholds $\tau_{c,0}$ (surface erosion) and $\tau_{c,S}$ (erosion behavior change) obtained from the cumulative erosion as a function of time by means of a slope criterion; Case A yields different values for $\tau_{c,0}$ and $\tau_{c,S}$ due to a change in the erosion behavior, case B yields equal values for $\tau_{c,0}$ and $\tau_{c,S}$ due to constant (steady-state) erosion.
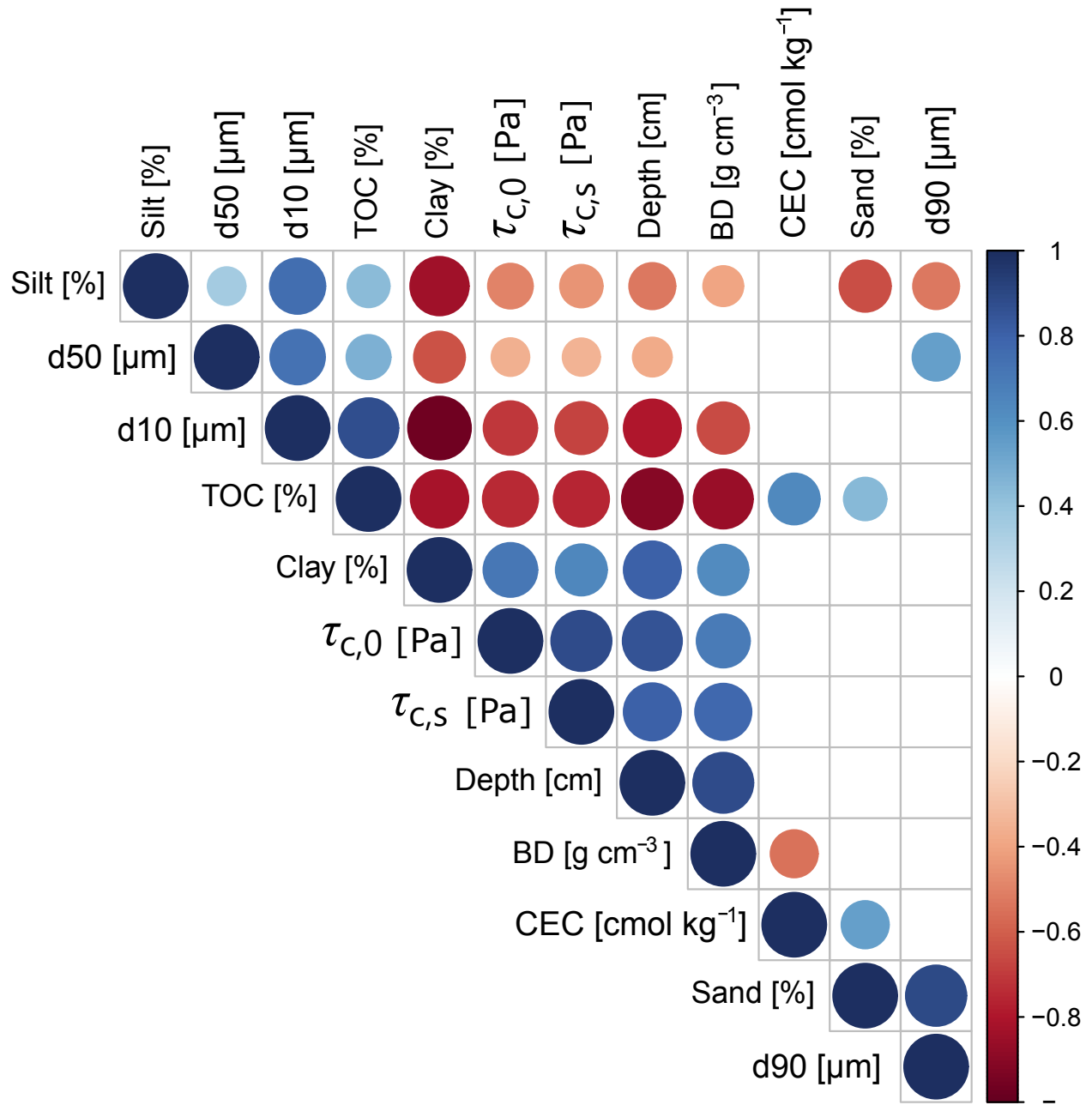
Fig. 4. Correlogram indicating the correlations (for a significance level $p \leq 0.05$) between the measured sediment characteristics and critical erosion thresholds for the sediment deposits of the GBS.
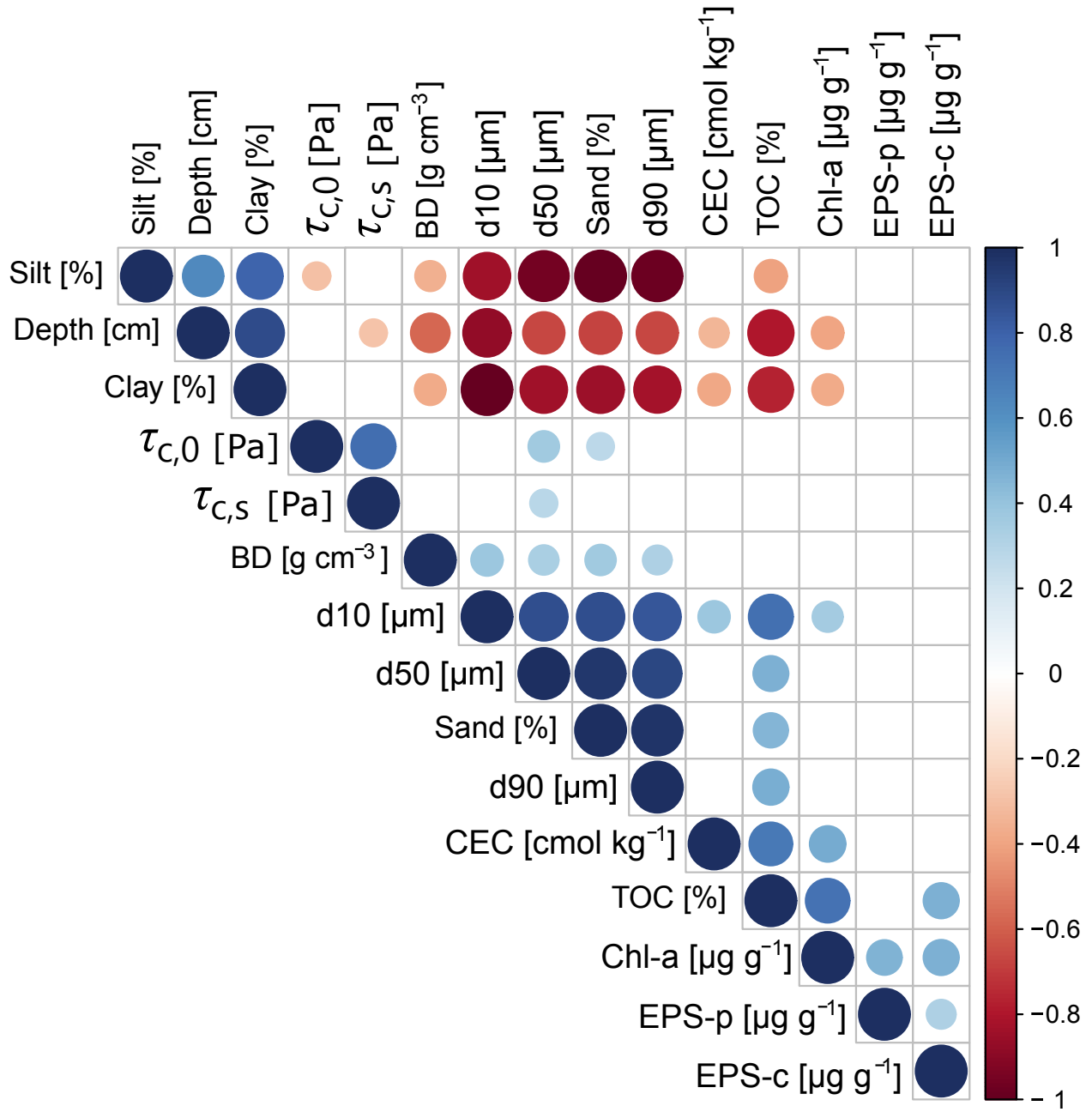
Fig. 5. Correlogram indicating the correlations (for a significance level $p \leq 0.05$) between the measured sediment characteristics and critical erosion thresholds for the sediment deposits of the SBT.
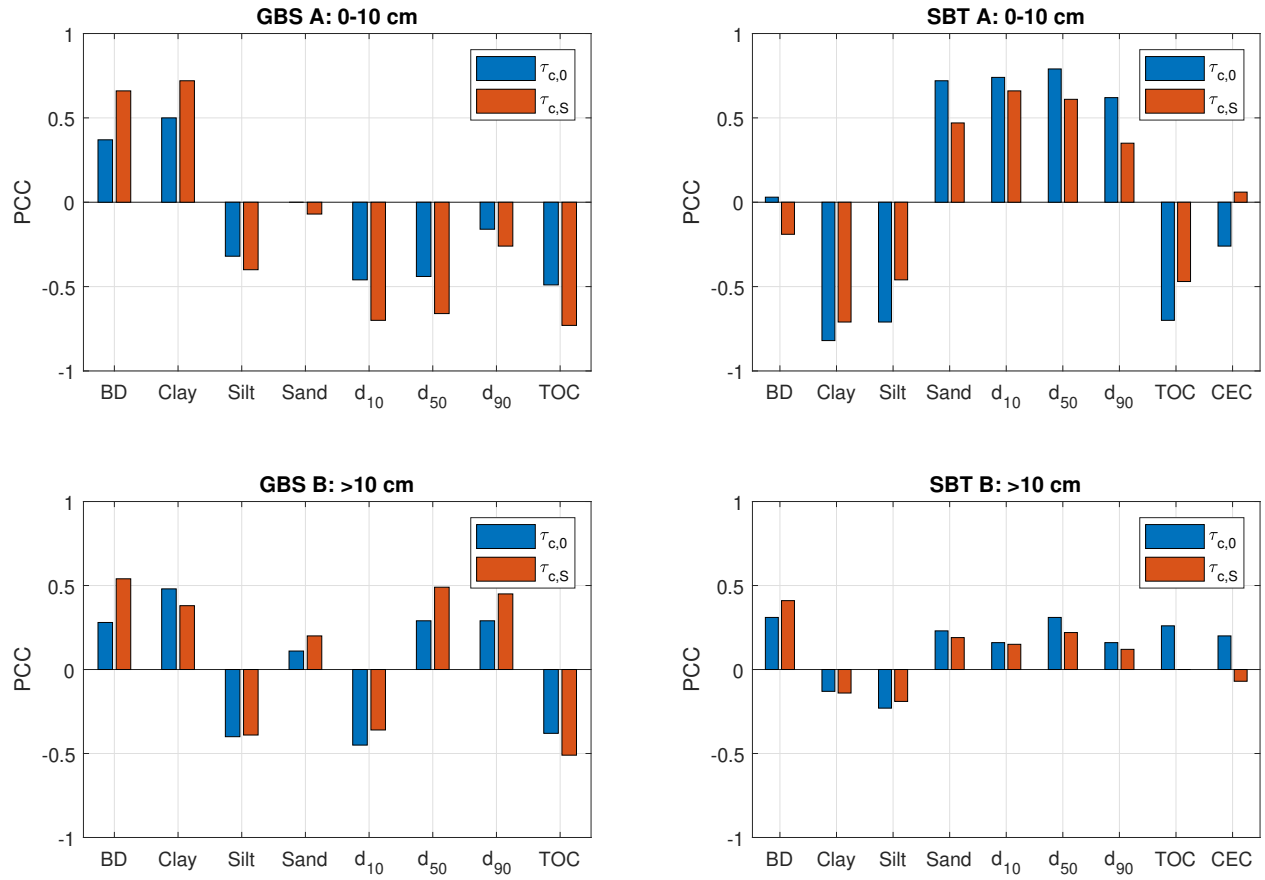
Fig. 6. Variation of correlation coefficients between erosion thresholds ($\tau_{c,0}$ and $\tau_{c,S}$) and sediment characteristics across two regions of sediment depth: A (0-10 cm) and B (>10 cm). The left panels indicate the correlations found for the GBS deposits, whereas the right panels indicate the correlations for the SBT deposits.
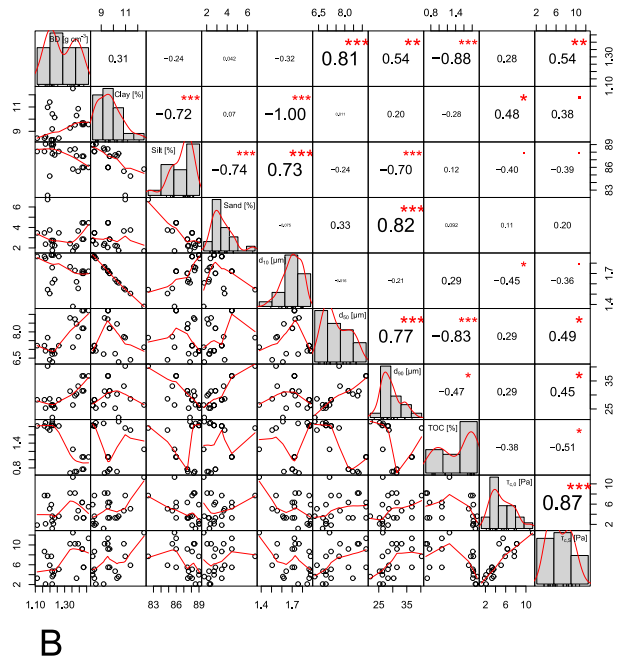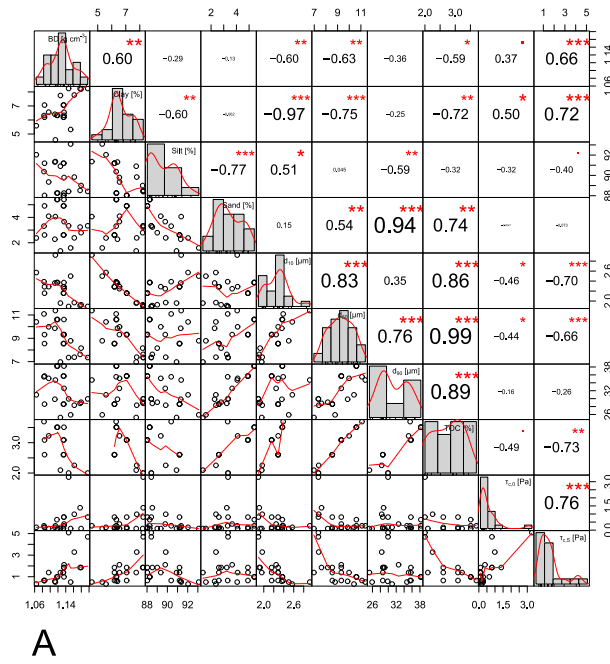
Fig. S1. Multivariate correlations between analyzed sediment parameters and critical erosion thresholds of the GBS deposits for the depth region A (0-10 cm) and B (>10 cm). The distribution of each variable is displayed as a histogram on the diagonal axis with an overlaid kernel density estimation. Below the diagonal axis, the scatter plots with fitted lines are displayed. Above the diagonal axis, the correlation coefficients and significance levels (*p*-values) of the relationship are indicated by the symbols *** (*p* = 0 - 0.001), ** (*p* = 0.001 - 0.01), * (*p* = 0.01 - 0.05), and ■ (*p* = 0.05 - 0.10).
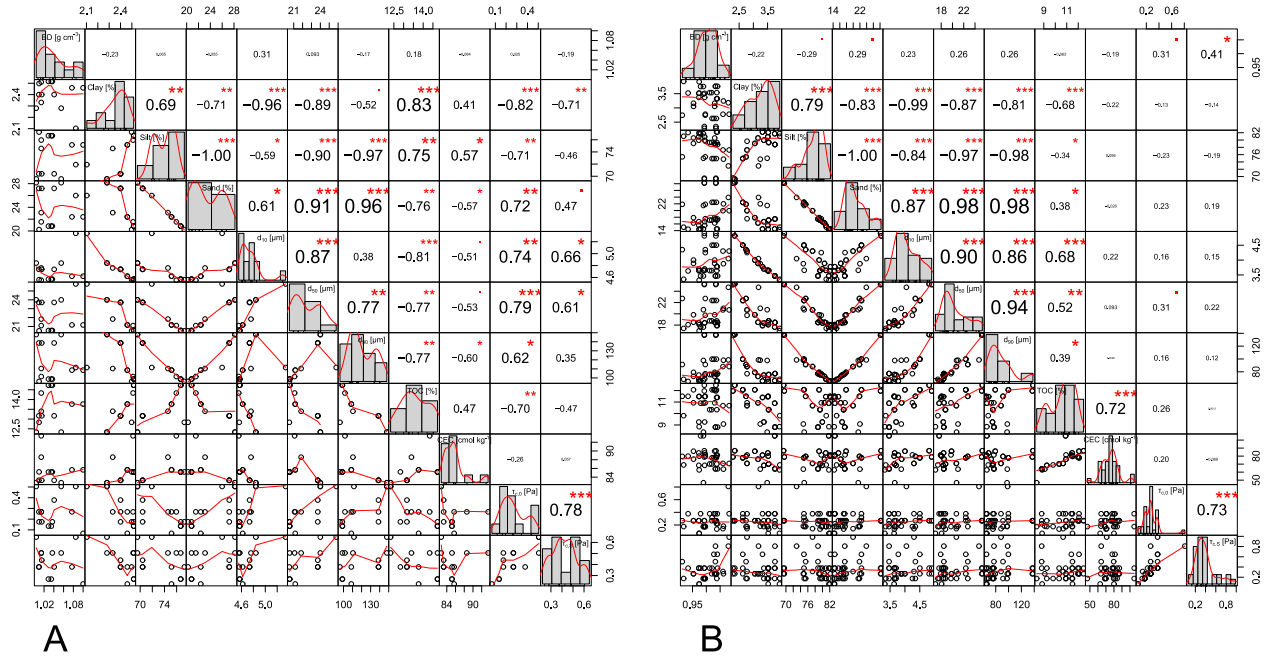
Fig. S2. Multivariate correlations between analyzed sediment parameters and critical erosion thresholds of the SBT deposits for the depth region A (0-10 cm) and B (>10 cm). The distribution of each variable is displayed as a histogram on the diagonal axis with an overlaid kernel density estimation. Below the diagonal axis, the scatter plots with fitted lines are displayed. Above the diagonal axis, the correlation coefficients and significance levels (*p*-values) of the relationship are indicated by the symbols *** (*p* = 0 - 0.001), ** (*p* = 0.001 - 0.01), * (*p* = 0.01 - 0.05), and ■ (*p* = 0.05 - 0.10).
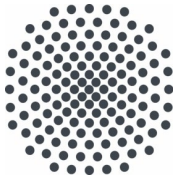
**Institut für Wasser- und
Umweltsystemmodellierung
Universität Stuttgart**

Pfaffenwaldring 61
70569 Stuttgart (Vaihingen)
Telefon (0711) 685 - 60156
Telefax (0711) 685 - 51073
E-Mail: iws@iws.uni-stuttgart.de
http://www.iws.uni-stuttgart.de

Direktoren
Prof. Dr. rer. nat. Dr.-Ing. András Bárdossy
Prof. Dr.-Ing. Rainer Helmig
Prof. Dr.-Ing. Wolfgang Nowak
Prof. Dr.-Ing. Silke Wieprecht

Vorstand *(Stand 21.05.2021)*
Prof. Dr. rer. nat. Dr.-Ing. A. Bárdossy
Prof. Dr.-Ing. R. Helmig
Prof. Dr.-Ing. W. Nowak
Prof. Dr.-Ing. S. Wieprecht
Prof. Dr. J.A. Sander Huisman
Jürgen Braun, PhD
apl. Prof. Dr.-Ing. H. Class
PD Dr.-Ing. Claus Haslauer
Stefan Haun, PhD
apl. Prof. Dr.-Ing. Sergey Oladyshkin
Dr. rer. nat. J. Seidel
Dr.-Ing. K. Terheiden

Emeriti
Prof. Dr.-Ing. habil. Dr.-Ing. E.h. Jürgen Giesecke
Prof. Dr.h.c. Dr.-Ing. E.h. Helmut Kobus, PhD

**Lehrstuhl für Wasserbau und
Wassermengenwirtschaft**
Leiterin: Prof. Dr.-Ing. Silke Wieprecht
Stellv.: Dr.-Ing. Kristina Terheiden
Versuchsanstalt für Wasserbau
Leiter: Stefan Haun, PhD

**Lehrstuhl für Hydromechanik
und Hydrosystemmodellierung**
Leiter: Prof. Dr.-Ing. Rainer Helmig
Stellv.: apl. Prof. Dr.-Ing. Holger Class

Lehrstuhl für Hydrologie und Geohydrologie
Leiter: Prof. Dr. rer. nat. Dr.-Ing. András Bárdossy
Stellv.: Dr. rer. nat. Jochen Seidel
*Hydrogeophysik der Vadosen Zone
(mit Forschungszentrum Jülich)*
Leiter: Prof. Dr. J.A. Sander Huisman

**Lehrstuhl für Stochastische Simulation und
Sicherheitsforschung für Hydrosysteme**
Leiter: Prof. Dr.-Ing. Wolfgang Nowak
Stellv.: apl. Prof. Dr.-Ing. Sergey Oladyshkin

VEGAS, Versuchseinrichtung zur
Grundwasser- und Altlastensanierung
Leiter: Jürgen Braun, PhD
        PD Dr.-Ing. Claus Haslauer

Verzeichnis der Mitteilungshefte

5   Plate, Erich: *Beitrag zur Bestimmung der Windgeschwindigkeitsverteilung in der durch eine Wand gestörten bodennahen Luftschicht*, und
Röhnisch, Arthur; Marotz, Günter: *Neue Baustoffe und Bauausführungen für den Schutz der Böschungen und der Sohle von Kanälen, Flüssen und Häfen; Gestehungskosten und jeweilige Vorteile*, sowie
Unny, T.E.: *Schwingungsuntersuchungen am Kegelstrahlschieber*, 1967

6   Seiler, Erich: *Die Ermittlung des Anlagenwertes der bundeseigenen Binnenschiffahrtsstraßen und Talsperren und des Anteils der Binnenschiffahrt an diesem Wert*, 1967

7   *Sonderheft anläßlich des 65. Geburtstages von Prof. Arthur Röhnisch mit Beiträgen von* Benk, Dieter; Breitling, J.; Gurr, Siegfried; Haberhauer, Robert; Honekamp, Hermann; Kuz, Klaus Dieter; Marotz, Günter; Mayer-Vorfelder, Hans-Jörg; Miller, Rudolf; Plate, Erich J.; Radomski, Helge; Schwarz, Helmut; Vollmer, Ernst; Wildenhahn, Eberhard; 1967

8   Jumikis, Alfred: *Beitrag zur experimentellen Untersuchung des Wassernachschubs in einem gefrierenden Boden und die Beurteilung der Ergebnisse*, 1968

9   Marotz, Günter: *Technische Grundlagen einer Wasserspeicherung im natürlichen Untergrund*, 1968

10   Radomski, Helge: *Untersuchungen über den Einfluß der Querschnittsform wellenförmiger Spundwände auf die statischen und rammtechnischen Eigenschaften*, 1968

11   Schwarz, Helmut: *Die Grenztragfähigkeit des Baugrundes bei Einwirkung vertikal gezogener Ankerplatten als zweidimensionales Bruchproblem*, 1969

12   Erbel, Klaus: *Ein Beitrag zur Untersuchung der Metamorphose von Mittelgebirgsschneedecken unter besonderer Berücksichtigung eines Verfahrens zur Bestimmung der thermischen Schneequalität*, 1969

13   Westhaus, Karl-Heinz: *Der Strukturwandel in der Binnenschiffahrt und sein Einfluß auf den Ausbau der Binnenschiffskanäle*, 1969

14   Mayer-Vorfelder, Hans-Jörg: *Ein Beitrag zur Berechnung des Erdwiderstandes unter Ansatz der logarithmischen Spirale als Gleitflächenfunktion*, 1970

15   Schulz, Manfred: *Berechnung des räumlichen Erddruckes auf die Wandung kreiszylindrischer Körper*, 1970

16   Mobasseri, Manoutschehr: *Die Rippenstützmauer. Konstruktion und Grenzen ihrer Standsicherheit*, 1970

17   Benk, Dieter: *Ein Beitrag zum Betrieb und zur Bemessung von Hochwasserrückhaltebecken*, 1970

18   Gàl, Attila: *Bestimmung der mitschwingenden Wassermasse bei überströmten Fischbauchklappen mit kreiszylindrischem Staublech*, 1971, *vergriffen*

19   Kuz, Klaus Dieter: *Ein Beitrag zur Frage des Einsetzens von Kavitationserscheinungen in einer Düsenströmung bei Berücksichtigung der im Wasser gelösten Gase*, 1971, *vergriffen*

20   Schaak, Hartmut: *Verteilleitungen von Wasserkraftanlagen*, 1971

21   *Sonderheft zur Eröffnung der neuen Versuchsanstalt des Instituts für Wasserbau der Universität Stuttgart mit Beiträgen von* Brombach, Hansjörg; Dirksen, Wolfram; Gàl, Attila; Gerlach, Reinhard; Giesecke, Jürgen; Holthoff, Franz-Josef; Kuz, Klaus Dieter; Marotz, Günter; Minor, Hans-Erwin; Petrikat, Kurt; Röhnisch, Arthur; Rueff, Helge; Schwarz, Helmut; Vollmer, Ernst; Wildenhahn, Eberhard; 1972

22   Wang, Chung-su: *Ein Beitrag zur Berechnung der Schwingungen an Kegelstrahlschiebern*, 1972

23   Mayer-Vorfelder, Hans-Jörg: *Erdwiderstandsbeiwerte nach dem Ohde-Variationsverfahren*, 1972

24   Minor, Hans-Erwin: *Beitrag zur Bestimmung der Schwingungsanfachungsfunktionen überströmter Stauklappen*, 1972, *vergriffen*

25   Brombach, Hansjörg: *Untersuchung strömungsmechanischer Elemente (Fluidik) und die Möglichkeit der Anwendung von Wirbelkammerelementen im Wasserbau*, 1972, *vergriffen*

26   Wildenhahn, Eberhard: *Beitrag zur Berechnung von Horizontalfilterbrunnen*, 1972

50   Mehlhorn, Hans: *Temperaturveränderungen im Grundwasser durch Brauchwasserein-leitungen*, 1982, ISBN 3-921694-50-7, *vergriffen*

51   Hafner, Edzard: *Rohrleitungen und Behälter im Meer*, 1983, ISBN 3-921694-51-5

52   Rinnert, Bernd: *Hydrodynamische Dispersion in porösen Medien: Einfluß von Dichteun-terschieden auf die Vertikalvermischung in horizontaler Strömung*, 1983, ISBN 3-921694-52-3, *vergriffen*

53   Lindner, Wulf: *Steuerung von Grundwasserentnahmen unter Einhaltung ökologischer Kri-terien*, 1983, ISBN 3-921694-53-1, *vergriffen*

54   Herr, Michael; Herzer, Jörg; Kinzelbach, Wolfgang; Kobus, Helmut; Rinnert, Bernd: *Metho-den zur rechnerischen Erfassung und hydraulischen Sanierung von Grundwasser-kontaminationen*, 1983, ISBN 3-921694-54-X

55   Schmitt, Paul: *Wege zur Automatisierung der Niederschlagsermittlung*, 1984, ISBN 3-921694-55-8, *vergriffen*

56   Müller, Peter: *Transport und selektive Sedimentation von Schwebstoffen bei gestautem Abfluß*, 1985, ISBN 3-921694-56-6

57   El-Qawasmeh, Fuad: *Möglichkeiten und Grenzen der Tropfbewässerung unter besonderer Berücksichtigung der Verstopfungsanfälligkeit der Tropfelemente*, 1985, ISBN 3-921694-57-4, *vergriffen*

58   Kirchenbaur, Klaus: *Mikroprozessorgesteuerte Erfassung instationärer Druckfelder am Beispiel seegangsbelasteter Baukörper*, 1985, ISBN 3-921694-58-2

59   Kobus, Helmut (Hrsg.): *Modellierung des großräumigen Wärme- und Schadstofftransports im Grundwasser*, Tätigkeitsbericht 1984/85 (DFG-Forschergruppe an den Universitäten Hohenheim, Karlsruhe und Stuttgart), 1985, ISBN 3-921694-59-0, *vergriffen*

60   Spitz, Karlheinz: *Dispersion in porösen Medien: Einfluß von Inhomogenitäten und Dichte-unterschieden*, 1985, ISBN 3-921694-60-4, *vergriffen*

61   Kobus, Helmut: *An Introduction to Air-Water Flows in Hydraulics*, 1985, ISBN 3-921694-61-2

62   Kaleris, Vassilios: *Erfassung des Austausches von Oberflächen- und Grundwasser in hori-zontalebenen Grundwassermodellen*, 1986, ISBN 3-921694-62-0

63   Herr, Michael: *Grundlagen der hydraulischen Sanierung verunreinigter Porengrundwasser-leiter*, 1987, ISBN 3-921694-63-9

64   Marx, Walter: *Berechnung von Temperatur und Spannung in Massenbeton infolge Hydra-tation*, 1987, ISBN 3-921694-64-7

65   Koschitzky, Hans-Peter: *Dimensionierungskonzept für Sohlbelüfter in Schußrinnen zur Vermeidung von Kavitationsschäden*, 1987, ISBN 3-921694-65-5

66   Kobus, Helmut (Hrsg.): *Modellierung des großräumigen Wärme- und Schadstofftransports im Grundwasser*, Tätigkeitsbericht 1986/87 (DFG-Forschergruppe an den Universitäten Hohenheim, Karlsruhe und Stuttgart) 1987, ISBN 3-921694-66-3

67   Söll, Thomas: *Berechnungsverfahren zur Abschätzung anthropogener Temperaturanoma-lien im Grundwasser*, 1988, ISBN 3-921694-67-1

68   Dittrich, Andreas; Westrich, Bernd: *Bodenseeufererosion, Bestandsaufnahme und Bewer-tung*, 1988, ISBN 3-921694-68-X, *vergriffen*

69   Huwe, Bernd; van der Ploeg, Rienk R.: *Modelle zur Simulation des Stickstoffhaushaltes von Standorten mit unterschiedlicher landwirtschaftlicher Nutzung*, 1988, ISBN 3-921694-69-8, *vergriffen*

70   Stephan, Karl: *Integration elliptischer Funktionen*, 1988, ISBN 3-921694-70-1

71   Kobus, Helmut; Zilliox, Lothaire (Hrsg.): *Nitratbelastung des Grundwassers, Auswirkungen der Landwirtschaft auf die Grundwasser- und Rohwasserbeschaffenheit und Maßnahmen zum Schutz des Grundwassers*. Vorträge des deutsch-französischen Kolloquiums am 6. Oktober 1988, Universitäten Stuttgart und Louis Pasteur Strasbourg (Vorträge in deutsch oder französisch, Kurzfassungen zweisprachig), 1988, ISBN 3-921694-71-X

95   Cirpka, Olaf: *Numerische Methoden zur Simulation des reaktiven Mehrkomponenten-transports im Grundwasser*, 1997, ISBN 3-921694-95-7, <u>*vergriffen*</u>

96   Färber, Arne: *Wärmetransport in der ungesättigten Bodenzone: Entwicklung einer thermischen In-situ-Sanierungstechnologie*, 1997, ISBN 3-921694-96-5

97   Betz, Christoph: *Wasserdampfdestillation von Schadstoffen im porösen Medium: Entwicklung einer thermischen In-situ-Sanierungstechnologie*, 1998, SBN 3-921694-97-3

98   Xu, Yichun: *Numerical Modeling of Suspended Sediment Transport in Rivers*, 1998, ISBN 3-921694-98-1, <u>*vergriffen*</u>

99   Wüst, Wolfgang: *Geochemische Untersuchungen zur Sanierung CKW-kontaminierter Aquifere mit Fe(0)-Reaktionswänden,* 2000, ISBN 3-933761-02-2

100 Sheta, Hussam: *Simulation von Mehrphasenvorgängen in porösen Medien unter Einbeziehung von Hysterese-Effekten*, 2000, ISBN 3-933761-03-4

101 Ayros, Edwin: *Regionalisierung extremer Abflüsse auf der Grundlage statistischer Verfahren*, 2000, ISBN 3-933761-04-2, <u>*vergriffen*</u>

102 Huber, Ralf: *Compositional Multiphase Flow and Transport in Heterogeneous Porous Media*, 2000, ISBN 3-933761-05-0

103 Braun, Christopherus: *Ein Upscaling-Verfahren für Mehrphasenströmungen in porösen Medien*, 2000, ISBN 3-933761-06-9

104 Hofmann, Bernd: *Entwicklung eines rechnergestützten Managementsystems zur Beurteilung von Grundwasserschadensfällen*, 2000, ISBN 3-933761-07-7

105 Class, Holger: *Theorie und numerische Modellierung nichtisothermer Mehrphasenprozesse in NAPL-kontaminierten porösen Medien,* 2001, ISBN 3-933761-08-5

106 Schmidt, Reinhard: *Wasserdampf- und Heißluftinjektion zur thermischen Sanierung kontaminierter Standorte*, 2001, ISBN 3-933761-09-3

107 Josef, Reinhold: *Schadstoffextraktion mit hydraulischen Sanierungsverfahren unter Anwendung von grenzflächenaktiven Stoffen*, 2001, ISBN 3-933761-10-7

108 Schneider, Matthias: *Habitat- und Abflussmodellierung für Fließgewässer mit unscharfen Berechnungsansätzen*, 2001, ISBN 3-933761-11-5

109 Rathgeb, Andreas: *Hydrodynamische Bemessungsgrundlagen für Lockerdeckwerke an überströmbaren Erddämmen*, 2001, ISBN 3-933761-12-3

110 Lang, Stefan: *Parallele numerische Simulation instätionärer Probleme mit adaptiven Methoden auf unstrukturierten Gittern*, 2001, ISBN 3-933761-13-1

111 Appt, Jochen; Stumpp Simone: *Die Bodensee-Messkampagne 2001, IWS/CWR Lake Constance Measurement Program 2001*, 2002, ISBN 3-933761-14-X

112 Heimerl, Stephan: *Systematische Beurteilung von Wasserkraftprojekten,* 2002, ISBN 3-933761-15-8, <u>*vergriffen*</u>

113 Iqbal, Amin: *On the Management and Salinity Control of Drip Irrigation,* 2002, ISBN 3-933761-16-6

114 Silberhorn-Hemminger, Annette: *Modellierung von Kluftaquifersystemen: Geostatistische Analyse und deterministisch-stochastische Kluftgenerierung,* 2002, ISBN 3-933761-17-4

115 Winkler, Angela: *Prozesse des Wärme- und Stofftransports bei der In-situ-Sanierung mit festen Wärmequellen,* 2003, ISBN 3-933761-18-2

116 Marx, Walter: *Wasserkraft, Bewässerung, Umwelt - Planungs- und Bewertungsschwerpunkte der Wasserbewirtschaftung,* 2003, ISBN 3-933761-19-0

117 Hinkelmann, Reinhard: *Efficient Numerical Methods and Information-Processing Techniques in Environment Water,* 2003, ISBN 3-933761-20-4

118 Samaniego-Eguiguren, Luis Eduardo: *Hydrological Consequences of Land Use / Land Cover and Climatic Changes in Mesoscale Catchments*, 2003, ISBN 3-933761-21-2

119 Neunhäuserer, Lina: *Diskretisierungsansätze zur Modellierung von Strömungs- und Transportprozessen in geklüftet-porösen Medien*, 2003, ISBN 3-933761-22-0

120 Paul, Maren: *Simulation of Two-Phase Flow in Heterogeneous Poros Media with Adaptive Methods*, 2003, ISBN 3-933761-23-9

144   Breiting, Thomas: *Techniken und Methoden der Hydroinformatik - Modellierung von komplexen Hydrosystemen im Untergrund*, 2006, ISBN 3-933761-47-6

145   Hrsg.: Braun, Jürgen; Koschitzky, Hans-Peter; Müller, Martin: *Ressource Untergrund: 10 Jahre VEGAS: Forschung und Technologieentwicklung zum Schutz von Grundwasser und Boden,* Tagungsband zur Veranstaltung am 28. und 29. September 2005 an der Universität Stuttgart, Campus Stuttgart-Vaihingen, 2005, ISBN 3-933761-48-4

146   Rojanschi, Vlad: *Abflusskonzentration in mesoskaligen Einzugsgebieten unter Berücksichtigung des Sickerraumes,* 2006, ISBN 3-933761-49-2

147   Winkler, Nina Simone: *Optimierung der Steuerung von Hochwasserrückhaltebeckensystemen,* 2006, ISBN 3-933761-50-6

148   Wolf, Jens: *Räumlich differenzierte Modellierung der Grundwasserströmung alluvialer Aquifere für mesoskalige Einzugsgebiete*, 2006, ISBN: 3-933761-51-4

149   Kohler, Beate: *Externe Effekte der Laufwasserkraftnutzung*, 2006, ISBN 3-933761-52-2

150   Hrsg.: Braun, Jürgen; Koschitzky, Hans-Peter; Stuhrmann, Matthias: *VEGAS-Statuskolloquium 2006,* Tagungsband zur Veranstaltung am 28. September 2006 an der Universität Stuttgart, Campus Stuttgart-Vaihingen, 2006, ISBN 3-933761-53-0

151   Niessner, Jennifer: *Multi-Scale Modeling of Multi-Phase - Multi-Component Processes in Heterogeneous Porous Media*, 2006, ISBN 3-933761-54-9

152   Fischer, Markus: *Beanspruchung eingeerdeter Rohrleitungen infolge Austrocknung bindiger Böden,* 2006, ISBN 3-933761-55-7

153   Schneck, Alexander: *Optimierung der Grundwasserbewirtschaftung unter Berücksichtigung der Belange der Wasserversorgung, der Landwirtschaft und des Naturschutzes*, 2006, ISBN 3-933761-56-5

154   Das, Tapash: *The Impact of Spatial Variability of Precipitation on the Predictive Uncertainty of Hydrological Models,* 2006, ISBN 3-33761-57-3

155   Bielinski, Andreas: *Numerical Simulation of CO_2 sequestration in geological formations*, 2007, ISBN 3-933761-58-1

156   Mödinger, Jens: *Entwicklung eines Bewertungs- und Entscheidungsunterstützungssystems für eine nachhaltige regionale Grundwasserbewirtschaftung*, 2006, ISBN 3-933761-60-3

157   Manthey, Sabine: *Two-phase flow processes with dynamic effects in porous media - parameter estimation and simulation,* 2007, ISBN 3-933761-61-1

158   Pozos Estrada, Oscar: *Investigation on the Effects of Entrained Air in Pipelines,* 2007, ISBN 3-933761-62-X

159   Ochs, Steffen Oliver: *Steam injection into saturated porous media – process analysis including experimental and numerical investigations*, 2007, ISBN 3-933761-63-8

160   Marx, Andreas: *Einsatz gekoppelter Modelle und Wetterradar zur Abschätzung von Niederschlagsintensitäten und zur Abflussvorhersage, 2007,* ISBN 3-933761-64-6

161   Hartmann, Gabriele Maria: *Investigation of Evapotranspiration Concepts in Hydrological Modelling for Climate Change Impact Assessment*, 2007, ISBN 3-933761-65-4

162   Kebede Gurmessa, Tesfaye: *Numerical Investigation on Flow and Transport Characteristics to Improve Long-Term Simulation of Reservoir Sedimentation*, 2007, ISBN 3-933761-66-2

163   Trifković, Aleksandar: *Multi-objective and Risk-based Modelling Methodology for Planning, Design and Operation of Water Supply Systems*, 2007, ISBN 3-933761-67-0

164   Götzinger, Jens: *Distributed Conceptual Hydrological Modelling - Simulation of Climate, Land Use Change Impact and Uncertainty Analysis*, 2007, ISBN 3-933761-68-9

165   Hrsg.: Braun, Jürgen; Koschitzky, Hans-Peter; Stuhrmann, Matthias: *VEGAS – Kolloquium 2007,* Tagungsband zur Veranstaltung am 26. September 2007 an der Universität Stuttgart, Campus Stuttgart-Vaihingen, 2007, ISBN 3-933761-69-7

166   Freeman, Beau: *Modernization Criteria Assessment for Water Resources Planning; Klamath Irrigation Project, U.S.*, 2008, ISBN 3-933761-70-0

191 Merkel, Uwe: *Unsicherheitsanalyse hydraulischer Einwirkungen auf Hochwasserschutz-deiche und Steigerung der Leistungsfähigkeit durch adaptive Strömungsmodellierung*, 2011, ISBN 978-3-933761-95-8

192 Fritz, Jochen: *A Decoupled Model for Compositional Non-Isothermal Multiphase Flow in Porous Media and Multiphysics Approaches for Two-Phase Flow*, 2010, ISBN 978-3-933761-96-5

193 Weber, Karolin (Hrsg.): *12. Treffen junger WissenschaftlerInnen an Wasserbauinstituten*, 2010, ISBN 978-3-933761-97-2

194 Bliefernicht, Jan-Geert: *Probability Forecasts of Daily Areal Precipitation for Small River Basins,* 2011, ISBN 978-3-933761-98-9

195 Hrsg.: Koschitzky, Hans-Peter; Braun, Jürgen: *VEGAS-Kolloquium 2010 In-situ-Sanierung - Stand und Entwicklung Nano und ISCO -,* Tagungsband zur Veranstaltung am 07. Oktober 2010 an der Universität Stuttgart, Campus Stuttgart-Vaihingen*, 2010,* ISBN 978-3-933761-99-6

196 Gafurov, Abror: *Water Balance Modeling Using Remote Sensing Information - Focus on Central Asia,* 2010, ISBN 978-3-942036-00-9

197 Mackenberg, Sylvia: *Die Quellstärke in der Sickerwasserprognose: Möglichkeiten und Grenzen von Labor- und Freilanduntersuchungen,* 2010, ISBN 978-3-942036-01-6

198 Singh, Shailesh Kumar: *Robust Parameter Estimation in Gauged and Ungauged Basins,* 2010, ISBN 978-3-942036-02-3

199 Doğan, Mehmet Onur: *Coupling of porous media flow with pipe flow,* 2011, ISBN 978-3-942036-03-0

200 Liu, Min: *Study of Topographic Effects on Hydrological Patterns and the Implication on Hydrological Modeling and Data Interpolation,* 2011, ISBN 978-3-942036-04-7

201 Geleta, Habtamu Itefa: *Watershed Sediment Yield Modeling for Data Scarce Areas,* 2011, ISBN 978-3-942036-05-4

202 Franke, Jörg: *Einfluss der Überwachung auf die Versagenswahrscheinlichkeit von Staustufen,* 2011, ISBN 978-3-942036-06-1

203 Bakimchandra, Oinam: *Integrated Fuzzy-GIS approach for assessing regional soil erosion risks,* 2011, ISBN 978-3-942036-07-8

204 Alam, Muhammad Mahboob: *Statistical Downscaling of Extremes of Precipitation in Mesoscale Catchments from Different RCMs and Their Effects on Local Hydrology,* 2011, ISBN 978-3-942036-08-5

205 Hrsg.: Koschitzky, Hans-Peter; Braun, Jürgen: *VEGAS-Kolloquium 2011 Flache Geothermie - Perspektiven und Risiken,* Tagungsband zur Veranstaltung am 06. Oktober 2011 an der Universität Stuttgart, Campus Stuttgart-Vaihingen*, 2011,* ISBN 978-3-933761-09-2

206 Haslauer, Claus: *Analysis of Real-World Spatial Dependence of Subsurface Hydraulic Properties Using Copulas with a Focus on Solute Transport Behaviour,* 2011, ISBN 978-3-942036-10-8

207 Dung, Nguyen Viet: *Multi-objective automatic calibration of hydrodynamic models – development of the concept and an application in the Mekong Delta,* 2011, ISBN 978-3-942036-11-5

208 Hung, Nguyen Nghia: *Sediment dynamics in the floodplain of the Mekong Delta, Vietnam,* 2011, ISBN 978-3-942036-12-2

209 Kuhlmann, Anna: *Influence of soil structure and root water uptake on flow in the unsaturated zone,* 2012, ISBN 978-3-942036-13-9

210 Tuhtan, Jeffrey Andrew: *Including the Second Law Inequality in Aquatic Ecodynamics: A Modeling Approach for Alpine Rivers Impacted by Hydropeaking,* 2012, ISBN 978-3-942036-14-6

211 Tolossa, Habtamu: *Sediment Transport Computation Using a Data-Driven Adaptive Neuro-Fuzzy Modelling Approach,* 2012, ISBN 978-3-942036-15-3

212 Tatomir, Alexandru-Bodgan: *From Discrete to Continuum Concepts of Flow in Fractured Porous Media,* 2012, ISBN 978-3-942036-16-0

237   Nuske, Klaus Philipp: *Beyond Local Equilibrium — Relaxing local equilibrium assumptions in multiphase flow in porous media,* 2014, ISBN 978-3-942036-41-2

238   Geiges, Andreas: *Efficient concepts for optimal experimental design in nonlinear environmental systems*, 2014, ISBN 978-3-942036-42-9

239   Schwenck, Nicolas: *An XFEM-Based Model for Fluid Flow in Fractured Porous Media*, 2014, ISBN 978-3-942036-43-6

240   Chamorro Chávez, Alejandro: *Stochastic and hydrological modelling for climate change prediction in the Lima region, Peru*, 2015, ISBN 978-3-942036-44-3

241   Yulizar: *Investigation of Changes in Hydro-Meteorological Time Series Using a Depth-Based Approach*, 2015, ISBN 978-3-942036-45-0

242   Kretschmer, Nicole: *Impacts of the existing water allocation scheme on the Limarí watershed – Chile, an integrative approach*, 2015, ISBN 978-3-942036-46-7

243   Kramer, Matthias: *Luftbedarf von Freistrahlturbinen im Gegendruckbetrieb*, 2015, ISBN 978-3-942036-47-4

244   Hommel, Johannes: *Modeling biogeochemical and mass transport processes in the subsurface: Investigation of microbially induced calcite precipitation*, 2016, ISBN 978-3-942036-48-1

245   Germer, Kai: *Wasserinfiltration in die ungesättigte Zone eines makroporösen Hanges und deren Einfluss auf die Hangstabilität*, 2016, ISBN 978-3-942036-49-8

246   Hörning, Sebastian: *Process-oriented modeling of spatial random fields using copulas*, 2016, ISBN 978-3-942036-50-4

247   Jambhekar, Vishal: *Numerical modeling and analysis of evaporative salinization in a coupled free-flow porous-media system,* 2016, ISBN 978-3-942036-51-1

248   Huang, Yingchun: *Study on the spatial and temporal transferability of conceptual hydrological models*, 2016, ISBN 978-3-942036-52-8

249   Kleinknecht, Simon Matthias: *Migration and retention of a heavy NAPL vapor and remediation of the unsaturated zone*, 2016, ISBN 978-3-942036-53-5

250   Kwakye, Stephen Oppong: *Study on the effects of climate change on the hydrology of the West African sub-region*, 2016, ISBN 978-3-942036-54-2

251   Kissinger, Alexander: *Basin-Scale Site Screening and Investigation of Possible Impacts of CO_2 Storage on Subsurface Hydrosystems*, 2016, ISBN 978-3-942036-55-9

252   Müller, Thomas: *Generation of a Realistic Temporal Structure of Synthetic Precipitation Time Series for Sewer Applications*, 2017, ISBN 978-3-942036-56-6

253   Grüninger, Christoph: *Numerical Coupling of Navier-Stokes and Darcy Flow for Soil-Water Evaporation*, 2017, ISBN 978-3-942036-57-3

254   Suroso: *Asymmetric Dependence Based Spatial Copula Models: Empirical Investigations and Consequences on Precipitation Fields*, 2017, ISBN 978-3-942036-58-0

255   Müller, Thomas; Mosthaf, Tobias; Gunzenhauser, Sarah; Seidel, Jochen; Bárdossy, András: *Grundlagenbericht Niederschlags-Simulator (NiedSim3)*, 2017, ISBN 978-3-942036-59-7

256   Mosthaf, Tobias: *New Concepts for Regionalizing Temporal Distributions of Precipitation and for its Application in Spatial Rainfall Simulation,* 2017, ISBN 978-3-942036-60-3

257   Fenrich, Eva Katrin: *Entwicklung eines ökologisch-ökonomischen Vernetzungsmodells für Wasserkraftanlagen und Mehrzweckspeicher,* 2018, ISBN 978-3-942036-61-0

258   Schmidt, Holger: *Microbial stabilization of lotic fine sediments*, 2018, ISBN 978-3-942036-62-7

259   Fetzer, Thomas: *Coupled Free and Porous-Medium Flow Processes Affected by Turbulence and Roughness – Models, Concepts and Analysis*, 2018, ISBN 978-3-942036-63-4

260   Schröder, Hans Christoph: *Large-scale High Head Pico Hydropower Potential Assessment*, 2018, ISBN 978-3-942036-64-1

261   Bode, Felix: *Early-Warning Monitoring Systems for Improved Drinking Water Resource Protection*, 2018, ISBN 978-3-942036-65-8

286   Michalkowski, Cynthia: *Modeling water transport at the interface between porous GDL and gas distributor of a PEM fuel cell cathode*, 2022, ISBN: 978-3-942036-90-0

287   Koca, Kaan: *Advanced experimental methods for investigating flow-biofilm-sediment interactions*, 2022, ISBN: 978-3-942036-91-7

Die Mitteilungshefte ab der Nr. 134 (Jg. 2005) stehen als pdf-Datei über die Homepage des Instituts: www.iws.uni-stuttgart.de zur Verfügung.